

Longitudinal Imaging of Pancreatic Islets Transplanted into the Anterior Chamber of the Eye

A thesis submitted for the degree of Doctor of Philosophy,
Imperial College London

Kinga Suba

2020

Section of Investigative Medicine

Division of Diabetes, Endocrinology and Metabolism

Department of Metabolism, Digestion and Reproduction

Imperial College London

Copyright Declaration

The copyright of this thesis rests with the author. Unless otherwise indicated, its contents are licensed under a Creative Commons Attribution-Non Commercial 4.0 International Licence (CC BY- NC).

Under this licence, you may copy and redistribute the material in any medium or format. You may also create and distribute modified versions of the work. This is on the condition that: you credit the author and do not use it, or any derivative works, for a commercial purpose.

When reusing or sharing this work, ensure you make the licence terms clear to others by naming the licence and linking to the licence text. Where a work has been adapted, you should indicate that the work has been changed and describe those changes. Please seek permission from the copyright holder for uses of this work that are not included in this licence or permitted under UK Copyright Law.

Declaration of Contributors

The majority of the work presented in this thesis was performed by the author. All collaboration and assistance are described below:

The islet in the eye imaging platform was developed at Karolinska Institute originally by Prof Per-Olof Berggren, Prof Alejandro Caicedo and Prof Stephan Speier.

Chapter 2:

Pearson R analysis and connectivity cut-offs were developed by Dr Victoria Salem and Prof Walter Distaso. Granger causality MatLab script was developed and performed by Dr Victoria Salem (Imperial College) and Prof Walter Distaso (Imperial College). Manual motion-correction FIJI macro was written by Mr Stephen Rothery. (FILM, Imperial College). Genotyping of transgenic animals used in this study was performed by Mr Yateen Patel.

Chapter 3:

Synthetic peptides were kindly donated by Prof Steven Bloom (Imperial College London). Peptides were weighed out and their purity tested by Dr James Minion (Imperial College London). The cAMP assay on G778 was performed by Mr Yateen Patel. Metabolic phenotyping of animals were carried out in collaboration with Mr Yateen Patel and Miss Aldara Martin-Alonso.

Chapter 4:

The Islet process FIJI macro was written by Mr Stephen Rothery (FILM, Imperial College London). qPCR measurements were conducted by Dr Stavroula Bitsi and Miss Aldara Martin-Alonso.

Acknowledgements

First and foremost, I would like to express my gratitude towards my primary supervisor Dr Victoria Salem who has been tirelessly mentoring and supporting me over the three years. She has majorly contributed to both my professional and personal development. I am also grateful to have shared this experience with such a fantastic team: Y.P, A.MA, in particular but also M.N, E.A, N.G, S.C, P.P, T.G, M.L. etc.

Secondly, I would like to thank Prof Guy Rutter for welcoming me in his lab and team. I would like to thank Dr Pauline Chabosseau for sharing her microscopy expertise with me. Additionally, I am also thankful to Stephen Rothery and Dr David Gaboriau for imparting their ImageJ wizardry on me. I thank Dr Gaelle Carrat for her patience and help.

Additionally, I would like to thank my friends for their encouragement throughout this experience. In particular, I would like to thank Dr Christopher Fassnidge for returning the favour, and keeping me sane during my PhD course. I am hugely grateful to Sebastien for only ever supporting me and treating me with kindness, especially during these challenging times.

Lastly, I am indebted to my parents for their continuous support

Contents

Copyright Declaration.....	2
Declaration of Contributors.....	3
Acknowledgements	2
Abstract	8
List of Figures.....	10
1 Chapter: General Introduction	12
1.1 Diabetes.....	12
1.1.1 Prevalence and disease burden.....	12
1.1.2 Type 1 Diabetes	13
1.1.3 Treatments for Type 1 Diabetes	14
1.1.4 Type 2 diabetes mellitus.....	15
1.1.5 Current T2DM Treatments	18
1.2 Islet Biology form the Macroscopic to the Microscopic.....	26
1.2.1 Tissue Architecture	26
1.2.2 Vasculature	30
1.2.3 Innervation	32
1.2.4 β -cell Identity.....	34
1.2.5 The Biochemistry of Insulin secretion: Insulin:Calcium Signalling Coupling.....	39
1.3 Methods for Studying Islet Biology.....	41
1.3.1 <i>In Vitro</i> Methods.....	41
1.3.2 <i>In Vivo</i> Methods.....	42
1.3.3 Longitudinal <i>in vivo</i> imaging of pancreatic islets implanted into the anterior chamber of the eye (ACE) 47	
2 Chapter: Functional Imaging of Islets Transplanted into the Anterior Chamber of the Eye.....	53
2.1 Introduction	53
2.1.1 β -cell to β -cell Electrochemical Coupling	54
2.1.2 Islet Connectivity	55
2.1.3 Connectivity Defined as Co-Activity of Cell Pairs.....	56
2.1.4 Hub Cells	57
2.1.5 Initiators and propagators	59
2.1.6 Functional Connectivity of β -Cells <i>In Vivo</i>	60
2.1.7 Aims and Hypothesis	62
2.2 Materials and Methods	63
2.2.1 Animal Husbandry	63

2.2.2	Islet Isolation.....	63
2.2.3	Human Islet Donors	64
2.2.4	Generation of Adenovirus Expressing AV-GCaMP6m	64
2.2.5	Infection of Islets with AV-CMV-GCaMP6m	65
2.2.6	Generation of the InsCre-GCaMP6f line	65
2.2.7	Pancreatic Islet Transplantation into the Anterior Chamber of the Murine Eye	65
2.2.8	Imaging Protocol.....	66
2.2.9	Image Analysis	67
2.2.10	Pearson R Analysis	68
2.2.11	Granger Causality Analysis.....	68
2.3	Results.....	69
2.3.1	AV-CMV-GCaMP6m-infected islets	69
2.3.2	High Glucose Levels Enhance β -Cell Connectivity in Ins1Cre-GCaMP6f-Expressing Islets	72
2.3.3	Enhanced β -Cell Connectivity in Ins1Cre-GCaMP6f-Expressing Islets under High Glucose Concentrations <i>in vivo</i>	73
2.3.4	Temporally-Defined Leader Cells are Highly Connected and Causally Predict the Behaviour of the Majority of Cell Studied in the Islet	79
2.3.5	β -cell connectivity in human islets transplanted into the ACE of BALB/c Nude mice.....	81
2.4	Discussion	85
2.4.1	Increased Connectivity of β -cells under High Circulating Glucose	85
2.4.2	Are Leader cells Hub cells? – Possibly, but no direct evidence	86
2.4.3	Hub versus Pacemaker β -cells	89
3	Chapter: The Effects of High Fat Diet and Chronic Glucagon Analogue Treatment on Islet Function <i>In Vivo</i>	92
3.1	Introduction	92
3.1.1	Glucagon	92
3.1.2	A case for the inclusion of glucagon receptor agonism in the anti-diabetic armamentarium.	93
3.1.3	Aims and Hypotheses	96
3.2	Materials and Methods	97
3.2.1	Study Overview.....	97
3.2.2	Peptide Synthesis of G778.....	98
3.2.3	cAMP Assay.....	98
3.2.4	Metabolic Phenotyping	99
3.2.5	<i>In Vivo</i> Imaging Experiments	99
3.2.6	<i>In Vitro</i> Imaging Experiments	100
3.2.7	<i>In Vivo</i> and <i>In Vitro</i> Imaging Analysis.....	100

3.2.8	Statistical Analysis.....	102
3.2.9	Longitudinal assessment of leaders.....	102
3.3	Results.....	104
3.3.1	<i>In Vitro</i> cAMP Assay Suggests that G778 Has a Similar Receptor Activation Profile as Native Glucagon	104
3.3.2	The effects of DIO on islet function.....	105
3.3.3	G778 Treatment Causes a Modest Weight-Loss	107
3.3.4	DIO and G778 Induced Weight-Loss Independent Effects on Islet Calcium Dynamics in a Directly-Observed Model	110
3.3.5	Longitudinal Assessment of β -Cell Connectivity and Leader Cells	114
3.3.6	The Effects of G778 on Islet Calcium Dynamics <i>In Vitro</i>	117
3.4	Discussion	121
3.4.1	High-Fat Feeding Causes a Diminution in Global Calcium Responses in the Majority of Transplanted Islets.....	121
3.4.2	A Long-Acting Glucagon Analogue Improves Glycaemia - The Role of Glucagon in Homeostatic Control of Glucose	123
3.4.3	Glucagon as an Insulin Secretagogue	124
3.4.4	Connectivity as a longitudinal read-out.....	126
4	Chapter: Investigating the Effects of β -cell Specific Overexpression of Epidermal Growth Factor Receptor on Islet Revascularization	128
4.1	Introduction	128
4.1.1	Clinical Management of Type 1 Diabetes Mellitus (T1DM).....	128
4.1.2	Impaired Awareness of Hypoglycaemia	128
4.1.3	Islet Transplantation as an Alternative Treatment.....	129
4.1.4	Current limitations of the technique.....	130
4.1.5	Engraftment of Transplanted Islets with Focus on Angiogenesis.....	131
4.1.6	Approaches to Improve Islet Vascularisation	132
4.1.7	Epidermal Growth Factor Receptor.....	133
4.1.8	Can Islets Be Engineered Pre-Transplantation to Improve Their Engraftment?	135
4.1.9	Hypotheses and Aims:	136
4.2	Methods.....	137
4.2.1	Animal Husbandry	137
4.2.2	Pancreatic Extraction and Islet Isolation	137
4.2.3	Adenoviruses	137
4.2.4	Transplantation of pancreatic islets into the anterior chamber of the eye (ACE)	137
4.2.5	<i>In Vivo</i> Imaging Experiments	137

4.2.6	FIJI Image Analysis	138
4.2.7	Statistical Analysis.....	139
4.2.8	qPCR Analysis.....	139
4.2.9	Complementary (cDNA) synthesis.....	139
4.2.10	qPCR.....	140
4.3	Results.....	141
4.3.1	Engraftment Success	141
4.3.2	Imaging Islet Blood Vessels in the Eye.....	141
4.3.3	Islet and Blood Vessel Volumes	143
4.3.4	Blood Vessel Network Analysis.....	145
4.3.5	β -cell identity	148
4.4	Discussion	150
4.4.1	Would adenoviral gene transfer be a viable clinical tool for improving islet transplantation? 150	
4.4.2	Is EGFR a Viable Target for Improving Islet Engraftment?	152
4.4.3	Is the Islet in the Eye a Viable Clinical Transplantation Site?	155
4.4.4	As a preclinical model for studying angiogenesis how does it compare to what we have already? 157	
4.4.5	Technical limitations encountered in this pilot project.....	160
5	General Discussion	162
5.1	Blood supply of transplanted islets	162
5.2	Nerve supply of transplanted islets.....	163
5.3	The Internal Milieu of the Eye	164
5.3.1	Endocrine-Exocrine pancreas cross talk	164
5.3.2	ECM in the Pancreas versus the Anterior Chamber	165
5.4	Imaging Islets under Anaesthesia	166
6	Appendix : Solutions	168
6.1.1	Mouse Islet Culture Medium:.....	168
6.1.2	Human Islet Culture Medium:	168
6.1.3	Krebs-Ringer Bicarbonate Buffer:.....	168
7	Appendix : Genotyping of Ins1Cre-GCaMP6f line.....	170
8	Appendix : FIJI Macros.....	172
8.1.1	Time-series manual ROI motion correction macro:	172
8.1.2	Islet process macro:.....	174
8.1.3	Tube Analyst macro:.....	174

9	Appendix: Granger Causality Analysis MatLab script	178
10	Appendix: Human Islet Donor Characteristics.....	179
11	Appendix : Conference Abstracts	180
	Bibliography.....	186

Abstract

Diabetes is a growing health problem associated with substantial health and socioeconomic costs. Current medications address hyperglycaemia and related complications, but a definitive cure for diabetes remains elusive. Pharmacotherapy with the potential to restore β -cell function is urgently needed. To this end, it is vital that we achieve a better understanding of islet function in both health and disease states. While major breakthroughs in diabetes research have traditionally resulted from *in vitro* experimentation, the crucial role of the pancreatic internal milieu is being increasingly recognised. The islet in the eye imaging platform is the first experimental tool which allows for the longitudinal and direct investigation of β -cell function in a non-invasive manner.

This thesis describes the application of this imaging platform to three divergent areas of islet research. Firstly the physiology of co-ordinated insulin secretion is examined. Pulsatile insulin secretion is physiologically relevant and is impaired in diabetes. The imaging platform is used to establish, for the first time *in vivo*, that the calcium waves that underlie insulin secretion arise from the co-ordinated activity of a heterogeneous group of β -cells.

Obesity is the greatest risk factor for developing Type 2 diabetes. The effects of high fat diet on islet calcium dynamics are incompletely understood. Hyperglucagonaemia is traditionally thought of as a contributing factor to diabetes disease progression. Emerging evidence however suggests that glucagon signalling has beneficial effects on food intake and energy expenditure. More recently, the insulin potentiating effects of intra-islet glucagon has been suggested. The imaging platform is developed to investigate the longitudinal effects of high fat diet and the subsequent weight-loss independent effects of a synthetic glucagon analogue on islet function.

Together, these two studies investigate the utility of the islet in the eye imaging platform to better our understanding of intercellular β -cell calcium dynamics in the acute and in a more chronic setting.

Islet transplantation has not provided a reliable cure for patients with Type 1 diabetes, due to a relative lack of suitable donors but, more importantly, because the majority of patients fail to achieve long term insulin independence. The reasons for transplant failure are manifold and poorly

understood, although engraftment failure is a major issue. There is a clear need to improve transplant success rates, especially if this can be achieved in line with a more reliable supply of β -cells/islets (for example stem-cell derived therapies). The last experimental chapter aims to investigate the effects of epidermal growth factor receptor (EGFR) overexpression in β -cells and whether this treatment improves islet engraftment. In particular, this chapter focuses on the angiogenesis of newly transplanted islets and whether the islet in eye platform is capable of longitudinally monitoring this process.

List of Figures

Figure 1.1.1.1 Changes in diabetes prevalence rates over between 1980 and 2014 by region.....	13
Figure 1.1.4.1. Schematic diagram of diabetes-related micro-and macrovascular complications.	18
Figure 1.2.1.1 Architecture of mouse and human islets.	29
Figure 1.2.5.1 Schematic diagram of the glucose stimulated insulin secretion in the β -cell.	40
Figure 1.3.3.1 Schematic diagram of the islet in the eye imaging platform.....	49
Figure 2.1.4.1 Schematic diagram summarising the properties of hub cells.	58
Figure 2.2.7.1 Photography of the microscopy set-up and mouse with islets transplanted in his eyes.....	67
Figure 2.3.1.1 Photography of the implanted islets in the mouse eye anterior chamber.	69
Figure 2.3.1.2 Representative Ca^{+2} traces of individual AV-CMV-GCaMP6m-expressing β -cells (n=6) transplanted into the eye.	70
Figure 2.3.1.3 Pooled data from four AV-CMV-GCaMP6f expressing islets displays increased cell connectivity under high glucose concentrations.	71
Figure 2.3.2.1 Representative image from a time-series experiment showing identified cells.....	72
Figure 2.3.3.1 Increased beta-cell connectivity under high circulating glucose conditions in InsCre-GCaMP6m islets (n=5).	74
Figure 2.3.3.2 Increased beta-cell connectivity under high circulating glucose conditions in InsCre-GCaMP6m islets (n=5).	76
Figure 2.3.3.3 Pooled data from five InsCre-GCaMP6f expressing islets showing enhanced connectivity under high glucose concentrations.....	77
Figure 2.3.3.4 Cartesian maps showing increased β -cell connectivity 3-dimensionally under high circulating blood glucose.....	78
Figure 2.3.3.5 Link probability distribution of β -cells follows a power-law distribution.... Error! Bookmark not defined.	
Figure 2.3.3.6 Temporally defined leaders are identical to those with the most number of connections as independently identified using Granger Causality analysis.....	81
Figure 2.3.4.1 Pooled data for average R and percentage connectivity measurements in non-diabetic human islets (n =11 islets).	83
Figure 2.3.4.2 Pooled data for average R and percentage connectivity measurements in diabetic human islets (n =2 islets; from the same donor).	84
Figure 3.2.7.1 Representative image sequences of the three different types of islet calcium behaviour. ...	100
Figure 3.2.9.1. C57BL6 mice received syngeneic InsCre-GCaMP6m expressing islets into the anterior chamber of their eyes.....	103
Figure 3.3.1.1 cAMP assay showing the affinity of G778 to glucagon, GLP-1 and GIP receptors as well as their endogenous ligands.....	105
Figure 3.3.2.1 Animals (n=64) on HFD display an impaired glycaemic profile at two months before the start of treatment.	106
Figure 3.3.3.1 G778 treatment resulted in a modest weight loss.	107
Figure 3.3.3.2 Cumulative food consumption of G778 and control groups over the course of the study. ...	108
Figure 3.3.3.3 Metabolic profiling of G778 and control groups at two weeks suggested a tendency for improved glucose tolerance.	108
Figure 3.3.3.4 Metabolic testing of control and G778-treated groups (n=8-9) showed a significant improvement in the glucagon analogue-treated group.....	110
Figure 3.3.4.1 Wave score of islets over the course of the study.	110

Figure 3.3.4.2 Graphs showing changes in calcium wave parameters in response to HFD and subsequent G778 treatment.	112
Figure 3.3.4.3 The effects of HFD and glucagon analogue treatment on wave propagation speed.....	114
Figure 3.3.5.1 Cross sections of islets at each imaging session showing leader cells.	115
Figure 3.3.5.2 β -cell connectivity changes in from baseline to DIO and 6 weeks of chronic G778 treatment.	117
Figure 3.3.6.1 Representative calcium traces under glucose only and glucose+G778 conditions.....	118
Figure 3.3.6.2 Graphs showing differences in islet calcium activity parameters in the presence and absence of 60nmol G778.	120
Figure 3.4.3.1 Systemic versus paracrine actions of glucagon.	125
Figure 4.1.7.1 The angiogenic and immune modulatory actions of EGFR.	134
Figure 4.2.6.1 Example images created in Fiji software using the Tube Analyst macro.	138
Figure 4.3.2.1. Images of AV-GFP-pAdTrack-vector and SNAP-EGFR-virus infected islets at day 14 and day 28.	142
Figure 4.3.2.2. Islet volume changes in AV-GFP-pAdTrack (Empty) virus (n=3) and SNAP-EGFR-virus (n=14) expressing islets.....	143
Figure 4.3.2.3 Blood vessel volume changes two and four weeks after transplantation.	144
Figure 4.3.2.4 Blood vessel volume changes relative to islet size.	145
Figure 4.3.2.5 Vessel branch characteristics in control and EGFR treated islets.	147
Figure 4.3.2.6 EGFR overexpression upregulates angiogenesis-related and β -cell maturity-related gene expression.....	149
Figure 4.4.5.1 An alternative to using TexasRed-Dextran to report on blood vessel morphology.	161

1 Chapter: General Introduction

1.1 Diabetes

Diabetes mellitus (DM) is a chronic, progressive disease characterised by the gradual loss of pancreatic (insulin-secreting) β -cell function resulting in hyperglycaemia. DM is classified as type 1 or type 2 depending on the underlying pathophysiological processes, which are considerably different. Ultimately, hyperglycaemia is defined as a fasting plasma glucose concentration of ≥ 7 mmol/L or ≥ 11.1 mmol/L at 2 hours following 75g glucose challenge test (WHO Recommendations 2006). More recently, glycated haemoglobin (HbA1C) has been approved for the diagnosis as well as the monitoring of glycaemia. This test provides a measurement of the amount of red blood cell haemoglobin that is glycated – the higher the percentage, the higher the prevailing (average) blood glucose has been over the past three months (Goldstein et al. 2004). A level of ≥ 48 mmol/mol (6.5%) is accepted for a diagnosis of diabetes (American Diabetes Association 2010). Hyperglycaemia in the presence of other symptoms (polyuria, polydipsia or weight-loss) satisfies diagnostic criteria for diabetes mellitus (Diabetes UK).

1.1.1 Prevalence and disease burden

Diabetes is a growing global health concern of immense proportions. According to a 2019 estimate, there were 3.9 million people with diabetes in the UK, a figure that has doubled over the past 20 years (Diabetes UK 2020). A further million are estimated to have developed the disease without yet being formally diagnosed. The vast majority (90%) of cases are Type 2, which is closely associated with the growing number of people living with obesity. Type 1 diabetes on the other hand, accounts for 8% of cases; rarer types of diabetes, for example monogenic forms, contribute to the remaining 2%. Diabetes is one of the leading preventable causes of morbidity and mortality in the UK and globally. Treatment of diabetes complications cost 10% of the NHS budget in 2018 and people with diabetes are five times more likely to require kidney dialysis or transplantation than the general population (Diabetes UK 2018). Type 2 diabetes is strongly associated with an increased risk of heart disease and stroke, the leading causes of death in the UK. In the present climate, it has also been demonstrated that patients with diabetes are significantly more likely to succumb to severe corona virus disease 2019 (COVID-19) and die from the virus (Zhu et al.

2020). This may be due to an already compromised immune system (chronic hyperglycaemia) or the presence of macro- or microvascular complications of diabetes that promote viral disease severity (Fang et al. 2020).

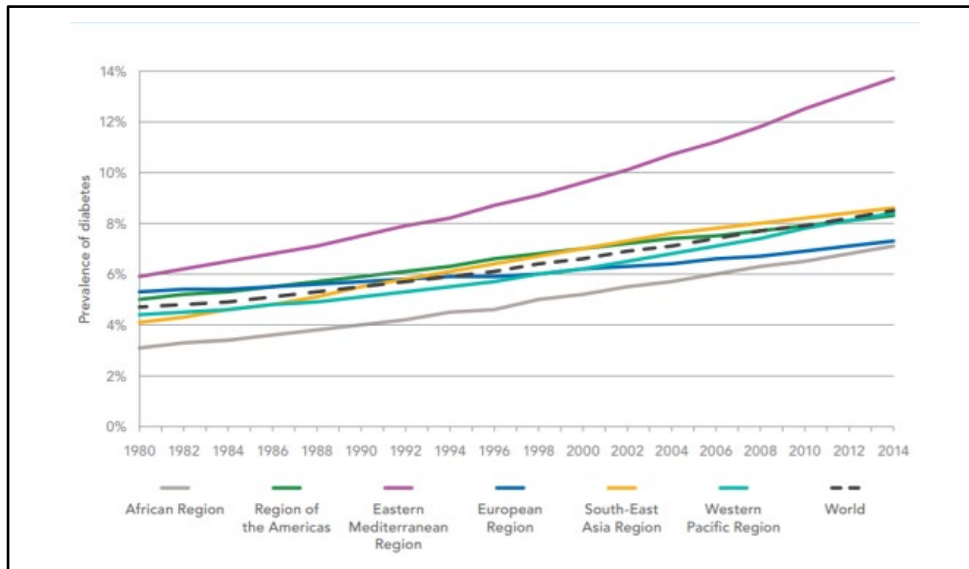


Figure 1.1.1.1 Changes in diabetes prevalence rates over between 1980 and 2014 by region.

Diagram adapted from WHO website.

Further to health costs, diabetes carries additional socio-economic costs, particularly those incurred due to reduced work efficiency or absenteeism. While this is a relatively under-researched area, the indirect costs of diabetes have been found to be higher than direct ones and it was estimated that in 2012 the cost of reduced productivity amounted to a staggering £9 billion. Approximately 37,000 and 288,000 working days were lost due to type 1 and type 2 diabetes respectively in 2010/11 in the UK alone (Hex et al. 2012).

1.1.2 Type 1 Diabetes

According to 2014 estimates, 387 million people were afflicted with diabetes world-wide, of which 5 to 10% suffered from type 1 diabetes mellitus (T1DM). The incidence of T1DM is increasing globally which many believe is the consequence of unprecedented environmental pressures present in our every-day lives (Gale 2002). T1DM is classically considered to be an autoimmune disease in which genetically susceptible individuals exposed to a number of environmental triggers develop an immune response specifically targeting pancreatic β -cells. In support of this, autoantibodies against β -cell specific antigens are present years before the onset of symptoms, suggesting an ongoing autoimmune attack.

At the start of the autoimmune response, dendritic cells and macrophages invade the pancreatic parenchyma and later present several β -cell specific antigens via the major histocompatibility complex (MHC class I) to naïve CD4+ T-cells (Gan et al. 2012; DiMeglio et al. 2018). The subsequent activation of cytotoxic CD8+ T-cells results in the induction of apoptotic pathways and mass β -cell destruction. Despite extensive β -cell destruction, glycaemia is maintained within a normal range initially by a pool of functional β -cells. Over time, the majority of β -cells become depleted and glycaemia gradually increases until overt diabetes develops (Zaccardi et al. 2016).

Complications of Type 1 Diabetes

Long-term microvascular complications in T1DM are a major cause of morbidity. For instance, diabetic retinopathy is the leading cause of blindness in the UK adult population. Vision is lost in the most advanced stages of proliferative diabetic retinopathy where the growth of new blood vessels surrounding the vitreous body posteriorly causes macular oedema and retinal hypoperfusion (Fong et al. 2004). Other serious microvascular complications include nephropathy which results first in protein leak from the nephrons, through to progressive loss of renal function, such that diabetes is also the leading cause of renal replacement therapy in the UK (Gross et al. 2005). The small blood vessels of nerves, the vasa nervorum, are also particularly prone to hyperglycaemic damage and this can cause a sensory neuropathy. If this occurs in the feet, alongside vascular damage, ulceration can occur (Juster-Switlyk and Smith 2016).

1.1.3 Treatments for Type 1 Diabetes

Since T1DM is the result of insulinopenia (loss of pancreatic β -cell mass), the central pillar of treatment is the use of exogenous insulin together with dietary management. Additionally, the importance of patient education on the carbohydrate-load of different food choices and desired glycaemic values is encouraged for best managing T1DM diabetes (NICE guidelines 2016). This encourages patients to self-administer doses of insulin that match their body's requirements. The Diabetes Control and Complications Trial (DCCT) compared a twice daily regime with more intensive, rigorous insulin interventions where multiple insulin injections and frequent glycaemic monitoring were encouraged. In the intensive therapy arm of the trial, the prevalence of microvascular complications was reduced, while the rate of severe

hypoglycaemic events did not increase substantially, causing a paradigm shift in the approach to T1DM management (Nathan et al. 1993). Exogenous insulin may be delivered via insulin pens or insulin pumps.

Typically, patients with T1DM are treated with a “basal bolus” regime: a long-acting insulin analogue is injected at night, which provides a constant background dose thereby removing the risk of slipping into diabetic ketoacidosis. Then, a short-acting insulin analogue is injected with meals – three times a day – at a dose calculated by the patient to match the carbohydrate-load being ingested. Modern insulin pump systems have been designed to remove the need for regular metered injections. They are placed subcutaneously and deliver a constant background infusion of insulin and can be programmed to deliver a bolus of insulin at mealtimes. Newer generation insulin pumps have the added benefit of continuous monitoring of glycaemia; closed loop insulin pumps deliver a pulse of insulin in accordance with the measured trend in glycaemic value (Hovorka et al. 2014), and some use Artificial Intelligence (AI) programmes to alter doses according to knowledge about other factors which may alter insulin dose responsivity e.g. recent exercise. While insulin pumps have been declared safe, a small proportion of patients develop "brittle" diabetes in which their glycaemia proves difficult to control (Plotnick et al. 2003; Gill et al. 1996). Patients with recurrent severe hypoglycaemic episodes are at risk of developing impaired hypoglycaemia awareness (IAH). In IAH patients, the glycaemic set-point for hypoglycaemia awareness is lowered to dangerously low values at which point tissue damage is likely to be already occurring. For this subset of patients, whole-organ pancreas transplantation offers an alternative and has been shown to reduce hypoglycaemic events and the rate of T1DM-related complications (Redfield et al. 2016). However, for the vast majority of patients with T1DM, pancreatic or islet transplantation has not been an effective treatment option (this is discussed in further detail in Chapter 4). In brief, the lack of organ donors and, crucially, the lack of long-term graft function limit this as a treatment. Newer approaches to replace β -cell mass, for example using stem cell technologies, remain in their infancy (Aguayo-Mazzucato and Bonner Weir 2010).

1.1.4 Type 2 diabetes mellitus

Type 2 diabetes mellitus (T2DM) is a chronic metabolic disorder characterised by the relative lack of insulin secretion on a background of insulin resistance. Obesity is a major risk

factor for developing T2DM. Clinically, obesity is defined as having a body mass index (BMI) of $\geq 30 \text{ kg/m}^2$ (WHO 2020). Besides weight gain, the specific centripetal accumulation of excess adipose tissue has been associated with an increased risk for cardiovascular disease, insulin resistance and T2DM (Cnop et al. 2002; Purnell 2003). While it is evident that both β -cell dysfunction and insulin resistance are present in T2DM, the relative contribution of each of these factors is less well understood and indeed, may vary across patient subgroups (Ahlqvist et al. 2018).

Insulin resistance

In obesity, non-esterified fatty acids (NEFA) are released from the excess adipose tissues. Increased plasma fatty acids have been shown to reduce glucose transport activity by directly interfering with upstream insulin signalling (Shulman 2000). Increased NEFA accumulation in cells can halt intracellular lipid metabolism and increase the content of fatty acid metabolites diacylglycerol (DAG), fatty acyl-coenzyme A (fatty acyl-CoA) and ceramide, which in turn phosphorylates serine/threonine residues on insulin receptor substrates 1 and 2 (IRS1 and IRS2). Through this pathway, NEFAs prevent IRS 1 and 2 from interacting with phosphatidylinositol-3-OH kinase (PI3K), rendering the cell insulin resistant (Kahn et al. 2006). Similarly, adipocyte derived retinol-binding protein 4 (RBP4) is elevated in obesity states and contributes to insulin resistance by reducing PI3K activity in the liver and enhancing the expression of gluconeogenic enzymes (Yang et al. 2005). An intriguing observation was that the pattern of fat distribution is a critical determinant of the extent of insulin resistance. On average, visceral and retroperitoneal fat cells are smaller and are more responsive to lipolytic actions of catecholamines than adipocytes in the subcutaneous compartment (Mårin et al. 1996). Thus, fat cells vary in their metabolic phenotype and contribution to insulin resistance according to their site.

β -cell dysfunction

Insulin resistant patients have established metabolic abnormalities well before frank T2DM occurs. In the pre-diabetic period, enhanced glucose stimulated insulin secretion and basal hyperinsulinaemia (in response to peripheral insulin resistance) has been well-documented. This finding is supported by an increase in islet size and insulin content in animal models of obesity-induced diabetes (Halban et al. 2014). The increased insulin secretory demand

posed on the endoplasmic reticulum (ER) causes cellular stress in β -cells until they eventually fail to produce and secrete adequate amounts of insulin. The toxic combination of chronic oxidative stress and induction of inflammatory pathways by hyperglycaemia and insulin resistance further exacerbates β -cell exhaustion and apoptosis (Donath et al. 2005; Cernea and Dobreanu 2013). Besides β -cell death, dedifferentiation may be another process by which loss of β -cell mass occurs. During dedifferentiation, cells lose their acquired specialised functions to regress into a progenitor cell-like state. In β -cells, this mechanism has been reported to involve the down-regulation of β -cell-enriched genes. Transcription factors which have been termed as master regulators of β -cell identity show a reduction in expression levels and binding in models of T2DM (Bensellam et al. 2018; Scheen et al. 2003).

There is a strong case for the existence of a degree of β -cell dysfunction years before the onset of diabetes symptoms. First degree relatives (FDR) of patients with diabetes show deranged insulin secretion and evidence for insulin resistance, despite their normal oral glucose tolerance test results. (Eriksson et al. 1989). Over the course of a 48-hour hyperglycaemic clamp experiment, FDRs of patients with diabetes showed evidence for shorter insulin secretion rates with reduced amplitude. As a result, the periodicity of normal diurnal insulin secretion is disrupted in FDRs and compensatory insulin secretion in response to sustained hyperglycaemia fails beyond 18 hours of hyperglycaemic clamping (Boden and Polansky 1999). Findings of the United Kingdom Prospective Diabetes Study (UKPDS) in 1999 suggested the presence of β -cell impairment 10 years prior to hyperglycaemia becoming evident (King et al. 1999; Turner and Holman 1995).

Complications of T2DM

Over 50% of patients with T2DM already have some element of microvascular disease (retinopathy) at the point of diagnosis. However, since this disease commonly presents in middle to older age, and is strongly associated with other manifestations of the metabolic syndrome (hyperlipidaemia and hypertension), by far the commonest cause of morbidity and mortality in T2DM is cardiovascular disease (Leon and 2015). Obesity is a major risk factor for T2DM, and independently also promotes atherogenesis. Meanwhile, hyperinsulinaemia also promotes atherogenesis as it increases collagen production and smooth muscle cell proliferation in vessels (DeFronzo 2010; Isomaa et al. 2001).

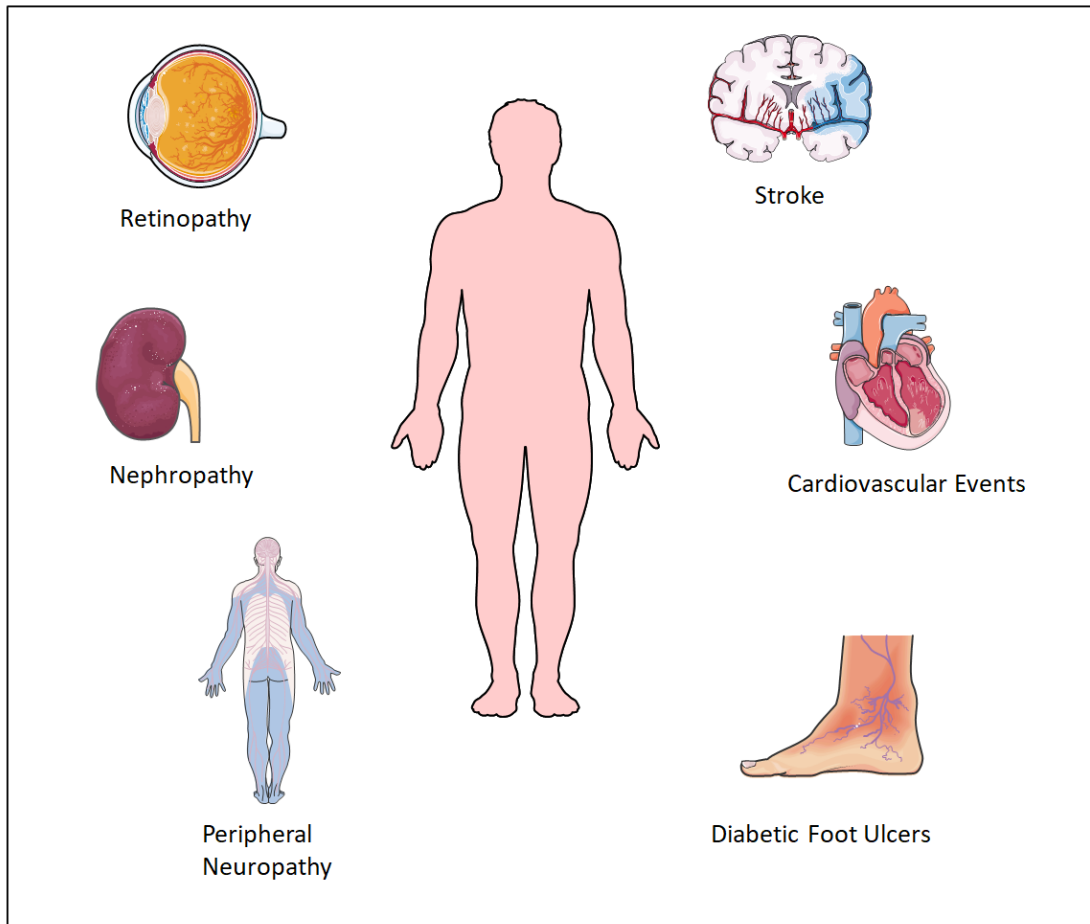


Figure 1.1.4.1. Schematic diagram of diabetes-related micro-and macrovascular complications.

1.1.5 Current T2DM Treatments

Lifestyle intervention

Aerobic exercise has been shown to effectively improve insulin sensitivity and lipid profiles of patients as well as increasing their cardiovascular fitness. Additionally, as diabetes is associated with an increased loss of muscle strength and function, resistance (strength) training can also prove beneficial (Colberg et al. 2016). Indeed, a meta-analysis investigating exercise intervention in T2DM patients found a modest added benefit when aerobic and resistance training was combined (Snowling and Hopkins 2006). The 2002 Diabetes Prevention Program (DPP), with over 3000 participants, investigated whether exercise as an intervention could prevent or delay the onset of diabetes in individuals with impaired glucose tolerance. Participants of the study were enrolled to follow standard lifestyle recommendations and receive either the diabetes medication metformin or placebo, or alternatively, to follow an intensive regime of lifestyle modifications. Interestingly, the incidence rate of diabetes was decreased by 58% in the rigorous lifestyle intervention group

versus 31% with metformin. Importantly, beneficial effects were similar regardless of sex or ethnicity of participants (DPP Research Group 2002). Following on from the DPP study, the Look AHEAD study investigated the positive effects of lifestyle changes in patients who had already developed T2DM (Look AHEAD Research Group 2006). Although the differences in cardiovascular risk factors were non-significant between groups, increased physical activity and diet positively impacted on the lipid profile, blood pressure and renal health of participants. Despite the evidence supporting lifestyle modification being a successful intervention, its potential with real-life patients is hampered by the growing tendency towards sedentary lifestyles. According to the WHO, globally, 31% of adults were insufficiently active in 2008, contributing to 3.2million deaths each year (WHO 2010). More recently work by Roy Taylor and Michael Lean for the UK DiRECT study has shown that strict caloric restriction in patients with established T2DM can have a profound effect on glycaemia. In their study of almost 300 patients with T2DM randomised to 3 months of a very low calorie diet (~850kcal/day via meal replacements, followed by a graded re-introduction of dietician-led healthy eating), compared with routine diabetes care, 36% of the intervention arm were in full remission from their diabetes (i.e. normoglycaemic and requiring no medications) at 2 years (Lean et al. 2018). This has led to a major change in practice at the primary care level in the UK (NHS Diabetes Prevention Programme 2016). However, there remain grave doubts as to whether such harsh lifestyle interventions are sustainable in the long-term.

Metformin

Metformin is currently the first-line treatment for people diagnosed with T2DM (NICE Guidelines 2016). The glucose lowering effects of metformin have been recognised since the 1950s and it has become established as a safe and effective treatment option, even in gestational diabetes (Rena et al. 2017; Lindsay and Loeken 2017). In the UKPDS study, patients in the metformin-arm showed 32% reduction in primary outcomes as well as 42% in diabetes-related deaths, supporting its use as first-line medication. The mechanism of action of metformin is not fully understood. As metformin is a positive charge carrier, its accumulation inside mitochondria is driven by the mitochondrial membrane potential ($\Delta\psi$) where it inhibits complex I of the electron transport chain (Owen et al. 2000).

Consequentially, the $\text{NAD}^+:\text{NADH}$ ratio and oxygen consumption rate of cells decreases, leading to a drop in the proton mediated synthesis of ATP (Viollet et al. 2012). Inhibition of mitochondrial function creates a cellular energy imbalance that is sensed by AMP-activated protein kinase (AMPK). Liver kinase B1 (LKB1) is an interacting partner of AMPK and plays a pivotal role in mediating the effects of metformin on hepatic glucose production (Shaw et al. 2005). Together, AMPK and LKB1 phosphorylate CREB-regulated transcription coactivator 2 (CRTC2), thereby preventing it from entering the nucleus. During hypoglycaemic states, CRTC2 translocates to the nucleus where it binds cAMP response element binding protein (CREB), which upregulates the expression of peroxisome proliferator-activated receptor- γ coactivator 1 α (PGC-1 α) in hepatocytes. In turn, PPAR-1 α drives the expression of gluconeogenic genes, phosphoenolpyruvate carboxykinase (PEPCK) and glucose-6-phosphatase (G6P), with the ultimate aim to raise blood sugar levels (Le Lay et al. 2009). By inhibiting the gene expression of gluconeogenic enzymes, metformin effectively reduces hepatic glucose production which has been implicated as a contributing factor in diabetes progression (Rines et al. 2016).

In addition, results of a randomized clinical trial on patients with diabetes suggest that metformin has other advantageous extrahepatic effects. Using fluorodeoxyglucose (FDG) tracers and positron emission tomography (PET) imaging modality, it was demonstrated that 26-week metformin treatment increases glucose uptake from the gut (Koffert et al. 2017). Animal studies suggest that the increased uptake was paralleled by an increase in AMPK phosphorylation (Duca et al. 2015). Furthermore, chronic metformin administration increased GLP-1 secretion which is putatively mediated by vagal afferents of the gut (Maida et al. 2011).

Sulfonylureas

Sulfonylureas potentiate insulin secretion by their direct action on β -cells. Sulfonylureas act to close ATP-sensitive K^+ channels (K_{ATP} -channel) (Rendell 2004). K_{ATP} -channels are formed by two distinct subunits, an inwardly rectifying K^+ channel (Kir6.x) and a sulfonylurea binding site (SUR), which form an octameric channel pore. In β -cells, K_{ATP} -channels are formed from the combination of Kir6.2 and SUR1 (Tarasov et al. 2004). Sulfonylureas act by inhibiting K_{ATP} -channels at two distinct sites with differing affinities; a low-affinity binding site is

provided by Kir6.2 while sulfonylureas bind the SUR1 subunit with high affinity (Proks et al. 2002). The inhibition of K⁺ influx results in the depolarization of the cell and thus amplification of insulin secretion (Sola et al. 2015; Tarasov et al. 2004). Channel blockade by sulfonylureas is never complete, the maximum achievable inhibition ranges between 60 to 80%. Since sulphonylureas continue to promote insulin secretion independently of prevailing circulating glucose levels, the major side effect associated with this class of drug is hypoglycaemia which, if severe or recurrent, can obfuscate the health benefits of tight glucose control (Roumie et al. 2012).

The progressive loss of functional β -cell mass in T2DM also means that the efficacy of sulfonylureas wanes over time. The effects of sulfonylureas, exogenous insulin and metformin on insulin secretory capacity were cross-compared in the UKPDS study. It was found that β -cell failure occurred in all three treatment groups and that there was no discernible difference in the rate of progression (Turner et al. 1999). In patients where secondary failure of β -cells sets in, the addition of long-acting exogenous insulin analogues to the treatment regimen provided adequate blood glucose control (Chow et al 1995). However, the added benefit of sulfonylureas in combination with insulin therapy was only seen in patients with a remaining functional β -cell reserve (Rendell 2004).

Thiazolidinediones

Peroxisome proliferator-activated receptors (PPAR) are a group of nuclear receptors which regulate the transcription of many genes related to adipogenesis, lipid metabolism and inflammation. Various dietary lipids and lipid metabolites bind PPARs, inducing a conformational change and recruitment of other co-factors. Of interest, PPAR γ is expressed in high levels in white and brown adipose tissues (WAT and BAT, respectively) to regulate lipid metabolism and insulin sensitivity (Saltiel and Olefsky 1996; Ahmadian et al. 2013). Generating PPAR γ null mice resulted in the absolute lack of adipose tissue in model animals, underscoring the significance of PPAR γ signalling in adipocyte differentiation (Barak et al. 1999). Thiazolidinediones (TZD) are synthetic, high-affinity PPAR γ -selective agonists which have been developed to improve insulin sensitivity. Fibroblast growth factors 1 and 21 (FGF1 and FGF21) have been identified as paracrine activators of PPAR γ in adipocytes. TZDs are reported to stimulate FGF21 release from WAT adipocytes, which ultimately leads to

increased adipogenesis in these cells (Sun and Scherer 2012; Dutchak et al. 2012). Unsurprisingly, TZD intake has been consistently linked to increased fat mass in both mice and humans (Picard and Auwerx 2002). High circulating free fatty acid (FFA) levels have been linked to insulin resistance therefore, the ability of TZDs to increase FFA uptake and adipogenic capacity of fat cells contributes to their insulin sensitizing yet weight gain effects. Interestingly, the anti-diabetic effects of TZDs may also be partially explained by their ability to re-distribute fat deposits from the peritoneal cavity to the subcutaneous compartments (Mori et al. 1999). Finally, the insulin-sensitizing effects of TZDs in lipodystrophic (whereby both WAT and BAT have been eliminated) animals suggests that TZDs ameliorate insulin resistance through other mechanisms (Burant et al. 1997). Indeed, similar to adipose tissue, TZDs improve insulin sensitivity in both skeletal muscle and liver in a PPAR γ -mediated manner (Hevener et al. 2007). Furthermore, TZDs inhibit the glucose uptake inhibitory actions of tissue necrosis factor α (TNF- α) in fat cells thus providing a clue for the existence of other PPAR γ -independent pathways (Hauner 2002).

Unfortunately troglitazone, a first generation TZD, was removed from the market due to serious liver toxicity. Safety concerns regarding the use of newer generation TZDs remain; rosiglitazone has been implicated in causing salt and water retention thus predisposing patients to congestive heart failure (Nesto et al. 2004). It has also been associated with an increased risk of bladder malignancy and osteoporosis. At present, only pioglitazone is used relatively widely as an insulin sensitising drug. Its better safety profile against other drugs in this class may be related to the fact that it also has PPAR- α agonist effects which promote additional triglyceride lowering benefits.

SGLT2 inhibitors

The latest generation of anti-diabetic medicines include the sodium glucose cotransporter (SGLT) 2 inhibitors, whose main site of action are the kidneys. Reabsorption of glucose from the glomerular filtrate occurs through SGLT 2, which are located at the luminal side of the proximal renal convoluted tubules. For every Na⁺ ion, one molecule of glucose is transported across to the basolateral membrane, where glucose transporters (GLUT) release glucose back into the circulation. Glucose reabsorption is an ATP-dependent process as glucose is transported across against a concentration gradient (Ferrannini and Solini 2012).

With increasing plasma glucose concentrations, the reabsorption of filtered glucose is also elevated until the maximum re-absorptive capacity is exceeded – therefore, patients with hyperglycaemia exhibit glycosuria. This is often referred to as the renal threshold and equates to a filtration rate of 260-350mg/min per 1.73 m² which occurs at 11mmol/L in humans. Above this threshold the fraction of glucose that is reabsorbed decreases while excretion of glucose in the urine increases, leading to glycosuria.

SGLT 2 inhibitors therefore block the renal resorption of filtered glucose in patients with T2DM. Excess glucose is effectively lost in the urine. Newly developed SGLT 2 inhibitors have been shown to increase glucose excretion in proportion to the GFR and plasma glucose concentrations (Ferrannini et al. 2013). Besides increasing glucose excretion, SGLT 2 inhibitors confer additional benefits to diabetic patients. Sodium accumulation in tissues has been positively correlated with cardiovascular risk. SGLT 2 inhibitors have been shown to reduce sodium concentrations in the skin of T2DM patients (Karg et al. 2018). Together with the osmotic diuretic effects to increase urine volume, SGLT 2 inhibitors have been shown to be advantageous in patients with hypertension (Ansary et al. 2019).

Recently, clinical trials have confirmed that SGLT 2 inhibitors improve cardiovascular outcomes in patients with T2DM, greater than expected for their relatively modest effect lowering HbA1c. This class of drugs typically confer a reduction of HbA1C of 0.5 to 0.7%. However they are associated with over 30% reduction in cardiovascular events and more recently have been shown to reduce the progression of diabetic nephropathy (Abdul-Ghani et al. 2016; Perkovic et al. 2019). Furthermore, early fears that the glycosuria incurred with this class of drug might increase the risk of serious urinary tract infection have not been borne out in meta-analysis (Liu et al. 2017). They are therefore fast becoming popular second line choices (after metformin) to treat patients with T2DM.

Incretin-based therapies

Pioneering work by Stephen Bloom and colleagues on characterising the physiology of gut hormones led to a surge of interest in their use in the pharmacotherapy of diabetes and obesity (Kreymann et al. 1989; Turton et al. 1996; Batterham et al. 2002). Following their discovery, the incretin properties of glucagon like peptide-1 (GLP-1) merited intense research attention. GLP -1 is one of the products of the proglucagon gene which also gives

rise to glicentin, glicentin-related pancreatic polypeptide, glucagon, oxyntomodulin and a proglucagon fragment (Müller et al. 2019). These peptides are primarily secreted as protein precursors and are subsequently processed by prohormone convertase enzymes in a tissue-specific manner. The proglucagon gene is widely expressed in enteroendocrine L-cells, pancreatic α -cells as well as in the brainstem. Proglucagon gene products are major players of energy homeostasis with wide-ranging functions; they potentiate glucose stimulated insulin secretion (GLP-1), induce thermogenesis (glucagon), have anorectic effects (GLP-1, oxyntomodulin) influence gastric emptying (GLP-1, GLP-2, glucagon) and others (Holst 2007). In addition, glucagon is considered to be a major counter-regulatory hormone in glucose metabolism, stimulating gluconeogenesis and glycogenolysis as well as the breakdown of aminoacids (for more details see Chapter 3; Habegger et al. 2010).

Endogenous GLP-1 has a half-life of just 2 minutes and is rapidly processed by plasma dipeptidyl peptidase-4 (DPP-4). One strategy to exploit the endogenous incretin system is based on the inhibition of DPP-4. Sitagliptin, a DPP-4 inhibitor, was developed and approved for use by the Federal Drug Administration (FDA) in 2006. This class of drugs are very well-tolerated and remain an important choice of drugs for diabetes. They effectively reduce HbA1c (by about 0.7 to 1.0 %) and are weight neutral (unlike sulphonylureas, which promote weight gain). They are particularly favoured for patients with advanced kidney disease, due to their low risk of hypoglycaemia. However, unlike the SGLT 2 inhibitors, there is no evidence that they reduce cardiovascular endpoints against placebo (Rosenstock et al. 2019).

The extraction of exendin, the first naturally available DPP-4 resistant GLP-1R agonist, inspired the development of synthetic GLP-1 analogues as treatments for T2DM. These agents had significantly longer half-lives due to their resistance to degradation and a proven efficacy at improving glycaemia (Raskin and Mora 2010). A combination of metformin and liraglutide, a synthetic GLP-1R agonist, proved to be better at normalizing blood glucose than metformin with sulphonylureas (Pratley et al. 2010). Due to the satiating effects of GLP-1 in the central nervous system (CNS), patients also experience a modest weight-loss however this tends to plateau over time (Mehta et al. 2017). Furthermore, liraglutide confers cardioprotective benefits in patients with diabetes (Marso et al. 2016). The weight-loss benefit of this class of drugs has been extended with longer-acting preparations. Daily

subcutaneous injections of liraglutide at high dose, if tolerated, produces 5-10kg weight-loss in clinic and has received FDA approval for the use in obesity in the absence of diabetes (Marso et al. 2016).

The acute incretin effects of GLP-1 involve a rise of intracellular cyclic AMP (cAMP) in target β -cells. The rise in cAMP leads to the activation of protein kinase A (PKA) which phosphorylates L-type voltage dependent Ca^{2+} channels, ultimately leading to depolarization and insulin secretion. Simultaneously, cAMP also activates Epac which has been associated with the priming and docking of insulin secretory vesicles (Müller et al. 2019). Since the incretin effect can only occur in the presence of glucose, these drugs do not cause hypoglycaemia. While they are effective, like other agents discussed above, they require the presence of a functional β -cell reservoir. At the cellular level, GLP-1R agonism has been associated with β -cell protective effects and inhibition of glucagon secretion, both of which are desirable outcomes in the context of diabetes. As side-effects, nausea and other digestive problems are especially discomforting for patients and they significantly limit the use of increased doses of GLP-1 analogues (Filippatos et al. 2014).

The latest additions to the anti-diabetic arsenal are single molecules with combined actions at multiple gut hormone receptors to provide a multipronged strategy targeting β -cell function and energy homeostasis. Recently, the beneficial effects of oxyntomodulin inspired the generation of GLP-1/glucagon receptor co-agonists. Oxyntomodulin is a proglucagon gene product that has affinity for both GLP-1 and glucagon receptors. In both mice and men, it was demonstrated to have weight-lowering effects while positively impacting on insulin secretion (Dakin et al. 2001; Wynne et al. 2005). The glucagonergic agonism is a likely contributing factor to weight-loss effects, as it was recently demonstrated to elevate energy expenditure in both rodents and humans (Salem et al. 2016). GLP-1/glucagon receptor co-agonists show superior weight-loss effects, improved lipid metabolism and glucose homeostasis in both humans and non-human primates. Importantly, GLP-1/glucagon receptor co-agonism affected both subcutaneous and visceral fat compartments to reduce bodyweight (Henderson et al. 2016). Therefore, the combined targeting of anorectic, energy expenditure and insulin secretory pathways holds a promising future in the development of anti-diabetes medications.

Bariatric surgery

Presently available pharmacotherapy options are able to control glycaemia and reduce the risk of developing diabetic complications but fail to restore β -cell functional capacity. The only intervention with established, long-term curative potential is bariatric surgery. An unexpected outcome of bariatric surgery to treat obesity was the observation that it induced diabetes remission (Pories et al. 1995). While it was initially thought that anti-diabetic effects are a corollary of weight-loss and improved insulin sensitivity, emerging evidence suggests otherwise. It is becoming increasingly recognised that bariatric surgery has direct effects on the β -cell. Evidence to support this notion rests on the observation that diabetes remission occurs days after surgery and before any significant weight-loss is achieved (Rubino et al. 2010). These striking results have been related to increased postprandial secretions of gut-derived GLP-1 (Larraufie et al. 2019). Additionally, circulating bile acids have been reported to increase post-surgery and are implicated in mediating some of the glucose-lowering effects (Albaugh et al. 2017).

A major issue with bariatric surgery is the invasiveness of the procedure. Peri-operative morbidity is more common among obese patients. In particular, an increased postoperative rate of myocardial infarction, wound infection and nerve injury has been reported (Bamgbade et al. 2007).

There remains much work to be done in achieving the goal of pharmacological reversal of β -cell dysfunction and a cure for diabetes. Many people believe that the key to this is a better understanding of β -cell biology and its role in the pathophysiology of diabetes.

1.2 Islet Biology from the Macroscopic to the Microscopic

1.2.1 Tissue Architecture

Macroscopic Anatomy

The pancreas is a complex organ with a multitude of exocrine and endocrine secretory functions. Exocrine secretions are performed by ductal acinar cells. In most species, including humans, the pancreas is a distinct organ with clear anatomical boundaries (Case 2006). In mice, on the other hand, the pancreas is a rather diffuse organ with no clear demarcation (Dolenšek et al. 2015). The human pancreas can be subdivided into three

major parts; the head, body and the tail. Similarly, three anatomical regions can be distinguished in mice, duodenal, splenic and gastric lobes. The human pancreas is encased in a fibrous capsule and is divided into distinct lobes and lobules (smaller subunits of lobes) by the surrounding connective tissue. Exocrine secretions from pancreatic acini are drained into intralobular (i.e. running within lobules) ducts which converge to form interlobular ducts (i.e. running between lobules) and terminate in the main pancreatic duct (Case 2006). The pancreatic duct enters the duodenum, running parallel to the common bile duct in humans. In response to a nutrient load, acinar cells of the exocrine pancreas secrete α -amylase, lipase and protease to participate in the breakdown of carbohydrates, fats and proteins, respectively. Exocrine secretions are under neuronal regulation with cholecystokinin, acetylcholine, vasoactive intestinal peptide and secretin being the main neurotransmitters to stimulate enzyme secretions (Leung and Ip 2006). Contrastingly, mouse exocrine secretions are drained into interlobular and pancreatic ducts which join the common bile duct before reaching the duodenum.

The venous drainage of the organ occurs into the hepatic portal vein in both rodents and humans (Mahadevan 2019). Species differences concern the localization and vessel network of pancreatic islets. In humans, islets of Langerhans are mostly interspersed within the lobules where they are each supported by their own insulo-acinar portal networks which drain into intralobular capillaries. In mice, on the other hand, islets are frequently found mainly interlobularly where their secretions enter the veins directly (Murakami et al. 1993).

Together, the duodenum and the head of the pancreas are supplied by the pancreaticoduodenal arcades which are anastomoses between the superior mesenteric and coeliac arteries. The body and tail of the pancreas are supplied by the splenic artery.

Microscopic Anatomy

Embedded in the pancreatic parenchyma, endocrine cells cluster together to form a single functional unit, called the islet of Langerhans. These micro-organs make up 1-4% of the pancreatic tissue yet receive 8-10% of pancreatic blood supply (Jansson et al 2016). There is a considerable variation in the organisation of islets across different species. Heterogeneity in tissue architecture putatively arises from differences in developmental processes,

metabolic requirements and physiological conditions (Steiner et al 2010). Within species as well as within individual variations also exist.

The five major endocrine cell types found in most islets are insulin-secreting β -cells (60-80% of cells in rodent islets), glucagon-secreting α -cells (15-20% of cells in rodent islets), somatostatin-secreting δ -cells (<10% of cells in rodent islets), ghrelin-secreting ϵ -cells (<1% of cells in rodent islets) and pancreatic polypeptide cells (PP-cells; <1% of cells in rodent islets). Rodent islets have a well-defined core and mantle structure where β -cells reside at the centre and are surrounded by α -cells at the perimeter. In humans, δ -cells represent 10% of the islet cells while β - and α -cells make up ~50% and ~40% of endocrine cells, respectively, thus human islets display a higher α to β -cell ratio than mouse islets (Dolenšek et al. 2015).

Challenging the notion that human islets are randomly intermingled, Bosco and colleagues recently reported that human islets are folded into a trilaminar plate where one layer of β -cells is pressed in between two layers of α -cells (Bosco et al. 2010). Interestingly, endothelial-specific CD34 labelling has revealed that the vast majority of endocrine cells in direct contact with blood vessels were α -cells, with only a select number of β -cells interspersed among them having direct access to the blood stream. Surprisingly, some of the β -cells that are located more distant to blood vessels displayed cytoplasmic extensions reaching between α -cells to make contact with endothelial cells (Bosco et al. 2010).

Together, these observations suggest that in human islets there is a greater number of heterotypic endocrine cell contacts (between α - and β -cells in particular) than there are in mouse islets (Brissova et al. 2005; Bosco et al. 2010).

Regional differences across the organ of the pancreas in terms of both the density and the make-up of islets exist. For example, Wang and colleagues reported a greater islet density in the tail region of the human pancreas compared to the head and neck regions (Wang et al. 2013). The endocrine cell-type composition of islets also varies in mice and humans; the head of the pancreas containing PP-cell rich and α -cell poor islets while in the neck and tail region, islets have a greater number of α -cells and lower number of PP-cells (Baetens et al. 1979; Yukawa et al. 1999 and Brissova et al. 2005). Interestingly, in T2DM there is a preferential loss of β -cells observed in the head region of human pancreata.

A comparative study of islets from several different species reported the size of human islets to be $50 \pm 29 \mu\text{m}$ versus $116 \pm 80 \mu\text{m}$ for mouse islets (Kim et al. 2009). However, it is important to mention that considerable heterogeneity exists even within the same individual and that, due to islet plasticity, islet size can be dynamically adjusted to meet the physiological demand of the organism (Ernst et al. 2011). Some islets have been found to be a collection of only about 10 cells, mostly β -cells, while others contained up to 1000 cells.

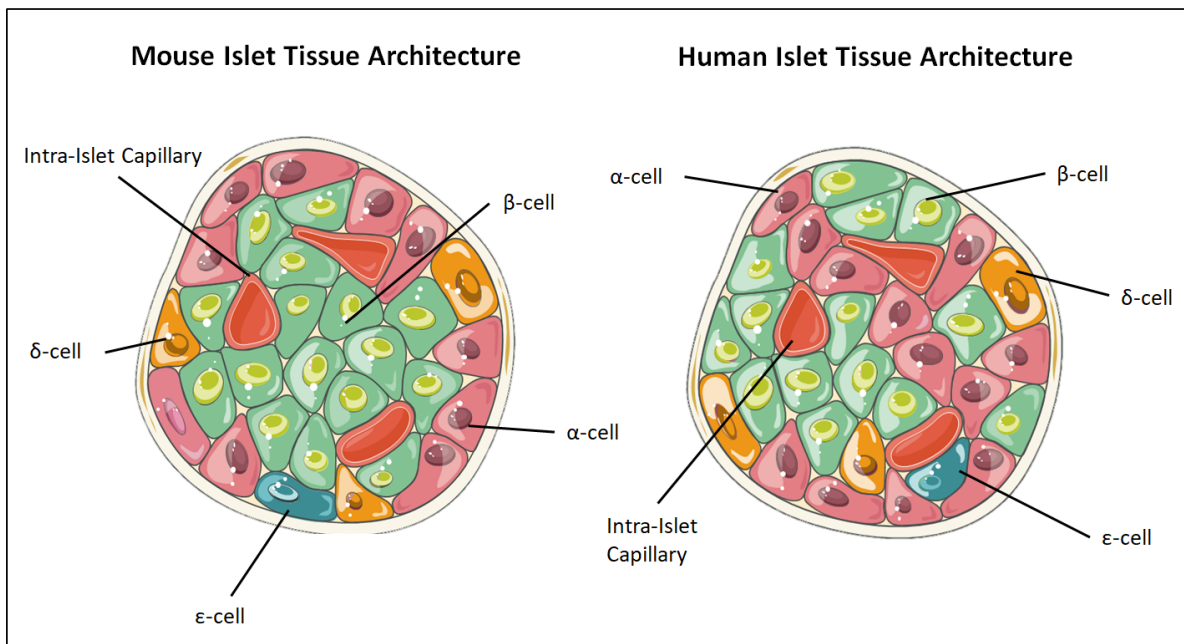


Figure 1.2.1.1 Architecture of mouse and human islets.

Mouse islets are characterised by a β -cell core and α -cell mantle while human islets fold into trilaminar plates, with more α - and β -cell intermingling. In addition to α -, β -, γ -, and ϵ -cells PP cells (<1%) are also found in both mouse and human pancreas.

Islet Paracrinology

Endocrine secretions from the pancreatic islet are the net result of the dynamic cross-talk between different types of endocrine cells. Somatostatin secreting δ -cells for example, inhibit the secretions of both α - and β -cells (Hauge-Evans et al. 2009). Interestingly, δ -cells were found to be activated during high circulating glucose levels and putatively play a role in terminating the insulin secretory response to prevent an insulin overshoot (Rodriguez-Diaz et al. 2019). Insulin released from β -cells has also been implicated as an autocrine factor influencing β -cell function. While it was shown that β -cells express insulin receptors, findings in the literature are inconsistent as to whether autocrine insulin signalling is

stimulatory or inhibitory in nature (Braun et al. 2012; Ammon et al. 1991; Aspinwall et al. 2000). Both human and mouse β -cells abundantly express GLP-1 and glucagon receptors (Huypens et al. 2000; Tornehave et al. 2008). GLP-1 receptor signalling in β -cells has previously been implicated in mediating the incretin effects of GLP-1 in a cAMP-dependent manner (Bateau 2008). More recently, glucagon receptor signalling in the β -cell was suggested to play a role in setting the glycaemic set-point in both mouse and human.

According to the model described by Rodriguez-Diaz and colleagues, a dynamic paracrine crosstalk exists between α - and β -cells to secrete the appropriate amount of insulin required to maintain normoglycaemia (Rodriguez-Diaz et al. 2018). Even more recent evidence has suggested that the paracrine effects of intra-islet glucagon are diminished in T2DM (Omar-Hmeadi et al. 2020).

1.2.2 Vasculature

Morphology of Islet Vasculature

Significant differences exist between mouse and human islets; human islets have been demonstrated to have smaller diameter islet capillaries and a relatively shorter islet vessel network (Cohrs et al. 2017). In the insulo-acinar system, 1-5 arterioles supply each islet and arborize into fenestrated capillaries. At the ultrastructural level, the basement membrane of capillaries is also reported to be thicker in human than in mouse islets (Brissova et al. 2015). Interestingly, islets from T2DM donors showed a tendency for increased vascular structures. Observations from animal models of obesity suggest that islets are hyperperfused at least in the prediabetic phase, which could explain the hypervascularity seen in human samples. Alternatively, compensatory mechanisms resulting from worsening β -cell function could account for the increased vessel numbers in T2DM. Additionally, human islet vasculature contains three times as many smooth muscle cells as that of mouse, where only the feeding arterioles are lined by smooth muscle cells. Interestingly, early evidence suggested that β -cells are polarised, with increased granulation at their apical side, facing arterioles (Bonner-Weir 1988). Almaca and colleagues have demonstrated that through aging, the islet vasculature acquires an inflammatory phenotype (Almaca et al. 2014).

Directionality and Velocity of Flow

Considerable debate exists surrounding the issue of blood flow directionality in the pancreatic islet. A consensus on this point is highly desirable as this clearly has physiological relevance to islet paracrinology. There exist three competing theories regarding the directionality of islet blood flow (Brunnicardi et al. 1996). According to the first theory, afferent arterioles arrive at the islet to perfuse the mantle region first, before branching out towards the core region, where β -cells reside in rodent islets. In this setting, non- β -cells can exert their influence on β -cell secretions. In contrast, the second theory posits that 1 to 3 afferent arterioles penetrate the islet core to then arborize to perfuse the periphery of islets. In line with this notion, β -cells are perfused first to modulate the secretions of α - and δ -cells (β -cell- α -cell- δ -cell) (Samols et al. 1988). Lastly, the third theory argues that feeding arterioles enter the islet at one pole and branch out into capillaries without a clear preference for the order of endocrine cells perfused (Ballian and Brunnicardi 2007).

According to this latter theory, islet blood flow and volume can be auto-regulated by means of external and internal gates made up of endothelial cells. Through this shunting mechanism the directionality of blood flow can be modulated in accordance with the metabolic demands of the animal; during hyperglycaemia blood could be directed to β -cells to facilitate glucose sensing and insulin secretions (Liu et al. 1993). Local vasoconstrictive activity in non-human primates was reported recently, providing evidence for the presence of blood shunting and auto-regulation mechanisms in this species (Diez et al. 2017). The blood flow pattern and its significance in islet paracrinology in humans are less clear due to the unique cytoarchitecture of human islets.

Comparing the filling rate of an intravenous bolus of dextran, Nyman and colleagues have shown that hyperglycaemic conditions increase islet blood flow velocity in the exteriorised pancreas model (Nyman et al. 2011). These observations aligned with earlier reports in rats where increased blood flow rate after a bolus of glucose was noted (Jansson and Hellerstrom 1983). The physiological relevance of this is that increases in islet blood flow post-prandially could facilitate insulin secretion and rapid delivery to target organs.

Contrastingly, hyperglycaemia did not elicit changes in the blood flow of the exocrine pancreas indicating the specificity of the vascular response. Intriguingly, small blood vessels

may even become recruited in hyperglycaemia as the same model noted some vessel branches with no flow during hypoglycaemia. Besides flowrate, islet capillary pressure also increases in islets subjected to hyperglycaemia from 3mmHg to 6mmHg, as measured in rat islets (Carlsson et al.1997). These observations suggest that the islet is capable of regulating its own perfusion independently from the rest of the pancreas. Opposite to rodent findings, islets transplanted into non-human primates have shown that blood perfusion was not different under hyperglycaemia (Diez et al. 2017). In the same study, focal vasoconstrictive activity was evident in sub-sectional areas of the islet, again pointing to the possibility of intra islet shunting.

The importance of blood perfusion is reflected by a myriad of observations. The islet vasculature possesses highly specific functions and is in a constant dynamic interaction with islet endocrine cells. Observations to support this notion include: 1) endothelial cells during development send instructive signals (vascular endothelial growth factor-A, in particular) to the dorsal endoderm to form the pancreatic bud and express insulin in β -cell progenitors, 2) β -cell interaction with pericytes allows islets to differentially increase blood flow rate and vessel diameter in response to a glucose stimulus, 3) endothelial cells secrete extracellular matrix proteins to support β -cell function and survival amongst other functions (Reinert et al. 2013; Lammert et al 2001; Yoshitomi and Zaret 2004; Almaca et al. 2018; Pieris et al. 2014; Nikolova et al. 2006; Parnaud et al. 2009).

1.2.3 Innervation Sympathetic Nervous System

The pattern of autonomic innervation in the islet has not been fully elucidated. Nevertheless, it is clear that both sympathetic and parasympathetic stimulation differentially influences pancreatic hormone release. Pre-synaptic splanchnic nerves make synapses at the level of the coeliac ganglia and use noradrenaline as the primary neurotransmitter (Ahren et al. 2000). Mouse islets are abundant in sympathetic nerve fibres, whose main site of action is the smooth muscle cells of intra-islet arterioles. In the perivascular space, this structure is collectively referred to as the sympathetic neurovascular complex. The anatomical positioning of sympathetic nerves suggests that while they have

direct influence on glucagon secretion from α -cells, they affect insulin secretion indirectly, by modulating vessel diameter.

However, there might be differences in human islet innervation pattern. Rodriguez-Diaz and colleagues for example, reported sparser sympathetic innervation pattern in human islets compared to mouse ones (Brissova et al. 2015; Rodriguez-Diaz et al. 2012; Rodriguez-Diaz et al. 2011). Meanwhile, using optical clearing techniques and 3-D imaging, Chiu and colleagues found evidence for similarities between the two species and demonstrated comparable innervation topology and density of human islets (Chiu et al. 2012). Sympathetic peri-islet nerve fibres were also found to undergo remodelling in streptozotocin-treated animals. Evidently, much more research in this area is needed to better characterise the function and innervation pattern of sympathetic nervous input to the islet (Taborsky 2011; Ahren 2012).

Parasympathetic Nervous System

Animal studies suggest rich innervation of islets by parasympathetic nerve fibres (Ahren 2000). The cephalic phase of insulin secretion was significantly diminished in rats undergoing abdominal vagotomy, highlighting the role of the vagus nerve in mediating insulin secretion (Berthoud and Powley 1990). Immunohistochemical and quantitative real-time polymerase chain reaction (qt-PCR) experiments have revealed the presence of muscarinic M1 and M3 receptor expression on the surface of β -cells in the human islet.

Further, evidence suggests that δ -cells express M4 receptors which on stimulation promote somatostatin secretion (Molina et al. 2014).

Paralleling findings from rodent studies, the cephalic phase of meal-stimulated insulin release has been shown to be vagally mediated in humans (Teff et al. 1991). The observation that the release of other islet hormones like glucagon and pancreatic polypeptide also require vagal stimulation lends further support for the presence of parasympathetic nerve fibres in the human islet (Ahren et al. 2006). Although muscarinic receptor expression has been demonstrated in human islets, the existence of cholinergic innervation in islets has been contested (Rodriguez-Diaz et al. 2011; Taborsky 2011).

Instead, some evidence points to the presence of vasoactive intestinal peptide (VIP) containing axons in human islets (Bishop et al. 1980). VIP- containing neurones have been linked to the parasympathetic system previously (Kimura et al. 1994). Thus, while human islets lack typical cholinergic parasympathetic fibres, they may receive parasympathetic input through VIP-containing neurones (Mazzone et al. 2002). Therefore, it is likely that acetylcholine in human islets acts as a paracrine factor released by α -cells rather than a *bona fide* neurotransmitter (Rodriguez-Diaz 2011).

In addition, sensory nerve fibres have also been observed in the islet and the main neurotransmitters in these are substance P and calcitonin gene-related peptide. While their role in hormone secretion remains unclear, sensory nerve fibres have been implicated in T1DM previously (Rodriguez-Diaz and Caicedo 2013; Razavi et al. 2006).

1.2.4 β -cell Identity

β -cell development and maturation involves tightly-controlled, dynamic changes in gene regulatory networks. Pancreatic duodenal homeobox 1 (PDX-1) has been termed as the master regulator of pancreatic development and is the first transcription factor (TF) to be expressed that commits early progenitor cells of the foregut to form the pancreatic bud (Gao et al. 2014). Over time, however, the expression of PDX-1 becomes confined to β -cells. With the selective ablation of PDX-1 in mature β -cells, multiple markers of β -cell identity are lost. Besides PDX-1, paired box 6 (PAX-6) is another early marker of the endocrine lineage which has also been implicated in the development of the central nervous system (CNS) and the eye. In the pancreas, PAX-6 expression was found to be critical for the maintenance of both α - and β -cell identity.

In adult β -cells, PAX-6 controls the expression of insulin, among other markers of β -cell identity (Gosmain et al 2012). The importance of PAX-6 is underscored by the observation that its selective knockdown in β -cells leads to a reduction in glucose-stimulated insulin secretion (GSIS) and insulin biosynthesis. Moreover, PAX-6 has been found to be down-regulated in leptin receptor deficient (*db/db*) insulin-resistant mice (Swisa et al. 2017).

Downstream to PAX-6, commitment to the β -cell differentiation pathway involves the expression of the basic helix loop helix neurogenic differentiation (NeuroD1) TF. Mutations in the NeuroD1 TF have been associated with maturity onset diabetes of the young (MODY-

1), a rare genetic form of diabetes (Malecki et al. 1999). Paradoxically, β -cell specific NeuroD1 null mice are glucose intolerant and display reduced insulin secretion despite elevated levels of insulin measured in the pancreata of these animals. However elevated levels of LDH and neuropeptide Y in this model hints that the insulin-laden but secretory deficient β -cells have an immature phenotype (Gu et al. 2016).

The last TF worth mentioning in this light is Nkx6.1, the specific expression of which has been shown to regulate glucose sensing and insulin biosynthesis. Its deletion results in rapid decline in β -cell insulin content. In parallel, neurogenin3 TF expression increases, suggesting that β -cells acquire a de-differentiated or less mature phenotype (Taylor et al. 2013). This may be of clinical relevance, since the process of acquisition of a de-differentiated, progenitor-like state of β -cells has been reported to occur in T2DM (Bensellam et al. 2018).

In summary, many molecules and transcription factors have been identified to be important in various aspects of β -cell maturity, identity and function. There is a large amount of heterogeneity between individual islets and β -cells. However, a precise molecular description of the typical β -cell is currently missing (Rutter et al. 2015).

Disallowed Genes in β -cells

Emerging evidence suggests that the maintenance of β -cell identity not only involves the selective enrichment of specific genes in β -cells but also the active suppression of disallowed genes, and this is physiologically important (Schuit et al. 2012). During postnatal maturation, the tissue specific expression pattern of genes occurs in parallel with the repression of disallowed genes. For example, while there are four different enzymes phosphorylating glucose, only glucokinase is expressed in mature β -cells while hexokinase expression is actively repressed (Schuit et al. 1999). In fact, earlier reports of hexokinase presence in the endocrine pancreas were later confirmed to have been due to exocrine contaminants. The *Slc16a1* gene is also deeply repressed in β -cells. *Slc16a1* encodes for a monocarboxylase transporter (MCT-1) which facilitates the diffusion of lactate and pyruvate in order to sustain anaerobic glycolysis. However, in β -cells MCT-1 expression is required to be very low in order to avoid the stimulation of insulin secretion by high ambient pyruvate in β -cells. The physiological relevance of this is brought to light by a rare condition called exercise induced hyperinsulinaemia, which results in exercise-induced hypoglycaemia due

to the inadequate repression of MCT-1 expression in β -cells (Otonkoski et al. 2007). It remains to be elucidated whether diabetes disease progression in humans involves the failure to repress disallowed genes. However Jonas and colleagues demonstrated the dynamic effects of hyperglycaemia on the gene expression profile of islets. Rats that developed hyperglycaemia after 80-90% pancreatectomy displayed hypertrophied and dedifferentiated β -cells in the remainder of their pancreata. Moreover, the remnant β -cells displayed de-repression of the *Ldha2* gene that encodes for lactate dehydrogenase (Jonas et al. 1999; Dominguez-Gutierrez et al. 2016).

Insulin Biosynthesis

In mature, functional β -cells insulin is stored in dense core granules as hexamers in the presence of zinc ions and favourable pH concentrations (Zn^{2+} 10mM; pH 6). Insulin is secreted as hexamers into the blood stream where they dissociate into monomeric forms due to electrostatic repulsive forces. The monomeric form of insulin consists of the 21 amino acid long-A and 30 amino acid long-B chains which are connected by a disulfide bond. The insulin gene encodes preproinsulin that is targeted to the endoplasmic reticulum for post-translational processing before a final maturation step in the Golgi apparatus. Subsequently, proinsulin enters premature secretory vesicles where it is cleaved to yield insulin and C-peptide (Fu et al. 2012). The main driver for insulin production is glucose metabolism; a glucose bolus in fasted rats elicited a three to four-fold increase in proinsulin mRNA in the ensuing 24 hour period (Welsh et al. 1985).

Glucose Sensing and Insulin Secretion

In β -cells, glucose is taken up via facilitated transport through glucose transporters (GLUT; encoded by the *SLC2A gene*). In rodent β -cells, the GLUT2 low affinity glucose transporter (with a K_m of 17mmol/L) is the prevalent subtype expressed. GLUT2 is also expressed in the proximal convoluted tubules of the kidney and liver hepatocytes. In the rodent pancreas GLUT2 functions as the glucose sensor of β -cells. Due to its high K_m value and transport capacity, glucose rapidly diffuses into cells where it is catalysed by glucokinase. Reduced expression of GLUT2 in β -cells has been noted in pre-clinical models of diabetes before (Thorens 2015; Thorens et al. 1990). The prevailing subtype of GLUT in the human β -cell has been a subject of debate. A selection of studies suggests that human and rodent tissue

differ in that human β -cells express the GLUT1 subtype (McCulloch et al. 2011; De Vos et al. 1995). GLUT1 is a high affinity glucose transporter (with a K_m of 3mmol/L) that is abundantly present in erythrocytes, the developing embryo, endothelial cells and epithelial-like barriers of the eye, brain, peripheral nerves (Augustin 2010). The relative importance of GLUT1 in glucose sensing of human β -cells was challenged more recently (Bunt and Gloyn 2012). *SLC2A2 gene* (encoding for GLUT2) loss of function mutations are the underlying cause of a rare type of neonatal diabetes. These patients present with low birth weight, lack of insulin secretion and with a requirement for insulin therapy, suggestive of islet dysfunction (Sansbury et al. 2012). Thus in humans the relative importance of the two GLUT isoforms remains to be fully elucidated.

Upon entry into the β -cell, glucokinase phosphorylates the glucose before its further processing through glycolysis. Since glucose-6-phosphate (G6P) is generated without allosteric inhibition, glucokinase itself is the controller of the rate of glycolysis and therefore this enzyme is regarded as the glucose sensor of the cell. The end-product of glycolysis is pyruvate, which is first converted by pyruvate kinase to acetyl-CoA that then reacts with oxaloacetate in a reaction catalysed by citrate synthase to obtain citrate, a component of the tricarboxylic acid cycle (TCA). With the activation of the TCA, $FADH_2$ and NADH are generated and the reduced equivalents of these are shuttled into the electron transport chain to be employed for ATP generation. ATP generated in mitochondria is transported back into the cytosol via adenine nucleotide translocator (ANT) and the elevated ATP levels trigger the opening of ATP sensitive K^+ channels, ultimately leading to the depolarization of the cell. Thus, metabolic activity is coupled to electrical activity via K_{ATP} channels. In turn, the depolarization of the cell leads to the opening of L-type voltage-dependent calcium channels and an influx of calcium. Elevated cytosolic calcium levels induce the mobilization and fusion of insulin secretory granules with the cell membrane through interaction with SNARE proteins (Xiong et al. 2017).

When glucose is elevated abruptly and sustained a period of time a characteristic biphasic insulin secretory pattern emerges. It has been proposed that secretory vesicles docked at the cell membrane are released rapidly in response to a glucose stimulus, constituting the first phase of insulin secretion. Before the second phase of secretion however, new

secretory vesicles are required to be primed and docked at the cell membrane, explaining the time-lag seen in the second phase of insulin secretion (Henquin 2012).

β-cell Impairments in Diabetes at the Ultrastructural Level

In T2DM, there are several impairments in insulin secretion. These include blunted or absent first phase insulin secretion. Over time, second phase insulin secretion also becomes affected ultimately even to non-glucose stimuli. Early studies on human islets have shown that glucose stimulated insulin secretion is diminished in type 2 diabetic islets while L-leucine or L-glutamine stimulated insulin secretion remained relatively intact in β-cells (Fernandez-Alvarez et al. 1994). In a different study, it was shown that diabetic islets secreted a lower amount of insulin upon stimulation with increasing glucose concentrations and needed a higher glucose threshold to stimulate insulin secretion (Deng et al. 2004, Marchetti et al. 2004). Glucose oxidation appears to be reduced in diabetes and this is partly explained by decreases seen in the activities of the many mitochondrial enzymes. Additionally, ultrastructural analysis of type 2 diabetic β-cells has revealed rounder mitochondria in reduced numbers (Parish and Petersen 2005). Interestingly, cells from T2DM patients did not increase their ATP content upon glucose stimulation (Haythorne et al. 2019). Accordingly, the ATP:ADP ratio was markedly lower in T2DM β-cells and there was an up-regulation of UCP2 and complexes I and V of the respiratory chain. Additionally, SNARE proteins involved in vesicle exocytosis were also down-regulated in type 2 diabetic islets (Aslamy and Thurmond 2017).

At the ultrastructural level, β-cells are characterised by the presence of electron dense core granules, whose size is around 300nm and their number is estimated to be 10,000 per cell. The mantle of the granules may contain proinsulin that is not yet fully processed. Also, the dense core can be absent or appear as grey, signifying that the cleavage of the precursor was insufficient. A portion of insulin containing vesicles is docked in close proximity to the cell membrane where they form the readily-releasable pool. Both total and the membrane-docked number of insulin granules are decreased in diabetes. Other cellular organelles also display changes to their structure; the endoplasmic reticulum for example appears more pronounced, concentrically arranged and show strong electron density due to the large number of ribosomes covering its surface. The ER volume in T2DM islets was found to be double that of normal β-

cells (Marchetti et al. 2007). The amount of apoptotic cells in T2DM islets is also increased compared to healthy individuals (Butler et al. 2003).

1.2.5 The Biochemistry of Insulin secretion: Insulin:Calcium Signalling Coupling Triggering Pathway

Under unstimulated conditions, cytosolic calcium levels are maintained at a very low level, four orders of magnitude below those in the extracellular compartment (Gilon et al. 2014). Cytosolic calcium oscillations in individual β -cells give rise to pulsatile insulin secretion and determine the kinetics of insulin pulses. Under resting conditions, the membrane potential of β -cells is set at -70mV. When the membrane potential is increased due to closure of ATP-sensitive K^+ channels, and surpasses a threshold of -50 to -55mV, the cell becomes depolarised. The change in membrane potential is sensed by voltage gated calcium channels (VGCC) which allow the influx of Ca^{2+} down their concentration gradient. Several types of calcium channels are expressed in β -cells but the predominant subtype is the L-type calcium channel in both human and mouse β -cells. L-type and P/Q-type VGCCs are high-voltage dependent and typically activate at -40mV or above. Distinct from mice, human β -cells also express T-type Ca^{2+} channels which give rise to transient currents. Importantly, T-type VGCCs become activated at -60mV and rapidly inactivate thereafter as the membrane potential becomes more depolarised. The cumulative effect of electrical activity through the various ion channels results in the generation of action potentials (APs). Periods of bursting activity (active phase) are interleaved with quiescent phases, following a cyclical pattern. A putative pacemaker-like role, driving these rhythmical changes inside β -cells, has been suggested for T-type VGCCs before (Rorsman and Braun 2013). Accordingly, calcium currents through T-type VGCCs initiate APs and bear a permissive role for L-type VGCCs and voltage-gated Na^+ channels to open and further depolarise the cell (Bhattacharjee et al. 1997). Theoretically, any stimulus that increases cytosolic calcium will culminate in insulin secretion, but insulin secretion is much more powerful when it is glucose stimulated than for example, when islets are electrically stimulated.

Insulin secretion in healthy humans and rodents follow a pulsatile pattern with a mean periodicity of \sim 5min. The observation that isolated β -cells secrete insulin in a pulsatile manner suggests that the ability for rhythmic hormone secretion is inherent to β -cells rather than being governed by external factors (Grotsky and Bennett 1966; Malaisse et al. 1979; Wollheim and Sharp 1981; Bertram et al. 2007). Islets display several types of oscillatory behaviours which are

classified on the basis of their periodicity. Slow calcium oscillations occur at 4 to 6 mins intervals while fast oscillations are at a rate of 1 min. The patterning of oscillatory behaviour is comparable between mice and humans which suggest conserved underlying mechanisms (Bertram et al. 2018).

Both metabolic and electrical oscillatory behaviours characterise islets and the comprehensive model to describe the interplay between these two parameters is termed the Dual Oscillatory Model (Bertram et al. 2007). According to the model, a third type of calcium oscillatory activity, compound oscillations underlie and determine pulsatile insulin secretion. Compound oscillatory activity of β -cells arises from the superimposition of fast oscillations over slow oscillations. It is believed that metabolic factors, primarily glycolysis, are major determinants of the slow component of compound oscillations, while ion fluxes (i.e. electrical activity) give rise to the fast element of compound oscillations. In support of this theory, oxygen consumption, insulin and Zn^{2+} patterns all show similar, compound oscillatory behaviour in β -cells (Civelek et al. 2012).

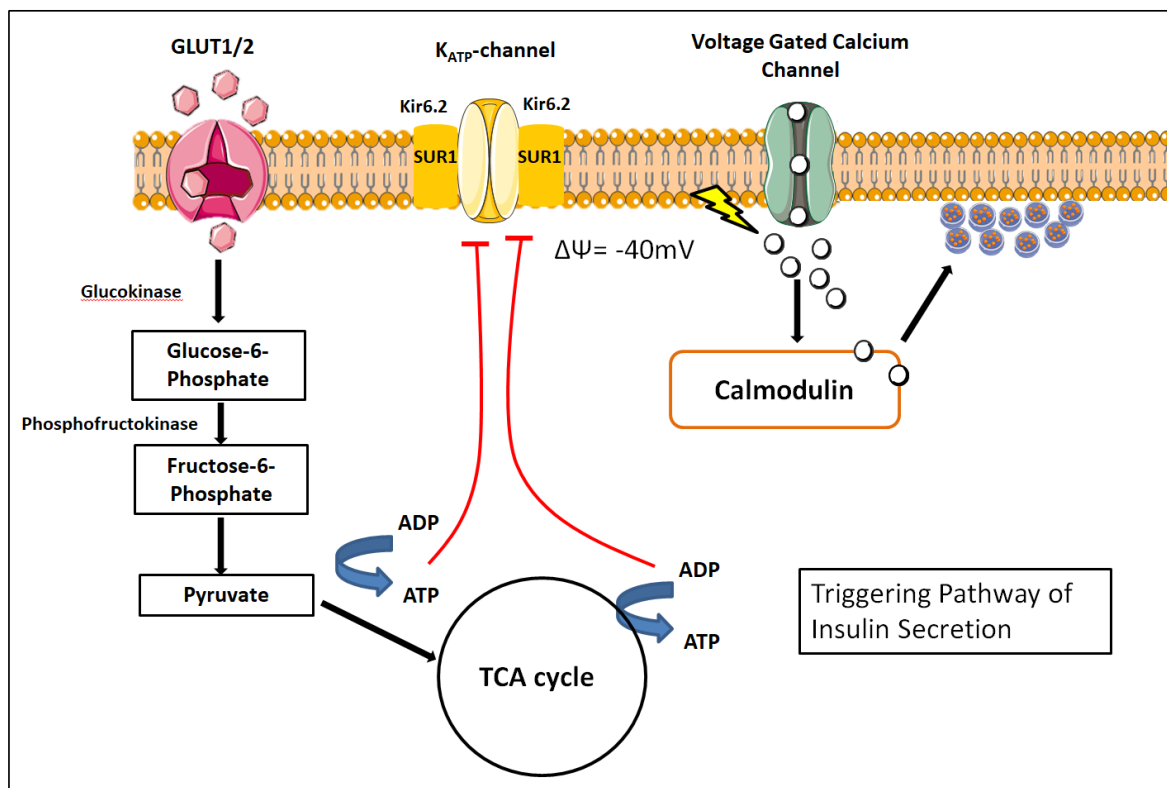


Figure 1.2.5.1 Schematic diagram of the glucose stimulated insulin secretion in the β -cell.

1.3 Methods for Studying Islet Biology

Before discussing the development of novel platforms to investigate some of the many unknowns in islet biology, it is useful to consider the most widely-used methods to date.

1.3.1 *In Vitro* Methods

The vast majority of our understanding of islet biochemistry has come from *in vitro* studies. Perhaps the best example of *in vitro* experiments that were translated to clinical applicability was the discovery and characterisation of K_{ATP} -channels embedded in the membrane of β -cells. Since the first observations of the hypoglycaemic effects of sulphonamides in 1942, a series of synthetic sulfonylurea compounds had been developed and used clinically (Henquin 1992). However, it was not until 1985 when the first line of evidence emerged regarding their actions at the SUR1 subunit of K_{ATP} -channels in β -cells. This has revolutionised the field and improved our understanding of insulin secretion from β -cells considerably.

However, there are many reported discrepancies between findings of *in vitro* and *in vivo* islet function, which highlight the fact that *in vitro* experimental conditions inherently lack the ability to fully recreate the *in vivo* microenvironment. For example, it has been reported that islets placed into an *in vitro* environment quickly lose both their Nkx6.1 and GLUT2 expression and that the overexpression of Nkx6.1 in islets *in vitro* and *in vivo* showed considerably divergent effects on β -cell proliferations (Weinberg et al. 2007).

The use of human islets in research

The increased effort to isolate human islets for research purposes and the development of programmes like the European Consortium for Islet Transplantation has made human islet tissue available to hundreds of scientists who study islet biology. It has allowed researchers to make important morphological distinctions between commonly used rodent islets and human islets. Research on human islets is however hampered by many difficulties: (i) the logistics of islet distribution is costly (ii) there can be variability between preparations (iii) tissues lose some of their features in the *in vitro* environment (iv) there is variability among people. Unlike islets fated for transplantation, there is no standardised testing of the functional quality of human islets used in research. Insulin secretion assays may be the only functional data collected on islets while other hormone secretions or measures of islet health are not routinely assessed (Nano et al. 2019).

1.3.2 *In Vivo* Methods

Metabolic phenotyping

Ultimately the most important (clinical) readout of islet function is the maintenance of euglycaemia. Since insulin secretion is only a small part of this complex homeostatic jigsaw (which also includes many other factors such as peripheral insulin resistance, nutrient load and hepatic glucose output), most translational studies focus on measurements of circulating glucose and insulin levels and then make inferences about the β -cell secretory component. The most basic and frequently used method of determining whole body glucose homeostasis is to perform an intraperitoneal (IPGTT) or oral glucose tolerance test (OGTT). Major factors governing glucose homeostasis are the rate at which insulin is secreted in response to a glucose challenge and the ability of insulin-target tissues to uptake glucose (Bowe et al. 2014; Ayala et al. 2010). While an overall picture on glucose handling can be gained through these tests, they do not elucidate underlying causative mechanisms for a particular glucose phenotype. In rodent models, there is relatively little consensus on the experimental protocol and a multitude of factors may impact on read-outs of a GTT. Among these, the time spent fasting prior to a GTT, the route of glucose administration, the strain, age and sex of the animals are all factors to consider as they influence glucose homeostasis. For example, insulin sensitivity decreases with age and therefore, it is generally advised that animals are age-matched for experiments.

The pharmacokinetics of glucose differs when administered orally versus intraperitoneally, with peak blood glucose measurements achieved at 15min and 30min, respectively (Andrikopoulos et al. 2008). Moreover, peak plasma glucose concentrations are significantly lower when glucose is administered orally, a phenomenon which has been attributed to the release of gut-derived incretins such as GLP-1 (Ahren et al. 2003).

Typically, a bolus of 1-2g/kg glucose is administered to animals after a period of 6 hours fast. It is important to mention that this type of dosing is only adequate when the body composition of animals can be assumed to be similar. The excess adipose tissue in high-fat fed animals will result in a higher overall body weight while their lean body mass, the major compartment of glucose disposal, will not be substantially different from control mice. Thus, when calculating a glucose dose, the lean body mass rather than the absolute weight of animals should be taken into consideration (Jorgensen et al. 2017). Additionally, stress induced by handling and the

peripheral tail nick can skew blood glucose read-outs towards higher values due to the release of catecholamines and therefore should be accounted for. To measure islet insulin secretory response *in vivo*, insulin measurements from blood samples may be taken. For these purposes, 5µl samples are sufficient from a peripheral tail nick and repeated measurements are also possible. For a more complete assessment of islet hormones, including glucagon and GLP-1 secretions, larger blood volumes are necessary. Because repeated tail nicking causes a large amount of stress in animals, alternative, more sophisticated *in vivo* methods are advised for the full profiling of islet hormones.

Insulin tolerance tests (ITT), which give a readout of insulin sensitivity, rest on the same principle as those laid out above for GTT. Here, a bolus of insulin is administered to fasted animals and the rate at which glycaemia returns to a normoglycaemic range is measured – more insulin sensitive animals will have a lower glucose nadir for example. It is imperative that the period spent fasting is carefully considered to avoid potentially fatal hypoglycaemic episodes. The extent to which glycaemic values decrease primarily indicates insulin sensitivity in the liver and skeletal muscles (Bowe et al. 2014).

Clamp studies

A much more refined but technically challenging technique is the surgical insertion of indwelling catheters, then clamping a specific element of metabolic flux e.g. glucose levels, in order to assess the contribution of other factors e.g. insulin secretion. The procedure itself is highly invasive but permits the examination with minimal handling in conscious, freely moving animals. Direct access to circulation is achieved through the insertion of intravenous catheters into the jugular vein where substances can be administered. Simultaneously, repeated blood sampling occurs from the carotid artery where sampling of larger blood volumes is attainable. The catheters are externalised at the back of the head and are secured in place to ensure that experimental animals cannot interfere with them. An equivalent to a GTT experiment is the set-up of a hyperglycaemic clamp. In this model, glucose is continuously infused to maintain a pre-determined hyperglycaemic value. Frequent blood sampling during the early stages of the clamp experiment allows for the assessment of both first and second phase of insulin release (Bowe et al. 2014; Ayala et al. 2010). In short, animals with impaired insulin secretory ability

require a lower glucose infusion rate to maintain their glucose clamped at 17mM than control animals that can secrete more endogenous insulin.

Hyperinsulinaemic-euglycaemic clamps were first described as a more advanced version of the ITT by DeFronzo and colleagues in 1979. This version of a clamp study is better suited to measuring insulin resistance rather than beta cell secretory function. Since then, this method has generally been accepted as the gold-standard for determining insulin sensitivity *in vivo* (DeFronzo et al. 1979). Indwelling catheters are surgically inserted as described above and insulin is administered intravenously to create a clamped hyperinsulinaemic environment. The high circulating insulin levels suppress the endogenous production of glucose and instead stimulate glucose uptake into insulin target tissues. Circulating blood glucose levels are monitored and infused at varying intervals to maintain euglycaemia. Animals with enhanced insulin sensitivity will require higher rates of glucose infusions for the maintenance of euglycaemia while more insulin resistant states will require lower glucose infusions. While hyperinsulinaemic-euglycaemic clamps provide fine details on insulin sensitivity, the invasive nature and technical demands of this procedure precludes it from being a standard technique in every laboratory.

Besides laboratory animals, clamp studies are also carried out in human participants, although they are also technically demanding to achieve. From clamp data, a number of quicker tests of human glucose metabolism have been extrapolated and validated. For example, the homeostasis model of insulin resistance (HOMA-IR) and quantitative insulin check index of insulin sensitivity (QUICKI) are frequently used to assess insulin sensitivity in humans, and can be calculated from a single sample for glucose and insulin. While HOMA-IR and QUICKI do not replace direct measurements of insulin resistance, they are acceptable substitutes in cases where direct assessments are not possible and quick results are desirable.

The above-mentioned techniques are excellent for the assessment of whole body glucose homeostasis however they are incapable of directly reporting on changes in β -cell function in real time. To address these, novel imaging platforms have been developed which allow for the examination of β -cell function directly.

***In vivo* imaging platforms – non invasive**

To date there is no clinically useful imaging methodology for pancreatic mass or function in humans. This is due to a mixture of problems with the small size of the islets within the pancreas, movement artefacts and a lack of high sensitivity and high signal to noise ratio of probes. Islets of Langerhans are challenging to image because individually they are below the spatial resolution of conventional positron emission tomographic (PET) and single photon emission computed tomographic (SPECT) imaging measurements. Radioligands can only be used to assess β -cell mass if they specifically accumulate in β -cells and are excluded from the exocrine tissue. The uptake of the tracer reports on islet tissue or β -cell volume and can be expressed as tracer signal divided by pancreatic volume or as integrated pancreas uptake (i.e. total tracer signal from the pancreas) (Eriksson et al. 2016). However, β -cells and non-neoplastic tissues tend to express only low levels of specific antigens on their cell surfaces.

Dihydrotrabenazine (DTBZ) is an antagonist of vesicular monoamine transporter 2 (VMAT2) and has originally been developed for use in labelling neurones. In pancreatic β -cells VMAT2 is expressed to transport monoamines from the cytosol to the secretory vesicles. ^{11}C -DTBZ imaging of the diabetic rat pancreas has shown a decline in islet mass with this type of radiotracer, highlighting its utility for pancreatic investigations (Souza et al. 2006). However, tested on T1DM human preparations ^{11}C -DTBZ showed non-specific staining and was inappropriate to use for quantifying islet mass (Fagerholm et al. 2010). Meanwhile, research by another group suggested that VMAT2 is not expressed in rodent islet tissue (Schafer et al. 2013). Importantly, the specificity of any VMAT2-based tracer is highly questionable as VMAT2 has been described in the literature as a marker for sympathetic nerve endings. As intra-islet blood vessels receive sympathetic nervous input it is likely that ^{11}C -DTBZ shows potential cross-reactivity with these nerve endings rather than signifying purely the islet mass (Weihe et al. 1994).

Evaluation of the [^{18}F]-labelled L-3,4-dihydroxyphenylalanine (L-DOPA) mouse and human islets implanted subcutaneously in recipient mice have shown that [^{18}F]-L-DOPA accumulates in islets. However, [^{18}F]-L-DOPA also shows non-specific staining in areas devoid of dopaminergic signalling (Eriksson et al. 2014). The clinical utility of the [^{18}F]-L-DOPA tracer is questionable, with some claiming its usefulness in identifying focal lesions of hyperinsulinism while others

report no difference in tracer uptake between healthy volunteers and those with insulinomas (Otonkoski et al. 2006).

GLP-1 receptor expression is almost exclusively limited to the β -cells in islets (Tornehave et al. 2008). With the intention of exploiting this specificity, GLP-1-based radionucleotide tracers have been developed for PET imaging. [^{111}In]-exendin was shown to be taken up by β -cells exclusively and overall as a good indicator of β -cell mass in a diabetic rat model (Brom et al. 2014). The same tracer applied to humans in SPECT modality uncovered a significantly reduced uptake of [^{111}In]-exendin in T1DM patients in comparison to healthy volunteers which is in line with the reduced β -cell mass that characterises this patient population. The pancreatic signal strength was also negatively correlated with the length of disease duration. However, a great amount of inter-individual variability was noted, with one individual with T1DM displaying higher pancreas signal than the average seen in healthy volunteers (Brom et al. 2014). In short, the use of radioligands to image pancreatic β -cell mass has not arrived at sufficient accuracy to distinguish disease states from healthy controls, let alone track disease progression over time.

The exteriorised pancreas imaging model in rodents

Recent advances in neuroscience with intravital imaging through a cranial window triggered a surge of research interest in the application of body windows to visualise peritoneal organs (Nimmerjahn et al. 2005; Weigert et al. 2010). Research questions addressed using the exteriorised pancreas approach involved investigating islet vasculature characteristics (Nyman et al. 2010; Carlsson et al. 1997). A recurrent challenge in these types of experiments is the presence of movement artefacts related to respiration and heartbeat of the animal. To combat this issue, stereotactic frames in various configurations have been developed with the aim to immobilise the body and negate undesired movement. Research efforts yielded the engineering of a compressive chamber under which the intestines could be externalised and imaged (Tanaka et al. 2010). A major concern with this approach however is that the applied pressure can inflict potential tissue damage on the organ investigated with devastating consequences on experimental read-outs. In the case of islet research more specifically, the mounting of the exteriorised pancreas on a micro-stage device has been successful. In this set-up, part of the pancreas is lifted up onto a micro-stage where movement can be better controlled by the experimenter while also avoiding tissue damage. Due to space limitations, the use of the micro-

stage device required modifying a traditional objective into a thin, stick-type objective (Cao et al. 2012). The key aspect of exteriorised organ models is the fact that the internal milieu remains intact and after sufficient motion correction, sub-cellular resolution can be achieved.

Furthermore, a major drawback with the exteriorised pancreas approach is that peritonitis precludes it from being used for the longitudinal assessment of islets. Moreover, due to the unique tissue architecture of the mouse pancreas, finding islets embedded in the parenchyma can be troublesome.

1.3.3 Longitudinal *in vivo* imaging of pancreatic islets implanted into the anterior chamber of the eye (ACE)

Immune-privileged sites

The first observation of ocular immune privilege was made by Peter Medawar in the 1940s. Skin allografts transplanted into the rabbit eye anterior chamber survived even though they remained avascular. With graft vascularization however, the process of allograft rejection was triggered (Medawar 1948). Erroneously it was thought that immune privilege in the eye is achieved by means of immune ignorance. It is now widely accepted that ocular environment is actually abundant in immunosuppressive factors which confer upon the "anterior chamber-associated immune deviation" (ACAID). Immune privilege is an evolutionary adaptation. Immune responses with high potential to inflict major collateral damage on the surrounding tissues are downplayed, while immune responses to serious threats remain intact.

ACAID is achieved with a multi-pronged strategy. Actors of the innate immune system are neutralised, since ocular cells express non-classical MHC1b molecules on their surface which have the capability to engage with inhibitory receptors on the surface of natural killer (NK) cells that prevent cytotoxicity. Binding of the cytokine Fas ligand (FasL) to its receptor on the surface of NK cells results in the apoptosis of them and thus prevents allograft rejection. Further, ocular cells are shielded from deleterious responses of the adaptive immune system; complement-mediated reactions are suppressed by the widespread expression of complement regulatory proteins on the surface of ocular cells. The limited lymphatic drainage of the eye curbs the accessibility of antigens to local lymph nodes. Thus, inflammatory cells originating from other

areas of the body are confronted with the aqueous humour which is abundant in immunosuppressive and anti-inflammatory factors in the eye (Niederkon 2006).

Consequently, the anterior chamber presents a transplantation site with a highly desirable anti-inflammatory internal milieu, and the cornea functions as a natural body window.

The anterior chamber of the eye (ACE) as an experimental tissue transplantation site dates back to 1873 (Moore et al. 1937). Since then, the ACE has been proven to be a versatile tool for transplantation studies and has been used to investigate the physiology of a wide array of different organs including the prostate, pineal gland cells, endometrial cells, adrenal glands and even embryonic hippocampal tissue with genetic predisposition to schizophrenia (Moore et al. 1937; Wragg et al. 1967; Markee 1978; Stromberg and Ebendal 1989; Freedman et al. 1992). Similarly, a large variety of examples can be found for experimental animals used ranging from mice, rhesus monkeys, chinchilla rabbits to cats (Freedman et al. 1992; Markee 1978; Moore et al. 1937; Jacobowitz and Laties 1970).

The first reported transplantation experiment involving pancreatic tissue is associated with Ernest Adegate in 1998. For his studies, rats were chosen as experimental animals and he had already documented the fact that transplanted islets become re-vascularised in the ACE. In fact, he hypothesized that newly grown blood vessels are likely to be a chimera of both host iridial and donor intra-islet vessels (Adegate, 1998). Later findings from confocal imaging experiments in the same model emerged to support this notion (Nyqvist et al. 2010). In 2008 Speier and colleagues applied the platform for the first time to investigate the biology of isolated islets (Speier et al. 2008).

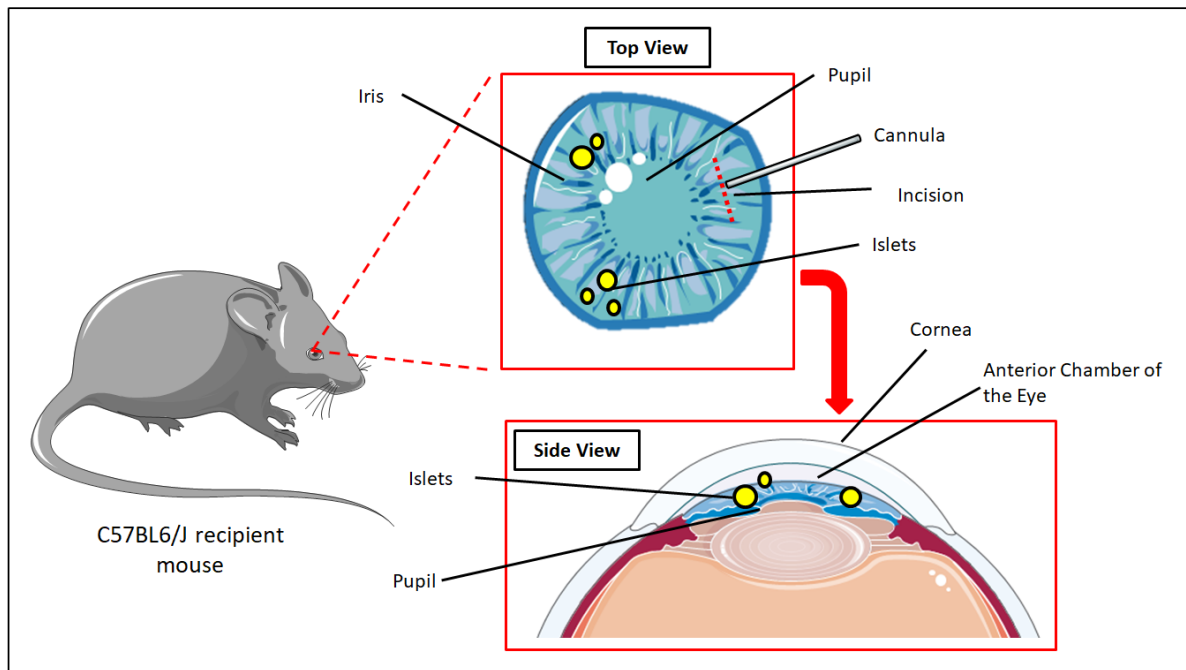


Figure 1.3.3.1 Schematic diagram of the islet in the eye imaging platform.

1.3.3.2. Vascularization and innervation of transplanted islets

As discussed in section 1.2.2. islet endocrine cell-vascular coupling is indispensable for the normal functioning of islets and only when the vascular aspect is recapitulated, can we obtain a more comprehensive understanding of integrative islet function in health and disease.

The role of islet vasculature in diabetic states is highlighted by the following findings: 1) endothelial cells from aged donor mice developed fibrotic, dysfunctional vasculature in a transplantation model, 2) the diabetic phenotype induced by streptozotocin treatment could be reversed by transplanting aged donor islets into young recipients with the ability to rejuvenate the vasculature, 3) islet vascular supply increases through dilatation in diabetic pre-clinical models, 4) vessel density selectively decreased in T1DM human donor islets while exocrine vessel network remained unchanged (Almaca et al. 2014; Dai et al. 2013; Canzano et al. 2019).

In the eye, islets re-establish a morphologically similar vessel network as that seen in the native pancreas. Besides the vessel network, very recently it was found that fibroblasts are also recruited to the transplantation site. These fibroblasts then secrete ECM proteins to re-constitute the basement membrane. Additionally, when mouse and human islet transplants

were compared in mouse recipients, it was found that the islet vessel architecture retained the phenotype of the donor (Nilsson et al. 2020).

Three days after transplantation, the iris blood vessel network is remodelled at the islet transplantation site and feeding vessels begin to grow around the islet. Subsequently, the iris blood vessels penetrating the islet parenchyma develop the islet vessel network which becomes denser and reaches its final topography by four weeks after transplantation.

Capillaries are more uniformly sized by week four and in terms of their diameter size they resembled that of native pancreatic islets. When islets are isolated from their native environment, they still contain a substantial amount of intra-islet endothelial cells. Donor islet endothelial cells have been shown to be important in the early stages of the re-vascularization process (Nyqvist et al. 2005; Nyqvist et al. 2011). As a result, the vessel network that forms in the ACE transplant is a chimera of both donor and recipient endothelial cells. At the ultrastructural level, endothelial cells are separated by a basement membrane and fenestrae, and are morphologically very similar to that in the native pancreas. Interestingly, the dynamics and the quality of the re-vascularization process is an age-dependent process. As shown by Almaca and colleagues, islets from 18month-old mice display the same vessel density as younger counterparts but their vessels show evidence for fibrosis and inflammation. Aged islets also have an increased number of intra-islet macrophages residing in them. Additionally, markers like intercellular adhesion molecule 1, colony stimulating factor 1 and vascular adhesion molecule are upregulated. However, when aged islets are transplanted into young recipients, the inflamed, fibrotic phenotype of the new vessels was reversed. These important observations imply that islet functionality *per se* does not change with aging although the vessel network supporting β -cells become fibrotic and inflamed which could lead to an overall reduced insulin secretory function. These observations suggest that the islet capillaries themselves could be a therapeutic target in diabetes treatment (Almaca et al. 2014).

Innervation in the ACE model

The innervation of islets is extremely important for generating an appropriate insulin secretory response to nutrient challenges. The feasibility of imaging autonomic innervation of islets transplanted in the ACE was demonstrated by Rodriguez-Diaz and colleagues with the use of VChAT-GFP expressing neurones. Accordingly, autonomic nerve fibres developed in close

apposition to the islet. Analyses by the same group have demonstrated that islets transplanted into the ACE receive both sympathetic and parasympathetic nervous input as indicated by their positive staining for tyrosine hydroxylase and vesicular acetylcholine transporter, respectively. The time course of re-innervation followed the time course of revascularization, suggesting that these processes run in parallel. The density of sympathetic and parasympathetic innervation was comparable to those of endogenous pancreatic islets. Therefore, this transplantation site offers the unique possibility of being able to selectively manipulate the parasympathetic tone of implanted islets (Rodriguez-Diaz et al. 2013).

Reporter islets versus metabolic transplantation

With regards to experimental design, there have been two prevailing strategies to investigate islet function in the ACE. During metabolic transplantation experiments, animals are rendered diabetic with streptozotocin treatment which eliminates 90% of their endogenous β -cells and induces hyperglycaemia. Normoglycaemia is restored in these animals by injecting a large number of syngeneic donor islets into the anterior chamber (Speier et al. 2008). It has been demonstrated that the anterior chamber is capable of accommodating a sufficient number of islets despite earlier concerns about physical space limitations at this transplantation site. Frequently, islets fuse together and aggregate into a homogenous tissue mass in these experiments, making it difficult to assess function of individual islets. In the reporter islet concept on the other hand, the endogenous pancreas remains intact and only a few (maximum 10) islets are implanted into the eye. With this approach it is assumed that islets investigated in the eye reflect the function and status of the endogenous *in situ* islets of the animal. Recently, a pilot study with a small number of patients to be receiving metabolic islet transplants into anterior chamber of their eyes was granted FDA approval (Shishido et al. 2016).

The reporter islet concept was first introduced by Illegems and colleagues who investigated the morphological changes in leptin deficient *ob/ob* mice. In this study, the effect of islet mass was investigated longitudinally in leptin deficient mice as they developed obesity and dysglycaemia. In this elegant paper, the investigators clearly demonstrated that the same morphological changes detected longitudinally in the eye reflected changes in the endogenous pancreas studied in comparator groups culled and histologically examined at equivalent time-points

(Ilegems et al. 2013). This established the utility of imaging individual islets in the eye as “reporter” isles for what is occurring in the pancreas of the transplant recipient.

Investigating β -cell mass *in vivo*

Islets transplanted into the eyes of a genetic model for obesity where animals are leptin deficient have shown that islets from leptin receptor KO mice had increased β -cell size and islets mass and this was associated with enhanced PI3K/Akt signalling. Islets from *ob/ob* donors also had an increased intra-islet blood vessel diameter which was thought to reflect the increased demand for insulin posed by chronic hyperglycaemia. Interestingly, exogenous provision of leptin was able to reverse these morphological differences as well as normalised glycaemia (Ilegems et al. 2013).

Summary of the aims and experiments in this thesis

The unifying theme of this thesis is the development of the eye platform as applied to basic and translational diabetes research. In Chapter 2 I will describe novel insights into the normal physiology and functional hierarchies of β -cells within the islet as applied to coordinated calcium activity and insulin secretion. In Chapter 3 I will present data to highlight the longitudinal power of the platform to describe changes in an obesogenic environment and in response to novel gut-hormone-based treatments for T2DM. Finally, in the last experimental chapter I will apply the technology to important questions about islet transplant biology (with relevance to T1DM treatment).

2 Chapter: Functional Imaging of Islets Transplanted into the Anterior Chamber of the Eye

2.1 Introduction

Highly synchronised calcium oscillations drive pulsatile insulin secretion from pancreatic β -cells – which is important for normal physiology and becomes defective in T2DM (Meier et al. 2005). Yet the way islets generate and sustain coordinated calcium oscillations remains incompletely understood. The islet of Langerhans, in common with many other biological systems, reveals the emergent phenomenon of wave-like behaviour which seems likely to occur as the result of its complex architecture of cellular subpopulations, electrical coupling, blood flow and nervous input. The basic question as to whether functional β -cell heterogeneity itself contributes to coordinated islet activity has become a hot topic in islet biology research.

β -Cell Metabolic Heterogeneity

Pioneering work by Pipeleers and colleagues in the 1980`s suggested that glucose induced insulin secretion is markedly higher in β -cells coupled to other islet cells than dissociated ones. Interestingly however, the higher rates of insulin secretion were not matched by elevated glucose metabolism in β -cells, as measured by 3-O-methyl-D-glucose. This observation suggested that the intercellular organisation of β -cells *per se* conferred an advantage and facilitated hormone release from cells (Pipeleers 1987). A functionally diverse population of β -cells was postulated from observations on glucose responsiveness, insulin content and replicative ability (Giordano et al. 1991; Schravendijk et al. 1992). Sensitivity to glucose was found to be linked to glucokinase expression, as highly glucose responsive cells were found to have on average, 60% higher glucokinase expression levels. The large variances seen in intracellular calcium responses of individual β -cells at high glucose appeared to parallel these findings (Pralong et al. 1990; Nunemaker et al. 2005).

Further evidence for metabolic heterogeneity among β -cells emerged from the assessment of the redox state of cells under increasing glucose concentrations. Glucose has previously been reported to alter NADH and FAD autofluorescence as it undergoes glycolysis and oxidative phosphorylation, respectively. Substantial differences in the redox state of cells were reported, with metabolic state remaining unchanged at high glucose concentrations in a subset of cells (Pipeleers et al. 2017; Kiekens et al. 1992). Additionally, a further division of labour is

exemplified by reported differences in Fltp (Flattp) protein expression levels where low expression characterises glucose unresponsive, proliferation-competent β -cells (Bader et al. 2016). In favour of high-level heterogeneity, one could argue that differences in metabolic rate, glucose-sensitivity and responsivity allow for more nuanced responses to stimuli, with subtle alterations in activity. If islets were a homogenous aggregate of cells this level of versatility in the system would be lost with detrimental consequences to the organism.

2.1.1 β -cell to β -cell Electrochemical Coupling

With such considerable β -cell diversity, it might seem a remarkable achievement that pancreatic islets have the ability to function as a coherent whole and mount uniform calcium and insulin secretory responses to a glucose challenge (Bergsten et al. 1994). Evidence suggests that gap junctions play a pivotal role in organising β -cells into a functional syncytium by electrochemically coupling them to one another. Gap junctions are protein complexes embedded in the cell membrane, made up of connexins and are selectively permeable to a variety of ions as well as larger molecules. Connexins can assemble as both hetero- and homomeric structures but in the case of β -cells, connexin 36 is the only isoform found to form gap junctional channels between β -cells (Benninger et al. 2008). The importance of cell-cell coupling in islets is underscored by observations from mice homozygous for connexin 36 deletion (Cx36^{-/-} KO) (Head et al. 2012).

Such genetic manipulation resulted in increased basal insulin secretion and more importantly, a lack of synchronised calcium oscillations and pulsatile insulin secretion (Ravier et al. 2005). Later, hyperglycaemic clamp studies confirmed that homozygous Cx36^{-/-} KO animals have a glucose intolerant phenotype (Head et al. 2012). Under physiological conditions, Cx36 channel conductance clamps any cells with closed K_{ATP} channels below threshold membrane potentials and the entire islet remains silent. Upon administration of a glucose bolus, a sharp transition from quiescent to insulin secretory phase takes place in WT islets. In the absence of gap junction coupling (Cx36^{-/-} KO) however, first phase insulin response to a glucose challenge is impaired. The rise in insulin levels occurs earlier, the amplitude of insulin secretion is reduced and the decay time to return to baseline insulin levels is also significantly longer in Cx36^{-/-} KO animals than in WT counterparts (Head et al. 2012). These observations suggested a pivotal role for gap junction coupling in the co-ordinated transition of β -cells from quiescent to a secretory activity. Further, electrophysiological characterisation of Cx36 deficient mice highlighted the

importance of gap junctions in confining β -cell response to a glucose concentration range by appropriately modulating β -cell membrane potential (Speier et al. 2007; Nguyen et al. 2014).

This has consequences for neonatal diabetic disorders where β -cells are inexcitable and fail to secrete insulin. In transgenic mice with Kir6.2 [AAA] mutation the ATP-binding subunit of the K^+ $_{ATP}$ -channel is rendered insensitive to intracellular rises of ATP and thus metabolic oscillations are decoupled from electrical activity in these animals. Consequentially, a sub-population of β -cells is permanently depolarised however, insulin secretion does not occur as the activity of these cells is suppressed by the majority of hyperpolarised cell population in a Cx36-dependent manner. Such intra-islet mechanisms could help preventing the occurrence of persistent hypoglycaemic hyperinsulinaemia (PHH) (Rocheleau et al. 2006). In another animal model of neonatal diabetes, ATP insensitive K^+ channels effectively shift the glucose dose-response of islets to the right, i.e. insulin secretion occurs at much higher glucose thresholds in β -cells. Importantly, >50% reduction in Cx36 coupling in these islets lifts the inhibitory tone of mutant K^+ $_{ATP}$ -channel expressing hyperpolarised β -cells over the rest of the population (Nguyen et al. 2014). This finding has potential therapeutic implications, whereby the modulation of gap junction conductance can overcome the insulin secretory failure of islets.

However, whilst heterogeneity in metabolic activity in β -cells may confer a more nuanced response to stimuli, and gap junctions may explain propagation of electrical activity, others have focussed on the possibility that β -cell heterogeneity actually underpins the ability of an islet to exhibit organised insulin secretory activity. In short, recent studies of islet function have reported the existence of a subpopulation of β -cells that serve to coordinate the electrical activity of the islet.

2.1.2 Islet Connectivity

To understand the concept of the islet as a functional unit it is important to explore what has been discovered about β -cell connectivity. The spatiotemporal dynamics of calcium oscillations from individual β -cells across the islet have been investigated *in vitro* using a number of techniques, particularly electrophysiology (limited to recordings from a small number of β -cells) through to islet-wide calcium imaging. Using different experimental and mathematical approaches a consensus opinion has been convened that functional heterogeneity in β -cells may underpin the observed phenomenon of coordinated calcium waves.

2.1.3 Connectivity Defined as Co-Activity of Cell Pairs

Stozer and colleagues investigated β -cell calcium responses through the lens of network theory. Network theory investigates the pairwise relations between discrete objects, which are termed nodes. In this interpretation, connectivity is defined as co-activity of cell-pairs (i.e. nodes) through Pearson R analysis of their calcium traces (Stozer et al. 2012). Functional connectivity between cell-pairs is defined as having a positive Pearson R-value above a pre-determined threshold, irrespective of Euclidean distance. Connections between cell-pairs are defined as edges and individual nodes (i.e. β -cells) can be characterised by the number of edges (i.e. connections) that they have. In network science this property is referred to as node degree. In order to describe a network's structure, the distribution of node degree can be quantified. Networks that show a high diversity in the distribution of connections follow a power-law distribution:

$$P(k) = Ak^{-\gamma};$$

Where A is a constant that ensures that the $P(k)$ values add up to 1 and the degree component γ is usually in the range $2 < \gamma < 3$ (although not always).

In these types of systems, there is no typical node (i.e. β -cell) that could be used to describe the rest of the nodes (i.e. β -cells) in terms of the number of their connections. Consequentially, the network is referred to as scale-free (Albert 2005). In the islet, under high glucose concentrations, an increased correlation between β -cell pairs was observed, with a disproportionately small number of cells bearing the majority of cell connections (Stozer et al. 2012; Stozer et al. 2013; Markovic et al. 2015).

Further characteristics of β -cell networks were obtained through calculating the average path length between β -cell pairs and clustering coefficients. Path length here is defined as the number of edges (i.e. connections) between two nodes (i.e. cells) along the shortest path connecting them. Meanwhile, the clustering coefficient of cell-pairs is determined by the ratio between the number of connections linking adjacent cells and the total number of possible connections between them. Stozer and colleagues found that with high glucose concentrations the average path length between β -cell pairs had become shorter while β -cells displayed a high propensity to cluster together (i.e. their average clustering co-efficient increased). Together, these three observations suggested that β -cells operate as parts of a scale-free network (Stozer

et al. 2012; Stozler et al. 2013; Markovic et al. 2015). When scale-free networks display a high level of clustering and short average path length, they are typically said to have small-world properties.

The myriad of examples in biological systems of similar small-world scale-free networks is highly suggestive of such topologies conferring an evolutionary benefit. This type of ordering lends robustness to biological systems as any random insult is unlikely to cause a major loss of connectivity within the system. On the other hand, due to the modular nature of scale-free networks, highly interactive hubs emerge which are selectively vulnerable to damage. This makes research into the physiological and pathophysiological relevance of hub cells extremely relevant – with the possibility that they may be highly tractable drug targets.

2.1.4 Hub Cells

With revised statistical tools, a highly-connected β -cell population was subsequently identified which were termed as hub cells. Using an approach previously used to uncover the small-world network properties of pituitary lactotrophs that become upregulated during lactation (Hodson et al. 2012), David Hodson and colleagues applied this analysis to pancreatic islets. The calcium traces from β -cells within *in vitro* imaged islets were binarized by Fourier transformation and the activity regime of each β -cell was plotted as a raster plot. The co-activity coefficient statistic was used to assess co-activity of cell-pairs (Hodson et al. 2012). A probability density function of connections revealed that, in agreement with Stozler's work, the distribution of the most highly connected hub cells follows a power law in keeping with small-world network theory. Furthermore, the time course of the most highly connected hub cells suggested that these cells were acting as pacemakers – with calcium traces that preceded and seem to entrain the activity of linked cells (Johnston et al. 2016).

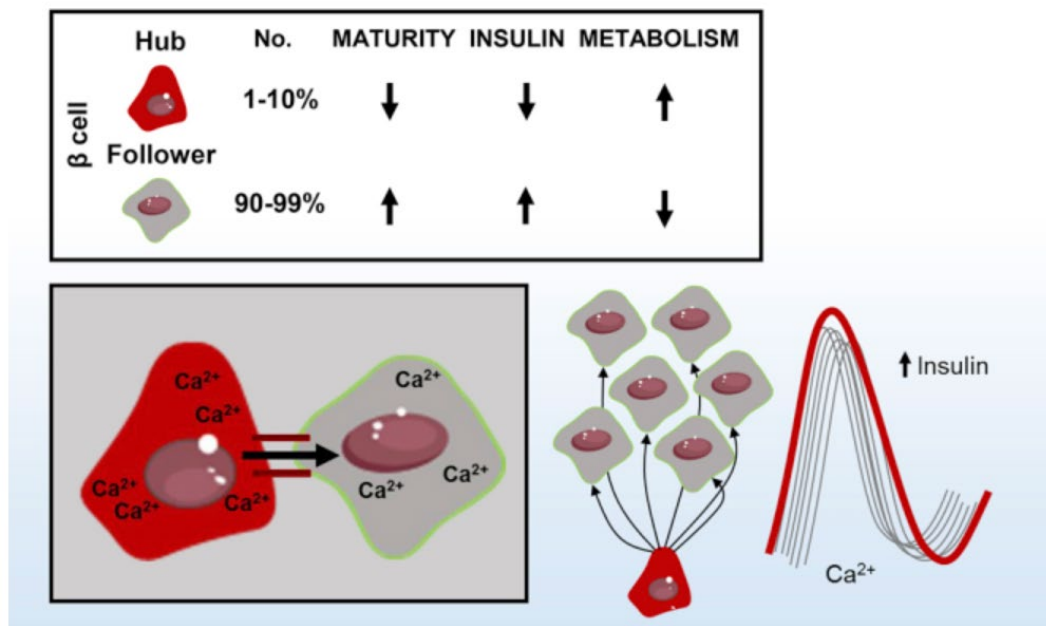


Figure 2.1.4.1 Schematic diagram summarising the properties of hub cells.

Image adapted from Johnston et al. 2016.

Hodson and Rutter went on to provide biochemical and interventional evidence of the functional relevance of hub cells. As unifying evidence for metabolic heterogeneity being linked to the existence of hub cells, they developed a model whereby hub cells could be selectively targeted using a laser to induce “photo uncaging” of β -cells that had been identified. Sorting of these cells revealed that hub cells are characterised by increased glucokinase expression levels, reduced expression of PDX1 and normal levels of the outer mitochondrial receptor TOM20, involved in peptide translocation. Interestingly, a crucial transcription factor NK6 homeobox (Nkx6.1) was almost absent from hub cells, suggesting an insulin hypo-secretory phenotype of these cells (Johnston et al. 2016; figure 6). Because no co-localisation of glucagon and insulin antibodies was detected in these cells, it is unlikely that hub-cells are multi-hormonal. Further, hub cells were not stained for neurogenin 3 (Ngn3) an early β -cell progenitor marker which suggested that hub population is unlikely to have an immature (i.e. progenitor-like) phenotype. Morphological characterisation at the sub-cellular level showed normal mitochondrial distribution and shape as well as endoplasmic reticulum content of these cells. Of note, the Ca^{2+} /ATPase SERCA2, a calcium transporter expressed in the sarco(endo)plasmic reticulum showed marked reductions in this sub-population of β -cells. Together, these experiments

uncovered a highly glucose-sensitive, hypo-secretory metabolic phenotype of hub cells which show signs of both mature and immature β -cell identity. The crucial experiment to ascertain the functional relevance of hub cells was performed using islets encoded to express an inhibitory halorhodopsin in its β -cells. The targeting of follower cells was without impact in terms of pan-islet calcium activity. On the other hand, the hyperpolarization of identified hub cells led to the derangement of synchronised calcium oscillations. To further examine the consequences of this intervention on insulin secretion, the group utilised the cell surface attached fluorescent Zn^{2+} probe JP-107 (Pancholi et al. 2014). Zn^{2+} is co-secreted with insulin and thus, can be used as a surrogate marker for insulin secretion. These sensors localize to the external surface of β -cells whereby their fluorescence increases upon coming into contact with Zn^{2+} . In this set-up, the temporary silencing of followers was without effect, as was evidenced by a linear increase in JP-107 fluorescence. In contrast, the silencing of a hub cell lowered Zn^{2+} release and thus, insulin secretion (Johnston et al. 2016; figure 5).

2.1.5 Initiators and propagators

Other groups have also successfully combined imaging techniques, mathematical tools and molecular biology to interrogate the islet as a functional unit. The Benninger lab has characterised the effects of electrical heterogeneity on islet function. Through the use of transgenic Kir6.2[Δ N30,K185Q] expressing islets in the presence of normal gap junction coupling (WT; Cx36^{+/+}) they provided evidence for critical behaviour within pancreatic islets. Kir6.2[Δ N30,K185Q] mutation causes the Kir6.2 subunit of K_{ATP} channels to be overactive and thus render β -cells inexcitable. With both experimental and computer simulation approaches, it was revealed that up to 20% of the β -cell population can be rendered inactive before any disruption to synchronised calcium oscillations occur. When 10-30% of cells are rendered inactive, critical behaviour emerges with a disruption in co-ordinated calcium oscillations. Beyond 30%, pan-islet calcium dynamics are completely deranged with only sporadic calcium activity visible. Through simulation experiments, it was revealed that in the presence of low gap junction conductance, a greater number of inactive cells are accommodated for before any apparent disruption to calcium oscillations. With increased gap junction coupling in the islet the critical threshold for the percentage of inexcitable cells was shifted to left (i.e. fewer cells necessary to disrupt calcium oscillations in this instance) (Hraha et al. 2014). Crucially, the

heterogeneous distribution of gap junction coupling was necessary for critical behaviour to emerge.

To investigate the effects of the spatial distribution of metabolic heterogeneity, Benninger and colleagues used a microfluidics device that allowed fine control over glucose concentrations of one side of the islet. In these experiments it was observed that waves were initiated from areas that were exposed to high levels of glucose and preferentially propagated away from the side that was exposed to high glucose. Importantly, the initiation site could be dynamically changed suggesting that there were no fixed wave initiation points. These observations suggested that islet wave initiation areas are characterised by high metabolic activity. In addition, they determined that K^+ and Ca^{2+} electrochemical gradients are not a determining factor in calcium wave propagation (Benninger et al. 2014). These initial findings were further extended, and it was revealed that wave initiation areas are more hyperpolarised and show reduced metabolic activity and therefore these cells were termed as wave initiators. Wave propagators on the other hand, were more excitable and displayed a higher metabolic rate and thus propagated calcium waves more efficiently (for more detail please see Section 2.4 Discussion) (Westacott et al. 2017).

2.1.6 Functional Connectivity of β -Cells *In Vivo*

To date, all work investigating the existence of β -cell functional hierarchies and their relationship to β -cell coordination had been done under *in vitro* conditions. The crucial question as to whether these emergent phenomena were retained or modulated *in vivo* was unknown. To this end, we established and optimised a powerful *in vivo* imaging platform in our lab to longitudinally monitor the calcium dynamics of pancreatic islets. Donor islets with β -cell specific GCaMP6f expression were transplanted into the anterior chamber of the eye and imaged under low and high glucose concentrations. With updated statistical tools, we provide evidence for the existence of functional β -cell connectivity and leader β -cells *in vivo*, furthering evidence for their physiological relevance.

The islet in the eye platform had been established at the Karolinska Institute, led by PO Berggren, applied to investigate islet morphology but not islet function. In this model, islets transplanted into the anterior chamber implant fully by one month, developing a functional capillary network as well as fully re-innervating. There is no immune-response mediated loss to

islets implanted into the anterior chamber due to the eye's unique environment in which pro-inflammatory responses are suppressed, aided by the use of a syngeneic model where possible. Since the transparent cornea acts as a natural optical window, fully implanted islets can be imaged in the eye and over time the same cells can be re-identified across different imaging sessions.

2.1.5. Aims and Hypothesis

- 1) To establish and optimise islet in the eye *in vivo* imaging platform in our lab in order to longitudinally investigate mouse and human β -cell function *in vivo*

***In vitro* aims:**

- 2) To generate a fluorescent calcium indicator in an adenovirus backbone

***In vivo* aims:**

- 3) To characterise the calcium dynamics of adenovirus infected mouse and human β -cells
- 4) To generate transgenic animals that express a fluorescent calcium reporter in their β -cells
- 5) To characterise calcium dynamics in transgenic islets
- 6) To analyse cell-pair coordination and the presence of functional heterogeneity *in vivo*

Hypotheses:

- 1) The islet in eye imaging platform is a suitable model to investigate *in vivo* calcium dynamics
- 2) β -cells calcium dynamics differ at low and high blood glucose levels
- 3) β -cells become more connected at elevated glucose levels and retain evidence of hub cell morphology *in vivo*.

2.2 Materials and Methods

2.2.1 Animal Husbandry

Male (18-25g) wild type (WT) C57BL6/J WT or Balbc/Nu recipient and syngeneic donor mice were group-housed in individually ventilated cages under controlled conditions (21-23°C; 12h light:12h dark cycle) with ad libitum access to standard chow and water. Transgenic animals were generated using the Cre/Lox system and sacrificed for their islets. In brief, InsCre animals (provided by J. Ferrer, Imperial College London) were crossed with mice that expressed the cytosolic calcium indicator GCaMP6f downstream of a LoxP-flanked STOP cassette. In essence this produced donor pancreatic islets with highly efficient expression of the calcium fluorophore GCaMP6f selectively in their β -cells. This study was conducted under the project licence PA03F7F07A (project licence holder Dr Isabelle Leclerc). All procedures were in compliance with the UK Home Office Animals (Scientific Procedures) Act 1986.

2.2.2 Islet Isolation

In order to digest the exocrine and connective tissue surrounding islets, filtered collagenase solution was prepared at 1mg/ml and kept on wet ice at all times (as described in Li et al. 2009; Ravier and Rutter 2010). WT and transgenic syngeneic donors were sacrificed (Schedule 1) and the peritoneum excised to reveal the internal organs. Next, the sphincter of Oddi was clamped and the common bile duct identified. Using a 30G needle, pancreata were perfused with 3-5ml collagenase solution via the common bile duct. Once fully sufflated, the pancreas was excised and placed in a tube on wet ice. Tubes were placed in a water bath and incubated at 37°C for 10mins to allow collagenase digestion to take place. Then a series of washing and centrifuging steps (1000RPM for 1min each time) followed to remove any connective tissue. At the end of the 4th round, islets were separated by generating a ficoll gradient with Histopaques 1119 and 1083 and serum-free RPMI-1640 medium. Tubes were centrifuged at 2500RPM for 20mins with slow deceleration to avoid intermixing phases. Islets settled at the interphase of second and third layers from where they were aspirated and incubated in a petri dish in RPMI-1640 medium supplemented with FBS, penicillin and streptomycin and glutamate at 37°C; 5% CO₂. Islets were left to recover overnight before implanting them into the anterior chamber of the eye.

2.2.3 Human Islet Donors

Human islets were sourced from multiple institutions including University of Alberta, Edmonton, Canada (Patrick Macdonald and James Shapiro) and University of Pisa, Italy (Piero Marchetti). Permission for the use of human tissue was provided at Imperial College London by the Charing Cross Research Ethics Committee, REC reference no. 07/H0711/114. Human islets were obtained post mortem with next-of-kin and local and ethical permission at the sites of procurement. Data from 11 individual human islets coming from four donors (age range was 14-74; non-diabetic; body mass index (BMI) of 21.5-29.6kg/m²). Data for two islets provided here came from a single donor diagnosed with Type 2 diabetes (female; 54 years old; BMI of 24.4kg/m²; type 2 diabetic for 10 years and insulin-dependent for the last 1.5 years prior to death). For more details on human donor characteristics please see 10 Appendix. To visualise calcium dynamics, human islets were infected with the adenoviral construct AV-GCaMP6m prior to their implantation into the anterior eye chamber of BALB/c Nude mouse recipients (as described in Section 2.2.7).

2.2.4 Generation of Adenovirus Expressing AV-GCaMP6m

Prior to the generation of Ins1-Cre driven GCaMP expression in mouse islets, or for use in human islets, it was necessary to develop a viral vector to attain β -cell specific expression of GCaMP. The cytomegalovirus (CMV) promoter driven GCaMP6m adenoviral construct (CMV-AV-GCaMP6m) was generated using the pAdEasy system as previously described (Luo et al 2007). Briefly, the pGP-CMV-GCaMP6m plasmid (Addgene plasmid # 40754) was digested using the restriction enzymes *Bgl*III and *Not*I to release the GCaMP6m fragment. The GCaMP6m fragment was then purified and ligated into the pShuttle-CMV vector (Addgene plasmid #16403). Through restriction enzyme analysis and sequencing the presence of the insert was confirmed after each step. BJ5183 electrocompetent *E. Coli* cells (Addgene plasmid #16398) whose DNA is prone to homologous recombination events were transformed with pShuttle-CMV-GCaMP6m. Selective growth medium was used so that only those BJ5183 bacterial colonies where recombination had taken place to express pAdEasy-CMV-GCaMP6m vector with a kanamycin resistance gene survived. Next, the pAdEasy-CMV-GCaMP6m construct was amplified in NEB-10 β competent *E. Coli*. (New England BioLabs) and subsequently the plasmid was purified. To become fully competent, AD293 viral packaging cells were planted in a 25cm² tissue flask and transfected them with the linearized pAdEasy-CMV-GCaMP6m construct in the presence of calcium-phosphate and incubated at 37°C; 5% CO₂ for approximately 3 weeks. Cells

containing virions were collected and lysed to release our construct. The virus was further amplified and subsequently purified by subjecting it to high speed, overnight centrifugation on a CsCl₂ gradient. Virus titration was performed using serial diluted viral stocks in AD293 cells using GCaMP6m fluorescence as guidance.

2.2.5 Infection of Islets with AV-CMV-GCaMP6m

C57Bl6/J WT donor islets were infected with an adenovirus construct expressing the calcium-sensitive fluorophore, GCaMP6m. Following isolation, islets were incubated overnight (at 37°C; 5% CO₂) with the pAdEasy-CMV-GCaMP6m viral construct at the multiplicity of infection (MOI) of 20.

2.2.6 Generation of the InsCre-GCaMP6f line

GCaMP^{flox/flox} animals were bought from the Jackson Laboratory (Stock No. 028865). Mice were bred from heterozygous or homozygous GCaMP^{stopflox/stopflox} animal crossed with animals expressing Cre-recombinase under the Ins1 promoter (kindly donated by Prof Jorge Ferrer, Section of Epigenomics and Disease, Imperial College London). The genotype of animals was determined using Kapa HotStart Mouse genotyping kit (Sigma-Aldrich; for details see 2 Appendix).

The two GCaMP6 constructs used herein are comparable in terms of their sensitivity to intracellular Ca²⁺ dynamics and their rate of fluorescence increase, with the signal decay time being marginally improved for the GCaMP6 construct with fast kinetics (i.e. GCaMP6f). (Chen et al. 2013). Due to similar kinetics, the comparison of changes in the 'M' and 'F' subtypes of GCaMP6 fluorescence was deemed appropriate here.

2.2.7 Pancreatic Islet Transplantation into the Anterior Chamber of the Murine Eye

C57BL6/J adenoviral infected WT or transgenic islets were transplanted into the eyes of syngeneic recipients. AV-GCaMP6m-expressing islets were infected the day before transplantation to allow virus penetration overnight. To start, animals were anaesthetised in an induction chamber with 5% isoflurane (mixed with 95% O₂). Pedal reflexes were checked to assess depth of anaesthesia and animals were placed in a stereotactic head holder under 2-3% isoflurane. Using a 25G needle an incision was made at the corneo-scleral junction with great care taken not to damage the iris. The needle was carefully removed and a 27G blunt end cannula pre-loaded with islets in 20µl RPMI medium was inserted into the ACE. Islets were

gently expelled with a manually operated 100µl Hamilton syringe that was attached to the cannula. Islets were left to settle on top of the iris and carprofen ointment was applied topically. Islets fully implanted over the course of 4 weeks.

2.2.8 Imaging Protocol

All *in vivo* imaging experiments were performed with a spinning disk confocal microscopy (Nikon Eclipse Ti, Crest spinning disk, 20x water dipping 1.0 NA objective). Prior to imaging, animals were anaesthetised in an induction chamber with 5% isoflurane 95% O₂ mix and placed in a stereotactic head holder on a heated stage. AV-transduced and transgenic islets GCaMP expressing islets were excited at 488nm at 300msec exposure time (100% laser power). All islets analysed for connectivity were imaged in stream modality at speed of 3Hz except for long-acquisition experiments where islets were imaged at 1Hz for 10mins at a time continuously. Image sequences were recorded under both low (<4mmol/L) and high (>12mmol/L) glucose levels with each image sequence consisting of 401 frames. The Z-depth was adjusted manually where possible, to correct for movement artefacts.

3-D imaging (XYZT) was carried out in stream modality at a rate of 3Hz (ex.:488nm) using a Piezo Nano-positioner attached to the 20x objective. The Piezo device allowed for rapid tissue sampling which we carried out with 10µm spacing. We imaged three consecutive cell layers meaning that there was approximately 900msec interval between two time-points of the same cell layer.

Blood glucose sampling during imaging sessions was carried out from a tail nick with a standard glucometer (Accu-Chek), prior to image acquisition or every 2mins during long acquisition time-series experiments. Cut-off values were determined as <4mmol/L (mean blood glucose being: 3.4mmol/L ± 0.63 SEM) and >12mmol/L (mean blood glucose being: 16mmol/L ± 2.9 SEM) for low and high blood glucose levels, respectively. To achieve blood glucose levels of ≤4mmol/L, insulin at 1U/kg (Actrapid) administered intravenously (IV) or intraperitoneally (IP). To elevate blood glucose levels 20% D-glucose dissolved in sterile saline solution was administered (up to 200µl for 30g mouse) via either IV or IP routes.

AV-CMV-GCaMP6m transduced human islets were transplanted into the ACE of BALB/c Nude mice (immunosuppressed) and cut-off values for glycaemia were determined to be <4mmol/L

and >7mmol/L, for low and high glucose conditions, respectively. Islets were imaged in stream modality at 3Hz with a total of 401 time-points per imaging session (ex.: 488nm).

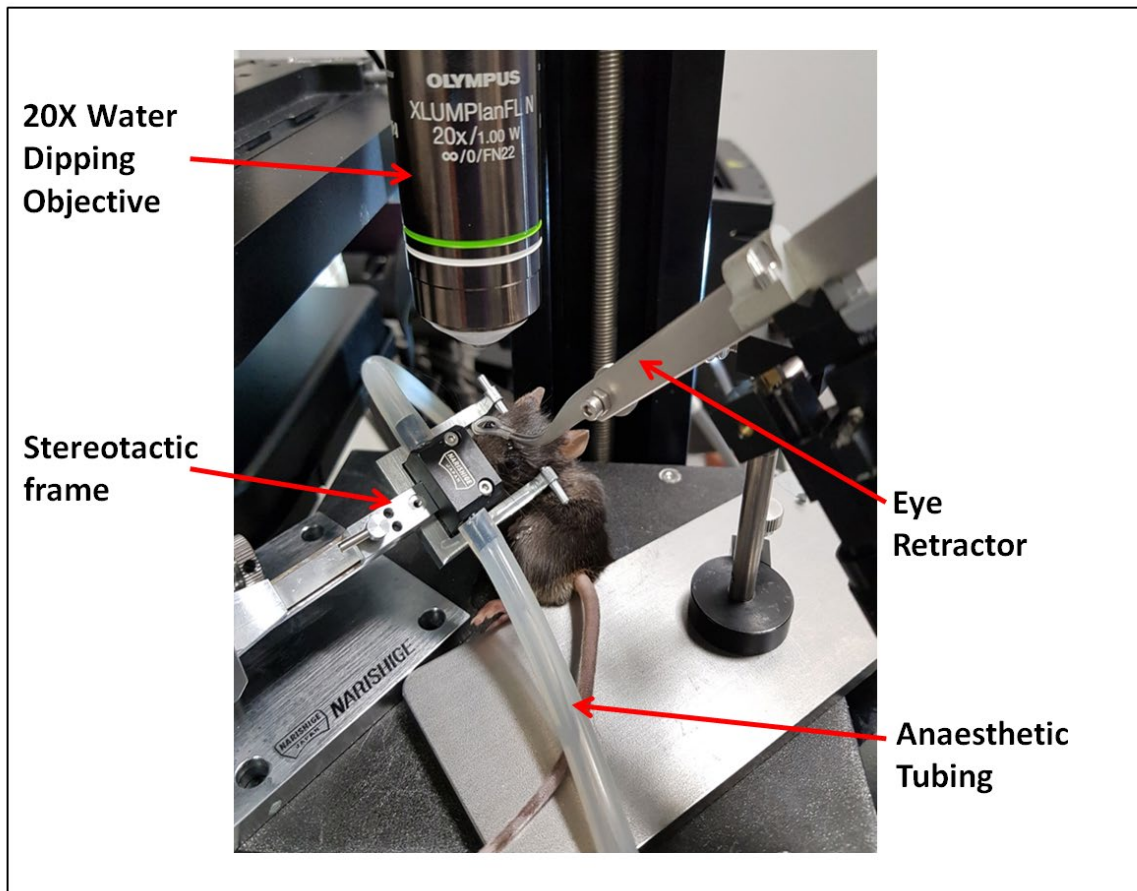


Figure 2.2.8.1 Photography of the microscopy set-up and mouse with islets transplanted in his eyes.

2.2.9 Image Analysis

All images (2048x2048 pixels; 16 bit) were processed and analysed using FIJI. This custom-made macro by Stephen Rothery (FILM, Imperial College London) allows the user to manually align a time-series experiment with a Region of Interest (ROI) as a point of reference.

Each frame in an individual sequence was checked and frames were removed if the image quality was poor or the Z-depth was different from the frame containing pre-determined ROIs for that particular image sequence. Image sequences were time-stamped to ensure that the absolute temporal information of files is maintained and not affected by the removal of frames.

Each identified cell was assigned an ROI which covered a subcellular region. As GCaMP6f is a cytosolic calcium indicator, it is excluded from the nuclei. This negative shadow of β -cell nucleus was used as guidance and ROIs were placed adjacent to these on images. Image

sequences were motion-corrected for each identified ROI individually to ascertain continuous sampling from the same cell. The XY coordinates of each ROI were also recorded and used to generate connectivity line maps (Johnston et al. 2016).

2.2.10 Pearson R Analysis

Pearson R correlation analysis of calcium traces was performed in MatLab. Calcium traces were normalised and smoothed using prospective time-points in the dataset. Pearson correlation between individual cell-pairs was determined, excluding autocorrelation and an R-value of 0.25 was set as threshold value to signify a connection. Data was resampled using boot strapping to increase accuracy of findings (R-values with $P < 0.001$ were deemed statistically significant). R-values were binned as follows: 0.25-0.50, 0.5-0.75 and 0.75-1 and considered to signify weak, medium or strong connections, respectively. Cartesian line maps showing beta cell connectivity were generated on the basis of cell XY coordinates and connections were assigned yellow, green or red depending on strength of connections. Heat-map matrices show the R-values for each individual cell pair, with an R value of 1 is assigned for autocorrelation.

2.2.11 Granger Causality Analysis

For Granger causality analysis, the time course of every individual ROI (β -cell) was compared with every other ROI using Granger causality analysis with a time lag of 1-3sec. This was then subjected to Bonferroni's multiple comparison test ($P < 0.001$). Thus, every ROI examined in the islet had a number assigned to it for the number of other cells in that islet to which it was statistically significantly causally associated. Since previously other people had noted that 1-10% of cells act as hubs (Johnston et al. 2016) the top 10% of cells in a given islet with the highest number of Granger connections were chosen and were defined as Granger Leaders. Cells identified through Granger analysis were compared with the Leader cells that were simply identified on an islet as the first to fire in a set of calcium waves. Granger analysis was performed by Dr Salem on the scripts she developed with Prof Distaso.

2.3 Results

2.3.1 AV-CMV-GCaMP6m-infected islets

AV-CMV-GCaMP6m-expressing islets successfully implanted into the anterior chamber and remained there throughout the lifetime of the animal (**Figure 2.3.1.1** >1year after transplantation).

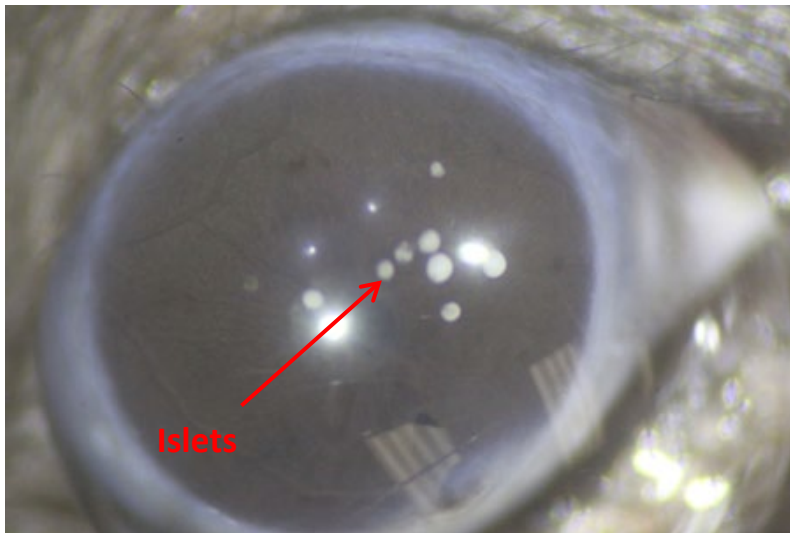


Figure 2.3.1.1 Photography of the implanted islets in the mouse eye anterior chamber.

After full implantation islets were imaged according to the protocol outlined above (n=5 animals).

Both intensity and the number of cells expressing the calcium indicator diminished over time. Nevertheless, as a proof of concept, we were able to interrogate the calcium dynamics of 10-15 cells in AV-CMV-GCaMP6m infected islets under both low and high circulating glucoses (**Figure 2.3.1.2 A**) There was an increase in spiking frequency and amplitude in β -cells upon IV administration of 20% D-glucose (**Figure 2.3.1.2 B**).

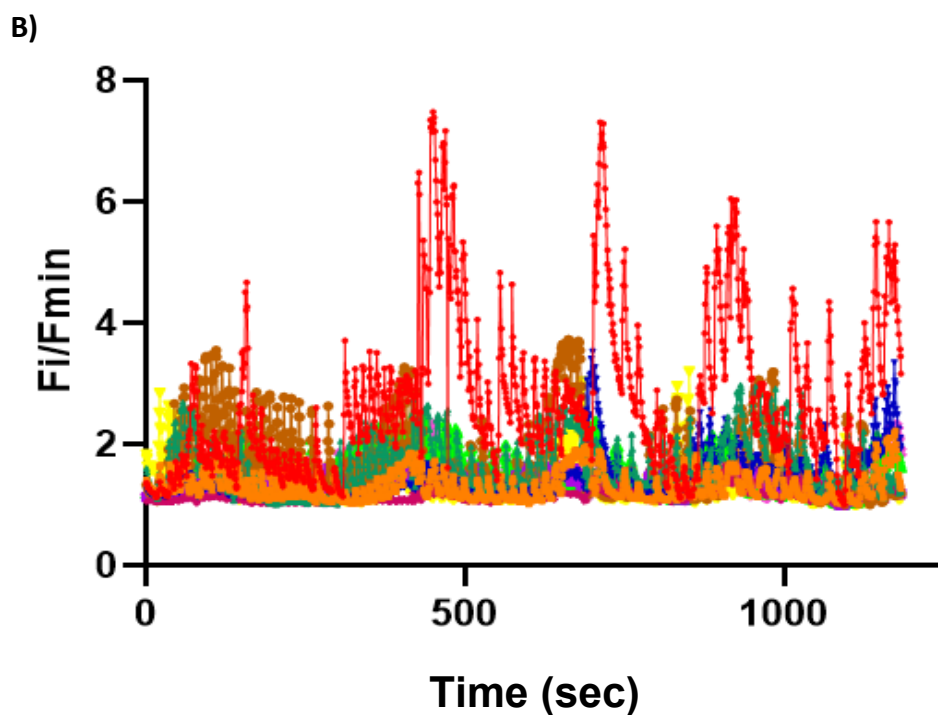
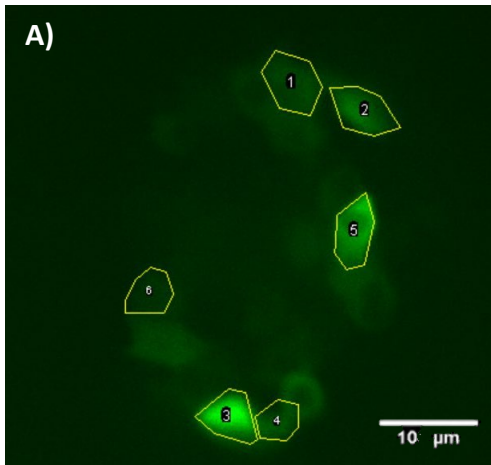


Figure 2.3.1.2 Representative Ca^{+2} traces of individual AV-CMV-GCaMP6m-expressing β -cells (n=6) transplanted into the eye. Ca^{+2} dynamics from β -cells implanted in the eye could be readily imaged (A). Ca^{+2} traces were normalised to the minimum intensity value within the sequence for each β -cell. The frame rate was 1 frame per second (B).

To assess cell coordination, the normalised calcium traces of cells were subjected to Pearson R correlation analysis which revealed an increased connectivity between cells under high glucose levels. Pearson R correlation analysis was performed to assess the level of connectivity between cells. With increased circulating glucose, the number and strength of

connections between cell-pairs increased, expressed as percentage connectivity and average correlation co-efficient values (**Figure 2.3.1.3 A and B.**). The proportion of Pearson connected cells increased from $38 \pm 11\%$ to $65 \pm 9\%$ ($n=5$; $P=0.028$) with a non-significant ($P=0.11$) rise in the mean co-efficient of connectivity from 0.54 ± 0.03 to 0.63 ± 0.04 (**Figure 2.3.1.3**). For small-world network analysis it was imperative that we increased the number of cells interrogated. For this purpose, we bred animals with the genetically encoded calcium indicator (GECI) GCaMP6f expressed under the control of Ins1 promoter.

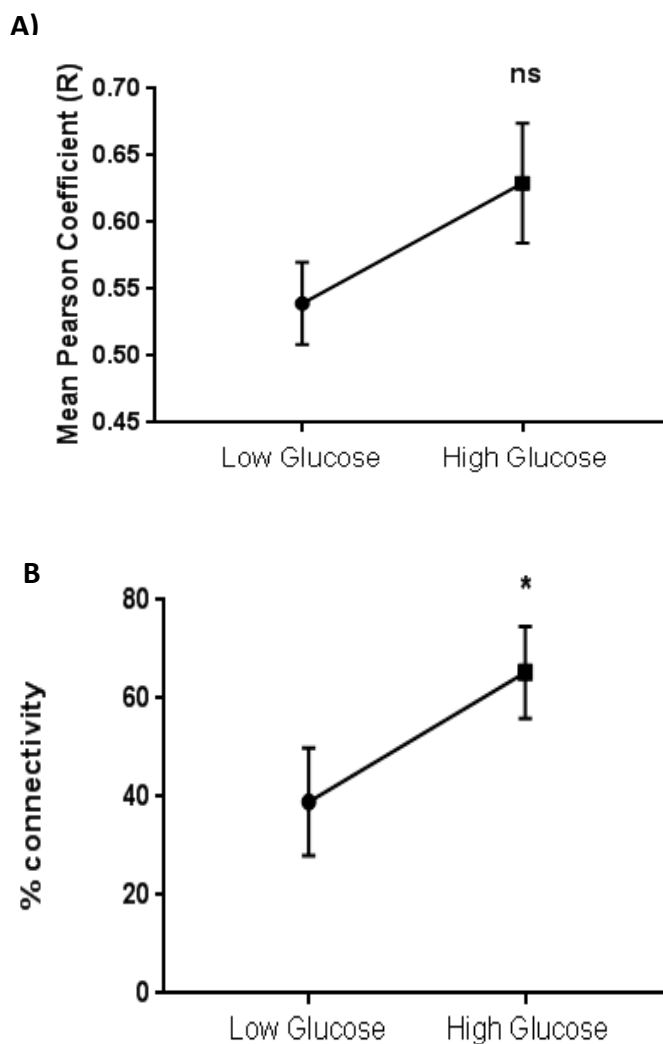


Figure 2.3.1.3 Pooled data from four AV-CMV-GCaMP6m expressing islets displays increased cell connectivity under high glucose concentrations. Both the average connectivity co-efficient (A) and the percentage connectivity (B) of β -cells increase under high circulating glucose conditions *in vivo* ($P < 0.001$ on a paired, two-tailed, Student's t-test).

2.3.2 High Glucose Levels Enhance β -Cell Connectivity in Ins1Cre-GCaMP6f-Expressing Islets

Through the use of transgenic Ins1Cre-GCaMP6f expressing islets we were able to achieve a β -cell specific expression of GCaMP. This type of genetic manipulation resulted in $\sim 95\%$ of all β -cells expressing the fluorescent calcium indicator (Thorens et al. 2015). Transgenic islets provided a calcium read-out that was superior to previously used virally loaded islets and therefore we used Ins1Cre-GCaMP6f expressing islets in the ensuing experiments (**Figure 2.3.2.1**).

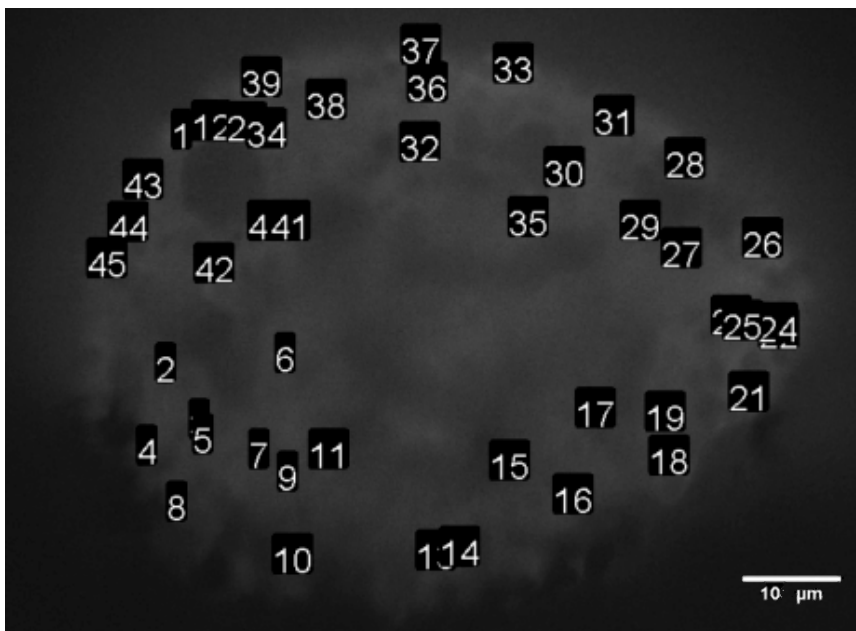


Figure 2.3.2.1 Representative image from a time-series experiment showing identified cells in an InsCre-GCaMP6f expressing islet. Regions of interests (ROI) (ie. cells; ~ 50 /islet) were identified in a contrast-enhanced cross section of the islet and their calcium responses were recorded under low (BM of <10 mmol/L) and high blood glucose (BM of >10 mmol/L).

With this method between 40 to 50 β -cells were identified in an individual islet. We successfully re-identified the same β -cells under low (<4 mmol/L) and high glucose (>12 mmol/L) and recorded their calcium activity (**Figure 2.3.2.1**). At high blood glucose levels, intracellular Ca^{2+} increased in the majority of β -cells with a small time lag and spread across the entire islet cross-section giving the impression of a ‘calcium wave’. This phenomenon was not observed previously in AV-infected islets presumably due to scarcity of AV-GCaMP6m signal in the islet core. We consistently observed the same behaviour in all

islets investigated at 8mmol/L blood glucose and beyond (n=10). Calcium waves were initiated at distinct sites and propagated at $120 \pm 3.4 \mu\text{m s}^{-1}$ (n = 5 wave bursts) velocity.

2.3.3 Enhanced β -Cell Connectivity in Ins1Cre-GCaMP6f-Expressing Islets under High Glucose Concentrations *in vivo*

Islets were quiescent under low blood glucose levels (**Figure 2.3.3.1** and **Figure 2.3.3.2**) and showed rhythmic calcium activity at elevated glucose levels. Pearson R-analyses of islets revealed that high circulating glucose results in elevated correlation co-efficient values of cell-pairs, as seen in Cartesian maps and heat matrices.

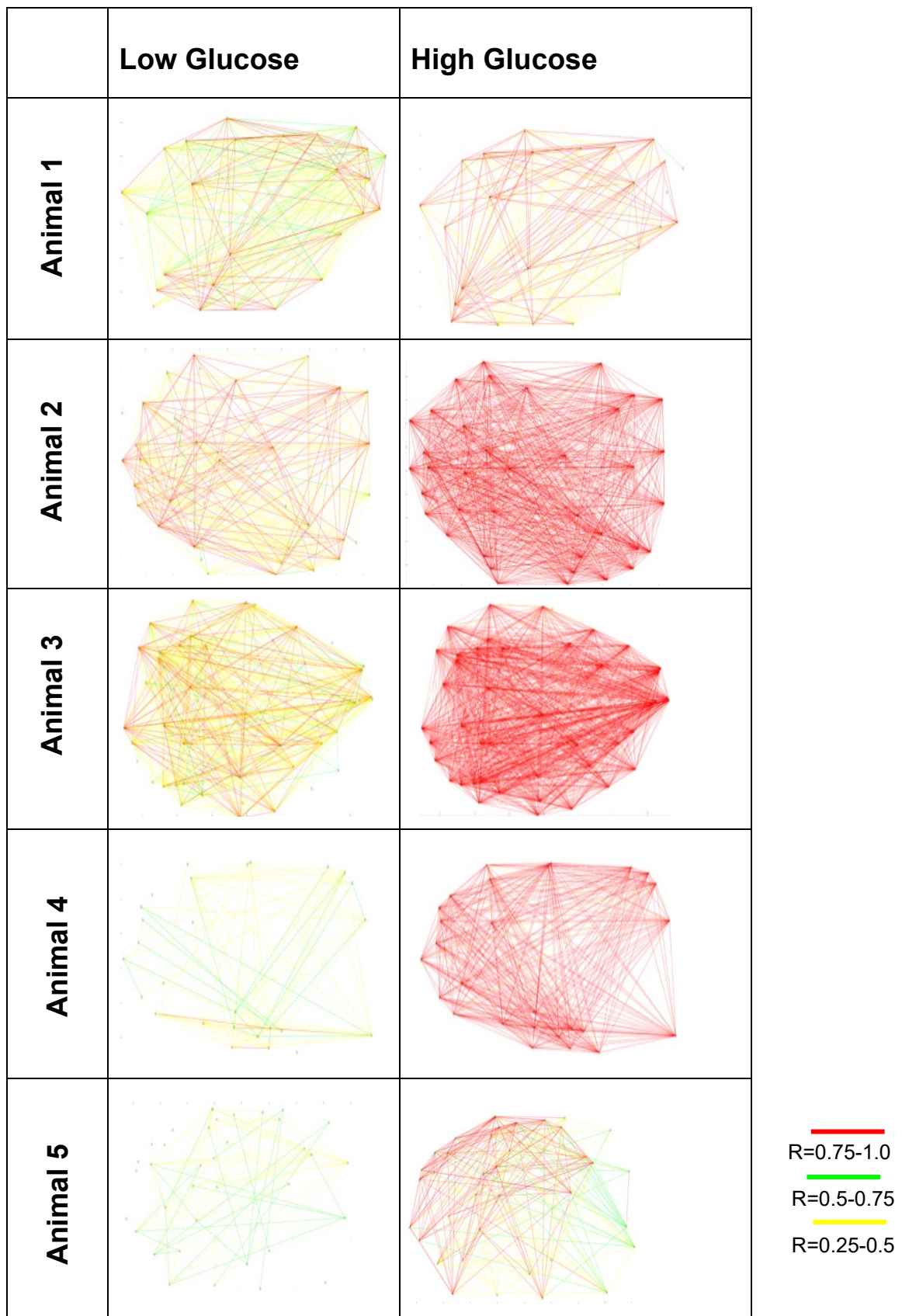


Figure 2.3.3.1 Increased β -cell connectivity under high circulating glucose conditions in InsCre-GCaMP6f islets (n=5).

β -cells displayed a highly synchronised behaviour under high blood glucose levels as reflected in an increase in the R-value of cell-cell connections. Individual cell connections were colour coded to demonstrate changes in the strength of connections.

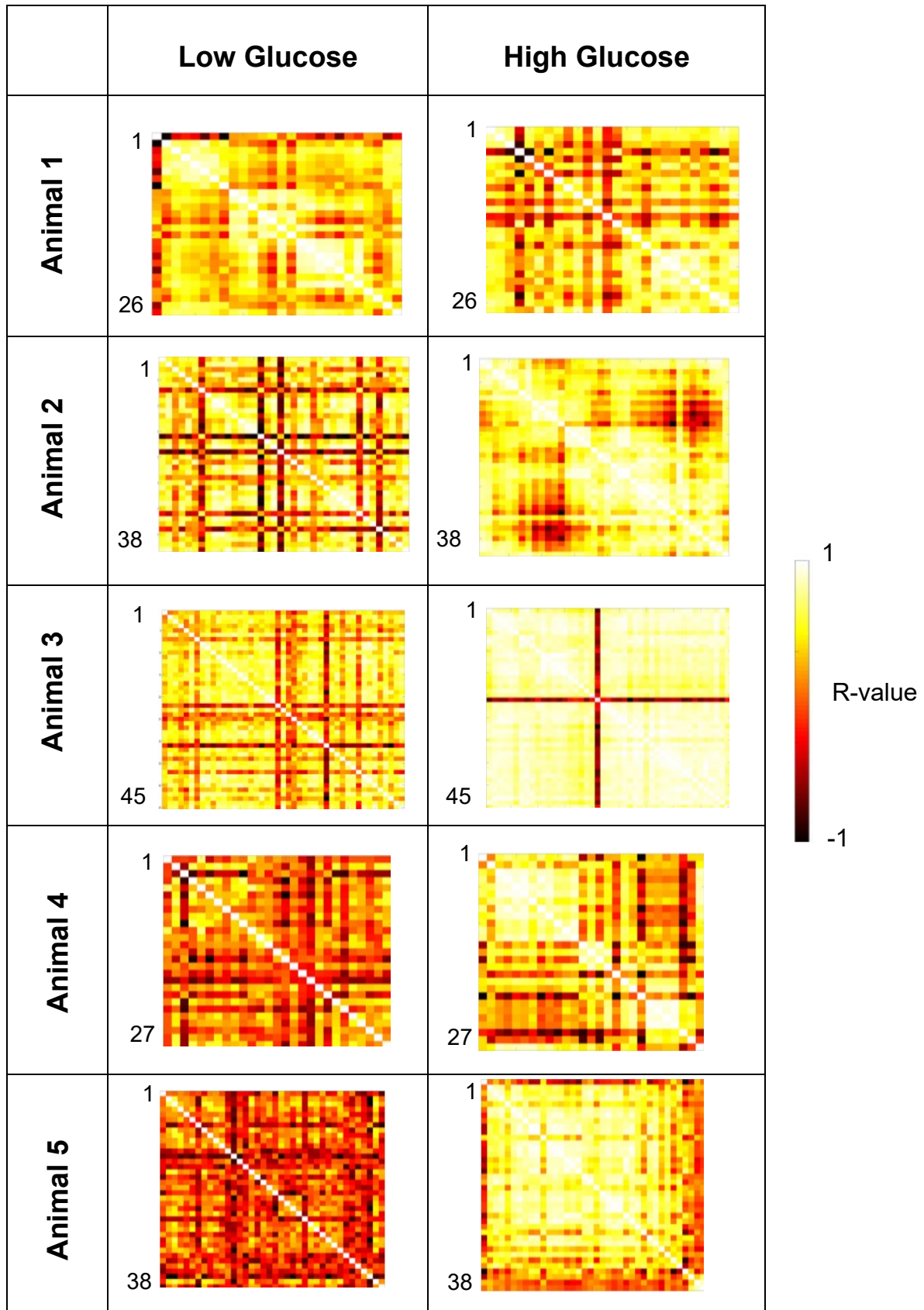
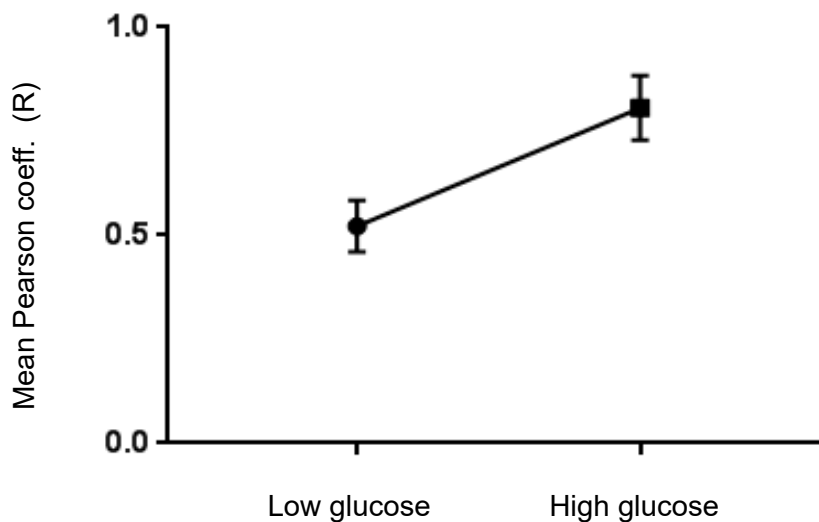


Figure 2.3.3.2 Increased β -cell connectivity under high circulating glucose conditions in InsCre-GCaMP6f islets (n=5).

Heatmaps showing Pearson R correlation co-efficient changes between all possible cell-pairs in a given islet. The Pearson R-value for cell autocorrelation is always 1 (see R-values of 1 denoted in white running diagonally across matrices.)

The average correlation co-efficient values increased from 0.46 ± 0.07 to 0.93 ± 0.09 (**Figure 2.3.3.3 A**; $P < 0.01$) and the percentage connectivity increased from $19.7 \pm 5.5\%$ to $88.8 \pm 5.9\%$ (**Figure 2.3.3.3 B**; $P < 0.001$). Similarly, β -cell connectivity increased when islets were subjected to a prolonged glucose stimulus (imaged for 10mins at 1Hz). Additionally, the use of an alternative anaesthetic agent, ketamine and xylazine did not abrogate the effects of high circulating glucose to enhance β -cell connectivity (data not shown).

A)



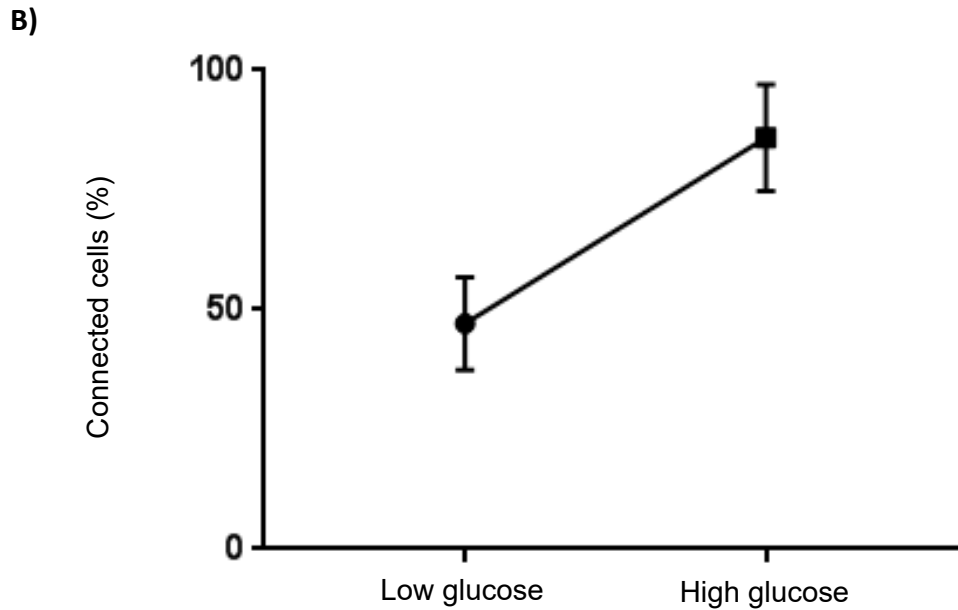


Figure 2.3.3.3 Pooled data from five *InsCre-GCaMP6f* expressing islets showing enhanced connectivity under high glucose concentrations.

The average connectivity co-efficient (A) and the percentage connectivity ($p < 0.01$) (B) of β -cells increase under high circulating glucose conditions in vivo ($p < 0.001$; paired, two-tailed, Student's t-test).

For the purposes of investigating whether β -cell connectivity extends over multiple cell layers, a Piezo device was installed which allowed the objective to be rapidly and accurately moved along the Z-direction. Results obtained mirrored those from single-plane recordings; elevated glucose levels enhanced β -cell connectivity between cells and encompassed cells from three consecutive cell layers (**Figure 2.3.3.4**).

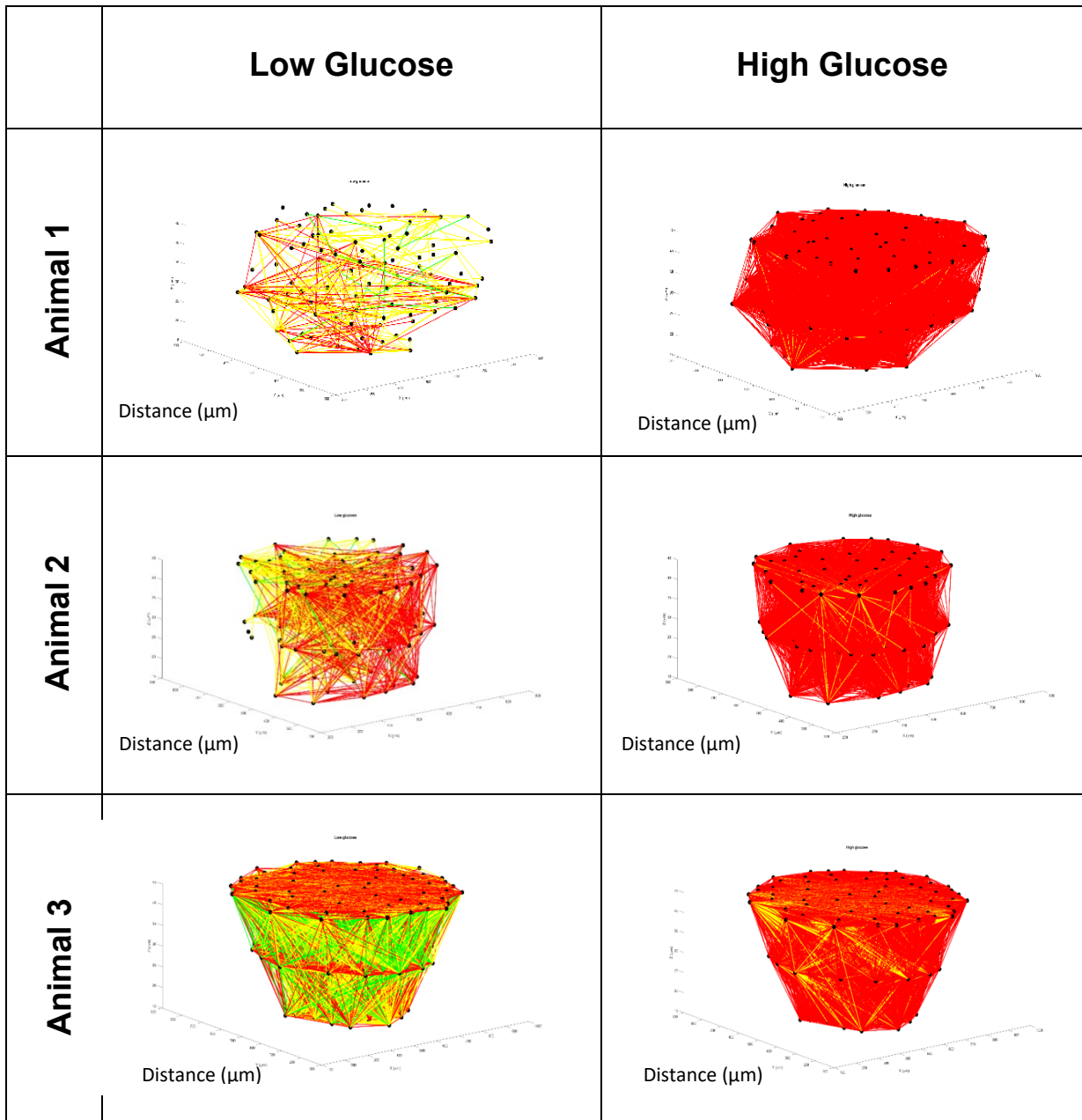
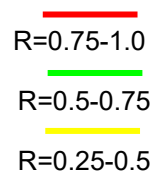


Figure 2.3.3.4 Cartesian maps showing increased β -cell connectivity 3-dimensionally under high circulating blood glucose.

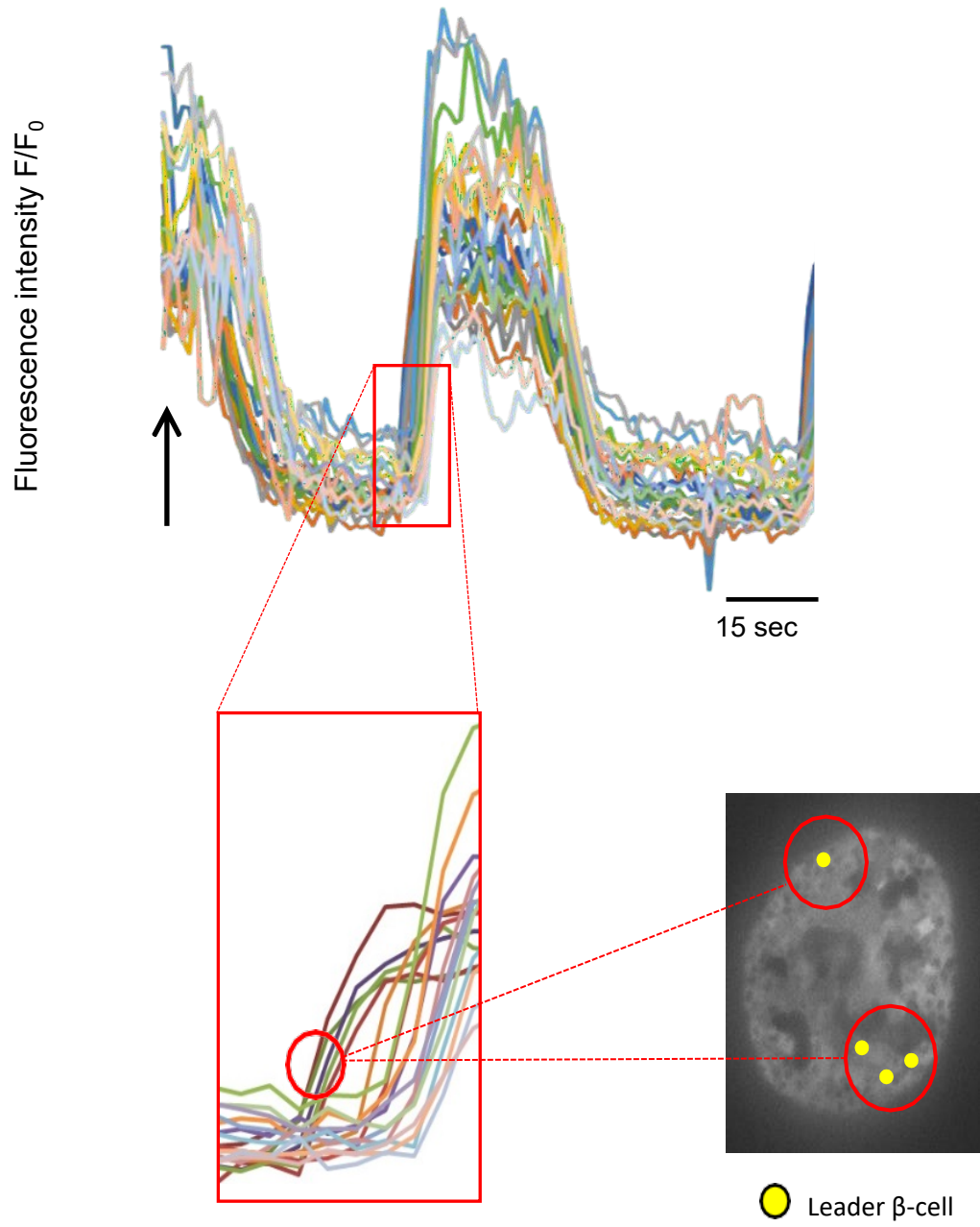
XYZT time-series experiments were recorded at 3fps with 10 μ m Z-spacing to ascertain capturing of three consecutive cell layers along the Z-plane. 3-dimensional findings were in agreement with recordings from a single Z-plane.



2.3.4 Temporally-Defined Leader Cells are Highly Connected and Causally Predict the Behaviour of the Majority of Cell Studied in the Islet

Johnston et al. identified hub cells as those that were highly connected to all other cells in the islet (i.e. the top 10% of cells harbouring the highest number of connections) and also happened to be pacemakers (i.e. their activity preceded and co-ordinated the activity of others). To test the role of highly connected β -cells in the initiation of a train of calcium waves, we first visually identified β -cells which consistently fired first, preceding the activity of the remainder of the population (**Figure 2.3.3.6 A**). We termed these cells as “leader cells”. Next, individual cell-pairs were subjected to Granger causality analysis to assess whether cells causally predicted the activity of one another. Granger cells that causally predicted the activity of the most number of cells were identified and compared against leader cells. Interestingly, leader cells tended to be those with the greatest number of causally linked followers, suggesting that this β -cell subpopulation might play a role in orchestrating calcium responses under high blood glucose levels in the living mouse (**Figure 2.3.3.6 B**). Of note, there was no clear preference for these cells to be located adjacent to each other or in the close vicinity of blood vessels.

A)



B)

Mouse islet (GCaMP6 driven by insulin promoter) [Number of ROIs i.e. cells analysed]	Temporally defined leader cell (numbered 1 – 4 i.e. the first responders to high glucose)	Number of cells to which the temporally-defined leader is causally connected on independent Granger analysis
#1 [26]	1	26
	2	26
	3	26
	4	26
#2 [26]	1	26
	2	26
	3	26
	4	26
#3 [44]	1	43
	2	44
	3	44
	4	44
#4 [27]	1	14
	2	13
	3	14
	4	15
#5 [38]	1	33
	2	35
	3	36
	4	36

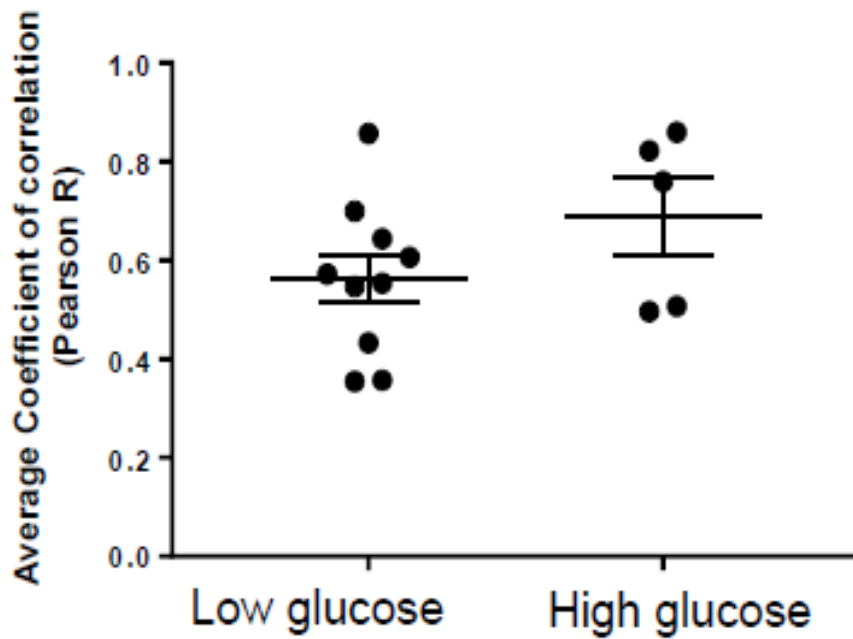
Figure 2.3.3.5 Temporally defined leaders are identical to those with the most number of connections as independently identified using Granger Causality analysis. A) Individual fluorescence intensity traces of 26 cells identified during a typical Ca^{2+} wave (superimposed in different colours) in a single islet. The zoomed-in image shows the point at which wave initiation occurs. Data collected at 1.0 frame s^{-1} , the calcium waves shown here occurred in the high glucose state (25 mM). Leader cells were visually identified as those cells where the rise in intracellular Ca^{2+} precedes the rest of the cell population (ie. followers). Highlighted in yellow are the positions of the temporally defined ‘leaders’. B) Summary table showing the number of cells causally linked to visually identified leaders.

2.3.5 β -cell connectivity in human islets transplanted into the ACE of BALB/c Nude mice

To increase the translatability of our findings we investigated the calcium behaviour of β -cells in human islets virally infected with AV-CMV-GCaMP6m. The AV construct was trophic for β -cells and excluded from other endocrine cell types. BALB/c Nude mice are immunocompromised and were used to allow for human islet xenograft transplantation.

Human islets successfully engrafted by one month post-transplantation. The correlation coefficient in human islets increased under high circulating glucose from 0.39 to 0.59. Additionally, percentage connectivity also increased from 56% to 76%, under low and high blood glucose conditions however the difference was non-significant (**Figure 2.3.4.1**).

A)



B)

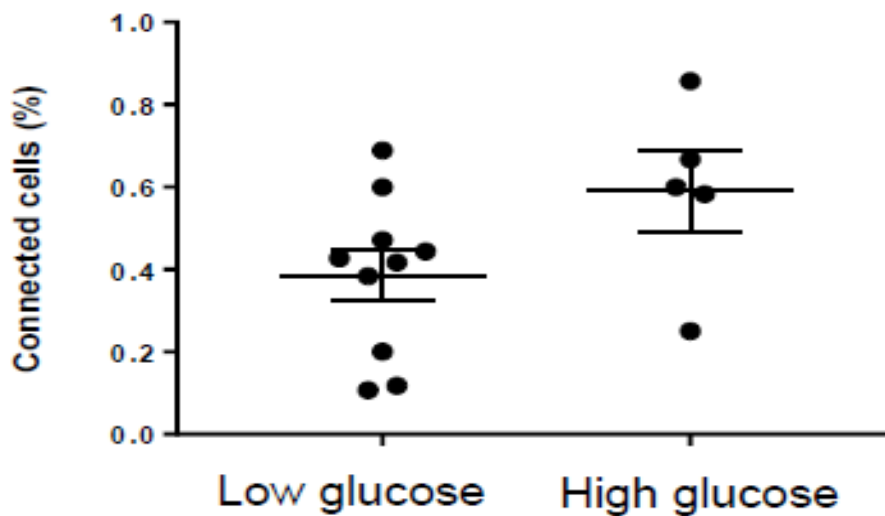


Figure 2.3.4.1 Pooled data for average R and percentage connectivity measurements in non-diabetic human islets ($n=11$ islets). Islets were imaged under low ($<4\text{mmol/L}$) and high ($>7\text{mmol/L}$) glucose conditions. There was a non-significant increase in both average correlation co-efficient (A) from 0.39 to 0.59 and percentage connectivity (B) from 56% to 76% ($p < 0.001$; paired, two-tailed, Student's t -test).

Interestingly, in the two islets investigated from a diabetic donor the opposite trend was observed; elevated blood glucose levels resulted in percentage connectivity decreasing from 30% to 20% and 29% to 27% in low and high conditions, respectively (**Figure 2.3.4.2**). While these preliminary findings are intriguing, data should be interpreted with caution. The two investigated diabetic islet samples were obtained from a single donor (and therefore may not be representative of all diabetic islets) and due to limited viral penetration, the β -cells interrogated in these instances are few ($<15\text{cells}$) and located circumferentially.



Figure 2.3.4.2 Pooled data for average R and percentage connectivity measurements in diabetic human islets ($n = 2$ islets; from the same donor).

Islets were imaged under low ($<4\text{mmol/L}$) and high ($>7\text{mmol/L}$) glucose conditions. Islets exhibited the opposite trend to non-diabetic human islets ($p < 0.001$; paired, two-tailed, Student's t -test).

2.4 Discussion

In the present study we demonstrated that β -cell connectivity exists in mouse islets 3-dimensionally and *in vivo*. The strength of connections increases with elevated glucose concentrations, irrespective of the anaesthetic used and they persist over a prolonged period of time. Moreover, we found evidence for scale-free network topology and identified cells with resemblance to previously identified hub cells. Time-series statistical tools, from the field of econometrics, independently identified these same cells as leaders of calcium waves. Findings from non-diabetic human islets mirrored these observations and displayed a tendency for increased connectivity under high circulating glucose. Surprisingly, islets from a human diabetic donor exhibited diminished β -cell synchronicity when the glucose was switched from low to high levels. Although it is beyond the scope of this project, it is of interest to mention that zebrafish islets displayed similar co-ordinated calcium responses with evidence to suggest a hierarchical organisation of zebrafish β -cells (Salem et al. 2019).

2.4.1 Increased Connectivity of β -cells under High Circulating Glucose

AV-CMV-GCaMP6m was trophic for β -cells due to their selective expression of coxsackie and adenovirus receptor (Takahashi et al. 2007). However, the expression of AV-CMV-GCaMP6m was limited to the periphery of the islet and expression levels gradually decreased over time (not quantified). Due to the circumferential expression pattern, it was not possible to comprehensively investigate calcium dynamics across the islet and therefore, virally mediated gene delivery systems are not robust enough to carry out meaningful connectivity analyses.

Calcium read-outs from pancreatic tissue slices provided the first evidence for small world network topology of the β -cell syncytium. Glucose-induced calcium responses subjected to Pearson R analysis revealed an increase in connectivity with a tendency for shorter intercellular path lengths and increased propensity for clustering (Stozer et al. 2012). Here, we further extend these initial reports and present evidence for increased β -cell connectivity under high circulating glucose levels in the living mouse. Earlier, the same connectivity distribution was recorded to exist, albeit only in a transient and stimulus-driven setting (Stozer et al. 2013). Addressing this, we imaged calcium responses under high

glucose levels for prolonged periods of time and demonstrated that highly synchronised β -cell behaviour continues to persist long after the glucose stimulus.

The validity of drawing conclusions on islet-wide calcium dynamics from observations on a single islet cross-section representing 5-15% of all β -cells was questioned recently (Lei et al. 2018). Consequentially, we employed a Piezo device which allowed for rapid tissue sampling across multiple cell layers without significant losses in temporal resolution. We observed co-ordinated β -cell responses to high glucose levels which traversed multiple cell layers thus demonstrating that functional connectivity is increased 3-dimensionally.

These tightly regulated calcium oscillations require β -cells to work as part of a functional syncytium and drive pulsatile insulin secretion (Klec et al. 2019). Under low circulating glucose conditions, the majority of β -cells are in a quiescent state resulting in low connectivity read-outs. With increasing glucose however, an increasing number of β -cells are recruited into the active phase, directly increasing the secretory output of individual islets. Cyclical elevations in intracellular calcium levels and pulsatile insulin release are physiologically important, as desensitisation of the β -cell secretory machinery and peripheral insulin receptors can be avoided (Jones et al. 1992).

3.4.2 Are Leader cells Hub cells? – Possibly, but no direct evidence

By the same approach developed for *in vitro* studies by Rutter and Hodson, a sub-population of super-connected β -cells was identified in this study which resembled previously characterised hub-cells *in vitro* (Johnston et al. 2016; data not shown). It was previously observed that hub cell responses repetitively preceded and outlasted the activity of the remainder population of cells. This type of behaviour was suggestive of a pacemaker-like quality to hub cells. By using stringent statistical analytical tools, we aimed to determine whether hub cells govern calcium responses *in vivo*.

To this end, β -cells that fired first in a train of calcium waves were visually identified and termed as leader cells. To better investigate the directionality of functional connections, visually identified first-responders were analysed using Granger causality statistic (Granger 1969). Granger causality analysis is a linear forecasting model which was originally developed in econometrics but is now also extensively used in the field of neuroscience. The principle idea behind Granger causality predictions is that causes both predict and precede

their effects and thus, sequence X 'Granger causes' Y if past values in the trajectory of X better predict the future of variable Y than previous values of Y. Granger leaders, that is cells that causally predicted the activity of the greatest number of other β -cells within a given islet, were identical to the β -cells previously identified as hubs. Interestingly, topological analysis of Granger leaders revealed an overlap for these β -cells to be located at wave initiation sites and to neighbour other Granger leaders (under medium to high glucose levels).

The original *in vitro* experiments that identified their regulatory role, utilised targeted optogenetic silencing of hub cells (which were identified in real-time) to reveal detrimental consequences for islet-wide synchronised calcium responses. This effect was rapidly reversed with cessation of laser-stimulated halorhodopsin channel opening. Importantly, the silencing of cells identified as followers did not perturb pan-islet calcium dynamics, demonstrating the hierarchical relationship between the two populations. Due to technical constraints, we were not able to experimentally test the regulatory role of hub cells in the living mouse. Of interest however, our collaborators using zebrafish as a model organism were able to show that laser ablation of leader cells (but not followers) resulted in the subsequent diminution of islet-wide calcium response to pericardial injections of glucose (data not shown, Salem et al. 2019).

Observations that hub cell silencing within a single confocal plane has islet-wide consequences were challenged by other research groups (Lei et al. 2018; Satin et al. 2020). Lei and colleagues addressed this question by 3-D computational modelling of mouse islets where hub cells were defined as a highly metabolic subpopulation with decreased insulin expression (Lei et al. 2018). In an attempt to model the experimental findings of Johnston and colleagues, the inhibition of hubs under unimodal and bimodal gap junction coupling were simulated. According to their findings, with unimodal gap junction coupling, where gap junction conductance is homogenous across the islet, a greater number of hubs were required to be silenced to disrupt islet-wide calcium dynamics. Furthermore, silencing of the same number of follower population had largely similar effects on islet calcium responses. In contrast, silencing of hub cells in the simulation setting where hubs are preferentially coupled (i.e. bimodal coupling setting) resulted in the inhibition of whole islet calcium responses and was more in line with findings of Johnston and colleagues. Altogether these

pointed to the conclusion that besides being highly metabolic, hub cells may also be preferentially gap junction coupled to the islet network.

In further support of this study, and that from this laboratory (Johnston et al. 2016), fluorescence recovery after photobleaching (FRAP) imaging of mouse islets revealed a small population of β -cells to be selectively highly coupled. FRAP is an established non-invasive experimental tool used for the assessment of gap junction coupling, where both the recovery rate and recovery level linearly correlate with gap junction function. A heterogeneous distribution of gap junction coupling was observed in both WT (i.e. Cx36^{+/+}) and heterozygous Cx36^{+/-} KO animals. Importantly, FRAP imaging experiments revealed the presence of a highly coupled sub-population of β -cells in mice. Moreover, gap junction coupling in the islet as a whole was increased at elevated glucose concentrations providing a mechanism by which β -cell connectivity emerges (Farnsworth et al. 2014). The increase in gap junction coupling seen under high glucose levels suggests that elevated and heterogeneous gap junction coupling might be mediating the synchronised behaviour of β -cells observed in this study.

On the other hand, Satin and colleagues called into question electrochemical coupling by gap junctions as the basis for β -cell connectivity and instead advocate for other diffusible factors as potential candidates for synchronising islet-wide calcium responses (Satin et al. 2020). The ability of a handful of hyperpolarised β -cells to propagate a hyperpolarising current across the entirety of the islet has been questioned and instead, it was argued that the inactivation of a hub cell could have inadvertently resulted in the depolarisation of an overlying δ -cell in the photoablation experiments performed by Johnston et al. According to Satin and colleagues activated δ -cells, in turn, could have led to the inhibition of followers, thereby governing pan-islet calcium responses. Lending support to this idea, Briant et al. have found evidence for electrical coupling between δ - and β -cells and showed that optical activation of β -cells results in somatostatin secretion from δ -cells (Briant et al. 2017). Further, in a more physiological setting, δ -cells were found to rapidly activate following a glucose challenge and silenced β -cells to achieve an appropriate secretory response (Rodriguez-Diaz et al. 2019). While the importance of paracrine input from δ -cells is becoming increasingly evident in the context of insulin secretion, the inhibitory tone over β -cells suggests a role for somatostatin and δ -cells in the termination of calcium waves rather

than in the initiation of them. Nevertheless, investigating the potential interaction between hub cells and δ -cells to coordinate islet calcium responses presents an exciting new research avenue. γ -aminobutyric acid (GABA) is an abundantly available neurotransmitter acting in an auto- and paracrine fashion to modulate hormone secretions from islet endocrine cells (Taneera et al. 2012). GABA shows multiple favourable actions within the islet; besides its anti-inflammatory properties it has also been reported to be trophic to β -cells (Soltani et al. 2011). Its physiological relevance is further highlighted by the finding that both GABA and the enzyme glutamic acid decarboxylase 65 (GAD65), important in the biosynthesis of GABA, are downregulated in diabetic human islet samples. Additionally, depending on the ambient glucose concentration, GABA appears to elicit highly divergent effects on islet calcium dynamics. GABAR stimulation at 6mM glucose in human islets resulted in the stimulation of insulin secretion, meanwhile, at supraphysiological levels, GABAR signalling inhibited insulin secretion (Braun et al. 2010). Further, Menegaz and colleagues showed that GABA is released in a periodically, setting the pace for pulsatile insulin secretion and affecting the magnitude of insulin pulses (Menegaz et al. 2019). Intriguingly, Menegaz and colleagues have identified a small fraction of the β -cell population which co-released their GABA with insulin in large dense-core vesicles (Rutter et al. 2020). It would be interesting to experimentally test the mode of GABA release from β -cells identified as leaders (through Granger analysis) or hubs (as identified by Johnston et al.) and the relevance of GABA in orchestrating islet calcium behaviour.

Other diffusible factors like nitric oxide (NO) and carbon monoxide (CO) have also attracted some research interest due to observations that they are both released in increased amounts under hyperglycaemia, following a rhythmical pattern and preceding calcium waves (Nunemaker et al. 2006; Lundqvist et al. 2003). Signal transmission between individual β -cells is modulated by any one of the above mentioned factors (including electrical conductance, and paracrine and diffusible factors) and the relative importance of these remains to be further elucidated (Farnsworth et al. 2014; Lei et al. 2018; Johnston et al. 2016; Rodriguez-Diaz et al. 2019; Menegaz et al. 2019).

2.4.3 Hub versus Pacemaker β -cells

The significance of gap junction coupling is demonstrated by the selective derangement of pulsatile insulin secretion and glucose intolerance in homozygous Cx36^{-/-} KO mouse models

(Benninger et al 2008; Benninger et al 2012; Head et al 2012). Paralleling our findings, the targeted activation of a specific group of channel rhodopsin 2 (ChR2) expressing β -cells resulted in calcium responses seen in >50% of the islet, indicating that wave propagation was effectively facilitated by these sets of β -cells but not others (Westacott et al 2017). Optogenetic targeting of β -cells therefore revealed regions of varying excitability across islets. Regions of heightened excitability could operate nearer the threshold required for depolarization and therefore are more efficient propagators of calcium waves. Simulating intra-islet variability of K_{ATP} channel density did not have a significant impact on ChR2 activated area, signifying that metabolic rate is a more important determinant of cell excitability. To test whether spatial segregation of metabolic activity underlies the spatiotemporal dynamics of calcium responses, the redox state of β -cells was interrogated through the NAD(P)H autofluorescent signal. A significantly positive relationship was found between ChR2 activated area and distance between cells supporting the idea that similarly excitable cells preferentially cluster together. This is consistent with our and Stozer and colleagues' idea that β -cells operate as part of small-world network, where clustering is high and intermodal distances are short (Stozer et al 2012; Stozer et al 2013). Strikingly, this type of spatial segregation was also demonstrated using the sliding window correlation statistic in the presence of incremental glucose increases. Of note, β -cells form local syncytia with their neighbours and gradually get recruited to match secretory demand (Markovic et al 2015).

On closer inspection of these wave initiation zones, both NAD(P)H and glucokinase activity were reduced suggesting that sub-regions of lower metabolic activity control the initiation of waves. ChR2-activated area was also significantly lower at initiation points than it was at wave termination points. In addition, K_{ATP} conductance was significantly higher at originating points than where calcium waves terminated, in line with other simulation predictions (Lei et al 2018).

Dynamic oscillator modelling predicts that nodes with the highest oscillation frequency act as pacemakers in a given system (Hraha et al 2014; Benninger et al 2008). Interestingly a significant negative correlation was found between NAD(P)H response and Ca^{2+} oscillatory frequency, where cells with higher metabolic activity show slower Ca^{2+} oscillations. Accordingly, as predicted by both static Boolean and dynamic oscillator models, a sub-

population of inexcitable β -cells suppresses calcium responses of the whole islet, provided that coupling surpasses a critical threshold. Contrastingly, in the pre-critical regime cell coupling is weak and inexcitable cells are unable to suppress the activity of more excitable β -cells (Hraha et al 2014; Westacott et al 2017; Gosak et al 2017). Accordingly, cells with higher metabolic rate are more depolarised, closer to firing and are more efficient at recruiting neighbouring cells. On the basis of computer based modelling the following distinction can be made between β -cell populations: pacemakers with high oscillatory frequency and low metabolic rate determine the synchronised islet behaviour, whilst highly excitable, metabolically active cells act as wave propagators. At sufficiently high level of glucose, all β -cells become depolarised and increased gap junction coupling facilitates synchronized calcium responses.

These findings contradict our own and those of Johnston and colleagues in which highly metabolically active hub cells are reported to govern pan-islet calcium dynamics. The differences in analytical tools used by the two groups make the comparison of results a difficult task. An inherent limitation of the immunostaining of islets in the study by Johnston and colleagues is that it is a semi-quantitative method and only represents a snapshot of hub cell glucokinase levels. Contrastingly, Westacott and colleagues measured dynamic changes in NAD(P)H levels simultaneously with calcium responses and therefore might offer a better understanding of wave initiator phenotype. The low insulin content reported by Johnston and colleagues is indicative of a hyposecretory status and is in alignment with predictions from dynamic oscillator modelling. Nevertheless, we were unable to metabolically phenotype leader cells here and it remains to be determined to what extent, and if there is any overlap between hub, pacemaker and leader cell populations.

3 Chapter: The Effects of High Fat Diet and Chronic Glucagon Analogue Treatment on Islet Function *In Vivo*

3.1 Introduction

3.1.1 Glucagon

The central role of insulin deficiency in diabetes pathophysiology was recognised almost a century ago. Glucagon was first discovered as a hyperglycaemic contaminant in pancreatic extracts (Feingold et al. 2000). Later its essential role in glucose homeostasis was recognised; under hypoglycaemic conditions, glucagon is released from the pancreas to stimulate glycogenolysis and gluconeogenesis in the liver. While the canonical hyperglycaemic effects of glucagon warranted its clinical use in severe cases of insulin-induced hypoglycaemia, the hormone attracted little clinical interest otherwise (Blackman 1961). This was about to change, when Roger Unger and Lelio Orci in their seminal work posited the bihormonal-abnormality theory of diabetes (Unger and Orci 1975). They proposed that elevated glucagon levels seen in diabetic patients actively exacerbate disease progression through increased hepatic glucose output. Thus, the bihormonal-abnormality theory cemented the view of glucagon driving T2DM pathophysiology for decades to come and provided the impetus for the development of glucagon receptor antagonists.

The bihormonal-abnormality theory rests on several observations of impairments in glucagon signalling in T2DM. For example, baseline plasma glucagon levels are elevated and are insufficiently suppressed following a carbohydrate-rich meal in individuals with T2DM (Baron et al. 1987; Raeven et al. 1987; D'Alessio 2011). On a background of hepatic insulin resistance, the net effect of hyperglucagonaemia is proposed to be an increase in hepatic glucose production thereby worsening the glycaemic profile. Furthermore, newly available treatment options targeting the GLP-1 signalling pathway have been shown to lower plasma glucagon levels (D'Alessio 2011).

Preclinical studies where chronic glucagon receptor blockade is achieved have shown an improvement in both glucose and insulin tolerance profiles of mice on high fat diet (HFD) (Winzell et al. 2007; Sloop et al. 2004). Through clamp experiments, it was revealed that the beneficial effects of chronic glucagon receptor antagonism on glycaemic profile were due to increased insulin secretion rather than increased insulin sensitivity (Sharma et al 2018).

Further, in a diabetes model where insulin resistance was induced by long-term insulin receptor antagonism, the blockade of glucagon signalling by monoclonal antibodies normalised glycaemia (Okamoto et al. 2017). Consistent with pharmacological studies, whole body *Gcgr*^{-/-} models reported lower blood glucose levels but results were confounded by the drastic increases in circulating GLP-1 levels and β -cell mass expansion (Gelling et al. 2003; Hancock et al. 2010). Nevertheless, an interesting observation was made that mice devoid of α -cells had better glucose tolerance profiles after streptozotocin (STZ)-induced β -cell destruction compared with WT animals. Despite reports on its protective effects against STZ, GLP-1 signalling was not assessed while β -cell mass was confirmed to have increased. This suggests that α -cell ablated animals had a larger β -cell reservoir prior to STZ conferring an advantage when compared with WT animals (Hancock et al. 2010; Kumar et al. 2007).

Thus, a recurrent theme emerges from these studies where a disruption of glucagon signalling results in enhanced GLP1 signalling, at least in studies where it is measured (Sorhede et al. 2007; Sloop et al. 2004; Gelling et al. 2003). In other cases, β -cell mass expansion is reported, directly explaining the increased insulin secretion seen after glucagon receptor blockade (Okamoto et al. 2017; Hancock et al. 2010). The insulinotropic and anti-apoptotic effects of GLP-1 on β -cell mass are well-established features and allow us to speculate that the normoglycaemic effects of glucagon receptor antagonists might be mediated by adaptive changes in the incretin axis rather than abolished glucagon signalling *per se*.

Furthermore, hepatic steatosis is a real concern with chronic glucagon receptor blockade as evidenced by the reported increase in fat accumulation in the liver cytoarchitecture and elevated plasma triglyceride levels (Hancock et al. 2010). Changes associated with liver function therefore might explain why, despite the initial successes, glucagon receptor antagonism has not been incorporated into any of the currently available anti-diabetic medications.

3.1.2 A case for the inclusion of glucagon receptor agonism in the anti-diabetic armamentarium

A recent re-discovery of glucagon's effects to increase energy expenditure in humans has shifted focus away from antagonising glucagon receptors to try and exploit the beneficial effects of glucagon on energy homeostasis. The ability of glucagon to raise energy

expenditure (EE) was first demonstrated in rodents and subsequently confirmed in humans. The thermogenic effects of glucagon arise within minutes after an intravenous infusion of glucagon in human subjects (Salem et al. 2016). The magnitude of thermogenic effects was comparable to cold exposure or β_3 -adrenergic receptor activation in brown adipose tissue (BAT). BAT has subsequently emerged as a candidate tissue for mediating the EE-elevating effects of glucagon after the early observation that direct application of glucagon to BAT tissue explants increases oxygen consumption in rodents. This was later contested by a series of studies in a variety of species and suggested that neither the glucagon receptor nor BAT are essential for glucagon-stimulated EE. In humans, cold exposure activated BAT activity, as assessed by ^{18}F -fluorodeoxyglucose positron emission tomography/CT (^{18}F -FDG PET/CT). However, subsequent glucagon infusions whilst increasing EE, failed to further stimulate BAT activity in an acute setting. These observations suggested that BAT activity is dispensable for glucagon stimulated EE (Salem et al. 2016). Among other candidates, catecholamines, fibroblast growth factor 21 (FGF-21) and bile acids have all been implicated in glucagon induced EE increase. Importantly, the EE effects of glucagon have been reported to be conserved in obese patients making it a plausible pharmacological target to consider (Tan et al. 2013). Moreover, glucagon injections in the arcuate nucleus elicited appetite suppressing actions in a PKA dependent manner (Quinones et al. 2015).

Oxyntomodulin is a naturally occurring peptide with affinities for both GLP-1 and glucagon receptors. In mice, oxyntomodulin was found to acutely improve glucose metabolism whilst its administration in overweight humans led to an overall negative energy balance through reduced appetite and increased movement-associated energy expenditure in a study (Wynne et al. 2006). These results proved that glucagon's lipolytic, thermogenic and satiating effects can be exploited and inspired the future development GLP-1 and glucagon based dual agonists. The fine balance between GLP-1 and glucagon agonism was investigated by Day and colleagues who developed single molecules with different potencies at each receptor (Day et al. 2009). In diet-induced mice the dual agonist with equal affinities for both GLP-1 and glucagon receptors showed superior weight-loss and glucose tolerance effects when compared with a GLP-1 analogue only *in vivo*. Increasing glucagon receptor efficacy was positively correlated with increased weight-loss and reduced adipose tissue. Poci and colleagues reported similar results and reasoned that the glucagonergic portion of

dual agonist compounds is more important in the fasted state where it accentuates catabolic effects of metabolism to enhance weight-loss (Pocai et al. 2009). Targeting GLP-1 receptors on the other hand, is crucial in offsetting the hyperglycaemic effects of glucagon and thus normalise glycaemia (Tan et al. 2013).

Although the resurgence of research interest in glucagon has provided many clues on its favourable metabolic effects and potential therapeutic utility in diabetes, its direct effects on islet function remain elusive. In order to address this gap in our knowledge, we implanted transgenic islets expressing a fluorescent calcium indicator into a cohort of mice, who were then fed a high-fat diet in order to induce obesity (DIO) and glucose intolerance. We longitudinally monitored the effects of DIO progression on islet function and subsequently treated animals with a daily injection of saline or a long-acting glucagon analogue over 40 days. In order to elucidate the weight independent effects of glucagon on islet function, we introduced a control group whose weight was matched to that of the glucagon analogue treated group.

3.1.3 Aims and Hypotheses

Hypotheses:

- Diet induced obesity (DIO) impairs islet-wide calcium dynamics *in vivo*
- Chronic treatment with a long-acting glucagon analogue induces weight loss in animals and rescues the impaired glucose phenotype
- Chronic treatment with a long-acting glucagon analogue has direct effects on islet function beyond the weight-loss-mediated processes

Aims:

- To establish the islet in the eye imaging platform for the longitudinal functional imaging of islets
- To assess the effects of HFD on metabolic health as well as islet function
- To assess the chronic effects of a long-acting glucagon analogue on glucose homeostasis and islet health on a background of high-fat feeding
- To assess the direct, weight-loss-independent effects of chronic glucagon analogue treatment on islet calcium dynamics both *in vivo* and *in vitro*

3.2 Materials and Methods

3.2.1 Study Overview

24 male C57BL6/J WT (25-30g) mice purchased from Charles River were housed in groups of four in ventilated individual cages under controlled conditions (21-23°C; 12 hour light: 12 hour dark cycle) with *ad libitum* access to standard chow and water. The animals received syngeneic Ins1Cre-GCaMP6f expressing islets into the anterior chamber of their eyes (as described previously in Chapter 2, Methods section 2.2.7). After full implantation (>4 weeks post-operation) the baseline calcium oscillations in islets were recorded (for imaging details see section 3.2.8. of this chapter). The metabolic phenotype of animals was assessed by intraperitoneal glucose and insulin tolerances tests (IPGTT 2g/kg; IPITT 1U/kg).

Following baseline recordings, animals were separated into individual cages and put on high-fat diet (HFD) for approximately 8 weeks to induce obesity and glucose intolerance. The energy density of high fat diet was 5.21kcal/g and composed of 20% kcal protein, 60% kcal fat and 20% kcal carbohydrate (Research diets; D12492). Weight and food intake measurements took place daily using a high-precision weighing scale. After establishing a glucose intolerant phenotype via IPGTT (1g/kg), animals were subjected to a second imaging session to assess the effects of HFD on islet function.

Subsequently, animals were uniformly distributed into three experimental treatment groups (n=8 per group) based on their weight. Animals were allocated to receive daily subcutaneous injections of either saline+Zn²⁺ (n=16) or the long-acting glucagon analogue G778 (n=8). G778 dosage was incrementally increased from 20nmol/kg to 160nmol/kg, using a previously established dose ramping protocol designed to avert sudden high dose nauseating effects. Briefly, mice received 12.5% of maximum dose (20nmol/kg) on the first day and 25% of maximum dose (40nmol/kg) for the following two days. A week was then allowed for animals to acclimatise to 50% of maximum dose (80nmol/kg) after which G778 dose was further increased to 160nmol/kg for the rest of the study (remaining 4 weeks).

As G778 treatment resulted in a modest weight loss, 8 out of the 16 animals on saline injections were allocated into a weight matched group. The food given to weight matched animals was determined based on the mean weight of the G778 group, the individual animal to which a weight-matched animal was pair-fed to and the food consumption of G778 group averaged over a four day period.

The islets of all three groups were imaged after 6 weeks of saline or G778 treatment and a final IPGTT was carried out before animals were sacrificed and their tissues harvested (brain, lungs, liver, striated muscle, white and brown adipose tissue). For a schematic diagram of the study see **Figure 3.2.9.1**). This study was conducted under project licence PPL750462 (project licence holder Prof Kevin Murphy). All animal procedures were approved and performed under the UK Home Office Animals (Scientific Procedures) Act 1986.

3.2.2 Peptide Synthesis of G778

The G778 analogue was designed and donated by Professor SR Bloom (Imperial College London). Peptides were synthesised by Bachem (UK) and underwent local testing for purity after aliquoting and freeze drying, according to well established protocols in the Bloom Drug Development programme. Prior to injections the long-acting G778 peptide was dissolved in sterile saline supplemented with Zn²⁺.

	1	2	3	4	5	6	7	8	9	10	11	12	13	14	15	16	17	18	19	20	21	22	23	24	25	26	27	28	29	30	31	32
GCG	His	Ser	Gln	Gly	Thr	Phe	Thr	Ser	Asp	Tyr	Ser	Lys	Tyr	Leu	Asp	Ser	Arg	Arg	Ala	Gln	Asp	Phe	Val	Gln	Trp	Leu	Met	Asn	Thr			
AnGLU	His	Ser	Gln	Gly	Thr	Phe	Thr	Ser	Asp	Tyr	Ser	Lys	Tyr	Leu	Asp	Ser	Arg	Arg	Ala	His	Glu	Phe	Val	Gln	Trp	Leu	Leu	Asn	Thr	His	His	NH ₂

Figure 3.2.2.1 The peptide sequence of long-acting glucagon analogue G778 and endogenous glucagon.

3.2.3 cAMP Assay

In order to confirm that the G778 analogue was an agonist of endocrine cell signalling, cyclic AMP accumulation was measured in stimulated PathHunter CHO-K1 cells. cAMP analysis was confirmed using homogenous time resolved fluorescence (HTRF), specifically the cAMP Gx Dynamic 2 cAMP kit (Cisbio, France). In all assays, cells were plated at 10,000 cells per well of a 96-well plate. The plated cells were incubated with the G778 for 30 minutes (acute incubation) at 37°C and the levels of cAMP were analysed as per manufacturer's instructions. Results were expressed relative to the endogenous ligand (i.e. glucagon for GCGR cells as well as other pre-proglucagon products GIP and GLP-1). No phosphodiesterase inhibitor was used. The fluorescence was measured using the Spectramax i3x Multi-Mode Detection Platform and read using SoftMax Pro version 6.5.1. (Molecular Devices, USA). cAMP assays were performed by Mr Yateen Patel.

3.2.4 Metabolic Phenotyping

Baseline IPGTT and IPITT experiments were carried out while animals were on normal chow (prior to first imaging session). After 8 weeks on HFD IPGTT and IPITT testing was repeated and a glucose intolerant phenotype was determined. Lastly, a final IPGTT was performed at 6 weeks of treatment to assess the effects of G778 and saline/weight matching (WM) treatments on the metabolic profile of animals.

Following a 5hrs-fast animals were weighed and an anaesthetic cream (lidocaine/prilocaine, EMLA™) was applied topically on the tip of their tail, prior to the start of glucose and insulin tolerance tests. Each animal was restrained and the lateral caudal veins were venepunctured using a sterile scalpel blade. A baseline reading at t=0 was taken using a glucometer (Novo Nordisk) and recorded which was followed by an intraperitoneal (IP) injection of either glucose (20% D-glucose at 2g/kg; Sigma-Aldrich) or insulin (1U/kg; Actrapid, Novo Nordisk). Subsequent blood glucose measurements were taken using a glucometer at 15, 30, 60, 90, 120, 150 and 180 minutes post-injection. At the end of experiments, mice were returned to their cages and food and water were placed back in hoppers.

3.2.5 *In Vivo* Imaging Experiments

All *in vivo* imaging experiments were conducted using spinning disk confocal microscopy (Yokogawa spinning disk, 20x water dipping 1.0NA objective; Cairn instruments). Image sequences were obtained by exposing islets to 488nm laser at 3Hz acquisition rate (a total of 401 frames per imaging session). Blood glucose was monitored through blood sampling from a peripheral tail nick using a standard glucometer (Accu-Chek). Islets were imaged three times over the course of the study; baseline recordings were carried out whilst animals were fed normal chow (Session 1) then repeated after 8 weeks on HFD (Session 2) and later, after 6 weeks of saline/WM or G778 treatment (Session 3). Islets were imaged on three occasions, at baseline, 2 months on HFD and 6 weeks after treatment. These will be referred to as imaging session 1, 2 and 3 within the text. Animals were imaged in the evening/night time i.e. when the long acting peptide was expected to be at maximal effect and when the animal was in his feeding phase.

Volumetric analyses of islets were carried out at the same time-points. Islets were imaged in Z-stack modality with 5µm spacing and exposed for 300msec with the 488nm laser.

3.2.6 *In Vitro* Imaging Experiments

All *in vitro* imaging experiments were conducted using a Yokogawa CSU22 Nipkow spinning disk microscope coupled with a Zeiss Axiovert M200 and x10/0.3NA objective (Zeiss). Volocity software was used to record image sequences which were acquired at a rate of 1Hz with 500msec exposure time using the 488nm laser. Ins1Cre-GCaMP6f islets were isolated from mouse donors (for protocol see Chapter 2, Methods section 2.2.2) and incubated overnight at 37°C, 5%CO₂. Prior to the start of the experiment, islets (15 islets at a time) were removed from RPMI-1640 full medium and placed in a 6-well cell suspension plate for pre-incubation in Krebs solution (for recipe please see Appendix 7.1.3.) with 3mM glucose for >1 hour. At the end of the incubation period, islets were placed in the centre of a metallic perfusion chamber with 1mL of 3mM glucose Krebs and the chamber was placed on a heated microscope stage. To start, islets were imaged at 3mM glucose concentration for 2 minutes, then at 7mM and 17mM glucose concentrations for 8 minutes each. As a positive control, islets were exposed to 2 minutes of 40mM KCl solution at the end of the experiment. Islets unresponsive to KCl were excluded from further analysis.

3.2.7 *In Vivo* and *In Vitro* Imaging Analysis

All image sequences were pre-processed using FIJI. Stream (rate of 3Hz; *in vivo* recordings) and time-series (rate of 1Hz; *in vitro* recordings) acquisitions were motion-corrected and re-aligned using the previously described custom-made macro (by Stephen Rothery, FILM facility Imperial College London; see Chapter 2, Methods section 2.2.9.).

Wave Index

Wave indices for individual islets were determined through visual assessment of image sequences, in a method developed for this particular project. Over the course of the study, four distinct types of β -cell calcium behaviour were evident (**Figure 3.2.7.1**). Type 1 activity was observed in quiescent islets where no calcium fluctuations were seen. Type 2 activity was characterised by calcium oscillations in individual cells or collection of cells without evident pan-islet calcium activity. Islets were described as displaying type 3 activity when calcium surges were seen in a larger area (20-50% of islet cross-section) or on the periphery of the islet, without the calcium oscillations being propagated across the imaged cross-section. Type 4 waves extended across the entire islet. Wave indices across all imaged islets were averaged by treatment and imaging session (**Figure 3.2.7.1**)

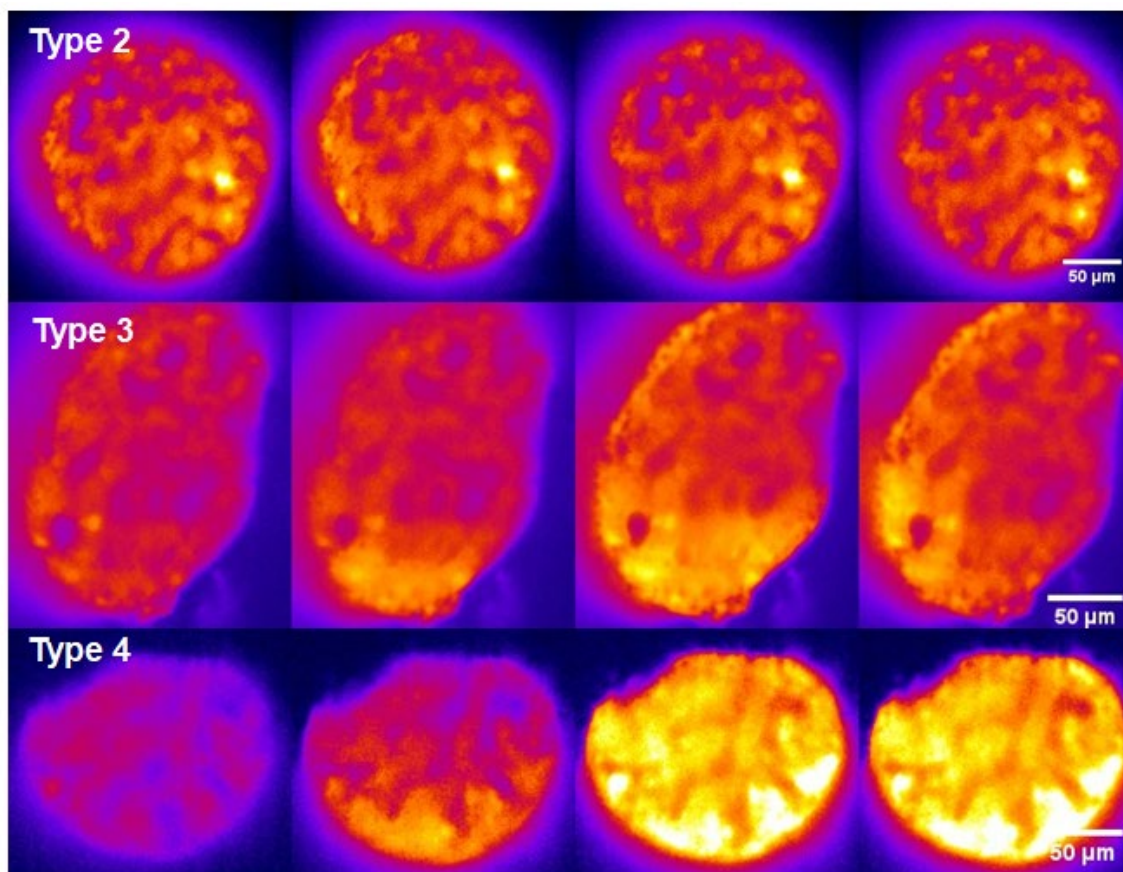


Figure 3.2.7.1 Representative image sequences of the three different types of islet calcium behaviour. Consecutive frames from a set of stream experiments are shown, where images were pseudo-coloured using the 'Fire' Look Up Table (LUT) in FIJI for demonstration purposes.

Waveform Analyses

Whole islet region of interest (ROI) read-outs were collected on the pre-processed motion corrected image sequences for both *in vivo* and *in vitro* experiments. Calcium traces normalised to the minimum value for each islet per imaging session (F_i/F_{min}) were plotted in GraphPad Prism 8. Calcium surges were identified and a genuine calcium response was determined as a 20% fluorescence intensity increase from baseline. Image sequences were cross-checked on FIJI to ascertain that all calcium surges were identified correctly. First, the XY coordinates of peak values were identified and then the amplitude of calcium surges were determined as $Y-1$. For wavelength measurements, two adjacent peaks were identified on calcium traces and their XY co-ordinates noted. Wavelength was calculated by subtracting the X value of the first peak from the X value of the second peak. Full width at half maximum (FWHM) was determined by first identifying the half maximum value of F_{peak} . The matching

two X co-ordinates were identified on both inclining (X_1) and reclining (X_2) arms of the wave and subtracted ($X_2 - X_1$) to determine the FWHM value.

Velocity

Wave propagation speed was assessed in *in vivo* imaging experiments with Ins1Cre-GCaMP6f expressing islets. The images were calibrated (voxel size: $0.3225\mu\text{m} \times 0.3225\mu\text{m}$) and the frame at which calcium surge is evident in the first β -cells is noted. The frame at which fluorescence intensity is increased in the entire islet is also noted and the number of frames elapsed between these two time-points is recorded. To translate this into seconds the frame numbers are multiplied by 0.3. To measure the diameter of the islet the linear ROI tool was used starting from the wave initiation point. Velocity was expressed as $\mu\text{m}/\text{sec}$.

3.2.8 Statistical Analysis

All data are expressed as mean \pm SEM unless specified otherwise. Weight loss and IPGTT data were analysed using two-way ANOVA with Bonferroni's post-hoc test. Values were considered statistically significant if $p < 0.05$. EC_{50} values were determined from the standard curves on log-log graphs.

3.2.9 Longitudinal assessment of leaders

Two islets – one in a G778 treated animal and one on a weight matched to G778 (WM to G778) group were identified. Specifically, the cross-sections imaged during sessions 1, 2 and 3 for these islets were directly comparable such that the same β -cell ROIs were re-identifiable longitudinally. Connectivity changes of Ins1Cre-GCaMP6f expressing islets were subjected to single-cell regions of interest (ROI) analysis to extract calcium traces of their individual β -cells for imaging sessions 1 (baseline), 2 (2 months on HFD), and 3 (6 weeks G778 treatment). ROIs were selected and manually motion-corrected as described previously in Chapter 2 Section 2.2.8. Pearson R correlation analyses were performed on prospectively smoothed datasets to determine connectivity changes between imaging sessions, generating Cartesian maps and heat matrices. Leader β -cells for waves in each imaging session (where they occurred) were visually identified and Granger causality analysis conducted to determine the directionality of connections (as described in Salem et al. 2019).

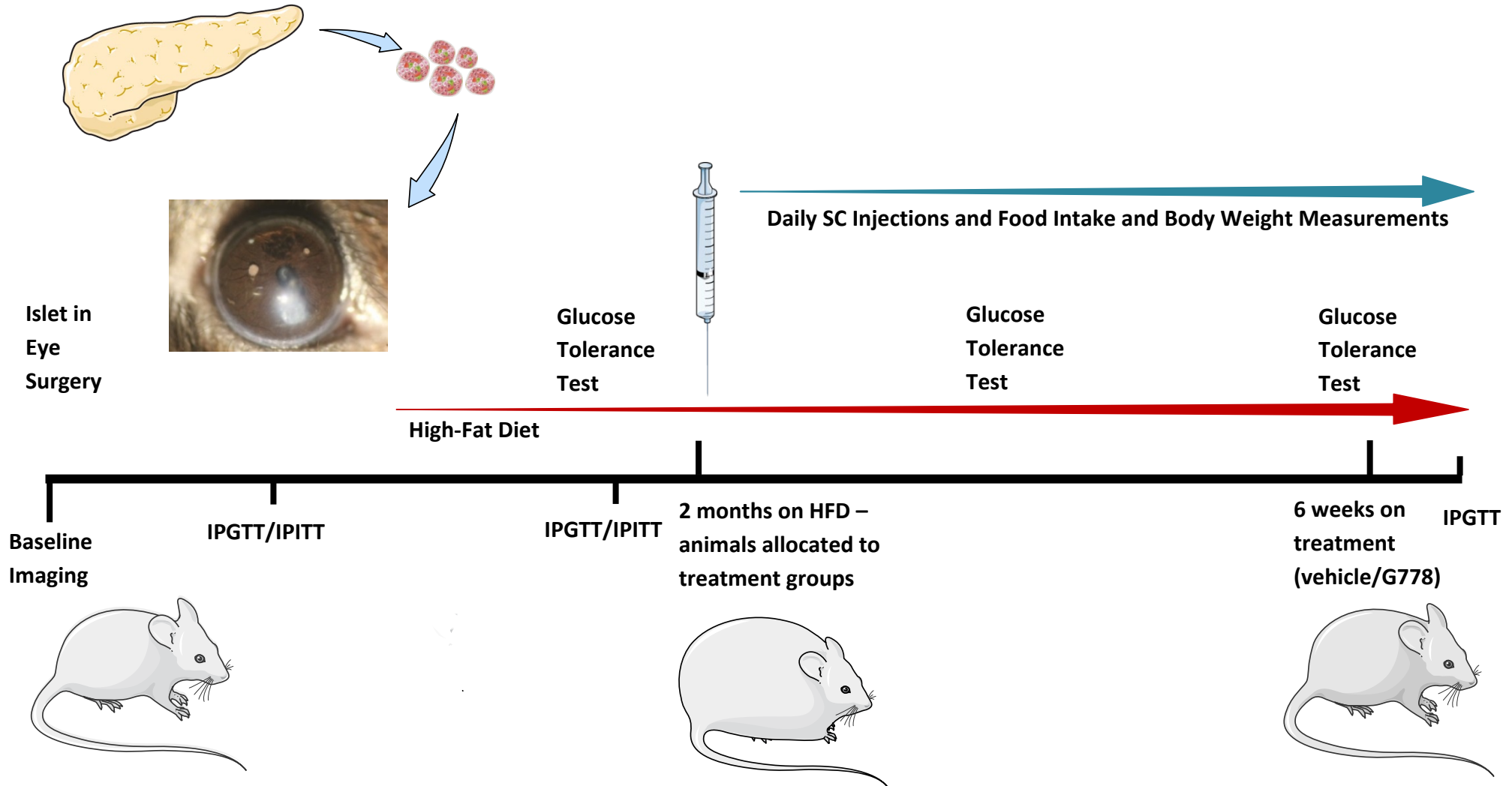


Figure 3.2.9.1. Schematic diagram of the study design.

C57Bl6/J recipients received syngeneic Ins1Cre-GCaMP6f-expressing islets in their eyes. Baseline imaging (ex.: 488nm; 3fps) and IPGTTs (2g/kg) were carried out prior to start of HFD. The effects of HFD on islet function were assessed at 2 months after start of HFD. G778 was administered via daily SC injections and dosage was incrementally increased to 160nmol/kg. Briefly, mice received 12.5% of max dose (20nmol/kg) on the first day; this was then increased to 25% max dose (40nmol/kg) for the subsequent two days. A week was then allowed for animals to acclimatise to 80nmol/kg dosage (50% max dose) after which G778 dose was increased to 160nmol/kg for the rest of the study. There was no sign of pica behaviour and glucagon analogue treatment was well-tolerated. Baseline imaging was carried out one month after transplantation to allow islet engraftment to complete. After 2 months on HFD islets were imaged again before commencing treatment. Additionally, transplanted islets were imaged after 6 weeks of treatment. Weight-matched groups were introduced at the start of injections and their food intake tightly controlled with the aim to match average body weight in the G778-treated group. IPGTTs were carried out 3months into HFD, then at 3 and 6 weeks into SC injection treatment. Animals were culled at the end of study and skeletal muscle, liver, BAT and WAT were harvested for analysis.

3.3 Results

3.3.1 *In Vitro* cAMP Assay Suggests that G778 Has a Similar Receptor Activation Profile as Native Glucagon

The glucagon, GLP-1 and GIP receptor activation profile of G778 is shown in **figure 3.3.1.1**. These peptides and their respective receptors were chosen because GLP-1 and GIP are well-established insulin secretagogues, and cross-reactivity between GLP-1 and glucagon receptors and their respective ligands has been reported in the pancreas previously (Müller et al. 2019). The efficacy of G778 to activate glucagon, GLP-1 and GIP receptors were compared with endogenous ligands of these receptors, namely, glucagon, GLP-1 and GIP. The EC₅₀ of G778 was 1.663e-010 at the glucagon receptor compared to the EC₅₀ of 2.390e-011 for endogenous glucagon. GLP-1 receptor binding potency of G778 was marginally higher than that of native glucagon, with EC₅₀ values of 2.083e-009 and 1.097e-008, respectively. Both synthetic G778 and endogenous glucagon was ineffective at cAMP activation through the GIP receptor (**Figure 3.3.1.1**). These results suggested that G778 closely mimics the actions of endogenous glucagon.

In data not presented here, earlier pharmacokinetic studies of this analogue confirmed a prolonged duration of action. In Wistar rats, peak plasma concentrations of the long-acting G778 peptide was achieved at 4 hours post-injection and circulating peptide could still be detected 48 hours after injection (Dr V Salem unpublished).

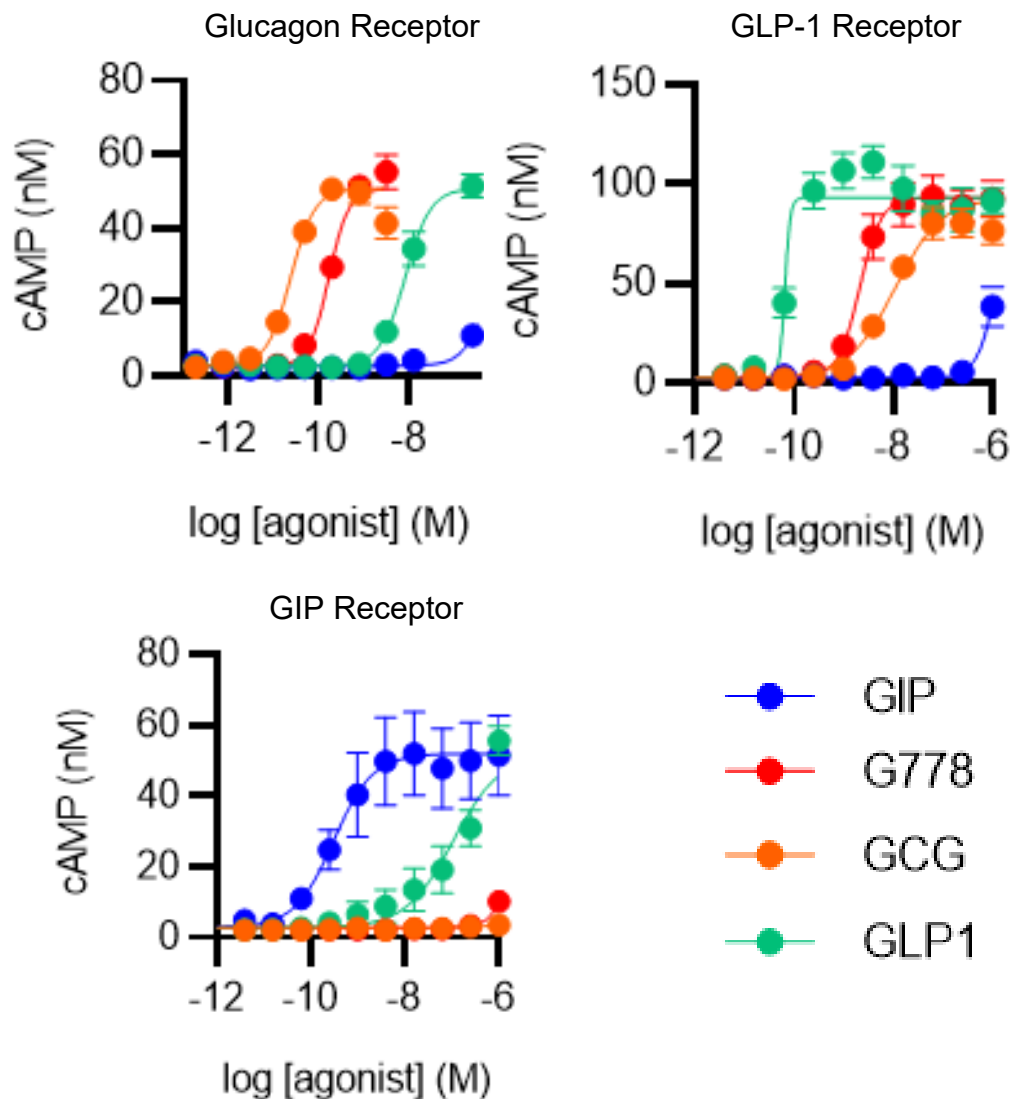


Figure 3.3.1.1 Potency of G778 at glucagon, GLP-1 and GIP receptors and the endogenous ligands of respective receptors. The EC_{50} of G778 versus glucagon at the glucagon receptor was $1.663e-010$ nM and $2.390e-011$ nM, respectively. In contrast, affinity at the GLP-1 receptor was $2.083e-009$ and $1.097e-008$ for G778 and glucagon, respectively

3.3.2 The effects of DIO on islet function

In order to induce a diabetic phenotype in our mouse cohort, we placed animals on HFD (60% kcal from fat) and monitored their glucose handling profiles by performing IPGTTs (2g/kg) and IPITTs (1U/kg) at regular intervals.

Two months into HFD, fasted blood glucose levels were slightly elevated at 8.6mmol/L (**Figure 3.3.2.1**). During baseline IPGTT the peak value at 15mins was 19.6mmol/L whereas after 2 months of high fat feeding the peak value was 24.3mmol/L at 30 minutes (AUC of 1783 ± 106 at

baseline versus 2884 ± 178 after HFD). Additionally, IPITT measurements suggested that HFD caused insulin resistance in our cohort of animals (AUC of 1145 ± 77 at baseline (on normal chow) versus 1000 ± 64 after 2 months HFD).

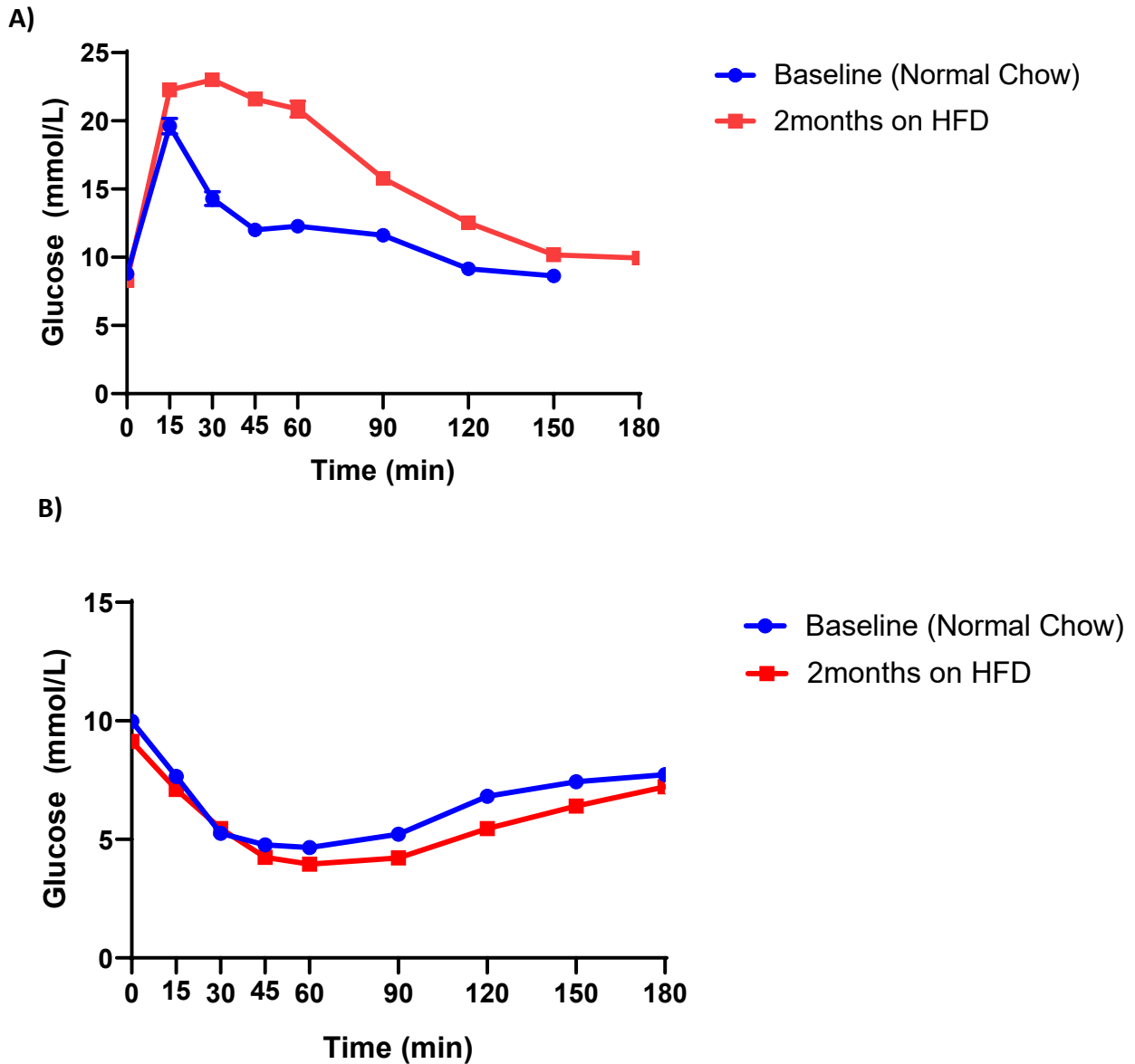


Figure 3.3.2.1 Animals on HFD display an impaired glycaemic profile at two months before the start of treatment. IPGTT (2g/kg) and IPITT (1U/kg) experiments suggested defects in insulin secretory function and mild insulin resistance (n=24).

3.3.3 G778 Treatment Causes a Modest Weight-Loss

The mean starting weight before treatment was comparable between groups, with an average body weight of 39.2g (± 1.9 SEM) for vehicle, 40.09g (± 1.3 SEM) for weight matched to G778 and 39.5g (± 1.6 SEM) for G778-treated groups (**Figure 3.3.3.1**).

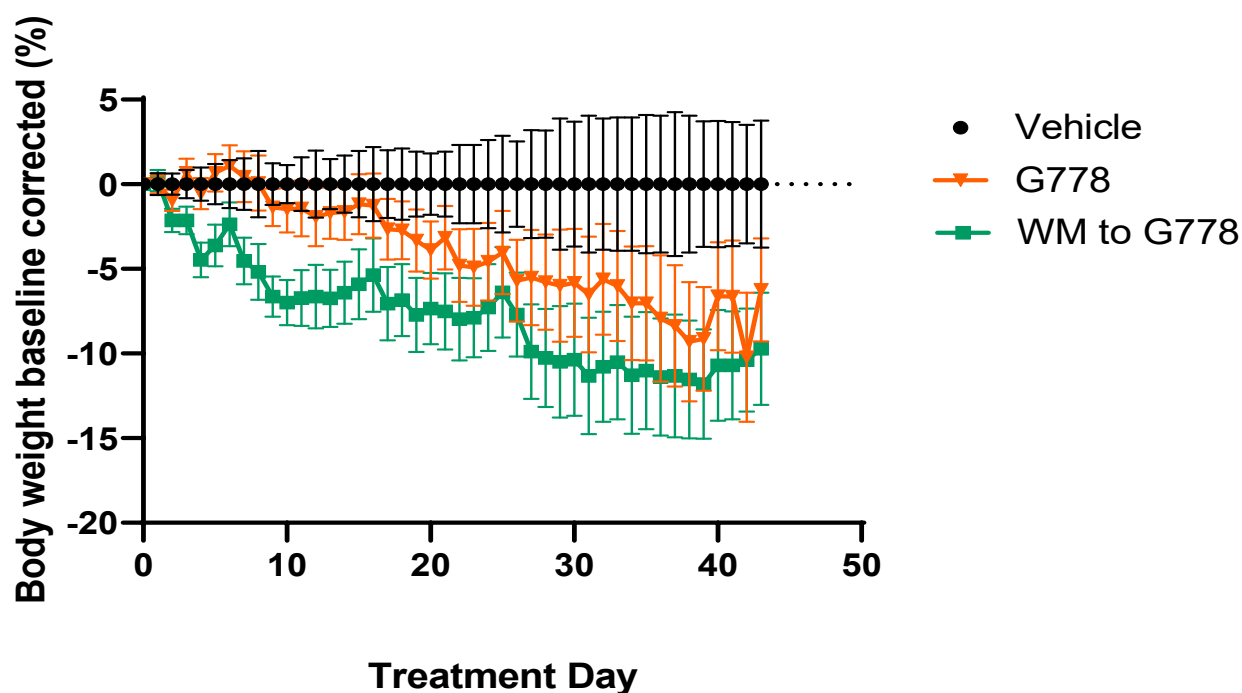


Figure 3.3.3.1 G778 treatment resulted in a modest weight loss. G778 treatment of mice (n=8 per group) resulted in a modest weight loss, the percentage body weight loss was significantly different between G778 and saline groups, as measured with two-way ANOVA and Bonferroni's multiple comparison test ($p=0.0298$). The mean weight of animals at the end of the study were 38.35g (± 2.221 SEM) for vehicle, 34.96g (± 0.4855 SEM) for weight-matched to G778 and 36.21g (± 1.558 SEM) for the G778-treated group.

There was a significant ($p=0.0298$) weight-loss with G778 treatment, -12.01% (± 1.97) for G778-group versus -2.3% (± 2.67) for saline treated group at the end of the experiment (Two-way ANOVA, Bonferroni's multiple comparison test). The body weight percentage change was comparable between G778 and weight-matched to G778 treated groups ($p=0.4461$). Importantly, body weight changes were not matched by a reduced food intake in G778-treated animals, confirming previous conclusions about the weight loss effects of glucagon being underpinned by energy expenditure rather than anorectic mechanisms (**Figure 3.3.3.1**)

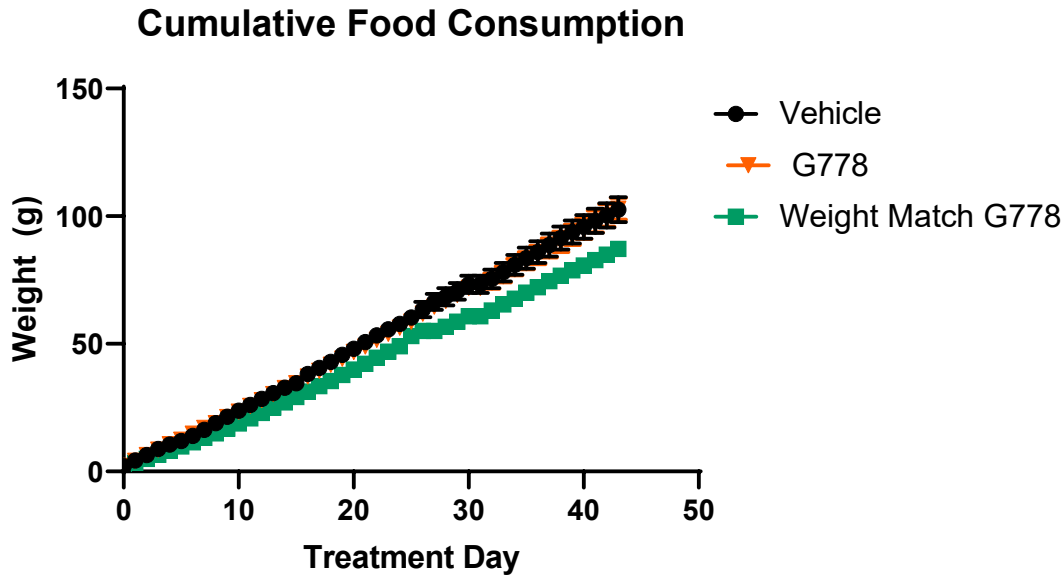


Figure 3.3.3.2 Cumulative food consumption of G778 and control groups. There were no apparent differences in the food intake of G778-treated animals when compared to the saline group. The weight matched group was given the appropriate food amounts to match the weight of the G778-treated mice and therefore these mice overall ingested a smaller amount of food than the other two groups (n=8; Two-way ANOVA; Tukey's test).

The first two weeks of G778 (at a dosage of 80nmol/kg) treatment resulted in a trend towards improved glucose tolerance observed at time-points 15, 30 and 45 mins compared with vehicle treated groups, albeit the difference was non-significant (p=0.111; **Figure 3.3.3.3**).

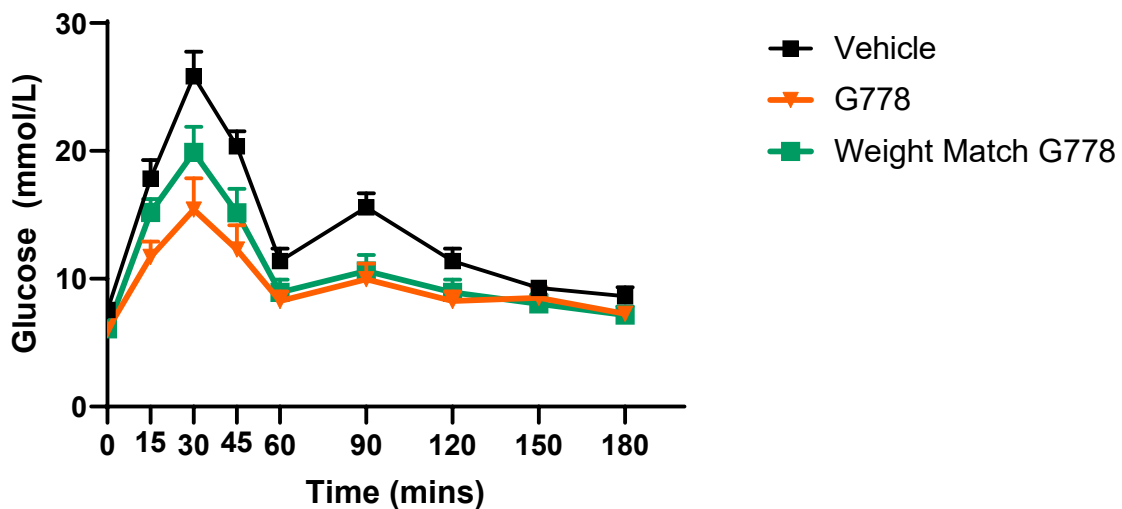


Figure 3.3.3.3 Improved glucose tolerance profile after 2-weeks glucagon-analogue treatment.

IPGTT (2g/kg) was performed at 2 weeks after the start of treatment (n=8-9/group). The average peak glycaemic values at 30min time-point were 15.4mmol/L, 19.9mmol/L and 25.8mmol/L for G778, WM to G778 and saline groups, respectively (n=8 per group; Two way ANOVA. Tukey's test)

By 40 days of treatment, G778 treated animals showed a striking improvement in glucose homeostasis compared with saline and weight matched (WM) groups. The average fasted circulating glucose was significantly different in G778 (4.3mmol/L) and vehicle treated (7.5mmol/L) groups (two-way ANOVA, Tukey's post-hoc test $p=0.0054$). Additionally, 15min blood glucose values were significantly lower for the G778 group compared with weight-matched counterparts (9.2mmol/L versus 18.5mmol/L; $p<0.001$). These results suggested that G778 improves glycaemia via weight-loss independent mechanisms (**Figure 3.3.3.4**).

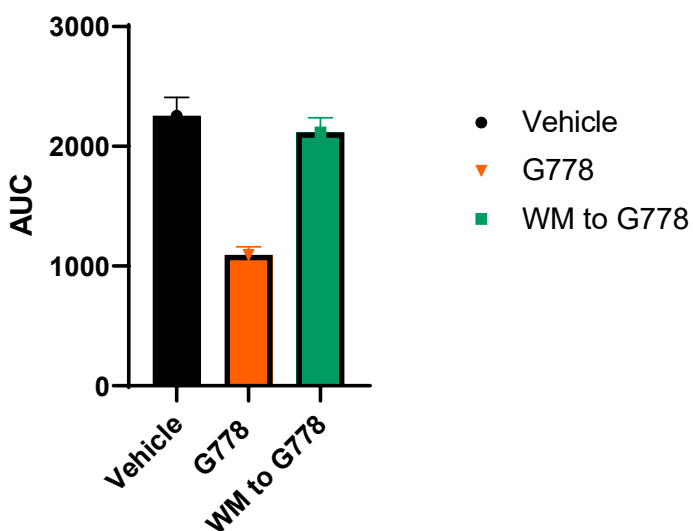
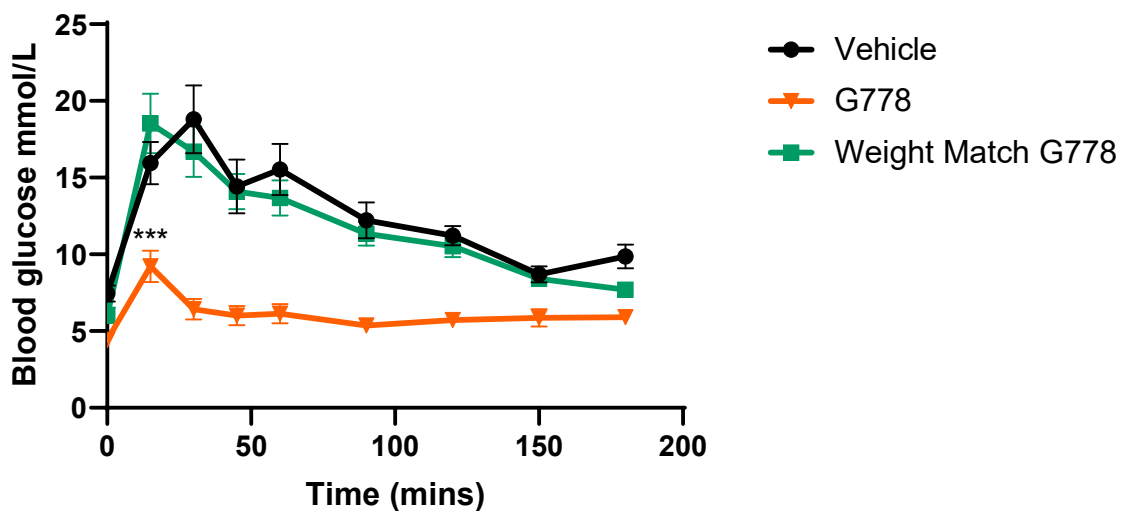


Figure 3.3.3.4 Improved glucose tolerance after 6-weeks glucagon analogue-treatment. IPGTT (2g/kg) results show a significant improvement in glucose tolerance of G778 treated group. Two-way ANOVA and Tukey's tests were used to analyse group differences ($p < 0.005$). Fasting glycaemia levels were 4.4mmol/L versus 6mmol/L and 7.5mmol/L for G778, WM to G778 and saline-treated groups, respectively. Peak glycaemic levels were 9.2mmol/L versus 18.5mmol/L and 18.8mmol/L for G778, WM to G778 and saline-treated groups, respectively.

3.3.4 DIO and G778 Induced Weight-Loss Independent Effects on Islet Calcium Dynamics in a Directly-Observed Model

In order to better understand the weight-loss independent processes that underpin the improvement in glucose homeostasis, we evaluated the calcium dynamics in Ins1Cre-GCaMP6f islets. There was a significant drop in the wave index of islets from baseline (mean value of 3.6) versus at two months on HFD (mean value of 1.5) in islets that were later receiving G778 treatment ($p = 0.032$). Additionally, the same trend was visible in islets of other groups, albeit non-significant. The wave indices suggested that some islets were less susceptible to the detrimental effects of the HFD (**Figure 3.3.4.1**).

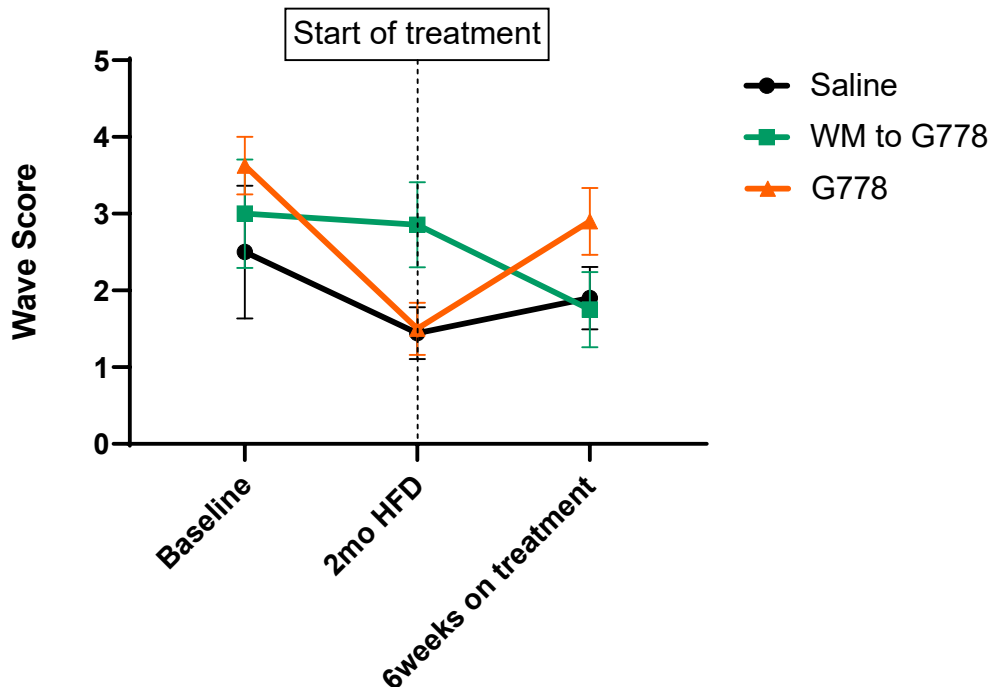
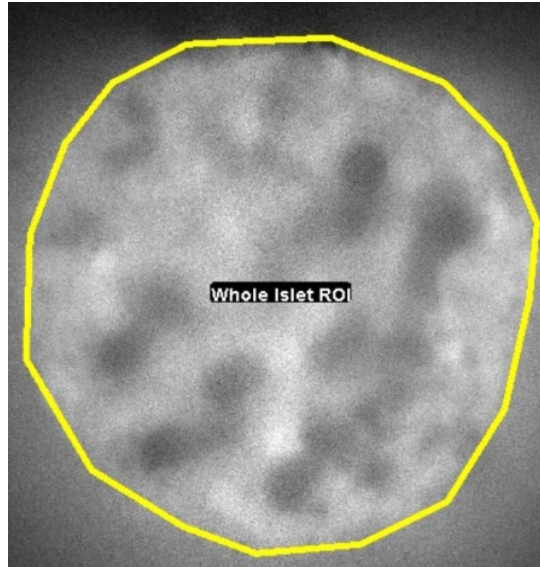


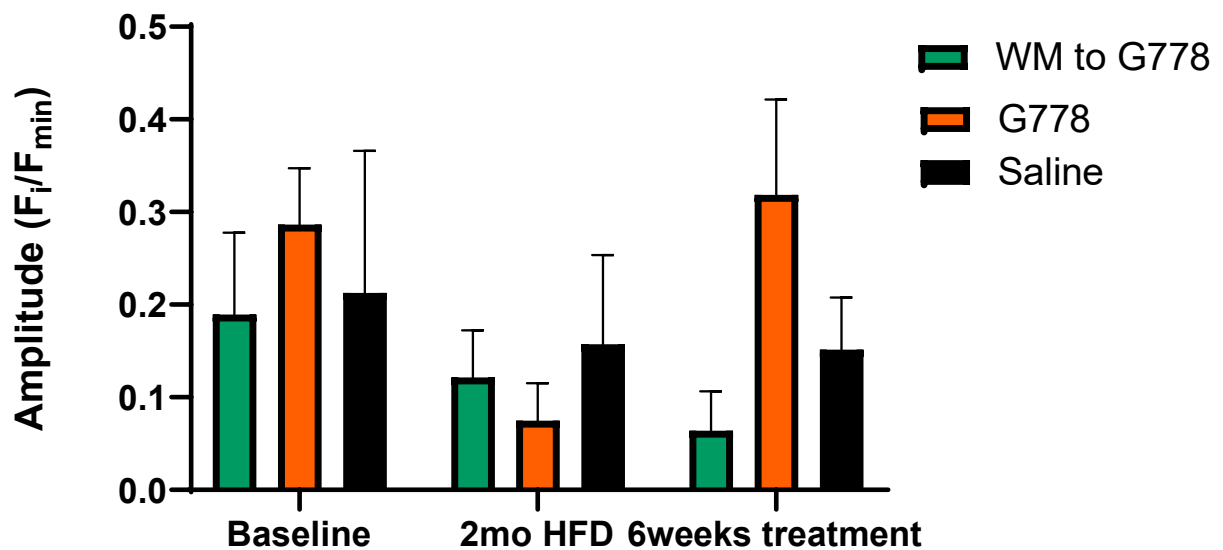
Figure 3.3.4.1 Wave index of islets over the course of the study. Overall, there was a tendency for decreased wave scores in all three experimental groups. The wave indices of islets subsequently treated with G778 showed a significant decrease between baseline and 2months on HFD (3.625 versus 1.5; $p = 0.032$ Two-way ANOVA; Tukey's multiple comparison test). Additionally, 6 weeks of G778 treatment

lead to elevated wave indices (from 1.5 to 2.9; $P=ns$ Two-way ANOVA; Tukey's multiple comparison test), a trend that was not observed in either of the saline treated groups (WM to G778 (baseline)n=4; WM to G778(2mo HFD)n=5; WM to G778(6week on treatment)n=8; G778(baseline)n=8; G778(2mo HFD)n=10; G778(6week on treatment)n=9; saline(baseline)n=3; saline(2mo HFD)n=5; saline(6week on treatment)n=6).

A)



B)



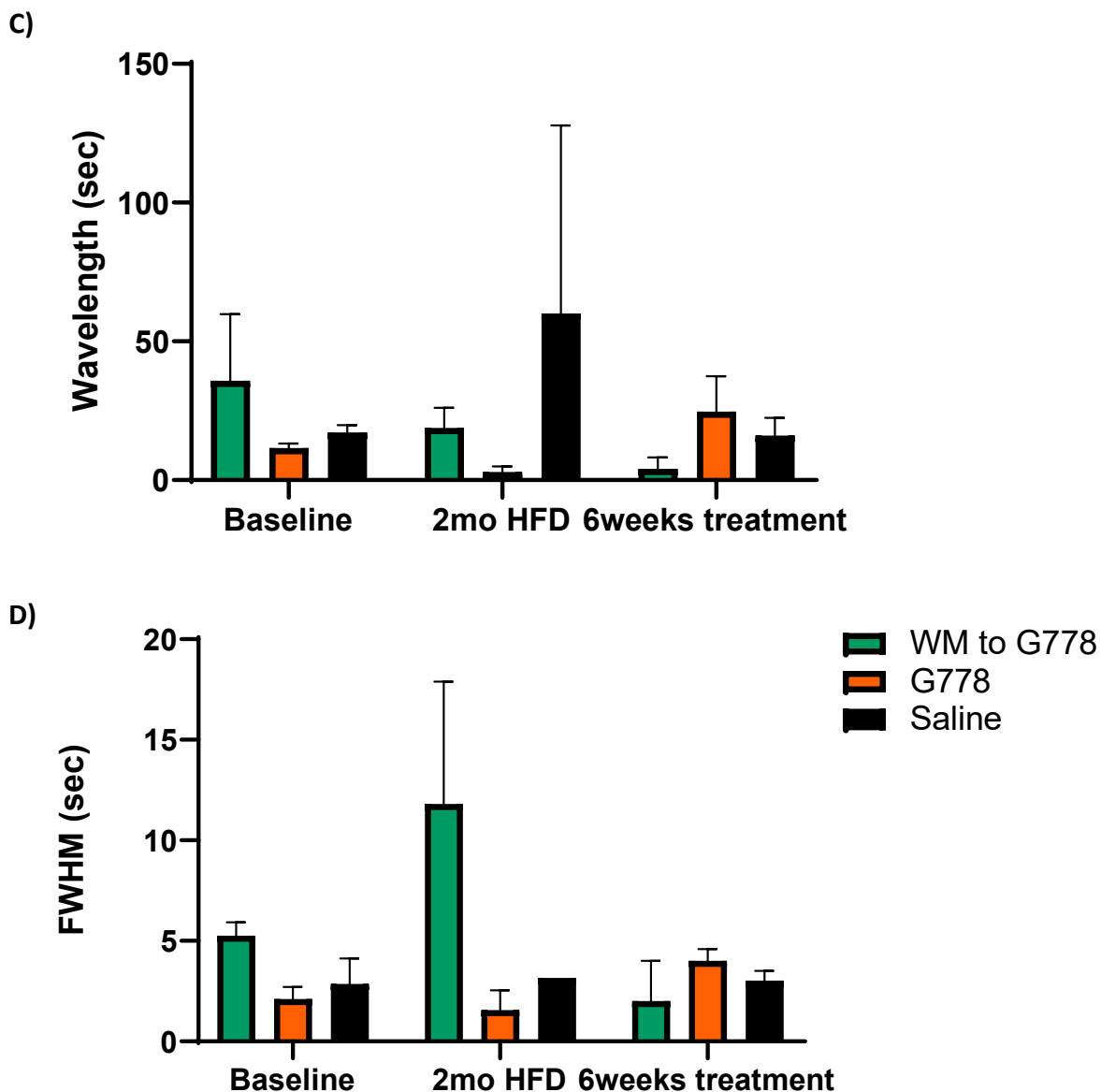


Figure 3.3.4.2 Graphs showing changes in calcium wave parameters in response to HFD and subsequent G778 treatment. The blood glucose levels were comparable between imaging sessions (i.e. high, >10mmol/L). With high-fat feeding there was a general trend for worsening waveform measures. Six weeks of G778 treatment reversed this tendency with increased average amplitude, wavelength and FWHM values (WM to G778 (baseline)n=4; WM to G778(2mo HFD)n=5; WM to G778(6week on treatment)n=8; G778(baseline)n=8; G778(2mo HFD)n=10; G778(6week on treatment)n=9; saline(baseline)n=3; saline(2mo HFD)n=5; saline(6week on treatment)n=6; Two way ANOVA, Tukey's test $P=0.2498$).

Paralleling the diminished calcium activity in islets in response to HFD, there was a trend towards reduced wave amplitudes, wavelength and full width at half maximum (FWHM) for all

islets studied. The average amplitude of calcium activity decreased from $0.29(\pm 0.06)$ at baseline to $0.07 (\pm 0.04)$ on HFD in animals that were subsequently enrolled into G778 treatment group (**Figure 3.3.4.2 B** $p=0.34$). Changes in the wavelength of calcium waves after HFD did not follow a clear pattern. Islets subsequently treated with G778 and weight-matching with saline showed a tendency for decreased average wavelength (11.6 ± 1.6 versus 3 ± 2 for G778 group and 35.8 ± 24 versus 22 ± 7.7 for weight-matched to G778; *ns*). In the meantime, the saline treated control group had a mean wavelength of $17.2 (\pm 1.8)$ initially at baseline which increased to $60.1 (\pm 48)$ after 2 months on HFD (**Figure 3.3.4.2 C**). There was a trend for decreasing FWHM values between baseline and HFD time-points; islets that later received saline treatment displayed baseline mean values of $2.9 (\pm 1.3)$ and 3.15 at 2 months on HFD, those that were later weight-matched to G778 had an average of $5.3 (\pm 0.7)$ at baseline and $11.8 (\pm 6.1)$ sec after HFD and finally, islets that were subsequently treated with G778 initially had an average of $2.1(\pm 0.6)$ at baseline and $1.6 (\pm 1)$ sec after HFD (**Figure 3.3.4.2 D**).

There was a non-significantly increased amplitude activity in the G778 group from after the 6-week treatment regimen with the average amplitude of (0.3 ± 0.06 on HFD versus $0.32 (\pm 0.1)$ after 6-week G778 regimen). Contrastingly, the average amplitudes in the weight matched to G778 and saline groups showed the opposite trend; with a decrease in average amplitude of $0.39 (\pm 0.01)$ to $0.18 (\pm 0.06)$ sec for the saline group and decrease from $0.12 (\pm 0.05)$ to 0.064 sec(± 0.04) for the weight-matched group (**Figure 3.3.4.2 B**).

Analysis of the wavelength of calcium activity suggested similar trends, except for the saline group, where there was an unexpected increase in average wavelength after 2 months of HFD (60.1 ± 48). Mirroring the wave index and amplitude changes, the wavelength in the weight-matched to G778 group decreased from $18.9 (\pm 7.2)$ to 4.1 sec by the last imaging time-point. On the other hand, G778 treatment caused islets to display calcium activity with longer wavelengths as this measure increased from $3 (\pm 2)$ to $24.7 (\pm 12.7)$ sec. FWHM values decreased over time in the control groups, from 3.15 ± 0 to $3 (\pm 0.5)$ and from $11.8 (\pm 6)$ to $0.6(\pm 0.6)$, for saline and weight matched group respectively (**Figure 3.3.4.2 D**).

Of note, circulating blood glucose levels were comparable between imaging sessions and groups. The average blood glucose levels across the groups were $10.6 (\pm 0.52)$ at baseline, $12.7 (\pm 0.6)$ at 2 months on HFD and $10 (\pm 0.3)$ during the last imaging session. Previously, we have

shown that circulating blood glucose levels of >10mmol/L enhances β -cell connectivity and consequently their calcium activity (Chapter 2). It is therefore unlikely that the diminished activity seen in response to HFD was due to low blood glucose levels during that imaging session. Overall, a general reduction in wave propagation velocity was observed across all groups, with G778 treatment not having a particular impact on this parameter of islet activity. There was only a single islet displaying type 4 (pan-islet) calcium activity for the saline group at baseline and 6 weeks after saline treatment (+HFD) and this islet showed high propagation velocities (120.8 at baseline versus 128.7 at the end of the experiment; **Figure 3.3.4.3**).

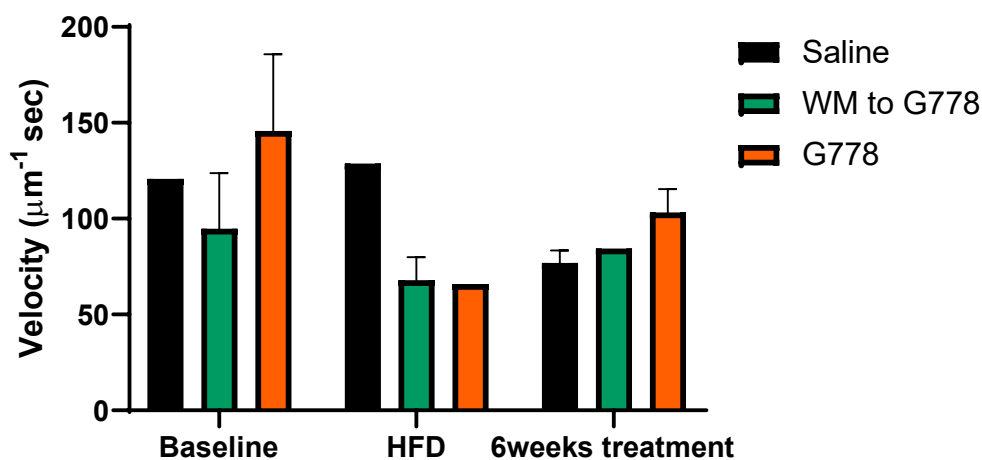


Figure 3.3.4.3 The effects of HFD and glucagon analogue treatment on wave propagation speed. The speed of wave propagation was investigated in islets displaying type 4 waving activity (wave propagated across the entirety of the islet; n=1-7). The average wave propagation speed was $96.1\mu\text{m}^{-1}\text{sec} \pm 12.18$ for the saline, $79.6\mu\text{m}^{-1}\text{sec} \pm 10.72$ for the weight-matched and $120.8\mu\text{m}^{-1}\text{sec} \pm 21.38$ for G778 groups. One-way ANOVA and Tukey's test showed that groups were not statistically significantly different however there was a tendency seen for slower wave propagation velocity among all three groups.

3.3.5 Longitudinal Assessment of β -Cell Connectivity and Leader Cells

Preliminary experiments on the longitudinal assessment of leaders in TWO islets that were longitudinally tracked within the same cross section revealed that the identity of leader cells dynamically changed between imaging sessions, although as described in Chapter 3, the visually identified leader cells and Granger defined cells overlapped well (**Figure 3.3.5.1**). Islet 1 was in an animal treated with G778 and islet 2 was treated with vehicle and weight-matched to G778 group. In islet 1 over subsequent imaging sessions, leaders emerged from the same quadrant

of the islet where they were previously seen, but in islet 2 new leaders after 6 weeks treatment (session 3) were located on the opposite side of the islet cross-section.

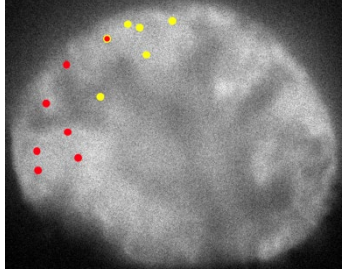
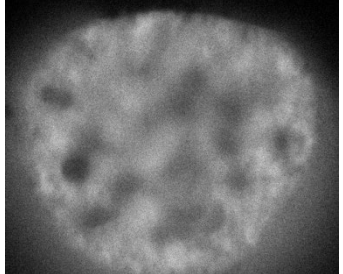
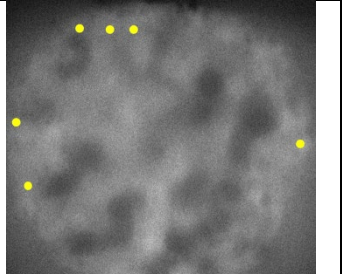
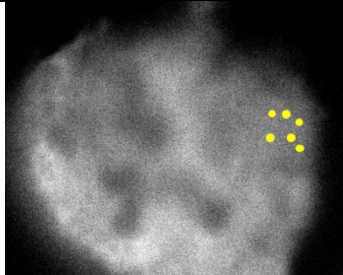
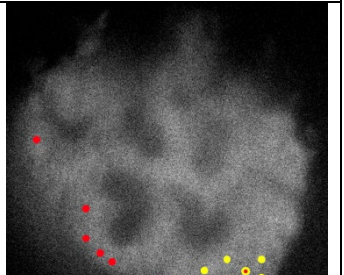
	Session 1	Session 2	Session 3
G778			
Leader cells	11, 47, 22, 41, 10, 12	Not identified as no wave captured in imaging sequence	14, 3, 49, 58, 45, 44
WM to G778	Video not analysed as cross sections were incomparable		
Leader cells		54, 21, 23, 25, 26, 24	56, 47, 18, 17, 55, 15

Figure 3.3.5.1 Cross sections of islets at each imaging session showing leader cells. The first 10% of β -cells to respond in a Ca^{2+} wave was visually identified in the recorded image sequences and highlighted in each islet cross section. These analysed islets had comparable cross sections throughout imaging sessions to ensure the accurate identification of the same β -cells over time. The positions of leader cells are highlighted in yellow. Where a Ca^{2+} wave with a different initiation site was captured in an image sequence, the leader cells are highlighted in red. Red markers with a yellow outline denote leader cells involved in both sites of Ca^{2+} wave initiation. Data is shown for G778 treatment group (Islet 1) and WM to G778-treatment group (Islet 2).

For islet 1 the average connectivity co-efficient was 0.97 at baseline which later reduced to 0.53 after 2 months on HFD. Interestingly however, 6 weeks of G778 treatment resulted in the increase of average connectivity co-efficient to 0.84. In islet 2, the average connectivity co-efficient at session 2 (2 months of HFD) was 0.82 and this further fell to 0.67 after 6 weeks of

weight-matching to G778 group. This observation suggests that DIO induces a progressive loss of β -cell connectivity and that weight-loss on its own is ineffective at reversing this trend.

When the number of connected cells was examined it was found that in islet 2 (WM to G778) under DIO 86% of cells were connected and this later dropped to 52%. In islet 1, all cells were connected at baseline, but percentage connectivity diminished to 44% after 2 months HFD and G778 treatment was only able to increase percentage connectivity back to 51% after 6 weeks. These very preliminary findings suggest that leader cells are not fixed over time and that G778 treatment was able to partially restore islet calcium dynamics, an effect that was better than weight-loss alone (**Figure 3.3.5.2**).

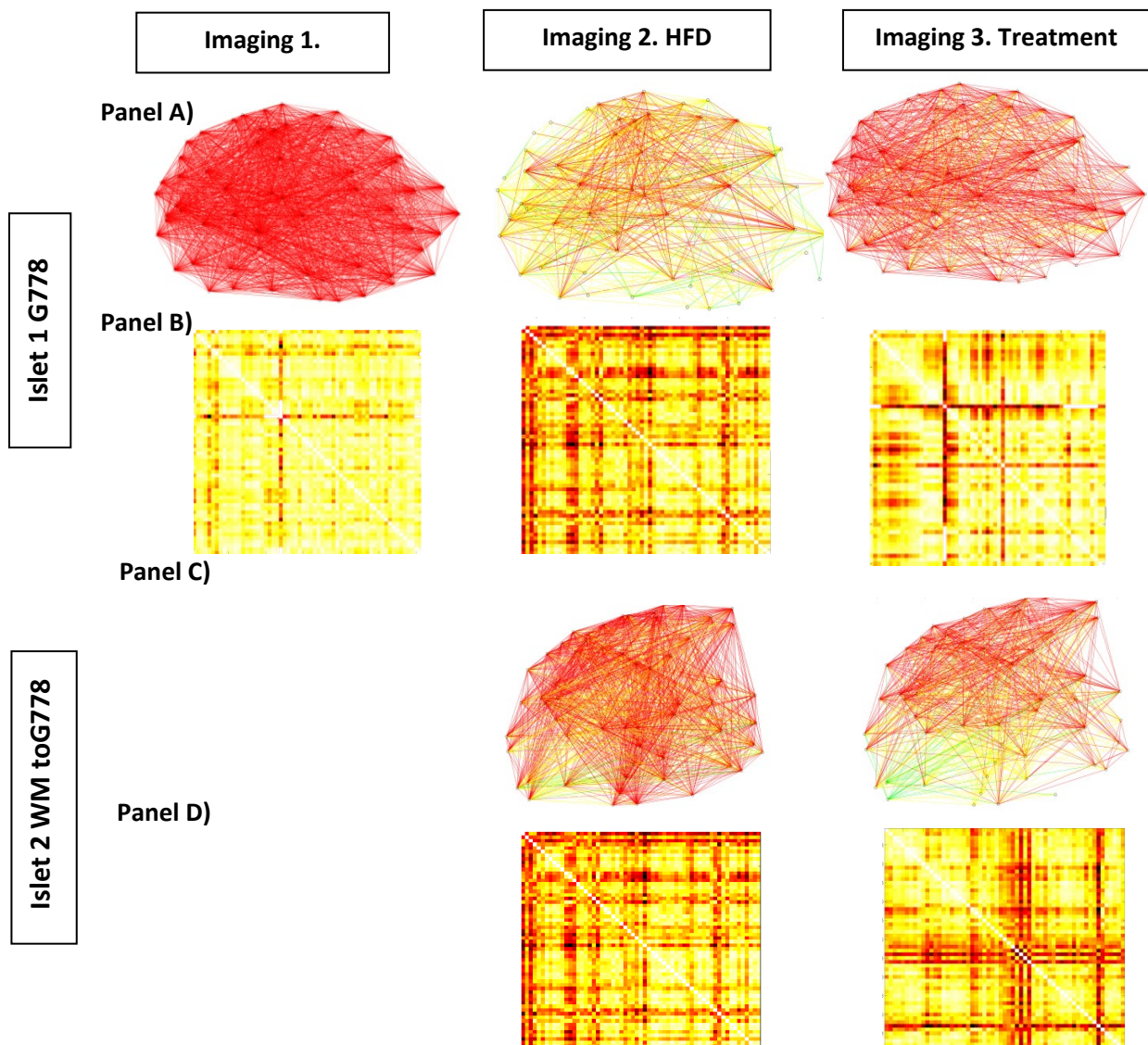
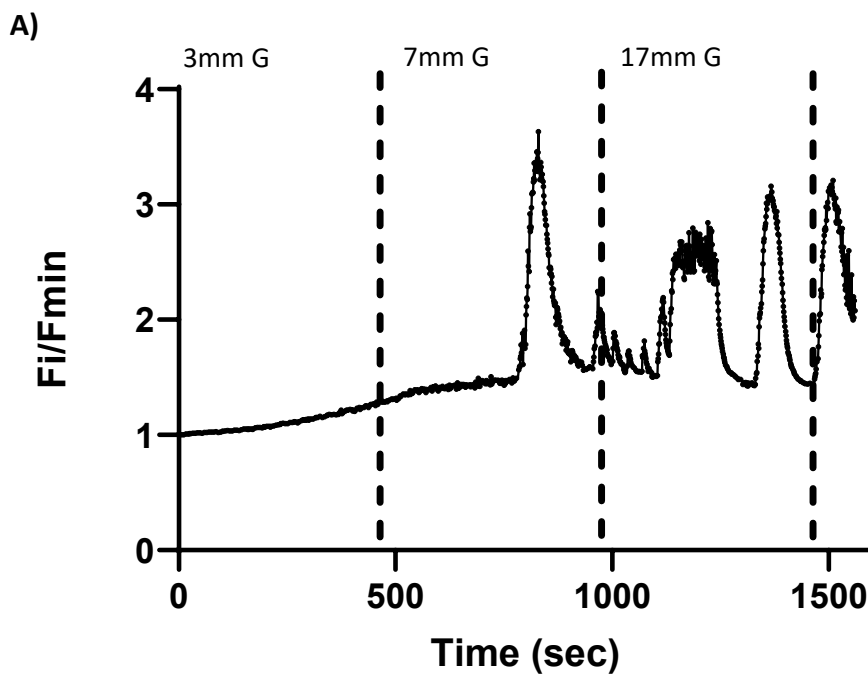


Figure 3.3.5.2 β -cell connectivity changes in from baseline to DIO and 6 weeks of chronic G778 treatment. Cartesian maps (Panels A and C)) showing connectivity changes over the course of 3 imaging sessions in G778- (Panel A) and WM to G778- (Panel C) treated islets. Cell pairs with a Pearson R of 0.25-0.5 have a green line connecting them, those pairs with Pearson R values of 0.5-0.75 have a yellow between them and finally those pairs whose connection was the strongest Pearson R of 0.75-1 have a red line connecting them. Heat matrices for these same islets are presented in Panels B (G778) and D (WM to G778).

3.3.6 The Effects of G778 on Islet Calcium Dynamics *In Vitro*

The striking effect of G778 on glycaemia prompted us to further and more directly investigate the effects of G778 on islet function. To this end, InsCre-GCaMP6f-expressing islets were isolated and calcium responses were recorded in the presence and absence of 60nmol G778 under increasing glucose concentrations (3mmol, 7mmol and 17mmol; **Figure 3.3.6.1**).



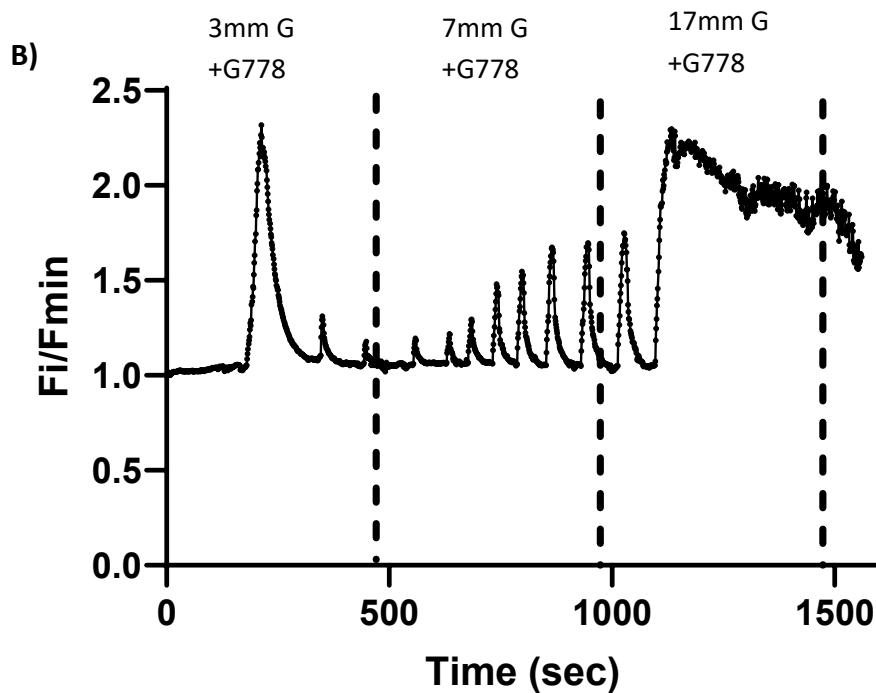


Figure 3.3.6.1 Representative calcium traces under glucose-only and glucose+G778 conditions.

The calcium trace of each islet was normalised to the minimum fluorescence intensity value measured for that islet in a given imaging session. Figure A) shows a representative calcium trace captured during glucose-only experiments and figure B) shows a calcium trace from glucose+G778 treated islets *in vitro*

At 3mmol glucose concentrations, β -cells are normally quiescent with little to no calcium changes. Indeed, this was the case during perfusion experiments with Ins1Cre-GCaMP6f islets. The addition of 60nmol G778 to 3mmol glucose however, incited calcium activity with average amplitude of $0.34 (\pm 0.18)$, average wavelength of $89.75 (\pm 36.5)$ and average FWHM values of $9.8 (\pm 3.3)$ (**Figure 3.3.6.2**).

Increasing the glucose concentration to 7mmol triggered a calcium response in islets where the mean amplitude was $0.52 (\pm 0.2)$, mean wavelength was $21.7 (\pm 9.7)$ and the FWHM $16.8 (\pm 7.7)$. At this concentration and in the presence of 60nmol G778, islets displayed mean amplitude of $0.31 (\pm 0.05)$, mean wavelength of $88.6 (\pm 17.9)$ and mean FWHM values of $20.28 (\pm 4.6)$. Therefore, while glucose only experiments elicited greater amplitude calcium responses from islets, the addition of G778 resulted in more sustained, longer-lasting calcium activity as evidenced by FWHM values. Wavelength read-outs suggested that the frequency of calcium activity is lower with the addition of the long-acting glucagon analogue G778. Islets perfused

with G778 and glucose displayed a calcium activity with longer wavelengths than islets in glucose only perfusions (88.6 versus 21.7; $p=0.36$) (**Figure 3.3.6.2**).

Lastly, islets were perfused with 17mmol glucose concentration which resulted in average amplitudes of 1.38 (± 0.07), average wavelengths of 105.7 (± 21.9) and average FWHM of 107.7 (± 20.1). Similarly to the trends seen under 7mmol glucose, the addition of 60mmol G778 lead to average amplitudes of 0.86 (± 0.05), average wavelengths of 121.1 (± 13.7) and average FWHM values of 138.9 (± 26.6). The amplitude of calcium activity was significantly larger in the glucose only perfusions compared to when G778 was co-perfused with glucose (1.38 versus 0.86 for glucose only and glucose+G778 perfusions, respectively $P=0.036$; Two-way ANOVA, Tukey's multiple comparison test). The wavelength of calcium activity on the other hand was longer in the G778 perfused group compared to glucose-only experiments; 121.1 versus 105.7 for 17mmol glucose+G778 and 17mmol glucose only perfusions, respectively. In parallel, FWHM values were also different in G778+ 17mmol glucose and 17mmol glucose only experiments (138.9 versus 107.7; $P=ns$; **Figure 3.3.6.2**).

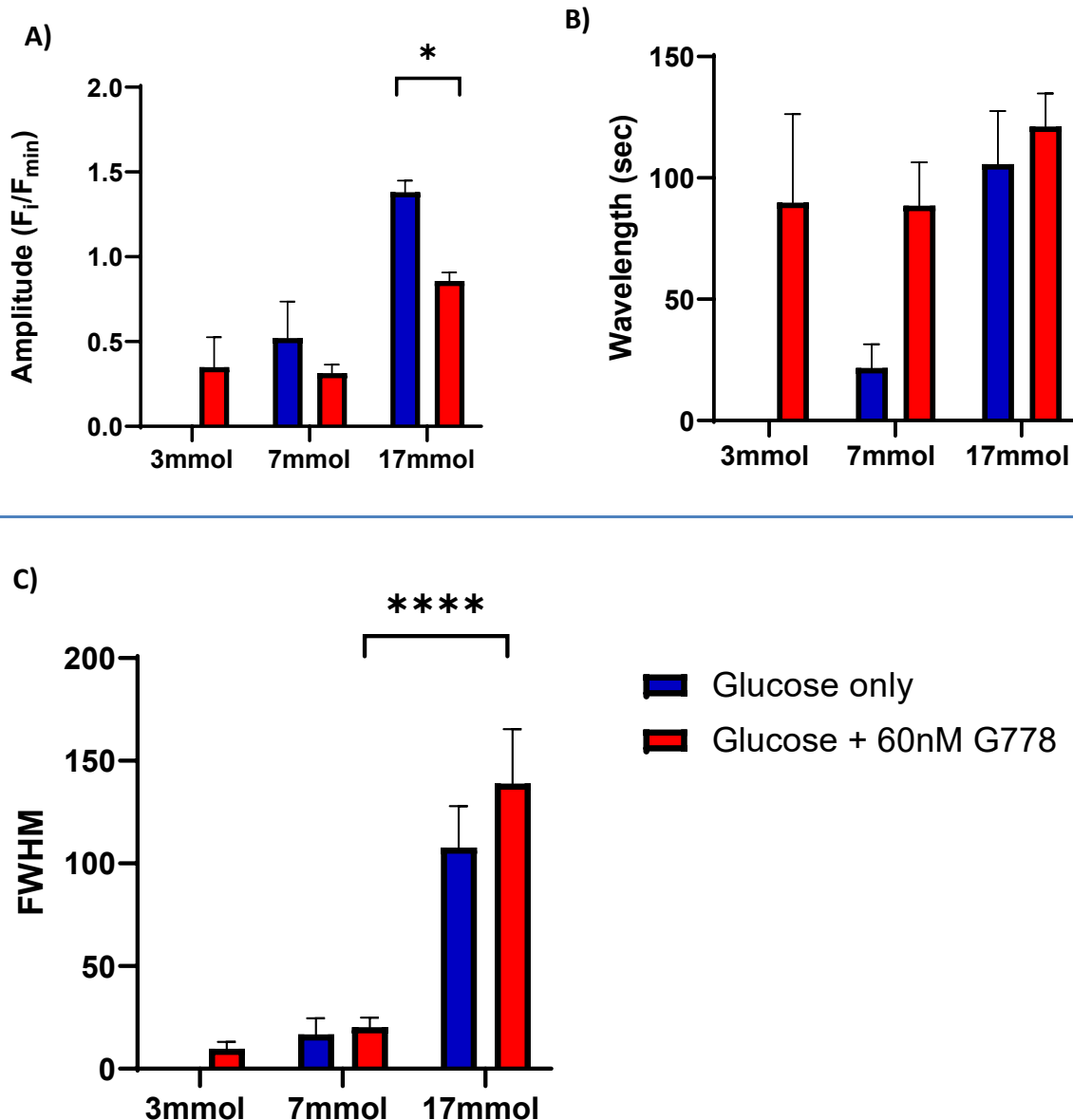


Figure 3.3.6.2 Graphs showing differences in islet calcium activity parameters in glucose-only and glucose+G778 experiments. Amplitude, wavelength and FWHM were analysed separately at each glucose concentration using Two-way ANOVA and Tukey's multiple comparisons test, $p < 0.001$. ($n = 17$ for glucose only group; $n = 28$ for glucose+G778 from 4 InsCre-GCaMP6f-expressing C57Bl6/J donors). The average amplitude of calcium activity was statistically significantly different between glucose only and G778-treated groups ($P = 0.0366$). Increasing the glucose concentration from 7mmol to 17mmol resulted in a statistically significant increase in FWHM in islets treated with 60nM G778 $P < 0.001$.

3.4 Discussion

This is the first time the direct effects of chronic glucagon treatment on islet function in DIO mice have been assessed *in vivo*. DIO mice exhibited a gradually worsening glycaemic phenotype and this was also reflected in the global diminution of islet calcium responsiveness under high glucose concentrations. Surprisingly, chronic glucagon treatment was able to partially rescue this phenotype as indicated by improved glucose tolerance of mice. After correcting for weight loss, *in vivo* islet read-outs suggested that the beneficial effects of glucagon are conferred at least in part by its ability to reverse calcium responsiveness. From our *in vitro* observations, we speculate that glucagon might normalise glycaemia by stimulating more robust and prolonged calcium responses at high glucose levels. Taken together, our data suggests that glucagon normalises glycaemia by directly orchestrating pan-islet coordinated calcium activity. Preliminary data from one islet in each group (G778 vs WM to G778) whereby the same cells were identified in the same cross section provided evidence that glucagon receptor agonism at least partially restores pan islet calcium activity.

3.4.1 High-Fat Feeding Causes a Diminution in Global Calcium Responses in the Majority of Transplanted Islets

With chronic high-fat feeding, we observed a tendency for diminished islet-wide calcium activity as reflected in the “wave indices” of transplanted islets. Consequentially, the majority of the islets displayed a reduction in all measures of wave characteristics, including amplitude, wavelength and full-width half maximum. Surprisingly however, some of the islets were more resilient to the effects of HFD than others (as reflected by lack of change in wave index at 2months HFD) and therefore the effects of weight-loss and G778 interventions should be treated with caution. It is likely that transplanted islets differ in their β -cell reserve capacity and that the detrimental effects of HFD become apparent at varying stages into high-fat feeding.

In general, there is a disparity between the acute versus chronic effects of free fatty acids (FFA) on islet function; the co-administration of lard oil and glucose after a period of fasting potentiated insulin secretion acutely *in vitro* (Nolan et al. 2006; Dobbins et al. 1998; Boden 2003). Later work has shown that acute effects of FFA are mediated through GPR40, an abundantly expressed receptor on the surface of β -cells, through Epac signalling (Song et al. 2013). Epac is a cAMP-regulated guanine nucleotide exchange factor whose binding to cAMP is activated by GLP-1 and plays a major role in cAMP mediated liberation of intracellular calcium

stores and calcium-dependent insulin exocytosis (Holz 2004). Thus, acutely FFAs potentiate insulin secretion both *in vitro* and *in vivo* (Chen et al. 2016).

The underlying mechanisms for the gradual loss of β -cells to propagate calcium waves in response to chronic HFD can be either intra- or intercellular in nature. Hoppa et al. has investigated in the past the effects of chronic exposure of islets to palmitate *in vitro*. Whilst membrane depolarization normally produces discrete regions of intracellular calcium in control islets, a more diffuse pattern of intracellular calcium signal was observed in cells subjected to palmitate. This finding was also reflected in a reduced coefficient of variation in the palmitate treated group where depolarization evoked a significantly less compartmentalised calcium response in β -cells. Under normal conditions, secretory granules of the readily releasable pool (RRP) are located in the close proximity of calcium channels and experience a rapid surge in local intracellular calcium concentrations upon depolarization. In palmitate treated β -cells, there were no topological differences in calcium surge and proximal granule discharge was inhibited by about 85%. All together these observations suggested that palmitate selectively decouples calcium channels from secretory vesicles of the RRP thereby impeding fast exocytotic responses to stimuli. With prolonged stimulus these secretory deficits could be ameliorated (Hoppa et al. 2009). Interestingly, the same group found that in mice on HFD the delayed rectifier K^+ current which is responsible for hyperpolarization, was reduced in a GPR40-dependent manner. Naturally, this leads to the prolongation of stimulus and allows β -cells to compensate for the secretory deficit arising from less efficient calcium channel clustering and their functional decoupling from RRP granules (Collins et al. 2010).

A more recent line of research focused on the effects of FFAs on cell-cell coupling and intercellular calcium dynamics. Carvalho and colleagues demonstrated that high-fat diet fed animals had down-regulated expression of connexin 36 (Cx36) which meant that gap junction coupling of β -cells was selectively altered. Further, tracer microinjection studies suggested that intercellular transfer was impeded in HFD islets compared to controls (Carvalho et al. 2012). Research from our lab has shown that chronic incubation of human islets with palmitate decreases Cx36 expression levels in a PKA-dependent manner and selectively attenuates incretin-stimulated calcium responses. The percentage of correlated cell pairs in response to GLP-1 treatment was also reduced in the palmitate group when compared with control islets. Very interestingly and conversely to human findings, islets from HFD mice showed disorganised

intracellular calcium oscillations in response to high glucose levels yet retained their responsiveness to GLP-1. These findings could also be recapitulated by incubating islets with palmitate thereby providing further evidence that FFAs have a direct effect on β -cell function and cell-cell coupling (Hodson et al. 2013). In accordance with these findings, in the same year it was found that mice on HFD for 8 weeks who had become insulin-resistant, had their GLP1Rs upregulated on the surface of their β -cells. Moreover, intestinal secretion of GLP-1 in the HFD was also elevated as well as GPR119 activation, providing further evidence that incretin-stimulated insulin secretion is preserved in rodent models of diabetes and compensates for the emerging insulin resistant phenotype (Ahlqvist and Ahren 2013).

3.4.2 A Long-Acting Glucagon Analogue Improves Glycaemia - The Role of Glucagon in Homeostatic Control of Glucose

The insulinotropic actions of glucagon were recognised as early as 1966 when the co-infusion of glucagon with glucose resulted in enhanced insulin secretion in contrast to a glucose-only stimulus (Huypens et al. 2000; Samols et al. 1966; Simpson et al. 1968). β -cells in isolation show poorer glucose competence than when they are juxtaposed to other endocrine cells, further highlighting the importance of paracrine crosstalk in islet function.

A major regulatory role for glucagon in the maintenance of human glycaemic set-point has been put forward by Rodriguez-Diaz and colleagues. Accordingly, the pancreatic islet functions as the glucostat of the body, and is responsible for glucose sensing and adjusting secretory behaviour to maintain glycaemia within a narrow homeostatic range. The actions of glucagon are twofold: when blood glucose levels drop beyond homeostatic values, glucagon secretion is stimulated and produces its canonical systemic hyperglycaemic effects. However, under hyperglycaemic conditions, α -cells act to amplify insulin secretion to match the secretory demand. Interestingly, the authors propose that species specific differences in homeostatic values arise from variations in islet α -cell content. Consequentially, islets with higher α -cell content display a tendency for lower normoglycaemic values (Rodriguez-Diaz et al. 2018). These putative dual modes of action were inadvertently separated in a study where glucokinase expression was selectively ablated in α -cells. Deletion of α -cell glucokinase led to an elevation in post-prandial glucagon levels, an improved glucose tolerance profile and higher insulin secretory capacity in young animals, supporting the notion that glucagon is an insulin secretagogue. Most striking of all, the insulin content of β -cells was not altered when

compared with WT controls and thus cannot account for better insulin secretion in α Gck-KO animals. Instead, it is plausible that enhanced paracrine signalling in this model improves β -cell function itself. It has to be noted however, that older animals eventually developed fasting hyperglucagonaemia and a pre-diabetic phenotype, underscoring the importance of α -cell glucokinase in glucose-mediated suppression of glucagon (Basco et al. 2018).

3.4.3 Glucagon as an Insulin Secretagogue

In the past year, a series of new studies emerged which further challenged the dogmatic views held on glucagon. Using designer inhibitory GPCRs, glucagon secretion was effectively inhibited in animals and led to drastic reductions in insulin secretion and impaired glucose handling. The phenotype could be reversed by exogenous glucagon, demonstrating that β -cells are capable of restoring normoglycaemia provided that a glucagonergic input is present (Zhu et al. 2019). In line with Zhu and colleague's findings, the investigation of pro-glucagon peptides in the context of insulin secretion yielded similar results. Of note, the paracrine input from pro-glucagon derived peptides establishes a β -cell tone mainly mediated by GLP-1 receptors and to a lesser extent, by glucagon receptors. The lack of paracrine signalling directly influences both triggering and amplifying pathways of insulin secretion putatively via reduced cAMP signalling (Capozzi et al. 2019a). In a series of *in vivo* and perfusion experiments, it was subsequently shown that β -cell activity is required for glucagon to stimulate insulin secretion. Under fasted conditions, a bolus of alanine challenge induced hyperglucagonemia whilst failing to stimulate insulin secretion. On the other hand, an IP injection of alanine produced elevated insulin and glucagon secretion simultaneously (Capozzi et al. 2019b). The incretin-like actions of glucagon at elevated glucose levels were also apparent in our perfusion studies with a synthetic analogue. Additionally, we observed a transient spike of activity in β -cells in the presence of the glucagon analogue at 3mmol glucose concentrations. The significance of this is unclear but we hypothesise that glucagon under low glucose might prime β -cells for a more efficient response at elevated glucose levels.

From the above studies, a dichotomy of paracrine versus systemic actions of glucagon transpires. Whilst seemingly contradictory, intra-islet glucagon signalling appears to be essential for optimal insulin secretion (**Figure 3.4.3.1**).

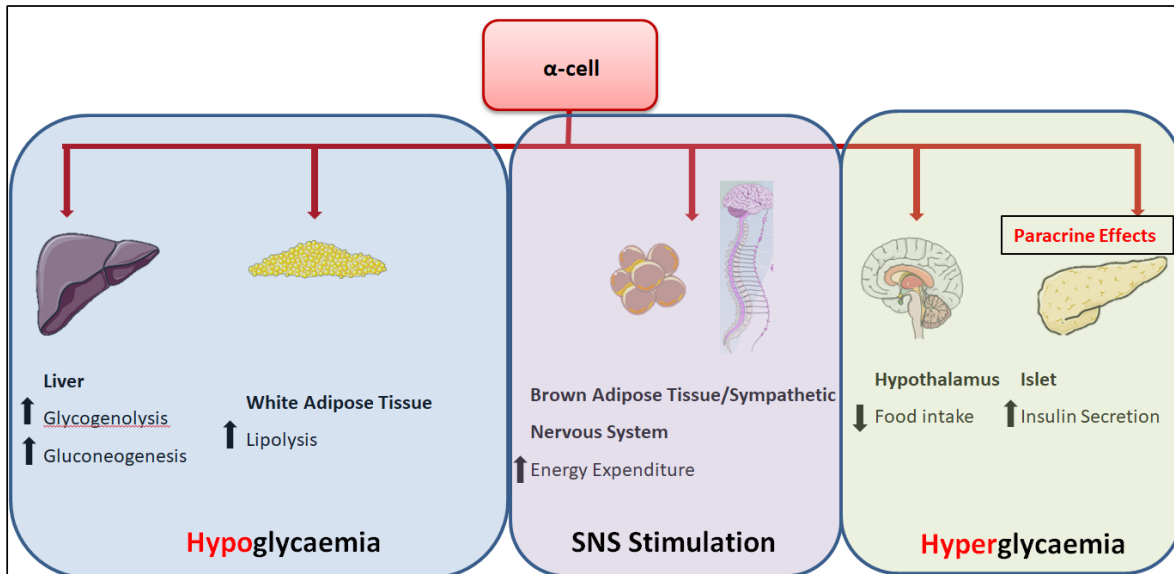


Figure 3.4.3.1 Systemic versus paracrine actions of glucagon.

In the context of diet-induced obesity, it seems plausible that β -cells remain responsive to incretins, at least in the early, pre-diabetic phase and this could account for the improved glycaemic profiles of our animals. Due to technical constraints it is currently not possible to measure intra-islet glucagon concentrations but it is assumed that levels are vastly different from peripheral concentrations. Studies indicate that whilst GLP-1 is only minimally effective at glucagon receptors, GLP-1 receptor produced EC_{50} values of 0.03nM and 3nM for GLP-1 and glucagon, respectively. Through titration experiments in $Gcg^{-/-}$ islets, the glucagon levels for insulinotropic actions was estimated to be between 0.3-1nM. Values are likely to be higher than these estimates as the mouse model in which this was investigated was reported to have increased GLP-1 receptor expression. Nevertheless, this suggests that our choice of 60nmol of G778 is in a range where the incretin-like effects should become apparent. The more pronounced effects of G778 at the concentration of 160nmol/kg *in vivo* on glucose homeostasis could be indicative of having pharmacologically achieved sufficient intra-islet concentrations to potentiate insulin (Finan et al. 2020).

Whether insulin secretion is promoted via effects at the individual β -cell level or they arise from improved signal transmission between β -cells remains to be further investigated.

3.4.4 Connectivity as a longitudinal read-out

Leader identification and Granger causality analysis revealed that the identity of leaders dynamically changes. In addition, leaders have been observed to emerge from contralateral areas of the islet cross-section while in others they originated from the same area. It was previously suggested by both Westacott and colleagues and Stozer and colleagues that cells with similar coupling conductance and metabolic activity preferentially cluster together (Westacott et al 2017; Farnsworth et al 2014; Markovic et al 2015). With this in mind, it is perhaps not surprising that while the exact identity of leaders change, they tend to derive from the same area of the islet as previously seen. However, the observation that leaders emerge from the contralateral side of the islet between imaging sessions suggests that the metabolic activity and gap junction conductance of cells may also dynamically change over time.

Our preliminary investigation into islet connectivity changes in response to DIO and subsequent G778 treatment have shown that β -cell connectivity is diminished in DIO and this can be partially rescued by chronic glucagon receptor agonism. Previously mentioned reductions in wave indices were mirrored by decreased connectivity in both islets investigated. The observation that both the number of cells and the strength of connections diminished in the WM group suggests that weight loss on its own is unable to fully resurrect pan-islet synchronised calcium behaviour. Chronic glucagon analogue treatment on the other hand, effectively increased the average connectivity co-efficient in the islet suggesting that the synchronised calcium response of β -cells was at least partially restored. A very intriguing finding however was that while the strength of connections increased with G778 treatment, the number of cells connected remained comparable to what was observed on HFD, prior to the intervention. Therefore improvements in islet calcium signalling are partially conferred by G778's ability to potentiate β -cell to β -cell communication between those cells which continue to exhibit a level of synchronicity after 2 months of DIO. This observation is in line with the notion that intra-islet glucagon acts in an incretin-like manner. Accordingly, in order for glucagon to stimulate insulin secretion β -cell activity is required (Capozzi et al. 2019b) and pan-islet calcium connectivity is only improved if there are still remaining functional β -cells whose activity can be amplified. Interesting questions arise from this observation – what percentage of the β -cell population has to remain functional in order for G778 to produce a positive effect? There is considerable heterogeneity among β -cells – does the metabolic status, gap junction and electrical conductance of the remainder functional reserve impact treatment success with

G778? Additionally, on the third imaging session a marginal increase (<10%) was observed in the number of connected cells. This raises the question whether it is possible to restore functional status of cells by glucagonergic agonism if given enough time.

4 Chapter: Investigating the Effects of β -cell Specific Overexpression of Epidermal Growth Factor Receptor on Islet Revascularization

4.1 Introduction

4.1.1 Clinical Management of Type 1 Diabetes Mellitus (T1DM)

T1DM is generally considered as a chronic autoimmune disease resulting in the destruction of insulin-producing pancreatic β -cells, leading to chronic hyperglycaemia leading to microvascular complications (for more detail on disease pathogenesis see to Chapter 1 Section 1.1.2). The landmark DCCT Trial confirmed that tighter glycaemic control in patients with T1DM dramatically reduces the risk of vascular complications and hence lengthens life (DCCT Trial American Diabetes Association 1987). Several formulations of synthetic insulin analogues have been developed, with a variety of durations of action. These are administered on multiple occasions throughout the day and are adjusted according to the patient's lifestyle and the carbohydrate load of their meals. Consequentially, patient education by specialist care providers is vital to best manage glycaemia in T1DM. Even so, T1DM is still associated with a reduced life expectancy and life-threatening diabetic emergencies. Weinstock and colleagues reported that at least 11.8% of patients had an episode of ketoacidosis and 4.8% of them experienced severe hypoglycaemia over a 12-month period (Weinstock et al. 2013; Natrass 2010).

4.1.2 Impaired Awareness of Hypoglycaemia

Repeated exposure to insulin-induced hypoglycaemia predisposes patients to a condition termed impaired awareness of hypoglycaemia (IAH) in which the perception of hypoglycaemia is either impaired or absent (Graveling et al. 2010). In these patients, the recurrent hypoglycaemic episodes elicit adaptive changes in the brain and autonomic system to lower the glycaemic threshold at which hypoglycaemic symptoms are perceived (Janssen et al. 2000). In addition to a lowered neuronal glycaemic set-point, hormonal counter-regulatory mechanisms are also impaired; glucagon and both cortisol and adrenaline levels are attenuated in response to hypoglycaemia in patients with IAH (Tesfaye and Seaquist 2010). As a result, the interval between the onset of hypoglycaemia-induced warning signs and the development of

neuroglycopenia is markedly diminished, putting patients at an increased risk of severe hypoglycaemia and death (White et al. 2009).

IAH is usually managed by a period of laxer glycaemic control in the expectation that running slightly higher blood sugars will allow the body's counter regulatory systems to reset. However, for a small number of patients with "brittle" diabetes, recurrent and severe hypoglycaemia can be debilitating (Vantghem and Press 2006). For this cohort of patients sometimes the only means of stabilising blood glucose is via pancreas transplantation. Whole organ pancreas transplantation is only indicated for patients alongside kidney transplant for end stage renal failure, since the graft failure rate of the pancreas alone is too high and the benefits do not outweigh the risk of the operation and subsequent need for lifelong immunosuppression. Nevertheless, for some patients, a pancreas-kidney transplant can be transformative. Besides better glycaemic control, microvascular complications are also reported to improve (Ludwig et al. 2010). The benefits conferred by whole-organ transplantation are difficult to interpret because often the patients for whom it is indicated already have advanced and irreversible complications and it may not confer survival benefit (White et al. 2009). Also, pancreatic transplant surgery is technically very challenging and there are significant peri-operative risks to consider.

4.1.3 Islet Transplantation as an Alternative Treatment

The transplantation of purified islets provides an alternative to whole-organ surgeries while achieving similar results with minimised surgical risks associated. The procedure involves the insertion of an ultrasound-guided catheter through which islets are carefully infused into the hepatic portal vein. Eventually, islets settle in the sinusoids of the liver where they later engraft. An important distinction with whole-organ transplants is that purified islet transplantation involves an avascular period of days during which the islets can only access oxygen and clear their metabolic waste-products by means of passive diffusion (Pepper et al. 2013). Being highly metabolically active organs the ischaemic attack may not be well-tolerated and indeed this procedure was limited by very poor transplant success rates in its infancy. With the advent of the Edmonton protocol in 2000, the peri-operative use of glucocorticoids was substituted with a different class of immunosuppressant agents (Shapiro 2000). In most clinics, the calcineurin inhibitor tacrolimus is now in use which exerts its effects by inhibiting the transcription of early T-cell activation genes for interleukin-2 (IL-2) and other cytokines (Tanabe 2003). The efficacy of

tacrolimus to prevent xenograft rejection is comparable to glucocorticoids and its implementation meant that glucose-elevating properties of glucocorticoid use could be avoided. However, the use of tacrolimus is not without its own set of limitations. Ironically, tacrolimus has a narrow therapeutic range and its long-term use has been associated with nephrotoxic complications. Nevertheless, the major benefit of islet transplantation is that it can restore glucose-regulated insulin secretion in patients, drastically reducing the risk of hypoglycaemia related fatalities. Accordingly, wide-range fluctuations in glycaemia have been reported to be corrected by the procedure (Ryan et al. 2001). The majority of patients undergoing surgery still have a functional reserve of transplanted islets at 5 years post-surgery but only about 10% of them maintain insulin independence at this time-point (Ludwig et al 2010). At present, the main aim of surgical intervention is to prevent life-threatening hypoglycaemic episodes and wide glycaemic fluctuations rather than the complete abandonment of diabetes medications. There is therefore great need and hope for improved islet transplant protocols that may allow this to become a viable treatment option as a cure for T1DM, open to many more patients.

4.1.4 Current limitations of the technique

According to the Edmonton protocol, an estimated number of 5000 islets/kg of recipient body weight is recommended for achieving notable improvements in glycaemia following transplantation (Shapiro 2000). In most instances however, multiple organ donors and islet injections are required to achieve sufficient numbers. The procurement of a large number of high quality purified islets is impeded by many factors related to the technical difficulties of islet purification and relative lack of islet donors. Islet isolation requires highly skilled personnel and the procedure is only available in a selected number of hospitals presently (Rother and Harlan 2004). Additionally, only 10-15% of patients manage to achieve insulin independence and implanted islet function only exceeds 20% of that seen in diabetic islets (Johansson et al. 2005). One potential reason behind reduced islet mass and function after transplantation could be that islets trigger an instant blood-mediated inflammatory reaction (IBMIR) when introduced into the hepatic portal vein. Tissue factor (TF) is a transmembrane protein that initiates blood coagulation and has been found to be expressed in increased numbers on the surface of endocrine cells in transplanted islets (Moberg et al. 2002). In a 7-day follow-up study after islet transplantation surgery, TF-mediated IBMIR was negatively correlated with insulin secretion in patients (Johansson et al. 2005).

Due to the lack of supply of high-standard islets and problems associated with engraftment, it is therefore imperative that islet transplantation is improved to maximise surgical outcome. Contrasting whole organ transplants, the vasculature of islets is severed upon purification and is not surgically anastomosed during the operation. Consequentially, islets undergo a significant amount of mechanical and ischaemic stress before angiogenesis would take place. During this time, the oxygen demand of highly metabolic islets is met by means of passive diffusion until re-vascularisation is completed. A delay in the formation of vascular network means that the core of the islet where oxygen diffusion is likely limited potentially becomes starved of oxygen and becomes necrotic. Indeed, transplanted islets were found to be poorly oxygenated as evidenced by the accumulation of the hypoxia marker pimonidazole in intrahepatic islets in mice (Olsson et al. 2011; Giuliani et al. 2005). Oxygen deprivation results in the triggering of apoptotic cascades which reduces β -cell mass and leads to the recruitment of immune cells to the transplantation site. A pro-inflammatory immune response can ultimately lead to the resorption of transplanted islets. Additionally, in those islets which have engrafted, it has been shown that vascular density is inferior to that seen in pancreatic islets *in situ* (Mattson et al. 2002).

4.1.5 Engraftment of Transplanted Islets with Focus on Angiogenesis

The process of engraftment entails the adaptation of transplanted tissue to the new internal milieu of the host organism. This is a complex process, involving the re-establishment of vascular and nerve supply, the expansion of the stromal supporting tissue and the reorganisation of endocrine tissue. Islet implantation occurs in one of two ways, islets can implant as separate entities or as aggregates of islets.

According to observations, islets begin to establish their vascular supply 3-5 days after transplantation and blood flow is re-established by 7-14 days. The commonest form of angiogenesis occurs through vascular sprouting of the microvasculature. Contrastingly, at the intrahepatic transplant site, it was found that tributaries of the hepatic artery are the major contributors of vessel supply to newly transplanted islets (Pepper et al. 2013), which might partially explain the poor vascular function of islets at this site.

During angiogenesis, highly motile blood vessel sprouts are formed on the parent vessel. The tip of these sprouts are characterised by many filopodial extensions and their primary aim is to sense and transmit pro-angiogenic signals from the surrounding tissue environment. Stalk cells

of vessel sprouts have a higher proliferative capacity and make up nascent blood vessels as well as playing a role in lumen formation (Betz et al. 2016). Vascular endothelial growth factor A (VEGF-A) is considered a major chemo-attractive signal for angiogenesis and it has been observed to increase intracellular calcium dynamics in tip cells of growing vessels (Yokoto et al. 2015). Additionally, tip cells also possess the required metalloproteolytic machinery for the breakdown of surrounding extracellular matrix (ECM), which then facilitates the remodelling and invasion of surrounding parenchyma. Subsequently, blood vessel sprouts differentiate into fully functional islet capillaries to provide nutrient and blood supply to endocrine cells (Staton et al. 2009). Resident endothelial cells in isolated islets have been shown to contribute to the early stages of angiogenesis by secreting instructive signals, like VEGF-A, to guide newly formed sprouts of the parent vessel (Nyqvist et al. 2005). At the end of islet engraftment, the vascular supply is a chimera of donor and recipient endothelial cells. Over time, the lining of islet blood vessels subsequently gets replaced by the recipient's endothelial cells (Brissova et al. 2004).

A means to aid transplantation could involve the targeting of immunomodulatory and angiogenic approaches or better still, the combination of these. Islets are highly-perfused, highly metabolic organs which are in constant and dynamic interaction with endothelial cells in both health and disease states (for more details on the importance of islet-vascular coupling please refer to Chapter 1 Section 1.2.2.). Therefore, the timely re-establishment of organotypic vessel architecture in newly implanted islets is critical for their normal functioning.

4.1.6 Approaches to Improve Islet Vascularisation

Encapsulation technologies have been devised to protect transplanted islets from host immune responses. The provision of adequate number of pores on the surface of these scaffolds allows nutrient and oxygen exchange in the initial avascular phase and later, the growth of blood vessels into the islet parenchyma. The size of pores should be a subject of careful consideration as these should be large enough to allow angiogenesis to occur but small enough to restrict access to immune cells. Clinical development of this biotechnology is still very much in its infancy. This is in part due to issues related to the biocompatibility of scaffold materials as these can elicit fibrotic processes and lead to islet cell death (Beck et al. 2007).

The provision of pro-angiogenic factors, VEGF and platelet-derived growth factor (PDGF), in matrices has shown promising results and has successfully shortened the initial, avascular period. The combination of hepatocyte growth factor (HGF) and VEGF infused into a Matrigel

produced synergistic effects, suggesting that multi-compound strategies are advantageous. Interestingly, in animal experiments fewer islets were necessary to restore glycaemia and the blood vessel density was higher in islets supported by combination of growth factors than a single growth factor Matrigel (Golocheikine et al. 2010).

Yet another possibility is the co-culturing of islets with stromal elements. The addition of mesenchymal stem cells (MSC), fibroblasts have been shown to be beneficial from an islet transplantation perspective (Kerby et al. 2013). The main function of MSCs is to degrade the ECM for sprouting endothelial cells to aid vascularisation of islets, to upregulate the angiopoietin and VEGF expression in islets and to suppress inflammatory responses. The combination of the above techniques is also possible, where co-cultured islets maybe embedded in an ECM scaffold. Co-transplantation methods resulted in increased glucose-stimulated insulin secretion from islets, higher graft oxygenation and improved glycaemia correction (Kerby et al. 2013). At present, all the methods described above are still in the preclinical phase of development.

4.1.7 Epidermal Growth Factor Receptor

The epidermal growth factor receptor (EGFR) belongs to the type 1 family of tyrosine kinase receptors, ErbB4. These receptors are single-transmembrane glycoproteins with an intracellular tyrosine kinase and C-terminal tyrosine domains (Wieduwilt and Moasser 2008). Upon binding, receptor dimerization and transautophosphorylation of the receptor occurs, followed by a series of intricate intracellular signalling cascades to influence gene expression. Among these, EGFR signalling activates mitotic Ras/mitogen-activated protein kinase and phosphatidylinositol 3-kinase/Akt pathways. Receptor dimerization is essential for the activation of intracellular tyrosine kinase domain and phosphorylation of the C-terminal tail. Originally extracted from mouse salivary glands, the proliferative properties of EGFR signalling were quickly recognised. The frequent EGFR overexpression seen in a variety of cancer types placed EGFR signalling as one of the main drivers of oncogenesis (Sigismund et al. 2018). Besides EGF, six other endogenous ligands have been described to bind to EGFR; these are transforming growth factor-alpha (TGF- α), amphiregulin, epiregulin, betacellulin, heparin-binding EGF-like growth factor and epigen. Normally, EGFR amplification has been associated with worse disease prognosis and therapeutic targeting of the pathway is often associated with developing resistance. Another interacting partner of EGFR is Stat3, with an apparent strong correlation

between EGFR expression levels (Quesnelle et al. 2007). The Stat family of transcription factors are important mediators of growth factor receptor signalling. Stat3 has been implicated in modulating immune responses to tumour cells as well as cell proliferation and thus, unsurprisingly, is frequently overexpressed in tumour cells (Quesnelle et al. 2007). Janus kinase (JAK) associates with the EGFR receptor and upon activation act as a connection link between the EGFR and Stat3. Once Stat3 is phosphorylated, it translocates to the nucleus where it modulates the expression of a multitude of genes. VEGF-A and LKB1 are amongst these genes and thus the overexpression of EGFR may confer benefit to the β -cell through the above outlined pathways (Keller and Schmidt 2017).

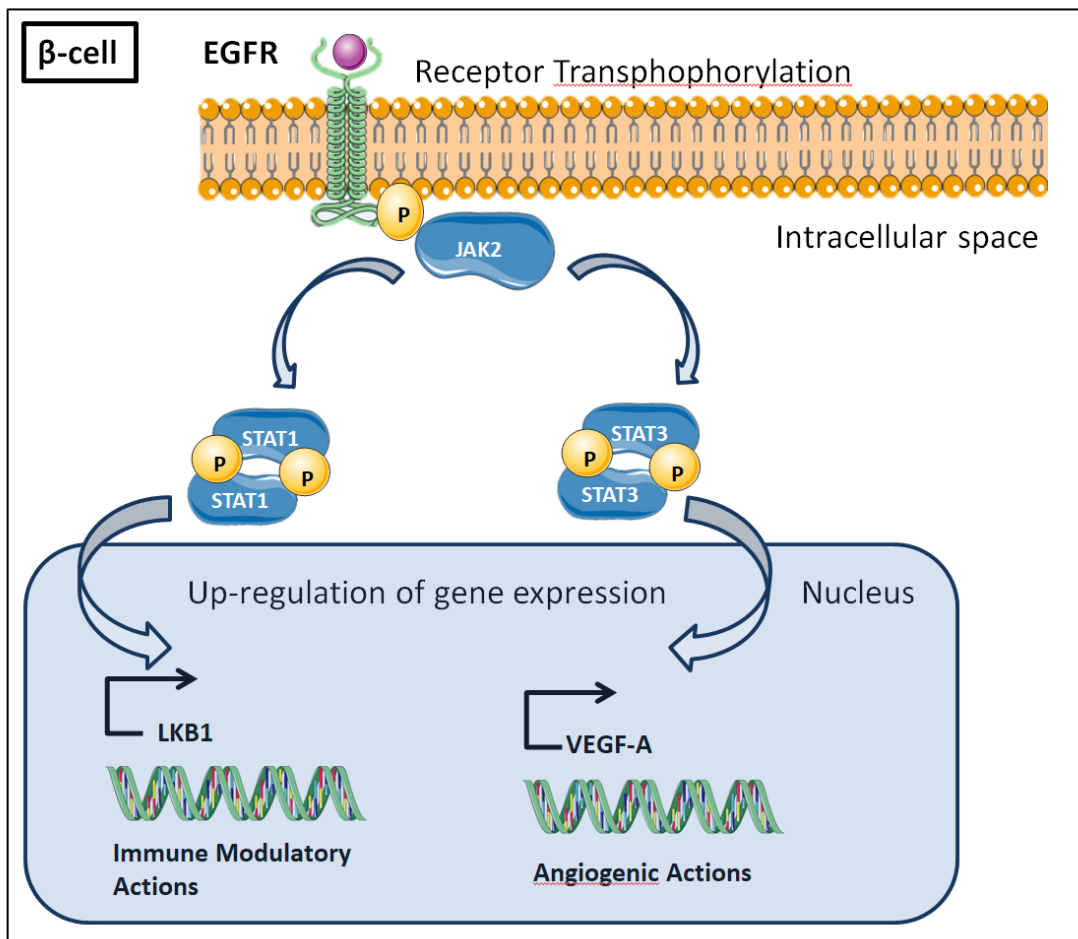


Figure 4.1.7.1 The angiogenic and immune modulatory actions of EGFR.

The calcium trace of each islet was normalised to the minimum fluorescence intensity value measured for that islet in a given imaging session.

4.1.8 Can Islets Be Engineered Pre-Transplantation to Improve Their Engraftment?

Ex vivo genetic engineering methods to deliver therapeutic and protective genes into β -cells have been considered as a means to improve islet transplantation rate. For viral mediated delivery, both adenovirus (Deng et al. 2003) and lentivirus constructs (Gallichan et al. 2008) have been utilised to achieve transient or stable gene expression levels, respectively. Meanwhile, other genetic modifications rely on RNA interference as a method to silence specific target genes encoding for pro-inflammatory proteins (Li and Mahato 2011). RNA interference is an evolutionarily conserved mechanism operating through small interfering RNAs (siRNA) (Castanotto and Rossi 2009). The therapeutic potential of siRNA-based approaches in islet transplantation was quickly recognised. Dendritic cells (DC) are important antigen presenting cells with immune regulatory roles. DCs can be found in islets where they promote T-cell differentiation and proliferation. Silencing of nuclear factor κ B (NF- κ B), an important transcription factor in DC differentiation, led to the development of a tolerogenic phenotype of DCs and improved islet engraftment (Li et al. 2007). Besides viral mediated delivery of siRNAs, other examples include conjugation to a magnetic nucleotide (Wang et al. 2013) but using liposomes as carriers have also been reported (Zhang et al. 2006). The challenges of RNA interference-based technologies are related to achieving their tissue specific delivery in order to achieve a localised effect.

In this study, we used the islet in the eye platform to visualise intra-islet vessel architecture and gain an understanding of the effects of β -cell specific overexpression of EGFR on angiogenesis. To this end, islets were imaged at 3, 14 and 28 days post-transplantation when islet engraftment is normally completed. The effects of upregulated EGFR-signalling on β -cell morphology was tested via qPCR analysis.

4.1.9 Hypotheses and Aims:

Hypotheses:

- 1) Enhanced signalling through β -cell EGFR results in better implantation success
- 2) Islets with β -cells overexpressing the EGFR show greater blood vessel density than control islets
- 3) β -cell function is improved in islets with enhanced EGFR signalling

Aims:

- 1) To visualise blood vessels in islets implanted into the ACE of syngeneic recipient animals
- 2) To track angiogenesis in transplanted islets and quantify vessel network characteristics in both EGFR-overexpressing and pAdTrack-AV expressing islets
- 3) To determine the influence of EGFR overexpression on β -cell specific genes

4.2 Methods

4.2.1 Animal Husbandry

Male C57BL/6 wild type (WT) were purchased and housed as described previously in Chapter 2. Section 2.2.1. This study was conducted under project licence PA03F7F07A (project licence holder Dr Isabelle Leclerc). All experiments were carried out in accordance with UK Home Office Animals (Scientific Procedures) Act 1986.

4.2.2 Pancreatic Extraction and Islet Isolation

Pancreatic islets were isolated from transgenic Ins1Cre-GCaMP6f expressing donors as described previously in Chapter 2. Section 2.2.2.

4.2.3 Adenoviruses

Viruses were generated using the pAdEasy system as described earlier in Chapter 2 Section 2.2.3. Islets were randomised to be infected with AV-SNAP-EGFR or AV-CMV-pAdTrack (herein referred to as 'Empty-virus' to denote that it lacks functional gene expression), a GFP-expressing empty shuttle vector. Islets were infected at the multiplicity of infection of 100 for both viruses and incubated (37°C; 5%CO₂) for up to 48 hours to allow for maximum viral penetration. The extent of virus uptake was assessed visually using a table top fluorescent microscope. Islets were re-infected if fluorescence was deemed insufficient. Adenoviruses preferentially infected β -cells due to their expression of coxsackie and adenovirus receptor. Both viral constructs were kindly donated by Dr Alejandra Tomas (Section of Cell Biology, Imperial College London).

4.2.4 Transplantation of pancreatic islets into the anterior chamber of the eye (ACE)

C57BL6/J recipient mice were randomised to receive AV-CMV-pAdTrack or AV-SNAP-EGFR expressing islets (n=5 per eye) in both of their eyes (n=3-4 mice per group). The procedure for transplanting islets into the anterior eye chamber is described in detail in Chapter 2 Section 2.2.6.

4.2.5 *In Vivo* Imaging Experiments

All *in vivo* imaging experiments were conducted using spinning disk confocal microscopy (Yokogawa spinning disk, 20x water dipping 1.0 NA objective; Cairn instruments). Mice anaesthetised with 5% isoflurane were placed in a head holder and onto a heated stage. Islets in the eye were imaged with interleaving 488nm and 561nm lasers in Z-stack modality at 5 μ m intervals. GFP-expressing β -cells were imaged at 488nm and islet blood vessels visualised by IV

injection of 200 μ l TexasRed-conjugated dextran (Invitrogen 3000MW; Neutral 10mg/1mL). To enhance signal in the 561nm channel in particular, islets were exposed to both lasers for 1000ms per stack and 2 by 2 binning at the point of acquisition. Islets were imaged at Day 3, 14 and 28 post-transplantation.

4.2.6 FIJI Image Analysis

All acquired images were pre-processed using a custom-made FIJI macro (Islet_process). The purpose of using “Islet_process” was to calibrate images (voxel size: 0.65 μ m x 0.65 μ m; depth: 5 μ m) and enhance the signal to noise ratio through a series of thresholding (rolling ball radius= 50) and filtering (Gaussian blur) steps. Z-stack images then were motion-corrected and re-aligned using the StackReg plugin (Rigid body). Vessel network analysis was carried out using the TubeAnalyst plugin. Images were thresholded such that the resulting tubular masks would cover the islet vessel network but excluding iris blood vessels. Tube radius and vessel radius were set for 3 μ m and 5 μ m, respectively. Using these parameters allowed us to reliably identify and map islet vessel network. With the use of TubeAnalyst we obtained a ‘thick skeleton’ map of the islet vasculature which was used to determine branching points and branch lengths. The maximum intensity projections (MIP) of pre-processed islet vasculature were superimposed on the binarised tubular mask and thick skeletal maps of individual islets to verify the accuracy of TubeAnalyst measurements. If skeletal maps and binarised masks were matching islet blood vessel MIPs measurements were saved and further analysis continued (**Figure 4.2.6.1**).

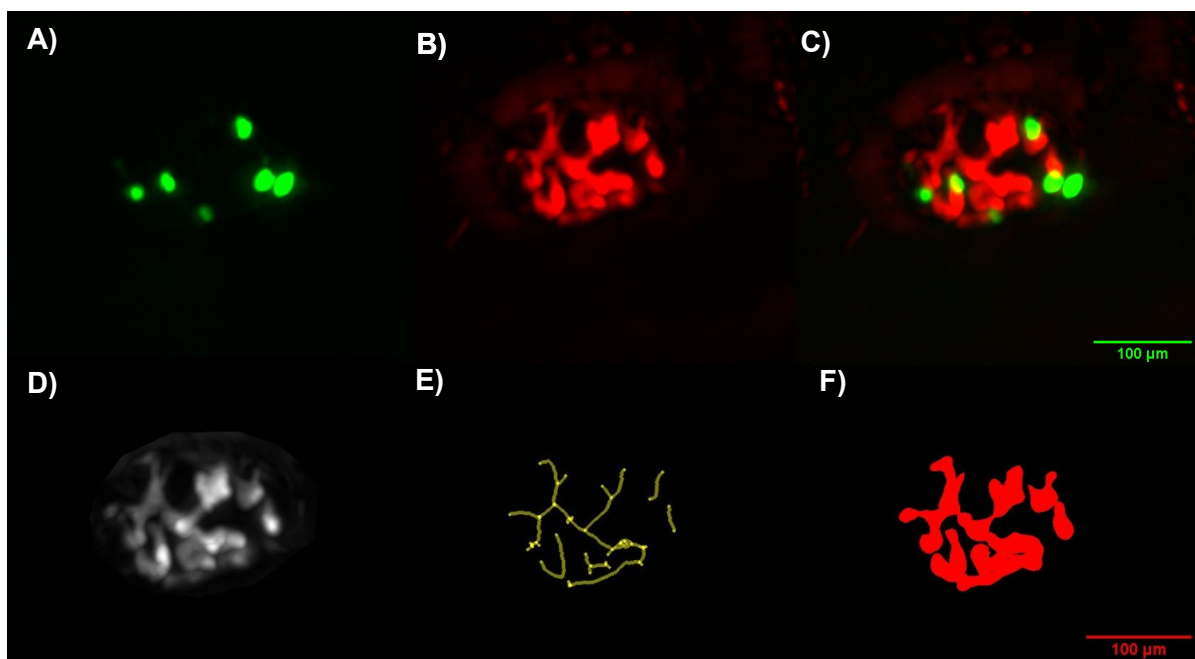


Figure 4.2.6.1 Representative images of blood vessel analysis using Fiji software and Tube Analyst

macro. Images (A) to (C) show multiple intensity projection images of beta-cells (ex.: 488nm) (A), blood vessels (ex.:561nm) (B) and the combination of the two (C). In the bottom panel a MIP of the vessel architecture is shown in (D), a thick skeleton to trace branching points in (E) and the binarized mask covering vessel network volume in (F). Results shown further below are the result of the combined analyses of images in represented in the bottom panel.

4.2.7 Statistical Analysis

Data were subjected to normality tests to determine the distribution of data. Blood vessel parameters for the two groups were analysed using repeated measures ANOVA. All data were analysed using Prism Graphpad Prism 8.2.1.

4.2.8 qPCR Analysis

qPCR analyses were carried out by an internal collaborator, Dr Stavroula Bitsi (Section of Cell Biology, Imperial College London). Islets isolated from WT C57Bl/6 donor mice were incubated with SNAPf-EGFR-AV or pAdTrack-AV as described above. After 24 hour of incubation period under standard conditions (37°C; 5% CO₂) islets were exposed to supra-physiological levels of EGF at 1µg/mL for up to four days.

To extract RNA, islets were collected in Eppendorf tubes and centrifuged at room temperature for 3 minutes at 200xg. The supernatant was discarded and 250µL of TRIsure (Bioline) was added to the pellet before vortexing and incubating for 10 minutes at room temperature. An additional 50µL of chloroform was added to the tubes, mixed by inversion and incubated for 3 minutes. Samples were centrifuged at 12000xg at 4°C for 15 minutes and the aqueous phase was collected. Then, 0.7µL of GlycoBlue™ Coprecipitant (Thermo Fisher) and 200µL of isopropanol (Sigma-Aldrich) was added. Samples were incubated overnight at -20°C.

Samples were centrifuged at 12000xg at 4°C for 15 minutes, the supernatant discarded, and pellets washed with 800µL 70% ethanol twice by centrifuging at 12000xg at 4°C for 15 minutes between the washes. RNA pellets were left to dry and subsequently re-suspended in 20µL of UltraPure DNase/RNase-Free Distilled Water (Thermo Fisher).

4.2.9 Complementary (cDNA) synthesis

cDNA was synthesised using a cDNA reverse transcription kit (ThermoFisher Scientific). A master mix of RT reaction was prepared using 5µL 10X RT buffer, 2µL 25X dNTP mix, 5µL 10X RT random primers 2.5µL Multiscribe reverse transcriptase and 5.5µL nuclease-free distilled water.

4µL of the resultant master mix was added to 6µL of each RNA sample and incubated at 25 °C for 10 minutes, 37°C for 120 minutes and 85°C for five minutes. cDNA from the two samples were diluted 1:5 using nuclease-free distilled water.

4.2.10 qPCR

A master mix of 80µL per primer was prepared using 48µL of fast-SYBR Green-Master Mix, 2.8µL of forward primer and 2.8µL of reverse primer and 16µL of distilled water. A summary of primers used can be found in table 1.

10µL of master mix for each primer was added to six of the wells in a MicroAmp Fast 96-well plate. 2µL of each cDNA was added to two of the wells each and 2µL of distilled water and cDNA master mix were added to the other wells. The 96-well plate was covered using MicroAmp optical adhesive film and samples were centrifuged at 1000RPM for 1 minute. A qRT-PCR was then performed (7500 Fast Real-Time PCR System) with the following cycling conditions: an initial denaturation step at 95°C for 20 seconds, then 40 cycles of 95°C for three seconds and 60°C for 30 seconds. Actin was used as a housekeeping gene and relative gene expression was calculated using the previously described Livak method. qPCR analysis of islets was performed by Dr Stavroula Bitsi and Miss Aldara Martin-Alonso.

4.3 Results

4.3.1 Engraftment Success

Empty-virus treated islets engrafted with a lower success rate than islets infected with AV-EGFR. In the former group 4 animals (8 eyes) were injected with empty-virus treated islets (5 islets per eye). Only 7 control islets (from 4 recipient mice) were noted 3 days after the eye transplantation and only 3 of these islets could be imaged on days 14 and 28. In the EGFR-overexpressing group (n=3 animals i.e. 6 eyes), 14 islets (from 3 different recipient mice) with the SNAP-AV-EGFR construct were imaged on both days 14 and 28. Thus the chances of successful implantation and imaging at day 28 was 7.5% in the empty vector treated islets compared with 47% in the EGFR-overexpressing islets (OR for implantation success 6.6 for EGFR islets $p < 0.001$ in chi squared contingency analysis).

4.3.2 Imaging Islet Blood Vessels in the Eye

The implantation process of islets was already underway at day three and was evidenced by increased TexasRed-dextran signal inside the islet. Interestingly, increased TexasRed signal was observed in all EGFR overexpressing islets on day 3 (data not shown) while only 1 control islet displayed TexasRed fluorescence signal on day 3. However, it was not possible to quantify vessel architecture characteristics at this point due to the immature nature of vessel networks at this time-point. Instead we focused our attention to later time-points days 14 and 28. Overall, both AV-pAdTrack-virus ('Empty-virus') and AV-EGFR islets displayed a tendency for more complex and tortuous vessel networks as days progressed from day 14 to day 28 post-transplant (**Figure 4.3.2.1**). Due to their location in the eye and shape of growing vessel network we were able to re-identify islets over time with confidence.

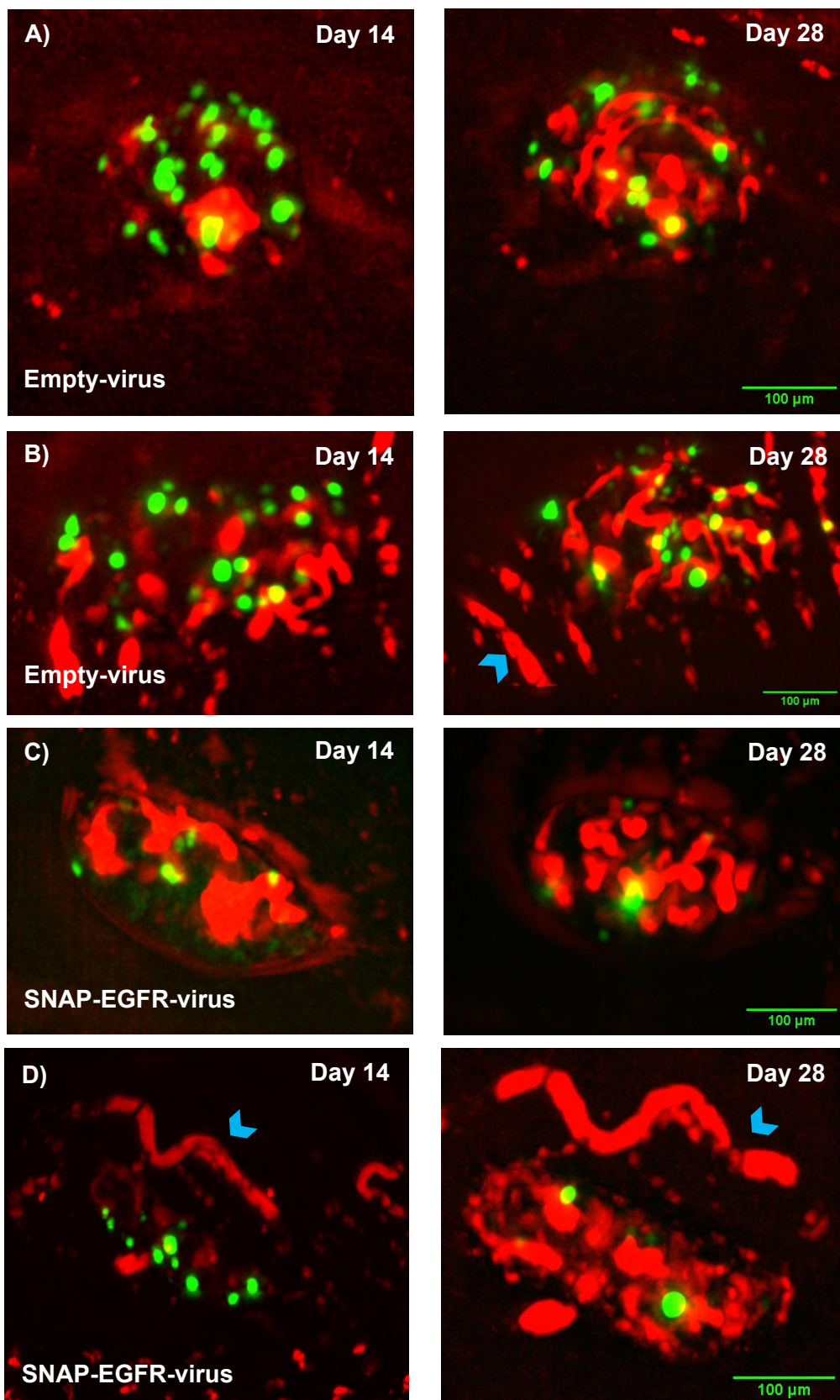


Figure 4.3.2.1. Images of AV-pAdTrack-vector (empty virus) and AV-EGFR-virus infected islets. AV-expressing β -cells and blood vessels were visualised using 488nm and 561nm lasers, respectively. Adenoviral linked GFP expression gradually decreased in islets whilst vessel architecture of implanted

islets increased in complexity as time progressed. Panels A) and B) show multiple intensity projections (MIP) of islets infected with empty-virus. Panels C) and D) show MIPs of SNAP-EGFR infected islets at days 14 and 28. Blue arrows point to iris blood vessels which were excluded from vessel network analysis.

4.3.3 Islet and Blood Vessel Volumes

Unexpectedly, mean islet volume did not appear to increase between 14 and 28 days post-transplant in the EGFR-over expressing group. The mean islet volume in the EGFR group was $2,617,000\mu\text{m}^3$ ($\pm 413,900$) on day 14 versus $2,218,000\mu\text{m}^3$ ($\pm 375,700$) on day 28 post-transplantation ($p=ns$). However, in the empty-virus treated group there was a significant rise in islet volume over time: $2,273,000\mu\text{m}^3$ ($\pm 662,500$) on day 14 versus $7,512,000\mu\text{m}^3$ ($\pm 2,063,600$) (Figure 4.3.3.1.).

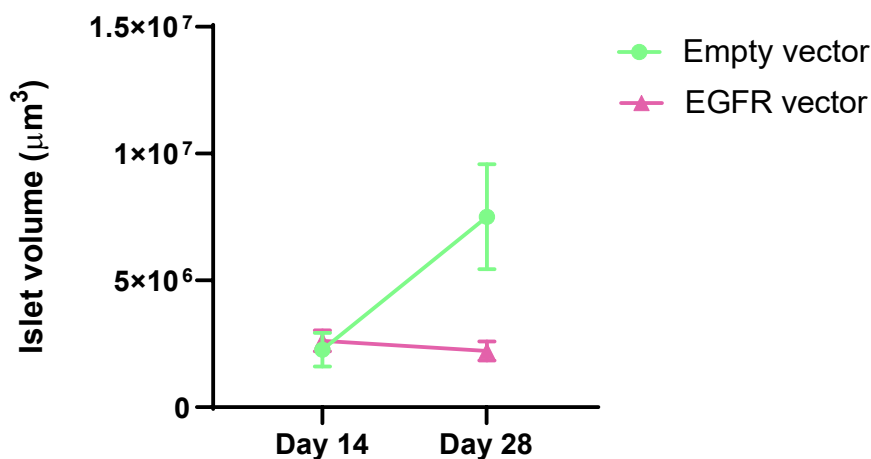


Figure 4.3.3.1. Volumetric changes in AV-pAdTrack (Empty) virus and AV-EGFR-virus expressing islets. Islets were comparable in size at day 14 between the two groups however there was a tendency for increased islet size by 28 day after transplantation in the AV-pAdTrack group (n=3) versus AV-EGFR-expressing group (n=14) (Two-way ANOVA, Tukey's test).

Due to the more prominent vascular structures of islets at days 14 and 28 we were able to quantify blood vessel volume of islets at these time-points. Blood vessel volume of the control

group showed an increasing tendency between days 14 and 28 and was larger on day 28 than EGFR-overexpressing islets (albeit non-significant). EGFR islets displayed comparable blood vessel volumes on day 14 and 28. On day 28 the mean blood vessel volume was 421,500 vs. 132,100 μm^3 for control and EGFR groups, respectively ($p=0.005$) (Figure 4.3.3.2).

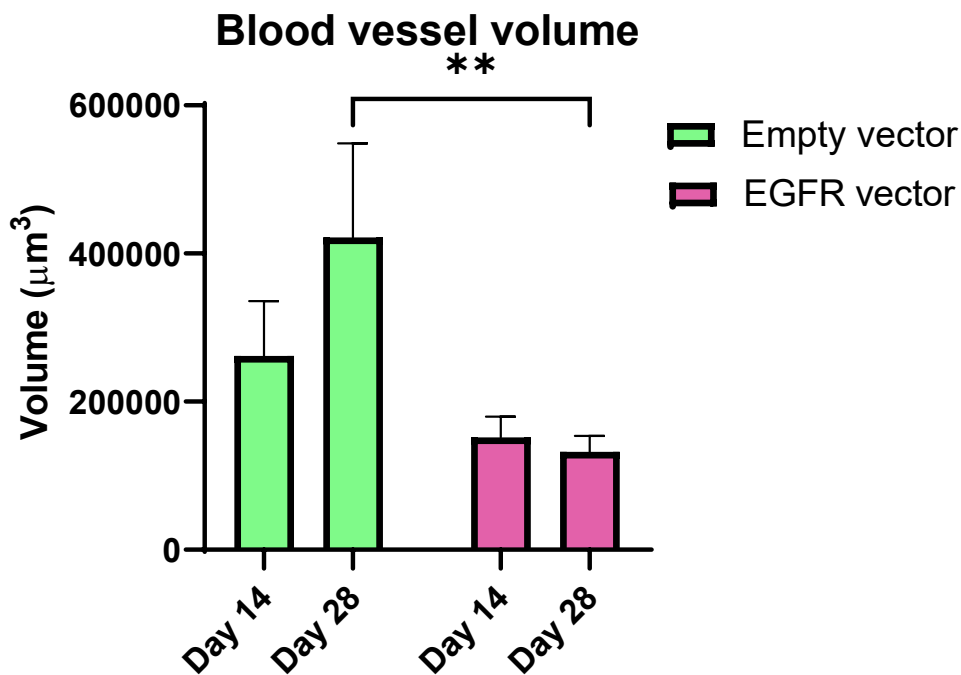


Figure 4.3.3.2 Blood vessel volume changes two and four weeks after transplantation. Blood volume increased in control islets but remained largely similar in the EGFR treated group, as visualised using IV TexasRed dextran (n=3; n=14, respectively). On day 28 AV-SNAP-EGFR infected islets displayed significantly smaller blood vessel volumes than control ones ($p=0.005$ Multiple comparisons ANOVA)

In order to control for islet size and to determine whether islets are better vascularised after adjusting for islet volume, we quantified blood vessel volume to islet size ratios. Here, we found that by day 28 islets in the EGFR group had marginally higher blood vessel density than did control islets 6.8 versus 5.6 with a difference of -1.18 (SEM of ± 2.9 ; $p=ns$) (Figure 4.3.3.3).

Percentage of blood vessel volume to islet size

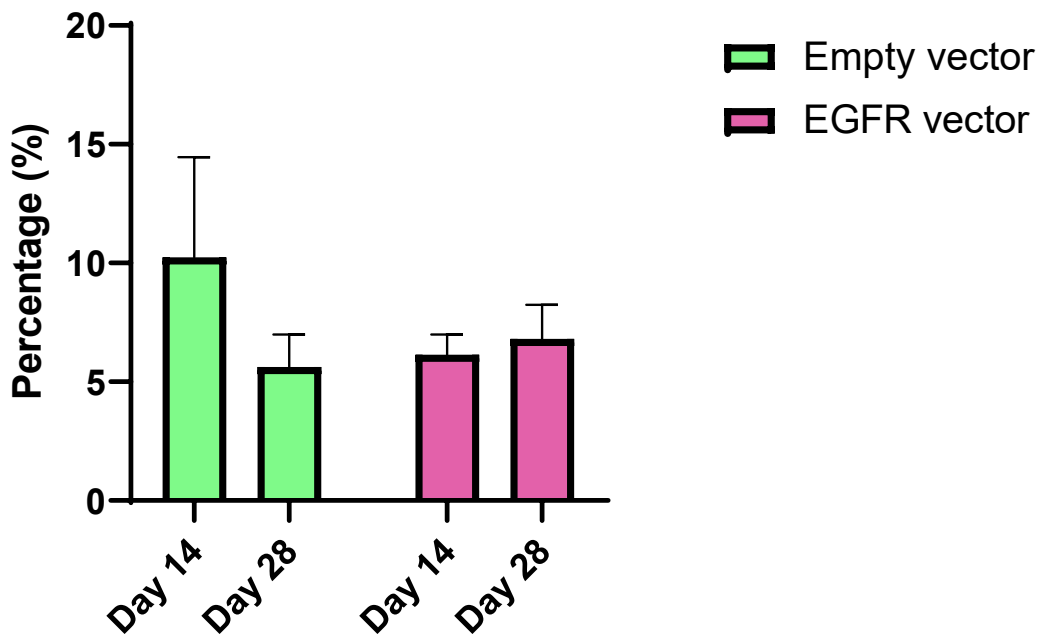


Figure 4.3.3.3 Blood vessel volume changes relative to islet size. EGFR treated islets demonstrated a higher blood vessel density than empty-virus treated group on day 28, however this difference was not statistically significant (repeated-measures ANOVA).

4.3.4 Blood Vessel Network Analysis

Next, we subjected the data to a more comprehensive vessel network analysis to better visualise and describe islet architecture differences between the two groups.

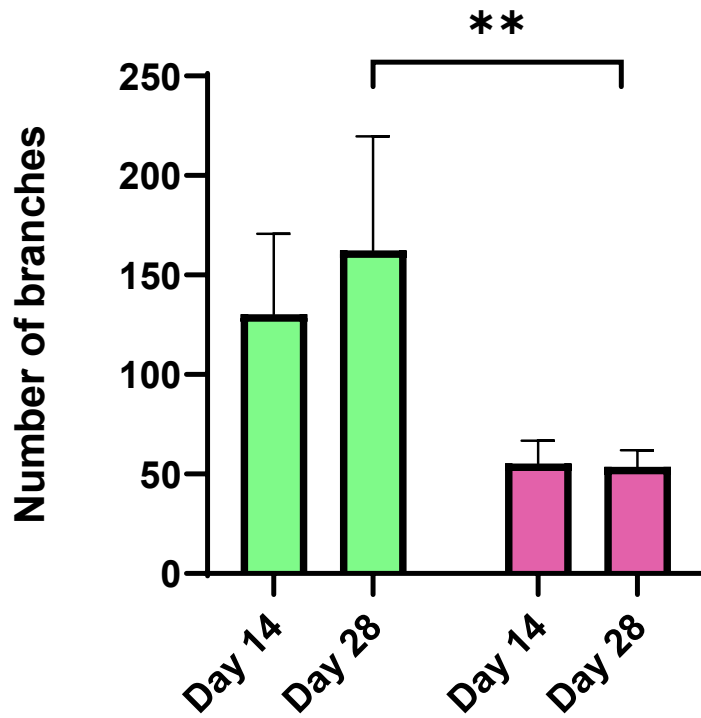
The tube analyst macro revealed the total number of branching points found within the islet vessel architecture. AV-EGFR-infected islets had fewer numbers of branches in their vessel network than did control islets (53.7 versus 162.3 in EGFR- and empty-virus infected islets, respectively). While the number of branches increased in control islets over time, in AV-EGFR-infected islets the number of branches remained unchanged. When comparing the average branch length between the two groups, it was observed that initially, EGFR islets had longer

branches (36 μm) than did controls (29 μm) but that numbers later dropped to levels similar to that of control islets at day 28 (**Figure 4.3.4.1**)

The vessel diameter between groups and on different imaging days was comparable and therefore unlikely to have affected blood vessel density measurements considerably (average vessel diameter for EGFR-treated islets: 11.51 μm on day 14 and 11.26 μm on day 28; and for control islets: 10.42 μm on day 14 and 11.32 μm on day 28).

Taken together, these results suggest that EGFR overexpression may promote very early vascularisation and thereby increase early implantation success but that by 28 days post implantation there is no effect on increasing blood vessel density or tortuosity (**Figure 4.3.4.1**).

A)



B)

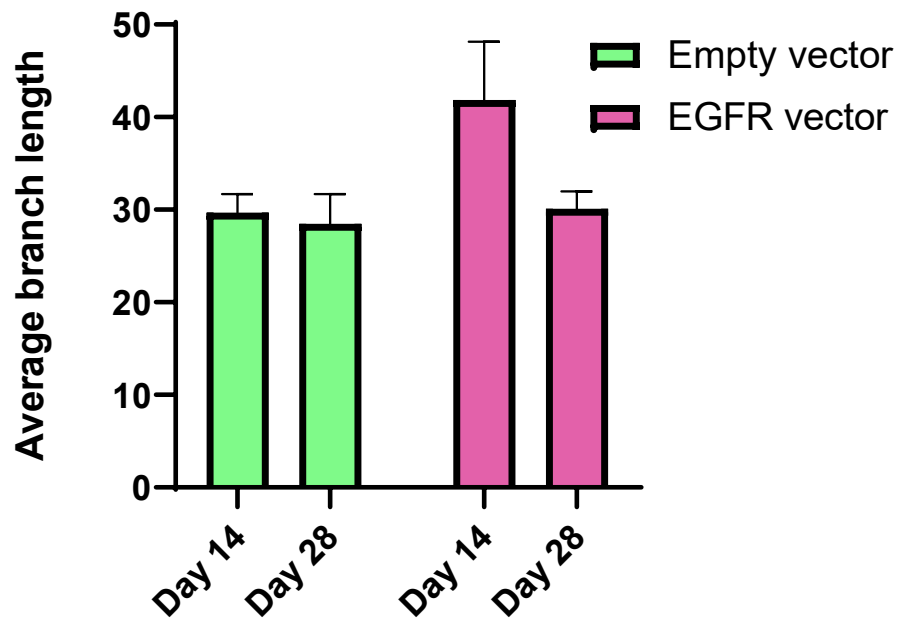


Figure 4.3.4.1 Vessel branch characteristics in control and EGFR treated islets. Control islets displayed a higher number of branches at 14 days with further increase by day 28. EGFR-treated islets on the other hand showed consistently lower numbers of branches in their vessel network at both experimental time-points. Average number of branches was 162.3 in control islets and 53.7 in EGFR-islets ($p=0.023$). The average length of branches was comparable between the two groups.

4.3.5 β -cell identity

After characterising vessel network, another important question remained regarding the function and identity of β -cells. To assess how overexpression of EGFR in β -cells impacted on β -cell identity genes, we subjected isolated islets infected with either AV-pAdTrack or AV-SNAP-EGFR viruses to qPCR analysis (Figure 4.3.2.6). In brief, it was found that in islets where EGFR was overexpressed, angiogenesis-related genes VEGFA and VEGFB were upregulated. In addition, markers of β -cell identity PDX-1, MafA and Kcnj11 were also expressed at higher levels than compared to control islets. β -cell disallowed genes on the other hand were down-regulated in these same islets as measured by qPCR (Figure 4.3.5.1.).

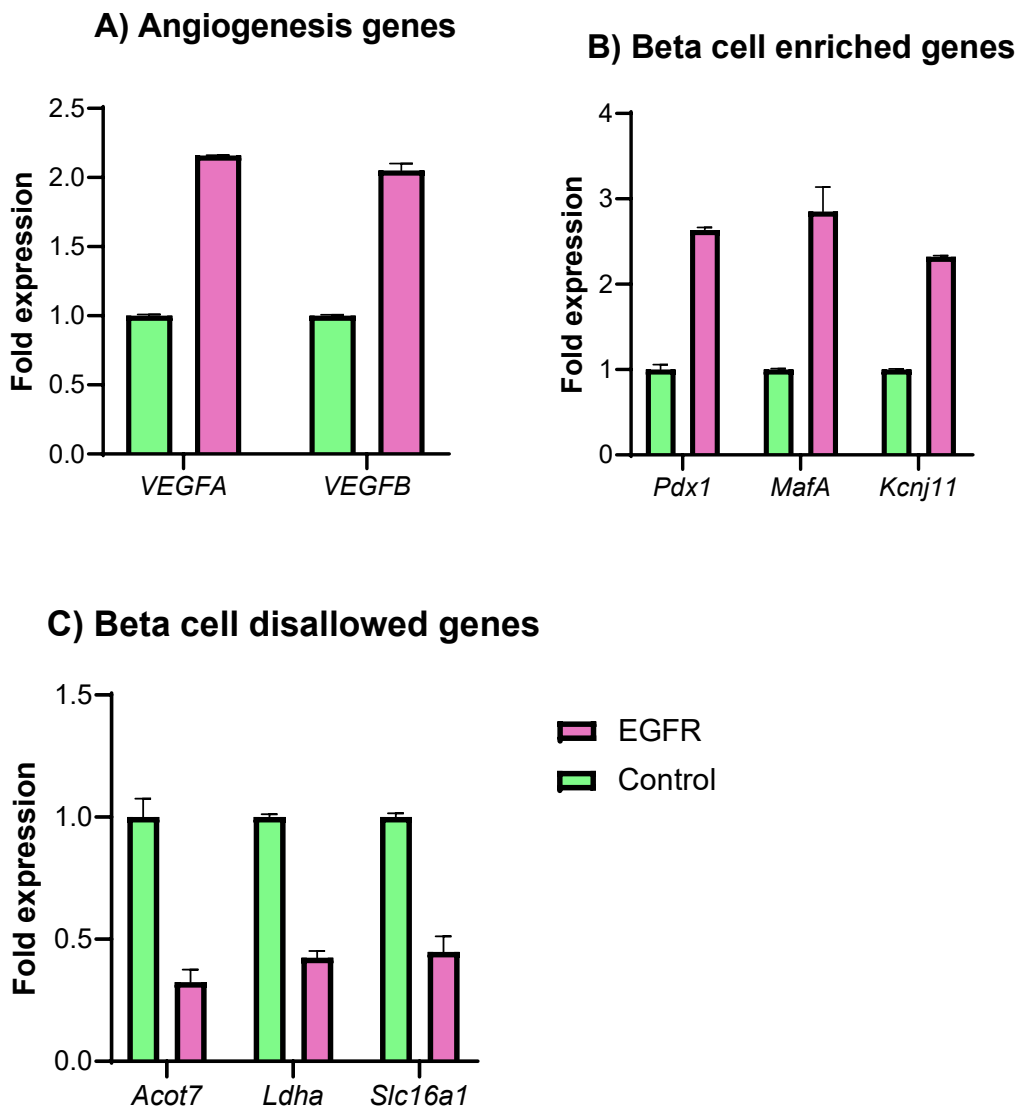


Figure 4.3.5.1 EGFR overexpression upregulates angiogenesis-related and β -cell maturity-related gene expression.

A) There was a 2.1 and 1.9-fold change in the expression of angiogenesis related genes, VEGFA and VEGFB, respectively, in EGFR-treated islets compared with controls. B) β -cell enriched genes showed a similar pattern in EGFR-treated islets with over 2-fold increase in their gene expression levels compared to controls. C) β -cell disallowed genes on the other hand, were down-regulated by 60-70%.

4.4 Discussion

In this study, we have demonstrated that islets where β -cells overexpress the EGFR have a statistically greater chance of successfully implanting. 47% of islets overexpressing EGFR implanted compared with only 7% control islets. Whilst blood vessel architecture could not be imaged and quantified at day 3, increased TexasRed signal was observed in EGFR overexpressing islets at this time-point (data not shown). Meanwhile, only 1 control islet displayed TexasRed fluorescence signal 3 days after transplantation. Although by 14 and 28 days blood vessel volume and density is not greater (adjusted for islet volume) in the EGFR-overexpressing islets, the increased transplant success rate and very early (day 3) imaging findings, supported the hypothesis that AV-mediated EGFR overexpression aids the early (hyperacute) implantation and vascularisation process. EGFR overexpression was also associated with increased markers of β -cell identity - qPCR analysis of EGFR overexpressing and control islets has shown that the overexpression of EGFR in β -cells results in the enhanced expression of angiogenesis-related (VEGF-A and VEGF-B) and β -cell enriched genes (PDX-1, MafA, Kcnj11). Taken together, these findings suggest that β -cell specific overexpression of EGFR promotes implantation in a transplant model and potentially improves beta-cell function. These results suggest a promising future avenue for research into engineering islets to promote transplant success rates.

4.4.1 Would adenoviral gene transfer be a viable clinical tool for improving islet transplantation?

In this study, a diminution in β -cell-specific GFP signal was observed in both AV-SNAP-EGFR- and pAdTrack-expressing islets. Achieving a uniform adenoviral load of infected islets can be challenging. We (chapter 2 section 2.3.1.) and others (Muniappan and Ozcan 2009) have observed in the past a reduced ability of adenovirus gene delivery systems to penetrate the islet. To achieve a more uniform AV expression pattern, islets can be dissociated into their single endocrine cell compartments for the period of viral incubation (van Krieken et al 2019). Prior to transplantation these islets can be re-assembled through 3-D culturing methods, such as the hanging-drop method. A much more ubiquitous viral expression pattern can be obtained by this means however, a significant alteration in the cytoarchitecture of re-assembled islets has been reported previously (van Krieken et al 2019). In pseudo-islets β -cells and α -cells were intermingled and while the gene of interest was overexpressed in these islets, this did not translate into an increased functional response *in vivo* (van Krieken et al 2019).

Our negative results on islet blood vessel tortuosity following β -cell-specific EGFR overexpression are not unprecedented. Olsson and colleagues have co-cultured islets with matrix metalloproteinase-9 (MMP-9), VEGF or fibroblast growth factor (FGF-2) prior to transplanting them under the renal capsule of recipient mice. There was no difference between control and growth factor-treated groups and there was a tendency for islet blood vessel density loss (Olsson et al. 2006). MMP-9 pre-treatment resulted in increased vessel tortuosity however this did not translate into improved islet function. It is possible that exposure of islets to extended periods of culturing (due to incubation with adenoviral constructs) induce the dedifferentiation of intra-islet endothelial cells and underlie the reduced rate of angiogenesis despite the presence of growth factors in culture medium (Giuliani et al. 2005). Indeed, Nyqvist and colleagues reported a dramatic loss of intra-islet endothelial cells over a period of 4 days. After 2 days of *in vitro* culturing, islets lost approximately 50% of intra-islet endothelial cells and combined FGF and VEGF treatment was ineffective in reversing endothelial cell loss (Nyqvist et al. 2005). Whilst AV infection of islets is traditionally assumed to have β -cell specificity, it is possible that some of the effects seen here are due to viral infection of remnant endothelial cells in the islets and that variation in this phenomenon could contribute to differences observed in vascularisation success. Therefore, culturing conditions and the means of gene transfer are factors to be carefully considered for future experiments.

Viral-based interventions all rely on the modification or deletion of some areas of the viral genome, that are involved in replication for example, thereby rendering adenoviral constructs less likely to induce an immune reaction. Because of the high expression level of AVs' cognate receptor, the coxsackie and adenovirus receptor (CAR), human tissues can be infected with high efficiency. AVs are the most commonly used vectors, accounting for >20% of gene therapy trials and some of them have already gained approval for clinical use. The AV-mediated delivery of the tumour suppressor gene p53 to patients with head and neck cancers has proven efficacy (Zhang et al. 2018). Other examples include the expression of the oncolytic protein, heat-shock protein 70 (Hsp-70), in tumour cells to induce their destruction. In addition, adenoviruses have been used for the introduction of a normal copy of CFTR in patients with cystic fibrosis (Knowles et al 1995). However, because AVs do not integrate into the host genome, the expression of the gene of interest is only transient, typically lasting up to 6-8 weeks. Whilst our understanding of the chronicity of AV-mediated genetic effects is still incomplete, it is arguable

that a limited effect on islet gene expression may be beneficial – to last the acute period of implantation only.

Alternative viral-mediated gene delivery systems with similar features include adeno-associated viruses (AAV) and gutless adenoviruses. AAVs are small non-enveloped viruses with a single stranded DNA genome that is approximately 5kb long. To date, no animal or human related diseases have been associated with AAVs despite most people showing seropositivity for the virus. AAVs are gutless viruses which cannot propagate by themselves and require the co-injection with helper viruses for sufficient AAV load. Their dependence on the presence of a helper virus provides safety control to limit virus spread in the body (Samulski and Muzyczka 2014). Very recently, a compound that relies on AAV-mediated gene delivery has received approval from the FDA to be used in patients, thus showing the real potential of these systems for clinical translation. Other examples that received both FDA and (European Medicines Agency) EMA approval include the use of an AAV-based vector system that was developed for use in rare, inheritable cases of severe pancreatitis.

Gutless adenoviruses lack all adenovirus genes and have comparable safety profiles to AAVs in that they show broad tropism for infection and high transfection efficiency. However, gutless adenoviruses are absolutely dependent on the presence of a helper virus to provide all the necessary cellular machinery for infection. During gutless AV production, the helper virus is present and actively replicates to provide helper functions to the gutless AV. Frequently, there is a small amount of contaminant helper AV in the resultant gutless AV product. While the amount of helper virus can be minimised, its complete removal is difficult. Through homologous recombination, the helper virus can generate replication competent adenoviruses which can actually trigger a host immune response (Yeung et al. 2012). Therefore, where possible other means of gene transfer should be given equal amount of consideration to avoid unwanted immune responses.

4.4.2 Is EGFR a Viable Target for Improving Islet Engraftment?

We observed a trend for improved vascular density in islets with β -cell specific overexpression of EGFR. In glioblastoma cells it was shown for the first time that EGFR signalling increases the secretion of VEGF (Goldman et al. 1993). Microvesicular cells in human malignant tissues have been shown to overexpress EGFRs. EGFRs can then be taken up by endothelial cells which activate the MAPK and Akt pathways to promote their survival. Moreover, increased EGFR

signalling in endothelial cells has been linked to the upregulation and secretion of VEGF to act on endothelial cells in an autocrine manner (Al-Nedawi et al. 2009). Additionally, EGFR signalling in tumour cells have been found result in the upregulation of neuropilin, which is a non-tyrosine kinase transmembrane protein. Originally, neuropilin has been characterised as a receptor for semaphorins and collapsins, proteins involved in the development of the nervous system. In human pancreatic adenocarcinoma cells, neuropilins have been shown to bind to growth factors including VEGF₁₆₅ and act as a co-receptor to them. The interaction of VEGF and neuropilin allows for the simultaneous binding of VEGF to both VEGFR-1 and VEGFR-2. Furthermore, EGFR signalling was associated with the activation of both Erk (MAPK pathway) and Akt (PI-3K pathway) suggesting their involvement in the upregulation of neuropilins in pancreatic cancer cells (Parikh et al. 2003). Considering the dual role of neuropilins in axon guidance and angiogenesis, the adenoviral overexpression of EGFR in β -cells could have conferred additive benefits in potentiating islet engraftment in the eye. Together, enhanced EGFR signalling promotes angiogenesis through multiple mechanisms.

In previous studies, where the naturally occurring ligand of EGFR, betacellulin was overexpressed, it was found that islets were in better health and this was also associated with improved islet function (Song et al. 2014). More specifically, the rate of re-vascularization in islets transplanted under the kidney capsule of streptozotocin-treated animals was enhanced. When exposed to cytokines, betacellulin virally transduced islets were protected from harmful effects when compared with control islets. Insulin secretion was also restored in animals exposed to cytokines after betacellulin treatment. These beneficial effects of betacellulin were linked to increased phosphorylated Akt expression and EGFR (Li et al. 2001). Furthermore, a study previously reported that betacellulin induces the expression of insulin and glucokinase in α -cells and thereby increases β -cell mass (Watada et al. 1996). It was presumed that actions of adenovirally overexpressed betacellulin were paracrine in nature and that no systemic effects may be induced with this method. Immunohistological examination of transplanted islets revealed that both β -cell size and numbers increased and thus contributed to the increased β -cell mass. Whether betacellulin is directly involved in the differentiation process of β -cells or acts by increasing survival rate of Pdx-1 expressing progenitors remains an open question. These findings are especially relevant in the context of T1DM where β -cell destruction is so

extensive. By improving β -cell survival, the demand on clinical islet isolation centres can be relaxed as fewer transplanted islets may be sufficient to provide better glycaemia control.

Evidence also points to an interaction between EGFR and GLP-1 signalling. Investigating the β -cell protective effects of GLP-1 agonism, it was uncovered that exendin treatment results in an increased rate of BrdU incorporation in β -cells, signifying enhanced rates of β -cell neogenesis. Mild glucose intolerance ensues when EGFR signalling is selectively depleted from β -cells in an inducible fashion. When exendin is administered to these mice, the desirable effects of GLP-1 signalling were depleted (Fusco et al. 2017). Interestingly, qPCR results have demonstrated an increase in the expression levels (2 to 3 fold increase) of master regulators of β -cell identity (PDX1 and MafA). Additionally, the gene encoding for inwardly rectifying K^+ channels was also up-regulated. These findings can be explained by one of two ways; expression levels could have increased due to increased β -cell mass, through EGFR-stimulated conversion of other endocrine cell types or the maturation of β -cells, previously trapped in a progenitor state.

Aside from the promotion of angiogenesis and islet survival, EGFR signalling has additional immunomodulatory functions which can be taken advantage of in the setting of clinical transplantations. Programmed cell death-1 (PD-1) is a transmembrane protein and is one of the immune check-points expressed on the surface of immune cells. Activation of PD-1 by its ligand PDL-1, leads to the induction of apoptosis of immune cells (Sasada et al. 2016). Many cancer types are characterised by PDL-1 overexpression and indeed, with EGFR overexpressing tumour cells it was found that EGFR signalling directly stimulates the expression of PDL-1 (Akbay et al. 2013). Studies independently have shown that these effects of EGFR were mediated by PI3K-Akt, MEK-ERK as well as the MAPK/Akt signalling (Azuma et al. 2014; Ota et al. 2015). Biopsies from patients seem more controversial regarding the link between EGFR and PDL-1 signalling, with some showing strong while others only weak correlation between the two signalling pathways. Thus, building on observations from tumour cells it is possible that EGFR overexpression in β -cells has favourable, immunosuppressive effects when islets are transplanted into the eye.

While the above studies demonstrate the potential benefits enhanced EGFR signalling may confer to improve islet engraftment, we should remain cautious and consider other effects of EGFR signalling. For instance, it has been shown that EGFR signalling participates in

cardiovascular complications of diabetes (Akhtar and Benter 2013). In the mesenteric arteries of diabetic rats, EGFR was found to be overexpressed where it promotes vessel walls to become fibrotic and, therefore, losing their elasticity. Additionally, there seems to be an increased propensity for vasoconstriction in EGFR-overexpressing coronary and mesenteric arteries coupled with decreased vasodilatory functions. On the whole, enhanced EGFR signalling resulted in smaller passive vessel diameters of resistance arteries, an increased vessel wall thickness and increased stiffness with elevated collagen type 1 content (Schreier et al. 2014).

To combat problems related to excessive EGFR signalling in cells, it would be of interest to design viral vectors that specifically target β -cells to avoid any unwanted effects in tissue surrounding islets. Also, besides having spatial control of EGFR overexpression, the temporal control of enhanced EGFR signalling would also be highly desirable. For example, a tetracycline-responsive element could be incorporated inside the viral vector. In this instance, overexpression of EGFR in cells only occurs when tetracycline is administered. Upon binding of tetracycline to its responsive element in the genome, the expression of EGFR can be permitted and terminated by withdrawing tetracycline.

4.4.3 Is the Islet in the Eye a Viable Clinical Transplantation Site?

Our results should be interpreted in the context of clinical practice. Currently, the hepatic portal vein is preferred as the transplantation site however this location has multiple drawbacks and an extrahepatic transplantation site is greatly needed. From a perspective of islet angiogenesis, striated muscle presents as an attractive option.

In adult organisms, angiogenesis is only initiated in a tightly controlled manner, in specific tissues during wound healing, in female reproductive organs, in the placenta and in striated muscles. Therefore, striated muscle confers obvious benefits to improve islet re-vascularisation and has shown some promising results as an experimental transplantation site. Physical exercise induces mechanical stress in striated muscles and has been shown to upregulate the expression of VEGFA, hypoxia inducible factor 1 β and matrix metalloproteinase 2, all of which are important players in angiogenesis (Svensson et al. 2010; Christofferson et al. 2010). While islets implanted onto the striated muscle were superior in their vascular supply, there was an increased volume of connective and fibrotic tissue surrounding islets, indicating an increased rate of apoptosis. The omentum is a collection of adipocytes embedded in connective tissue that hangs over the intestines inside the peritoneal cavity (Bartholomeus et al. 2013). Due to its

accessibility, rich vascular supply and capacity to hold a high number of islets, the omentum has received clinical attention as an alternative islet transplantation site (Stice et al. 2018). Whether the omental pouch can be used as a stand-alone transplantation site requires further evaluation. The spleen, on the other hand, offers a tissue environment that is similar to the endogenous pancreas however, it is flawed by the increased incidence of haemorrhage as well as the facilitated access of lymphocytes to transplanted islets (Merani et al. 2008).

To this date, there have been no reports of similar issues outlined above with the use of the eye as a transplantation site. In fact, the anterior chamber has already been considered in clinical practice. In a baboon model that was previously rendered diabetic, Perez and colleagues implanted pancreatic islets into the eye and demonstrated that they remain functional over the period of 357 days. Remarkably, only <15% of all implanted islets failed to graft, a significant improvement considering the islet survival rate at other clinically used transplantation sites. Within three months, exogenous insulin requirements of animals decreased substantially and remained at 60% of doses required prior to transplantation (Perez et al. 2011). Further, islets become highly vascularised by 24 days post-transplantation in a manner that closely resembles to the native islet vessel architecture (Alamaca et al. 2014). A major concern for the clinical adaptation of the islet in the eye platform has been associated with the potential collateral damage to the eye during surgery. Perez and colleagues have addressed these concerns and carried out a histological examination of baboon eyes receiving islet transplants. There were no morphological changes to the eyes and there were no signs of abnormal pupillary reflex or behavioural cues that would suggest impaired vision. The only reported ophthalmic pathology was the occurrence of cataracts which agrees well with our own experiences using the platform and can be effectively treated.

In titration studies, it was estimated that the murine anterior chamber is capable of accommodating sufficient number of islets for diabetes reversal to occur. The number of islets adjusted to the animal's body weight ranged from 75IEQ (equivalent to 2500IEQ/kg in humans) to 500IEQ (i.e. 17000IEQ/kg in humans) and were equally successful at treating diabetes albeit the rate at which this occurred differed. For reference, the benchmark Edmonton study from 2000 recommended the use of 5000IEQ/kg with multiple transplant surgeries likely being necessary (Shapiro 2000). The added benefit of the unique, immunosuppressive ocular environment means that the systemic use of immunosuppressive agents which bear potential

nephrotoxic complications can be limited. In fact, the feasibility of the targeted delivery of the immunosuppressant agent rapamycin to islets in the eye has already been demonstrated. Here, rapamycin was delivered in slow-releasing microparticles and co-injected with islets into the anterior eye chamber. While islet graft survival rate improved in the presence of rapamycin particles, potential systemic effects of rapamycin treatment were not assessed. These are important questions to address as the major hurdles associated with systemic rapamycin treatment relate to its nephrotoxic effects with long-term use (Fan et al. 2019). More recently, the transplantation of islets into the eye chamber gained approval by the FDA to be tested on a small number of human subjects (Shishido et al. 2018). Concerns over ocular alterations related to the eye surgery have recently been addressed, with an innovative smart contact lens that is able to report on intra-ocular pressure (IOP) changes. IOP was found to be transiently increased shortly after surgery however, IOP values remained within a safe margin even during this time (Kim et al. 2020).

4.4.4 As a preclinical model for studying angiogenesis how does it compare to what we have already?

Under normal circumstances, most endothelial cells are in a senescent, non-proliferative state. Placing endothelial cells in an *in vitro* culture induces adaptive changes in endothelial cells to proliferate and thus results in an artificially induced angiogenic state. This can lead to erroneous conclusions when testing pro-angiogenic factors *in vitro*, potentially overestimating their angiogenic potential. In addition, vessel networks throughout the body have been found to display organ specific morphology and cell-cell contacts (Craig et al 1997; Marcu et al 2018). Phenotypically, we distinguish between continuous vessels where endothelial cells completely cover the internal vessel wall; fenestrated, where endothelial cells are connected via fenestrae and are permeable to macromolecules; and sinusoidal where endothelial cells are only loosely connected and the basement membrane is discontinuous. A further layer of complexity is provided by the functional heterogeneity in the control of vasoconstriction, vasodilatation, blood coagulation, antigen presentation and atherogenesis. Through continuous passaging and without the tissue context and endogenous cues, endothelial cells lose their organ-specific morphology. While *in vitro* assays allow for the direct interrogation of specific molecular pathways, their inherent limitation is that observations may not pertain in a more complex, *in vivo* situation.

The capillary-like tubular arrangement of endothelial cells *in vitro* has been achieved by the use of biomaterial scaffolds into which endothelial cells combined with mesenchymal cells can be seeded. These platforms are suitable to study the later-stages of vessel differentiation during angiogenesis. Matrices maybe loaded with different angiogenic factors, dependent on the research question concerned and constituents of the scaffold material can also be altered (Staton et al. 2009). However, the most widely used biomaterial, Matrigel, is a tumour endothelial cell matrix with potent angiogenic factors which likely skew any interpretation of vessel morphogenesis (Andree et al. 2019). More importantly, vessel networks that form using this method have been shown to lack a lumen and, therefore, these vessels are not functional structures.

Further culturing refinements include the co-culturing of endothelial cells with mural cells. Mural cells are perivascular support cells such as pericytes and vascular smooth muscle cells. In the case of the islet, evidence has emerged for their important support functions in the islet where they control local blood flow by adjusting vessel diameter. In order to study angiogenesis in human tissues, an important advancement is the commercial availability of human collagen I hydrogel which can be loaded with human umbilical vein endothelial cells (HUVECs) and supplemented with stromal elements to study 3-dimensional vessel networks (Andree et al. 2019). The use of human tissue derived matrices is highly desirable as their growth factor levels are not so high and inter-species differences are likely to elicit adverse responses and disrupt the growing vessel network.

Bridging the gap between *in vitro* and *in vivo* assays is the aortic ring assay. The aortic ring assay is a more sophisticated method which involves the dissection of a 1mm-section of rodent aorta embedded into a collagen gel. Vessel sprouting occurs from the excised tissue which means that some aspects of the *in vivo* environment are retained and repeat passaging is avoided in these systems. Also, control over the tissue environment is maintained, with test substances may be added or removed to the collagen mounting medium (Masson et al. 2002). An obvious drawback of these assays is that angiogenesis in the body typically occurs in microvessels whereas the aorta is the largest artery in the body. The importance of using microvascular tissues in angiogenesis assays is further highlighted by the finding that the metalloproteinase expression profiles of the micro- and macrovessels have been found to differ *in vitro* (Jackson

and Nguyen 1997). Additionally, dissections are technically challenging and therefore their quality may vary which potentially further impacts angiogenesis read-outs (Goodwin 2007).

Model organisms for the *in vivo* assessment of angiogenesis, apart from mice, include the use of zebrafish larvae. While the use of zebrafish larvae is associated with low costs, high-throughput and a good optical accessibility, there has been debate over its utility. Vasculogenesis, the generation of *de novo* vessels, and angiogenesis occur simultaneously in the developing zebrafish embryo and, therefore, the model has been criticised for the fact that it is not possible to distinguish these two mechanisms.

In vivo methods to study angiogenesis in islet transplant models largely rely on the implantation of isolated islets and the installation of a body window. Typical sites include the dorsal cutaneous fold and kidney capsule but there are examples for the brain as transplantation site. Islets can be seeded into various different biomaterials as scaffolds and subsequently implanted cutaneously into mice. Results with these approaches have shown that islets remain functional inside the scaffold material and can sustain normoglycaemia in animals rendered diabetic previously (Yap et al. 2013; Elizondo et al. 2020). The biomaterial can be resected at the required time-points to investigate the extent of angiogenesis. While these approaches have the added benefit of the *in vivo* context, they only allow for single time-point assessment as it requires sacrificing the recipient animal. Our model on the other hand has allowed us to longitudinally monitor the process of angiogenesis of the same islets and within the same recipient animal. Additionally, the use of scaffolding materials carried the risk of triggering an immune response and can increase blood vessel growth to the area that is independent from the intra-islet angiogenesis. The interpretation of results can be troublesome as it can be challenging to distinguish between transplant blood vessels and those that are corollary to the surgery *per se*. Contrastingly, with the islet in the eye model, we did not encounter problems with identifying vessel structure belonging to the islet and distinguishing them from those of the iris.

To date, there have only been positron emission tomographic (PET) and magnetic resonance imaging (MRI)-based imaging approaches applied to study angiogenesis longitudinally (Witkowski et al. 2009; Hathout et al. 2008). In the study where islet vascularisation was investigated over time, the islets were implanted under the kidney capsule which has been

shown to provide sub-optimal vessel supply to islets and islets usually suffer from hypoxia (Hathout et al. 2008; Carlsson et al. 2001). The oxygen tension in renal capsule islets has been estimated to be around 2mmHg in diabetic mice compared to 40mmHg in healthy islets *in situ*. Indeed, by day 180, islets from under the renal capsule were no longer present and may have suffered from an immune system-mediated attack. In contrast, based on our experience (Chapters 2 and 3), islets after full implantation remain functional throughout the lifetime of the animal and allow for the assessment of time-points beyond those investigated here. Another significant drawback with the use of both MRI and PET scanning is that they lack spatial resolution, and functional assessment of islets is virtually impossible.

Besides MRI imaging techniques, renal capsule-implanted islets can also be accessed optically through an abdominal body window (van Gurp et al. 2016). Using this method, islets were found to be vascularised by the host vasculature which partially agrees with our findings. The abdominal body window allowed for repeated imaging for up to two weeks but this is an invasive method and the surgical intervention likely impacts angiogenesis to the kidney capsule site, making it difficult to interpret results. Additionally, the insertion of a foreign material inside the body cavity can potentially elicit systemic inflammatory responses which affect glycaemia, islet survival and ultimately mortality of the animal. We demonstrate here that the longitudinal assessment of angiogenic processes in a minimally invasive *in vivo* imaging model is feasible and addresses many of the above-mentioned shortcomings of alternative techniques.

4.4.5 Technical limitations encountered in this pilot project

This study has been particularly challenging from a technical perspective and has required expertise from multiple fields of research. For the visualisation of blood vessels, we used TexasRed-conjugated dextran which we injected intravenously. Mouse IV injections require advanced technical expertise and, consequentially, injection volumes may show slight variations between different mice and time-points. This will have a direct effect on the blood vessel read-out at the point of acquisition. Whilst efforts have been made at the time of data collection to enhance the signal as much as possible, it cannot be excluded that the reduced availability of TexasRed signal hindered the visibility of the full extent of vessel architecture. We tested an alternative method to visualise blood vessels; transgenic Tie2 driven GFP-expressing mice were also tested for islet architecture. In these mice, the vessel walls of islets were readily visualised at wavelength 488nm. However, during analysis, it was not feasible to resolve finer

details of the vessel network and reconstruct it. Additionally, our adenovirus constructs were also GFP-based and thus it is likely that signal bleed-through would have been an issue (**Figure 4.4.5.1**). The ultimate aim of improving islet implantation would be to enhance islet function in patients so that they can better control their glycaemia or even stop insulin therapy. Therefore, crucial experiments would have to include the functional assessment of islets following the overexpression of EGFR in their β -cells.



Figure 4.4.5.1 An alternative to using TexasRed-Dextran to report on blood vessel morphology. Transgenic animals expressing GFP under the Tie2 endothelial-specific promoter were visualised using the 488nm laser.

In conclusion, here we demonstrated the feasibility of using the islet in eye platform for the longitudinal examination of blood vessel architecture of transplanted islets. Additionally, we provide evidence that islets treated with AV-EGFR prior to transplantation display a higher engraftment rate and have a survival benefit over control islets. On the other hand, against our predictions, EGFR-overexpression failed to increase blood vessel density of islet grafts. Therefore, enhanced EGFR signalling might confer benefits at the early stages of engraftment and promote islet graft survival.

5 General Discussion

The findings and limitations of each potential application described in this thesis were dealt with separately in their respective chapters and here, more general limitations of the islet in eye platform will be discussed. In this thesis, the application of the islet in eye platform was demonstrated to answer three different experimental questions. These projects required the tailoring of the platform to best suit each research topic explored. In summary, in the previous chapters the islet in the eye imaging platform was applied to investigate β -cell coordination under high glucose and in an acute setting, then β -cell function was assessed longitudinally in response to high-fat feeding and chronic glucagon treatment and finally, the characteristics of islet implantation was investigated when the EGF receptor was overexpressed in β -cells. While the utility of the platform is clearly demonstrated, the islet in the eye technique is not without limitations.

5.1 Blood supply of transplanted islets

The eye orbit is supplied by the ophthalmic branch of the internal carotid artery, with considerable variations in its course in humans (Hayreh 2006). The central retinal artery provides further blood supply to the eye sockets while drainage occurs into the ophthalmic and central retinal veins. It is difficult to tell what the capillary pressure is like in the iridial vessels but the blood pressure of the ophthalmic artery was reported to be approximately 70mmHg (Hayreh 1971). While this has not been described in the literature previously, it is likely that the capillary pressure in the iridial vessels supporting transplanted islets are similar to that seen in the native pancreas (40mmHg). In the native islets a high proportion of islets are supplied by the insulo-acinar network with a topology that resembles the kidney glomerulus. Based on our observations (Chapter 4) and those of others (Nyqvist et al., Almaca et al.), islets transplanted into the anterior chamber develop a vascular network with similar morphology.

Transplantation experiments on recipients of simultaneous kidney pancreas (SKP) transplants have shown that the hepatic portal drainage of islet secretions did not confer any metabolic benefit (Petruzzo et al. 2006). SKP with both types of venous drainage were able to normalise glycaemia, in fact insulin secretion was even higher in patients with systemic drainage of transplanted islets, presumably due to the removal of hepatic clearance (Pepper et al. 2013; Petruzzo et al. 2006). Jampol and colleagues reported that the pO_2 of the aqueous humour in the rabbit eye is approximately 63.5mmHg and that this is likely reflecting the pO_2 of the iridial

blood vessels (Jampol et al. 1988). For the normal functioning of the islet it was estimated that pO_2 values of 40-50mmHg at the perimeter of the islet should be sufficient to supply all β -cells with their required oxygen concentration. Thus, in the eye, the oxygen supply of transplanted islets is likely to be good and even exceed values necessary for islet function (Evron et al. 2018). In fact, general anaesthetics with 100% oxygen supply in patients have been found to elevate the pO_2 values to 170mmHg (Sharifipour et al. 2013). During our imaging recordings islets are investigated under similar conditions therefore it is likely that at the point of data collection pO_2 is high in islets in the eye.

In the rabbit eye it has been previously shown that mechanical damage to the cornea increases the protein content of the aqueous humour (Mestriner and Haddad 1994). In fact, it has also been proposed that the aqueous humour not only surrounds the iris but also penetrates it thus disrupting the blood-aqueous barrier (BAB). The BAB is established by the tight junction of the non-pigmented epithelial cells of the ciliary epithelium. Tight junctions include adherens and gap junctions which lie in the ciliary body and iridial vessels dynamically regulate the content and the passage of molecules. There is evidence to show that leukocytes can break the BAB therefore, tight junctions act as active gate keepers of the anterior chamber associated immune deviation (ACAID) (Coca Prados 2014). Shear stress to the cornea elicited the break-down of BAB and evidence was found for leukocyte invasion two days after surgery. In addition, in the rabbit eye, there was evidence for the induction of angiogenesis by this type of shear trauma to the cornea (Goes et al. 2008). These observations could explain the fact that, following surgery, we occasionally observed a reduction in islet numbers (<20% of those injected) while on the whole, islets are generally well-tolerated due to the unique anti-inflammatory milieu of the ACE.

5.2 Nerve supply of transplanted islets

Parasympathetic input to the eye arises from two sources: 1) the Edinger-Westphal preganglionic cell cluster of the oculomotor (III) cranial nerve and 2) other preganglionic neuronal cell bodies which lie in the superior salivatory nucleus and their axons run together with the facial (VII) cranial nerve. Sympathetic innervation of the eye on the other hand, arises from pre-ganglionic neurones located in the C8-T2 segments of the spinal cord. Nevertheless, early islet in eye transplant models confirmed that sympathetic activation of the eye (visible with pupil dilatation) reduced insulin secretion from implanted islets and parasympathetic

activation produced the opposite effect – which mirrors autonomic signalling in the endogenous pancreas, suggesting that the eye islets are appropriately innervated. Clearly the local dynamics though are different, although the full implications of this are poorly understood (Rodriguez-Diaz et al 2012).

Parasympathetic fibres from the pterygopalatine ganglion, when stimulated, significantly increase iridial blood flow while sympathetic innervation has the opposite effect. While in some animals this has been found to compensate for changes in intraocular pressure or mean arterial pressure, in humans there was no evidence to support iridial blood vessel autoregulation in response to intraocular pressure changes.

Sensory innervation to the islet has received relatively little research attention and their role is poorly understood. The exact significance of these nerve fibres in health and disease processes is not clear but in pre-clinical models of both T1DM (Winer et al. 2003) and T2DM (Gram et al. 2007) islets were found to have reduced sensory innervation. New research suggests that 5-hydroxy-tryptophan (5-HT) co-released with insulin might activate 5HT3 receptors on vagal sensory afferents (Makhmutova et al. 2019). Thus putatively, this pancreas-brain signalling axis can have an effect on islet physiology and hormone secretion. So far the presence of sensory nerves have not been demonstrated in islets transplanted in the eye and with that, it is possible that an important and currently incompletely understood aspect of islet physiology is not recapitulated.

5.3 The Internal Milieu of the Eye

5.3.1 Endocrine-Exocrine pancreas cross talk

Evidence suggests the existence of a continuous interstitial matrix connection between the endocrine and exocrine pancreas. The potential significance of this physical connection is highlighted by the observation that islet exocrine interface is lost in T2DM. With disease progression, islets lose their desmosomal and adherens junctions between acinar tissue and a fibrous capsule develops around them. Consequentially, endocrine-exocrine connections are severed with T2DM. The widening of peri-islet interstitium has also been observed in diabetic *ob/ob* mice, with hyper-cellularity and increased pericyte infiltration to this compartment. Therefore, extensive evidence exists for the fibrotic remodelling of endocrine and exocrine pancreas during T2DM. Further, the intimate link between the endocrine and exocrine pancreas

is illustrated by their shared vascular network, the insulo-acinar portal system where the venous drainage of exo- and endocrine tissue is collected (Hayden et al. 2009). Moreover, during development, duct cells reportedly secrete growth factors to stimulate the development of early endocrine progenitors (Bertelli and Bendayan 2005).

Such reports on exocrine abnormalities in diabetes and the anatomical positioning of the islet with respect to the exocrine pancreas, all point to a cross-talk between the two compartments that is physiologically relevant. Thus, severing ties with the exocrine pancreas could affect islet function. This is an inevitable aspect of the islet isolation process and of the islet in the eye imaging platform presented here. On the other hand, this distinction may serve an interesting way of trying to understand the modulating effect of the exocrine interface, by the very fact that it can be inferred from its absence in the eye.

5.3.2 ECM in the Pancreas versus the Anterior Chamber

Pancreatic islets have been found to be strongly adherent to the extracellular matrix of the native pancreas which suggests that it provides important support functions. The importance of the ECM is highlighted by findings where co-culturing with ECM components aids later transplantation of islets. ECM-islet interactions have been implicated in regulating islet survival, insulin secretion, proliferation and cell migration during organ development. Recently, it was shown that β -cell interaction with integrins was important in the expression of fibroblast growth factor receptor (FGFR), a growth factor important for promoting survival of β -cells (Stendahl et al. 2009; Kilkenny and Rocheleau 2008).

Human islets are encapsulated by peri-insular basement membrane which is a special type of ECM that consists of laminins, non-fibrillar collagen linked to nidogen and entactin. During the islet isolation process the peri-insular basement membrane is destroyed and this is also reflected in the decreased integrin expression of islets (Wang et al. 1999). Very recent research has provided evidence that the peri-insular basement membrane can be reconstituted in islets transplanted into the eye (Nilsson et al. 2020). In addition, these recruited fibroblasts appeared to secrete ECM proteins such as collagen IV, nidogen 2, laminin-1 γ , perlecan and fibrillary collagen amongst others.

5.4 Imaging Islets under Anaesthesia

The choice of anaesthetic throughout the studies presented above was isoflurane. Isoflurane is a volatile anaesthetic whose mechanism of action is incompletely understood. It is assumed that volatile anaesthetics induce sedation and muscle relaxation through putative actions at the γ -aminobutyric acid (GABA), glycine and N-methyl-d-aspartate (NMDA) receptors expressed in the CNS and the spinal cord (Hawkley and Maani 2019).

In vitro experiments with rat islets incubated with isoflurane have shown that isoflurane reduced glucose-stimulated insulin secretion while basal insulin secretion levels remained unchanged (Desborough et al. 1993). Recently, some work has been done to ascertain the effects of a range of anaesthetics on islet function and insulin resistance in mice. In reality, all anaesthetic agents affect glucose homeostasis in some way, although isoflurane has relatively less effects on islet secretory activity compared to others (Windelow et al. 2016). In our hands, prolonged exposure to isoflurane causes a rise in glucose in C57BL/6J mice but interestingly, the reverse effect (hypoglycaemia) in BALB/c Nude mice. However, there is a good window of about 30 minutes at the start of imaging of normoglycaemia in which to capture unconfounded calcium images.

Isoflurane had been observed to change intraocular pressure values: the intraocular pressure (IOP) decreased from 14.1mmHg to 9.9mmHg in mice at which point it stabilised. (Kim et al. 2007). In a recent report, the issue of IOP was addressed using a novel smart contact lens that is able to report on changes in IOP. While the eye surgery slightly elevated IOP in the ensuing days, values remained within the normal range and returned to baseline values after 1 week of transplantation (Kim et al. 2020).

Taken together, this thesis provides three examples of the application of a novel *in vivo* imaging platform to interrogate pancreatic islet biology. The three sets of experiments demonstrate the versatility of the approach, covering basic research of normal function and physiology through to pre-clinical studies relevant to both Type 1 and Type 2 diabetes. The major advantage of this model, as well as the ground-breaking inroad to studying the islet in real time and *in vivo*, is the ability to repeatedly image and collect longitudinal datasets. A firm understanding of the limitations of this platform is vital in order to draw nuanced conclusions and apply it to the right

research questions. However, it is clear that the future potential of this platform is great and we have only just begun.

6 Appendix : Solutions

6.1.1 Mouse Islet Culture Medium:

RPMI-1640 (Sigma-Aldrich)

50mL Foetal Bovine Serum (Sigma-Aldrich)

Penicillin/Streptomycin (15mL)

Glutamate (15mL)

6.1.2 Human Islet Culture Medium:

RPMI-1640

50mL Foetal Bovine Serum

Penicillin/Streptomycin

Amphotericin (200µl)

5.5mM Glucose

6.1.3 Krebs-Ringer Bicarbonate Buffer:

Mixed Hepes Bicarbonate Buffer (4X) in distilled H₂O:

	Per 1L
Hepes 40mM	9.53g
NaHCO₃ 8mM	0.672g
NaCl 40mM	2.338g

Mixed Salts Buffer (5X) in distilled H₂O:

	Per 1L
NaCl 650mM	37.98g
KCl 18mM	1.326g
NaH₂PO₄ 2.5mM	0.345g
MgSO₄ 2.5mM	0.616g
CaCl₂ 7.5mM	1.120g

In order to make 200mL Krebs-Ringer Bicarbonate Buffer: 50mL Hepes-Bicarbonate (4X) solution with 40mL Mixed Salts (5X) solution to 110mL distilled H₂O.

The solution was bicarbonated for 20mins and adjust to a pH of 7.4 prior to use.

Digestion Master mix:

17.6 μ l H₂O, 2 μ l Extraction buffer and 0.4 μ l Extraction enzyme

PCR Master mix:

0.5 μ l of each 10 μ M primer, 5 μ l Genotyping Mix dye, 1 μ l and H₂O to add to a total of 10 μ l

7 Appendix : Genotyping of Ins1Cre-GCaMP6f line

Genotyping for this project was kindly performed by Mr Yateen Patel.

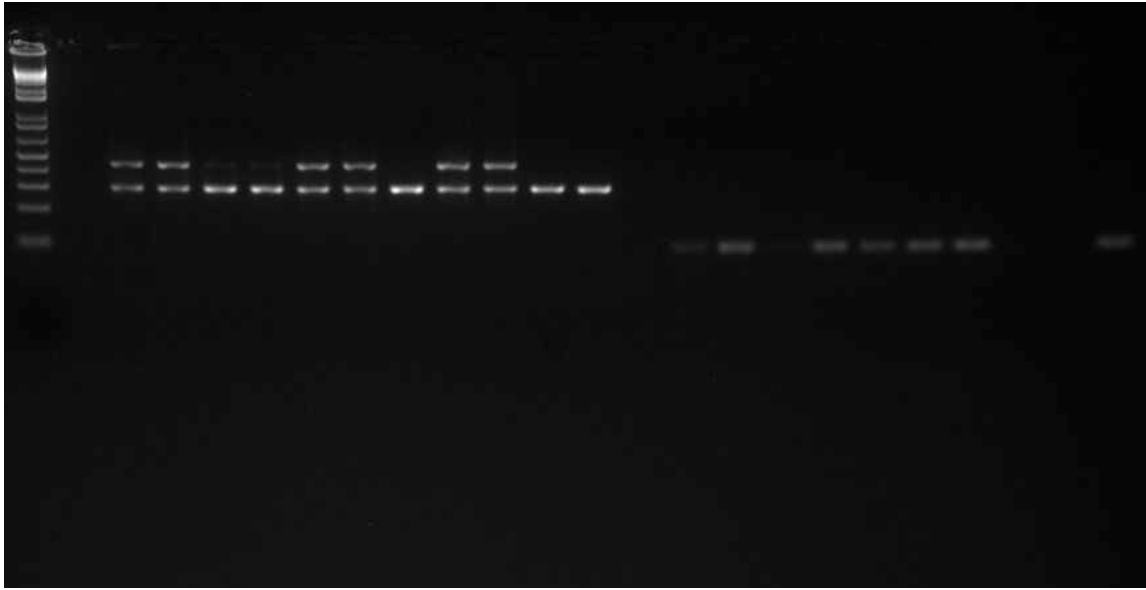
Genotyping was performed using KAPA mouse genotyping kit (KK7532). Ear biopsies (<2mm²), were taken using a sterile ear puncher and were transferred to 96-well plates and digested in 22µl proteinase K digestion mix. Samples were heated in a thermal cycler (Veriti™ 96- Well Thermal Cycler, Applied Biosystems) for 10 minutes at 75°C for optimal catalytic activity of the enzyme and 5 minutes at 95°C to the inactivate the enzyme. Samples were stored at -20°C until further use.

	Sequence
Mutant forward	5'-ACG AGT CGG ATC TCC CTT TG-3'
Wild-type forward	5'-AAG GGA GCT GCA GTG GAG TA-3'

After proteinase digestion of DNA 1µl was added to 22µl of the mastermix. Using a thermocycler, the DNA was initially denatured at 95°C for 3 minutes. The samples were subsequently cycled 35 times at 95°C (15 sec), 60°C (15 sec) and 72°C (15 sec) before being incubated at 4°C until later use.

3µl of the 6X DNA loading buffer was added to the DNA product and was run on a 2% agarose Type-II A gel. The agarose gel was made in 1X TEA buffer with 0.5µg/ml of ethidium bromide. The gel was run in 1 x TAE at 150mV for 30 minutes. The size of DNA bands were determined using a 1kb plus ladder (Invitrogen).

Genotyping for this project was kindly performed by Mr Yateen Patel.



GCaMP^{f1/f1} was 500bp long and endogenous calmodulin 300bp while Cre recombinase was 100bp large.

8 Appendix : FIJI Macros

8.1.1 Time-series manual ROI motion correction macro:

The macro can be freely available from: <https://www.imperial.ac.uk/medicine/facility-for-imaging-by-light-microscopy/equipment/software---fiji/>

```
New
File Edit Language Templates Tools Tabs
Series.txt
482 ////////////////////////////////////////////////////////////////////5
483
484 macro "Manually Align Images in a Time Series Action Tool - C999 V06cc C999 V66cc C444 V566c C000 006cc 066cc L32e2 L3251 L3254 Le2b1 Le2b4"
485 {
486 //macro to manually allign frames
487
488 //initialise
489 fn=getTitle();
490 roiManager("Reset");
491 run("Set Measurements...", "area mean min centroid bounding display redirect=None decimal=3");
492 getDimensions(OrigHldth, OrigHeight, channels, slices, frames);
493 getVoxelSize(px, py, pz, unit);
494 run("Duplicate...", "title=Temp duplicate");
495 run("Clear Results");
496
497 origImageChannels=channels;
498 origImageSlices=slices;
499 origImageFrames=frames
500
501
502
503
504 //check to make sure it is a time series
505 if (frames==1 && slices==1){
506     exit("This is not a time series");
507 }
508 if (frames==1 && slices!=1){
509     con=getBoolean("Image has only 1 frame, but " + slices + " slicess, do you want to convert slices to frames for alignment");
510     if (con==1){
511         run("Stack to Hyperstack...", "order=xyzct(default) channels=1 slices=" + frames + " frames=" + slices + " display=Color");
512         getDimensions(OrigHldth, OrigHeight, channels, slices, frames);
513
514         Stack.setUnit("frame");
515     }
516 }
517
518
519 range="";
520 if (slices>1){
521     range="duplicate frames=";
522 }
523 }
```

```
New
File Edit Language Templates Tools Tabs
Series.txt
524
525
526 range="";
527 if (slices>1){
528     range="duplicate frames=";
529 }
530
531 //get position info
532 Xpos=newArray(frames);
533 Ypos=newArray(frames);
534
535 title = "Add Position";
536 msg = "Draw an ROI\n press OK to continue";
537 waitForUser(title, msg);
538 roiManager("Add");
539
540 for (fr=0;fr<frames;fr++){
541     Stack.setFrame(fr+1);
542
543     title = "Add Position";
544     msg = "Frame "+fr+1+" - Move ROI to correct position\n press OK to continue";
545     waitForUser(title, msg);
546     run("Measure");
547     Xpos[fr]=floor(getResult("BX", fr)/px);
548     Ypos[fr]=floor(getResult("BY", fr)/py);
549 }
550
551 Array.getStatistics(Xpos, Xmin, Xmax, Xmean, XstdDev);
552 Array.getStatistics(Ypos, Ymin, Ymax, Ymean, YstdDev);
553
554 Xcanvas=OrigHldth+(Xmax-Xmin);
555 Ycanvas=OrigHeight+(Ymax-Ymin);
556
557 setBatchMode("hide");
558
559
560 //enlarge canvas
561 selectWindow("Temp");
562 run("Select None");
563 run("Canvas Size...", "width=Xcanvas height=Ycanvas position=center zero");
564 }
```

```

New
File Edit Language Templates Tools Tabs
Series.txt
517
518
519 range="";
520 if (slices>1){
521 range="duplicate frames=";
522 }
523
524 //get position info
525 Xpos=newArray(frames);
526 Ypos=newArray(frames);
527
528 title = "Add Position";
529 msg = "Draw an ROI\n press OK to continue";
530 waitforUser(title, msg);
531 roiManager("Add");
532
533 for (fr=0;fr<frames;fr++){
534
535 Stack.setFrame(fr+1);
536
537 title = "Add Position";
538 msg = "Frame "+fr+1+" - Move ROI to correct position\n press OK to continue";
539 waitforUser(title, msg);
540 run("Measure");
541 Xpos[fr]=floor(getResult("BX", fr)/px);
542 Ypos[fr]=floor(getResult("BY", fr)/py);
543 }
544
545 Array.getStatistics(Xpos, Xmin, Xmax, Xmean, XstdDev);
546 Array.getStatistics(Ypos, Ymin, Ymax, Ymean, YstdDev);
547
548 Xcanvas=OrigWidth*(Xmax-Xmin);
549 Ycanvas=OrigHeight*(Ymax-Ymin);
550
551 setBatchMode("hide");
552
553
554 //enlarge canvas
555 selectWindow("Temp");
556 run("Select None");
557 run("Canvas Size...", "width=Xcanvas height=Ycanvas position=Center zero");
558

```

```

New
File Edit Language Templates Tools Tabs
Series.txt
548 Xcanvas=OrigWidth*(Xmax-Xmin);
549 Ycanvas=OrigHeight*(Ymax-Ymin);
550
551 setBatchMode("hide");
552
553
554 //enlarge canvas
555 selectWindow("Temp");
556 run("Select None");
557 run("Canvas Size...", "width=Xcanvas height=Ycanvas position=Center zero");
558
559
560 //first image extraction
561 selectWindow("Temp");
562 Stack.setFrame(1);
563 makeRectangle(Xpos[0]-Xmin, Ypos[0]-Ymin, OrigWidth, OrigHeight);
564 //run("Duplicate...", "");
565 run("Duplicate...", range+1);
566 if (slices>1){
567 run("Add Slice", "add=frame prepend");
568 }
569 rename("new");
570
571
572
573 //image extraction
574 for (i=1;i<frames;i++){
575 selectWindow("Temp");
576 Stack.setFrame(i+1);
577 makeRectangle(Xpos[i]-Xmin, Ypos[i]-Ymin, OrigWidth, OrigHeight);
578 //run("Duplicate...", "");
579 run("Duplicate...", range+i+1);
580 rename("next");
581
582 run("Concatenate...", " title=[new] image1=[new] image2=[next] image3=[-- None --]");
583 }
584
585 //finish up
586 rename("Aligned "+fn);
587 Stack.setFrame(1);
588 if (origImageSlices>1 && origImageFrames>1){

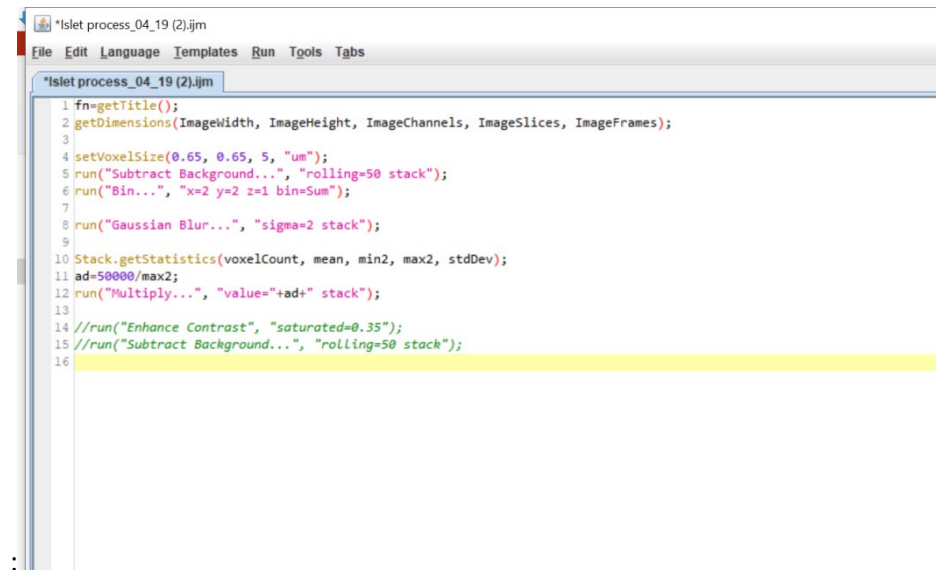
```

```

New
File Edit Language Templates Tools Tabs
Series.txt
588 Stack.setFrame(1);
589 makeRectangle(Xpos[0]-Xmin, Ypos[0]-Ymin, OrigWidth, OrigHeight);
590 //run("Duplicate...", "");
591 run("Duplicate...", range+1);
592 if (slices>1){
593 run("Add Slice", "add=frame prepend");
594 }
595 rename("new");
596
597
598
599 //image extraction
600 for (i=1;i<frames;i++){
601 selectWindow("Temp");
602 Stack.setFrame(i+1);
603 makeRectangle(Xpos[i]-Xmin, Ypos[i]-Ymin, OrigWidth, OrigHeight);
604 //run("Duplicate...", "");
605 run("Duplicate...", range+i+1);
606 rename("next");
607
608 run("Concatenate...", " title=[new] image1=[new] image2=[next] image3=[-- None --]");
609 }
610
611 //finish up
612 rename("Aligned "+fn);
613 Stack.setFrame(1);
614 if (origImageSlices>1 && origImageFrames>1){
615 run("Delete Slice", "delete=frame");
616 //run("Stack to Hyperstack...", "order=xyctz(default) channels=origImageChannels slices=origImageSlices frames=origImageFrames display=Color");
617 }
618 run("Stack to Hyperstack...", "order=xyctz(default) channels=origImageChannels slices=origImageSlices frames=origImageFrames display=Color");
619 setBatchMode("exit and display");
620 selectWindow("Temp");
621 close();
622

```

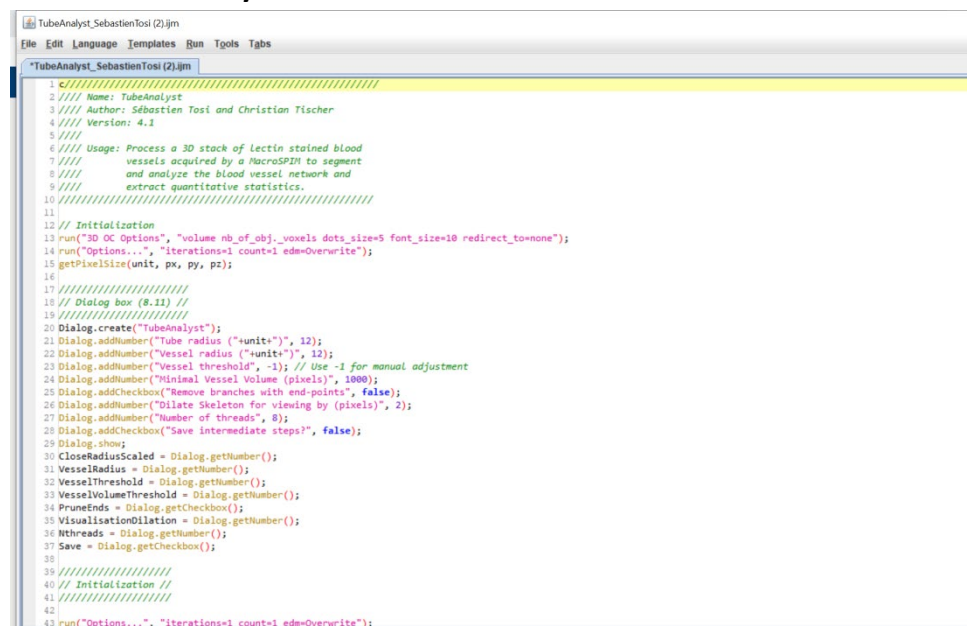
8.1.2 Islet process macro:



```
*Islet process_04_19 (2).ijm
1 fn=getTitle();
2 getDimensions(ImageWidth, ImageHeight, ImageChannels, ImageSlices, ImageFrames);
3
4 setVoxelSize(0.65, 0.65, 5, "um");
5 run("Subtract Background...", "rolling=50 stack");
6 run("Bin...", "x=2 y=2 z=1 bin=Sum");
7
8 run("Gaussian Blur...", "sigma=2 stack");
9
10 Stack.getStatistics(voxelCount, mean, min2, max2, stdDev);
11 ad=50000/max2;
12 run("Multiply...", "value="+ad+" stack");
13
14 //run("Enhance Contrast", "saturated=0.35");
15 //run("Subtract Background...", "rolling=50 stack");
16
```

The macro was custom written for this project (Chapter 4) by Stephen Rothery (FILM Facility, Imperial College London).

8.1.3 Tube Analyst macro:



```
TubeAnalyst_SebastienTosi (2).ijm
File Edit Language Templates Run Tools Tabs
*TubeAnalyst_SebastienTosi (2).ijm
1 #####
2 /// Name: TubeAnalyst
3 /// Author: Sébastien Tosi and Christian Fischer
4 /// Version: 4.1
5 ///
6 /// Usage: Process a 3D stack of Lectin stained blood
7 /// vessels acquired by a MacroSPIM to segment
8 /// and analyze the blood vessel network and
9 /// extract quantitative statistics.
10 #####
11
12 // Initialization
13 run("3D OC Options", "volume nb_of_obj_voxels dots_size=5 font_size=10 redirect_to=none");
14 run("Options...", "iterations=1 count=1 edm=Overwrite");
15 getPixelSize(unit, px, py, pz);
16
17 #####
18 // Dialog box (§.11) //
19 #####
20 Dialog.create("TubeAnalyst");
21 Dialog.addNumber("Tube radius (+unit)", 12);
22 Dialog.addNumber("Vessel radius (+unit)", 12);
23 Dialog.addNumber("Vessel threshold", -1); // Use -1 for manual adjustment
24 Dialog.addNumber("Minimal Vessel Volume (pixels)", 1000);
25 Dialog.addCheckbox("Remove branches with end-points", false);
26 Dialog.addNumber("Dilate Skeleton for viewing by (pixels)", 2);
27 Dialog.addNumber("Number of threads", 8);
28 Dialog.addCheckbox("Save intermediate steps?", false);
29 Dialog.show;
30 CloseRadiusScaled = Dialog.getNumber();
31 VesselRadius = Dialog.getNumber();
32 VesselThreshold = Dialog.getNumber();
33 VesselVolumeThreshold = Dialog.getNumber();
34 PruneEnds = Dialog.getCheckbox();
35 VisualisationDilation = Dialog.getNumber();
36 Nthreads = Dialog.getNumber();
37 Save = Dialog.getCheckbox();
38
39 #####
40 // Initialization //
41 #####
42
43 run("Options...", "iterations=1 count=1 edm=Overwrite");
```



```

TubeAnalyst_SebastienTosi (2).ijm
File Edit Language Templates Run Tools Tgbs
*TubeAnalyst_SebastienTosi (2).ijm
28 Dialog.addCheckbox("Save intermediate steps?", false);
29 Dialog.show;
30 CloseRadiusScaled = Dialog.getNumber();
31 VesselRadius = Dialog.getNumber();
32 VesselThreshold = Dialog.getNumber();
33 VesselVolumeThreshold = Dialog.getNumber();
34 PruneEnds = Dialog.getCheckbox();
35 VisualisationDilation = Dialog.getNumber();
36 Nthreads = Dialog.getNumber();
37 Save = Dialog.getCheckbox();
38
39 ///////////////////////////////////////////////////
40 // Initialization //
41 ///////////////////////////////////////////////////
42
43 run("Options...", "iterations=1 count=1 edm=Overwrite");
44 OriginalTitle = getTitle();
45
46 ///////////////////////////////////////////////////
47 // Closing (8.5) //
48 ///////////////////////////////////////////////////
49
50 // Physical units to pixels conversion
51 IJ.log("CloseRadiusScaled = "+CloseRadiusScaled+unit);
52 IJ.log("CloseRadiusPixX = "+d2s(CloseRadiusScaled/px,2));
53 IJ.log("CloseRadiusPixY = "+d2s(CloseRadiusScaled/py,2));
54 IJ.log("CloseRadiusPixZ = "+d2s(CloseRadiusScaled/pz,2));
55
56 // Filtering: closing to fill hollow tubes
57 run("Duplicate...", "title=tmp duplicate");
58 run("3D Fast Filters", "filter=Maximum radius_x_pix="+d2s(CloseRadiusScaled/px,2)+" radius_y_pix="+d2s(CloseRadiusScaled/py,2)+" radius_z_pix="+d2s(CloseRadiusScaled/pz,2)+" Nb_cpus="+d2s(Nthreads,0));
59 rename("Maximum");
60 run("3D Fast Filters", "filter=Minimum radius_x_pix="+d2s(CloseRadiusScaled/px,2)+" radius_y_pix="+d2s(CloseRadiusScaled/py,2)+" radius_z_pix="+d2s(CloseRadiusScaled/pz,2)+" Nb_cpus="+d2s(Nthreads,0));
61
62 // store output
63 if(Save==true){
64     rename("Closed_8-5");
65     run("Save");
66 }
67 rename("Closed");
68
69 // Cleanup
70 selectImage("Maximum");

```

```

TubeAnalyst_SebastienTosi (2).ijm
File Edit Language Templates Run Tools Tgbs
*TubeAnalyst_SebastienTosi (2).ijm
67 rename("Closed");
68
69 // Cleanup
70 selectImage("Maximum");
71 close();
72
73 ///////////////////////////////////////////////////
74 // Enhancement of filamentous pixels (8.6) //
75 ///////////////////////////////////////////////////
76
77 // Work on the closed image
78 selectImage("Closed");
79 run("Tubeness", "sigma="+d2s(VesselRadius,2)+" use");
80 if(Save==true)
81 {
82     rename("Tubeness_8-6");
83     run("Save");
84 }
85 rename("Tubeness Filtered");
86
87 ///////////////////////////////////////////////////
88 // Segmentation (8.7) //
89 ///////////////////////////////////////////////////
90
91 // Work on the image after tubeness filtering
92 selectImage("Tubeness Filtered");
93 run("Duplicate...", "title=mask duplicate");
94
95 // Convert to 8-bit for threshold normalization
96 Stack.getStatistics(voxelCount, mean, min, max);
97 setMinAndMax(min,max);
98 run("8-bit");
99
100 // If lower bound of threshold is set to -1 --> user interaction
101 if(VesselThreshold == -1)
102 {
103     run("Threshold...");
104     waitForUser("Treshold vessels");
105 }
106 else setThreshold(VesselThreshold,255);
107 run("Convert to Mask", "method=Default background=Dark");
108 setSlice(nSlices/2);
109

```

```

TubeAnalyst_SebastienTosi (2).jlm
File Edit Language Templates Run Tools Tgbs
*TubeAnalyst_SebastienTosi (2).jlm
1103 run("Threshold...");
1104 waitForUser("Threshold vessels");
1105 }
1106 else setThreshold(VesselThreshold,255);
1107 run("Convert to Mask", "method=Default background=Dark");
1108 setSlice(nSlices/2);
1109
1110 // Analyze connected components, remove too small objects and apply LUT
1111 run("3D Objects Counter", "threshold=128 min.="+VesselVolumeThreshold+" max.="+nSlices*getWidth()*getHeight()+ " objects statistics summary");
1112 run("Random");
1113 if(Save==true){
1114     rename("LabelMask_8-7");
1115     run("Save");
1116 }
1117 rename("Label Mask");
1118
1119 // Total vessel volume
1120 totalVolume = 0;
1121 stack_getUnits(Xunit, Yunit, Zunit, Timeunit, Valueunit);
1122 for(i=0; i<nResults; i++)totalVolume = totalVolume + getResult("Volume ("+Xunit+"^3)", i);
1123 IJ.renameResults("Results","Statistics for Binarized tubes"); // Rename results table
1124
1125 // Cleanup
1126 selectImage("Mask");
1127 close();
1128
1129 // store output
1130 selectImage("Label Mask");
1131
1132 // Fill holes (8.9) //
1133 // Fill holes (8.9) //
1134 // Fill holes (8.9) //
1135
1136 // Mark on the label mask
1137 selectImage("Label Mask");
1138
1139 // Fill holes
1140 run("Duplicate...", "title=Tmp duplicate");
1141 setThreshold(1,255);
1142 run("Convert to Mask", "method=Default background=Dark");
1143 run("Fill Holes", "stack");
1144
1145 // Fill holes

```

```

TubeAnalyst_SebastienTosi (2).jlm
File Edit Language Templates Run Tools Tgbs
*TubeAnalyst_SebastienTosi (2).jlm
1145 // Fill holes
1146 // Skeletonization + analysis (8.8) //
1147 // Skeletonization + analysis (8.8) //
1148
1149 setThreshold(1,255);
1150 run("Convert to Mask", "method=Default background=Dark");
1151 rename("Binarized tubes");
1152 run("Duplicate...", "title=Skeleton duplicate");
1153 run("Skeletonize (2D/3D)");
1154
1155 // Remove end-point branches by pruning
1156 if(PruneEnds) run("Analyze Skeleton (2D/3D)", "prune=none prune"); // no circular pruning, but end-point pruning
1157 else run("Analyze Skeleton (2D/3D)", "prune=none"); // no circular pruning, no end-point pruning
1158 IJ.renameResults("Results","Skeleton Results"); // rename results table for saving it from being overwritten by other "Results"
1159
1160 // Change analyzed skeleton colors
1161 run("Macro...", "code=v=(v==127)*127+(v==30)*192+(v==70)*255 stack");
1162 if(Save==true){
1163     rename("Analyzed_skeleton_8-8");
1164     run("Save");
1165 }
1166 rename("Analyzed skeleton");
1167
1168 // Thicken analyzed skeleton
1169 run("3D Fast Filters", "filter=Maximum radius_x_pix=2.0 radius_y_pix=2.0 radius_z_pix=2.0 Nb_cpus="+d2s(Nthreads,0));
1170 // Changes the LUT
1171 run("Fire");
1172 if(Save==true){
1173     rename("ThickSkeleton_8-8");
1174     run("Save");
1175 }
1176 rename("ThickSkeleton");
1177
1178 // Statistics extraction (8.10) //
1179 // Statistics extraction (8.10) //
1180 // Statistics extraction (8.10) //
1181
1182 // Total vessel length
1183 IJ.renameResults("Skeleton Results", "Results"); // make table accessible
1184
1185 totalLength = 0;
1186 nBranches = 0;
1187 for(i=0; i<nResults; i++) {

```

```
TubeAnalyst_SebastienTosi (2).jfm
File Edit Language Templates Run Tools Tgbs
TubeAnalyst_SebastienTosi (2).jfm
152 // Total vessel length
153 IJ.renameResults("Skeleton Results", "Results"); // make table accessible
154
155 totalLength = 0;
156 nBranches = 0;
157 for(i=0; i<nResults; i++) {
158     totalLength = totalLength + getResult("n Branches", i)*getResult("Average Branch Length", i);
159     nBranches = nBranches + getResult("n Branches", i);
160 }
161
162 IJ.renameResults("Results","Skeleton Results");
163
164 // Total imaged volume
165 selectImage(OriginalTitle); // select the image containing the segmented vessels
166 totalImagedVolume = getWidth()*px*getHeight()*py*nSlices*pz;
167
168 // Mean vessel x-section and diameter
169 meanCrosssection = totalVolume / totalLength;
170 meanDiameter = 2*sqrt(meanCrosssection/PI);
171
172 print("");
173 print("Results");
174 print("-----");
175 print("Total length = " + totalLength + unit);
176 print("Number of branches = " + nBranches);
177 print("Average branch length = " + totalLength/nBranches + unit);
178 print("Mean vessel cross-section = " + meanCrosssection + unit + "m^2");
179 print("Mean vessel diameter = " + meanDiameter + unit);
180 print("Total vessel volume = " + totalVolume + unit + "m^3");
181 print("Total imaged volume = " + totalImagedVolume + unit + "m^3");
182 print("Volume fraction occupied by vessels = " + totalVolume/totalImagedVolume);
183
184
185 // Results visualization (8.11) //
186 //-----//
187
188 // Load original stack, Label mask and analyzed skeleton in 3D viewer
189 run("3D Viewer");
190 //call("ij3d.Image3DViewer.setCoordinateSystem", "false");
191 call("ij3d.Image3DViewer.add", OriginalTitle, "None", OriginalTitle, "0", "true", "true", "true", "2", "0");
192 call("ij3d.Image3DViewer.add", "Label Mask", "None", "Label Mask", "0", "true", "true", "true", "2", "0");
193 call("ij3d.Image3DViewer.add", "ThickSkeleton", "None", "ThickSkeleton", "0", "true", "true", "true", "2", "0");
194 //call("ij3d.Image3DViewer.startAnimate");
```

The Tube Analyst macro was written by Dr Sebastian Tosi (Advanced Digital Microscopy Core Facility – IRB Barcelona) and is freely available from:

<http://adm.irbbarcelona.org/image-j-fiji>

9 Appendix: Granger Causality Analysis MatLab script

The MatLab Script was developed by Dr Victoria Salem and Prof Walter Distaso and is available upon request from: v.salem@ic.ac.uk.

10 Appendix: Human Islet Donor Characteristics

Gender and Age of Donor	BMI	Diabetic/Non-Diabetic
Male, 74 years old	29.2	Non-diabetic
Male, 14 years old	21.5	Non-diabetic
Female, 65 years old	28.8	Non-diabetic
Male, 50 years old	22.9	Non-diabetic, died of cardiovascular complications
Female, 54 years old	24.4	T2DM for 10 years, insulin-dependent for 1.5 years

11 Appendix : Conference Abstracts

Diabetes UK Professional Conference, London UK, March 2018 (poster presentation):

Measuring real-time islet blood vessel responses to hormonal challenges using the platform of transplanted islets in the anterior chamber of the murine eye

K SUBA¹, MS Nguyen-Tu¹, P Chabosseau¹, GR Carrat¹, I Leclerc¹, DCA Gaboriau², SM Rothery², V Salem¹, GA Rutter¹

¹Section of Cell Biology and Functional Genomics, Department of Medicine, Imperial College London, London, UK, ²FILM, Facility for Imaging by Light Microscopy, Imperial College London, London, UK

Aim: Transplantation into the anterior chamber of the eye (ACE) serves as a novel platform for longitudinal *in vivo* imaging of islet biology. Here, we use this approach to assess the time course effects of acute hormonal challenges on islet blood vessel dynamics *in vivo*.

Methods: C57BL6 mice received syngeneic donor islets (n = 12, 2 to 5 islets per animal) into the ACE. Following full implantation (>4 weeks), mice were anaesthetised (isoflurane) in a stereotaxic frame and the implanted islets visualised with confocal microscopy (CrestOptics spinning disk, 20× water dipping 1.0 NA objective; Nikon eclipse Ti microscope). Islet vasculature was visualised following tail vein injection of TexasRed-conjugated dextran. At different imaging sessions, mice randomly received 0.2-ml intraperitoneal injections of saline, noradrenaline (1mg/kg) or glucagon (1mg/kg). Z-stacks (ex.:561nm, 1-µm increments) were acquired at 5-min intervals post injection up to 30min. Images were analysed with ImageJ and Huygens software.

Results: Noradrenaline did not produce a global change in islet blood vessel calibre during the imaging period; however, subanalysis of individual vessels may produce evidence of shunting which will be further explored. Glucagon injection resulted in a sustained increase in islet blood vessel surface area from 5 to 30 min post injection.

Conclusion: We demonstrate that the ACE is a useful platform for studying real-time islet vascular responses, with great potential. Even though glucagon is also considered a “stress hormone”, we provide evidence for divergent effects on islet blood vessel responses with noradrenaline.

**American Diabetes Association 78th Scientific Sessions, Orlando (FL) USA, 2018
(poster presentation):**

Real-Time In Vivo Imaging of Whole Islet Ca²⁺ Dynamics Reveals Glucose-Induced Changes in Beta-Cell Connectivity in Mouse and Human Islets

VICTORIA SALEM, **KINGA SUBA**, ALDARA MARTIN ALONSO, PAULINE L. CHABOSSEAU, ELENI GEORGIADOU, THEODOROS STYLIANIDES, LINFORD BRIANT, DAVID HODSON, GAELLE CARRAT, ISABELLE LECLERC, DAVID C. GABORIAU, STEPHEN M. ROTHERY and GUY A. RUTTER

Imaging of Ca²⁺ dynamics in the intact islet in vitro has recently been subjected to connectivity analysis informed by similar approaches in neuronal systems. This has revealed the existence of intercellular networks between individual β cells which are increased by high glucose. Here, we sought to investigate if network connectivity also exists in islets in vivo under conditions of near-normal vascularisation and innervation. Donor mouse (C57BL/6J) islets were infected with adenovirus expressing the Ca²⁺ sensor GCaMP6m and transplanted into the anterior chamber of the eye in syngeneic recipients. Under isofluorane anaesthesia, fully implanted islets were imaged using a spinning disk confocal microscope (Nikon Ti-E, 25 x water dipping 1.0 NA objective, 300ms exposure time, 1 frame per second, 488nm excitation). Mean baseline blood glucose was 19mM and rose to >30mM following an IP bolus of 1.5g/L glucose. Human islets were infected with AV-GCaMP6m, transplanted into a nu/nu mouse recipient and imaged under conditions of normoglycaemia (blood glucose 3.9-4.9 mM followed by hyperglycaemia (blood glucose >30 mM). As circulating blood glucose increased, the proportion of connected cells in mouse islets rose from 65.5% to 88.3% (n=3 islets in 3 different animals, p=0.02) whilst the coefficient of correlation (a measure of the strength of the connectivity) showed a tendency to increase from 0.34 to 0.44 (p=NS). Data from human islets also revealed a tendency towards a rise in connectivity from 58.3% to 63.9% in response to rising circulating glucose. These data demonstrate that functional connectivity of Ca²⁺ dynamics between β cells is conserved in vivo in both mouse and human islets, with enhanced connectivity patterns observed in response to rising blood glucose levels. This technique, which allows β cell connectivity to be examined prospectively over time, will provide a powerful new approach for assessing its significance in health and disease.

Society for Endocrinology BES Conference, Glasgow UK, 2018:

Glucose regulates pancreatic [beta] cell Ca²⁺ dynamics and connectivity in vivo in the anterior chamber of the mouse eye

Victoria Salem¹, **Kinga Suba¹**, Aldara Martin-Alonso¹, Luis Fernando Delgadillo Silva², Nadeem Akhtar², Neda Mousavy¹, Eleni Georgiadou¹, David Gaboriau¹, Stephen Rothery¹, Theodoros Stylianides³, Piero Marchetti⁴, Linford Briant⁵, Nikolay Ninov², David Hodson⁶, Walter Distaso¹ & Guy Rutter¹

Background and Aims: β cell connectivity is a feature of pancreatic islets in vitro but its existence in vivo, when innervated and continuously perfused with blood, has not yet been demonstrated. We imaged islets engrafted in the anterior chamber of the mouse eye (ACE) to explore this question.

Methods: Mouse (C57BL6, Ins1Cre::GCaM6mf/f) or human islets infected with adenovirus to express GCaMP6m, were engrafted and Ca²⁺ imaging performed under anaesthesia. Glucose or insulin were administered intravenously to achieve low glucose (4–6 mM) or high glucose (25–30 mM) conditions. Data were collected on a spinning disc confocal microscope using a 20 \times , 1.0 NA water immersion objective (3 Hz). Following movement correction, Ca²⁺ traces were analyzed with Image J. Connectivity analysis was performed with custom-built scripts in Matlab.

Results: Ca²⁺ waves spreading across the islet in 5/5 animals were observed. Even at low glucose concentrations, β cells form a highly connected syncytium. Increasing glucose concentrations augmented the proportion of connected β cells from 65 to 86% (n=5; P=0.02) and correlation strength (Pearson R with bootstrapping) from 0.34 \pm 0.07 to 0.46 \pm 0.08 (n=5; P=0.05). Granger causality analysis indicated that cells which responded first during Ca²⁺ pulses were causally linked to the activity of the largest number of other β cells in the islet. Moreover, the presence of a super-connected β cell subpopulation (8.7 \pm 3.6% of cells) was revealed by signal binarisation and Monte Carlo randomization. Pearson connectivity was increased from 58.3% to 63.9% (n=1 animal) in engrafted human islets

Conclusions: We demonstrate intercellular connectivity between β cells within the islet in vivo under conditions of normal islet perfusion and innervation. These findings are consistent with the existence of islet pacemaker cells which coordinate Ca²⁺ dynamics and possibly pulsatile insulin secretion in the physiological setting.

American Diabetes Association 79th Scientific Sessions, San Francisco (CA) USA, 2019 (oral presentation):

Hub Cells Orchestrate 3-Dimensional Pancreatic Beta-Cell Ca²⁺ Dynamics In Vivo

VICTORIA SALEM, LUIS F. DELGADILLO SILVA, **KINGA SUBA**, ALDARA MARTIN ALONSO, WHEI-CHANG KIM, VASILIKI KALOGIANNI, NADEEM AKHTAR, NEDA MOUSAVY GHARAVY, ELENI GEORGIADOU, ISABELLE LECLERC, LINFORD BRIANT, DAVID HODSON, WALTER DISTASO, NIKOLAY N. NINOV and GUY A. RUTTER

Aim: In-vitro studies reveal a subpopulation of β cells which co-ordinate insulin release from pancreatic islets. This connectivity has not been established in 3 dimensions across the islet or in the living animal. We investigated this in the living zebrafish *D. rerio* or in mouse islets engrafted in the anterior eye chamber (ACE), using the recombinant Ca²⁺ sensor GCaMP6 under the insulin promoter/C57Bl6, *Ins1Cre:GCaM6^{f/f}*.

Methods: Whole islet live imaging of *D. rerio* primary islets in situ at an acquisition rate of 0.8Hz, covering 700 μ m, was achieved using resonant scanner technology with a Leica inverted laser scanning confocal system, using a 25X/N.A. 0.95 water lens. Fully vascularized islets in the murine ACE were imaged under isoflurane anaesthesia on a modified Nikon Ti-E spinning disc confocal microscope (20x 0.75 NA water immersion objective, 3 Hz frame rate).

Results: 3-dimensional β cell connectivity (Pearson R statistic) significantly rose to 88% across the zebrafish islet in response to glucose stimulation. Focused ablation of the co-ordinating “hub” (but not follower) β cells significantly attenuated the subsequent response to a glucose challenge. In mouse islets, high circulating glucose levels were also associated with a significant rise in 3D beta cell connectivity from 65 to 86% (n=3; p=0.02). Granger causality analysis on these islets revealed that even on prolonged (>10 minute) glucose stimulation, pan-islet connectivity was sustained and the most highly connected cells were those in the region of the islet from which Ca²⁺ waves emanated. Binarized signal analysis (n=6) separately confirmed the presence of a highly-connected β cell subpopulation (8.7 \pm 3.6% of cells).

Conclusions: These studies evidence beta cell “hubs” which are responsible for the initiation and sustained coordination of the Ca²⁺ response to glucose across fish and mouse islets in vivo.

Society for Endocrinology BES Conference, Brighton UK, 2019 (oral presentation):

Modulation of EGFR expression to increase islet transplantation success

Usama Ali, **Kinga Suba**, Stavroula Bitsi, Aldara Martin Alonso, Yateen Patel, Isabelle Leclerc, Guy A Rutter, Stephen Rothery, Victoria Salem & Alejandra Tomas

Background: Islet transplantation is an established treatment for type 1 diabetes mellitus. However, many recipients do not achieve independence from exogenous insulin since up to 50–70% of islets are lost post-transplant. An important factor determining transplant success is graft vascularisation. The epidermal growth factor receptor (EGFR) is a key pro-survival and proliferation factor. Here, we investigate for the first time if EGFR overexpression in pancreatic islets improves engraftment in an in vivo mouse model.

Methods: We generated adenovirus encoding human EGFR alongside a GFP reporter in order to overexpress this protein in primary tissue. Following successful infection (as assessed by GFP expression), control (empty vector) or EGFR-infected islets were transplanted into the anterior chambers of the eyes of syngeneic mice (n=12 eyes randomly receiving either EGFR or control islets). Islet volume and blood vessel density/branching were assessed longitudinally over 30 days using confocal microscopy. To assess implantation, beta cell identity and function, expression of angiogenesis (eg VEGF), beta-cell enriched (eg Pdx1 and MafA) and beta-cell disallowed (eg Acot7 and LdhA) genes was determined by qPCR from identically infected islet groups (in vitro).

Results: Blood vessel density increased significantly over 30 days for both groups of islets ($P < 0.05$), with EGFR-overexpressing islets demonstrating greater density compared to control islets at 30 days. qPCR results showed that EGFR-overexpressing islets had increased gene expression of angiogenic factors. Furthermore, consistent with preserved beta cell identity, beta-cell enriched factors were upregulated compared to control islets, while beta-cell disallowed genes were further repressed.

Conclusion: This is the first study to demonstrate that EGFR overexpression can promote the vascularisation of transplanted pancreatic islets in vivo. The transcriptional profiling of these islets also suggests an improved potential for beta-cell regenerative capacity and function. Further studies are underway to fully investigate the therapeutic potential of this intervention.

American Diabetes Association, 80th Scientific Sessions, Virtual Conference, 2020:

Chronic administration of a long-acting glucagon analogue results in enhanced insulin secretory activity in a directly-observed murine model

Aims: GLP-1 (GLP-1R) and glucagon (GCGR) receptor dual agonists are in development to treat Type 2 Diabetes. The effects of chronic GCGR agonism on weight loss are well-documented, its direct influence on islet function remains poorly understood. We investigated the chronic in vivo effects of a long acting glucagon analogue G778 on pancreatic islet calcium dynamics.

Methods: C57Bl/6 (n=9 per group) mice with diet-induced obesity received daily subcutaneous (SC) injections of G778 100nmol/kg or saline (and calorie restricted to achieve weight matching) for 40 days. All mice had islets with beta-cell specific expression of GCaMP6f implanted in the anterior chamber of the eye as a direct, longitudinal readout of beta-cell function in vivo with confocal microscopy. Such islets were separately tested in vitro to measure the effects of G778 on whole islet calcium dynamics.

Results: At 40 days, there was a non-significant difference in body weight loss between the saline and G778-treated groups ($0.9g \pm 1.1$ vs $3.4g \pm 0.7$ $p=0.07$), but a marked improvement in glucose tolerance (15 min glucose on a 2mg/kg IPGTT 15.9 mmol/L vs 9.2 mmol/L $p<0.001$). Islet readouts suggest that glucagon receptor agonism was able to restore calcium activity of islets in DIO mice in vivo. In vitro findings confirmed that G778 promoted calcium waves of longer duration and hence heightened connectivity (despite no change in amplitude) above 7mM glucose ($p=0.05$).

Summary: Our data suggest that the glucagon element of a glucagon/GLP-1 analogue has weight-loss independent effects on insulin secretory function, promoting more robust and sustained beta-cell calcium responses

Bibliography

Abdul-Ghani, M., Del Prato, S., Chilton, R. & De Fronzo, R. A., 2016. SGLT2 inhibitors and cardiovascular risk: Lessons learned from the EMPA-REG Outcome study. *Diabetes Care*, 1 5, 39(5), pp. 717-725.

Adeghate, E., 1998. Host-graft circulation and vascular morphology in pancreatic tissue transplants in rats. *The Anatomical Record*, 1 8, 251(4), pp. 448-459.

Adeva-Andany, M. M. et al., 2016. *Glycogen metabolism in humans*. s.l.:Elsevier B.V..

Aguayo-Mazzucato, C. & Bonner-Weir, S., 2010. *Stem cell therapy for type 1 diabetes mellitus*. s.l.:s.n.

Ahlkvist, L. et al., 2016. Defective insulin secretion by chronic glucagon receptor activation in glucose intolerant mice. *Journal of Endocrinology*, 228(3), pp. 171-178.

Ahlqvist, E. et al., 2018. Novel subgroups of adult-onset diabetes and their association with outcomes: a data-driven cluster analysis of six variables. *The Lancet Diabetes and Endocrinology*, 1 5, 6(5), pp. 361-369.

Ahmadian, M. et al., 2013. Ppar γ signaling and metabolism: The good, the bad and the future. *Nature Medicine*, 19(5), pp. 557-566.

Ahrén, B., 2000. *Autonomic regulation of islet hormone secretion - Implications for health and disease*. s.l.:Springer Verlag.

Ahrén, B., 2012. *Islet nerves in focus-Defining their neurobiological and clinical role*. s.l.:Springer.

Ahrén, B., 2015. *Glucagon - Early breakthroughs and recent discoveries*. s.l.:Elsevier Inc..

Ahrén, B., Holst, J. J. & Mari, A., 2003. Characterization of GLP-1 effects on β -cell function after meal ingestion in humans. *Diabetes Care*, 1 10, 26(10), pp. 2860-2864.

Ahrén, B., Wierup, N. & Sundler, F., 2006. *Neuropeptides and the regulation of islet function*. s.l.:American Diabetes Association.

Akbay, E. A. et al., 2013. Activation of the PD-1 pathway contributes to immune escape in EGFR-driven lung tumors. *Cancer Discovery*, 12, 3(12), pp. 1355-1363.

Akhtar, S. & Benter, I. F., 2013. *The role of epidermal growth factor receptor in diabetes-induced cardiac dysfunction*. s.l.:Tabriz University of Medical Sciences.

Albaugh, V. L. et al., 2017. *Bile acids and bariatric surgery*. s.l.:Elsevier Ltd.

Almaça, J. et al., 2014. Young capillary vessels rejuvenate aged pancreatic islets. *Proceedings of the National Academy of Sciences of the United States of America*, 9 12, 111(49), pp. 17612-17617.

Almaça, J. et al., 2018. The Pericyte of the Pancreatic Islet Regulates Capillary Diameter and Local Blood Flow. *Cell Metabolism*, 6 3, 27(3), pp. 630-644.e4.

- Al-Nedawi, K. et al., 2009. Endothelial expression of autocrine VEGF upon the uptake of tumor-derived microvesicles containing oncogenic EGFR. *Proceedings of the National Academy of Sciences of the United States of America*, 10 3, 106(10), pp. 3794-3799.
- Alsahli, M. & Gerich, J. E., 2017. *Renal glucose metabolism in normal physiological conditions and in diabetes*. s.l.:Elsevier Ireland Ltd.
- Ammon, H. P., Reiber, C. & Verspohl, E. J., 1991. Indirect evidence for short-loop negative feedback of insulin secretion in the rat. *Journal of Endocrinology*, 128(1), pp. 27-34.
- Andrée, B. et al., 2019. Formation of three-dimensional tubular endothelial cell networks under defined serum-free cell culture conditions in human collagen hydrogels. *Scientific Reports*, 1 12, 9(1), pp. 1-11.
- Andrikopoulos, S. et al., 2008. Evaluating the glucose tolerance test in mice. *American Journal of Physiology - Endocrinology and Metabolism*, 12, 295(6), pp. E1323-32.
- Anon., n.d. *Diabetes Prevalence 2019 | Diabetes UK*. [Online] Available at: <https://www.diabetes.org.uk/professionals/position-statements-reports/statistics/diabetes-prevalence-2019>
- Anon., n.d. *Impaired awareness of hypoglycaemia: a review | Elsevier Enhanced Reader*. [Online] Available at: <https://reader.elsevier.com/reader/sd/pii/S1262363610704705?token=5C6511C385C4F18E5566C56B2F5F3799D67B4FBC4185AF3D50D3141AE78EF9D1532836AF8A548577C4C8DA81CF18806D>
- Anon., n.d. *Molecular Imaging: A Promising Tool to Monitor Islet Transplantation*. [Online] Available at: <https://www.ncbi.nlm.nih.gov/pmc/articles/PMC3195545/>
- Anon., n.d. *The Journal of Clinical Investigation*.
- Ansary, T. M., Nakano, D. & Nishiyama, A., 2019. *Diuretic effects of sodium glucose cotransporter 2 inhibitors and their influence on the renin-angiotensin system*. s.l.:MDPI AG.
- Arifin, D. R. & Bulte, J. W., 2011. *Imaging of pancreatic islet cells*. s.l.:NIH Public Access.
- Arrojo e Drigo, R. et al., 2019. Structural basis for delta cell paracrine regulation in pancreatic islets. *Nature Communications*, 1 12, 10(1), pp. 1-12.
- Aslamy, A. & Thurmond, D. C., 2017. *Exocytosis proteins as novel targets for diabetes prevention and/or remediation?*. s.l.:American Physiological Society.
- Aspinwall, C. A. et al., 2000. Roles of insulin receptor substrate-1, phosphatidylinositol 3-kinase, and release of intracellular Ca²⁺ stores in insulin-stimulated insulin secretion in β -cells. *Journal of Biological Chemistry*, 21 7, 275(29), pp. 22331-22338.
- Association, A. D., 2010. *Diagnosis and classification of diabetes mellitus*. s.l.:American Diabetes Association.

Augustin, R., 2010. The protein family of glucose transport facilitators: It's not only about glucose after all. *IUBMB Life*, 15, 62(5), pp. NA-NA.

Ayala, J. E. et al., 2010. *Standard operating procedures for describing and performing metabolic tests of glucose homeostasis in mice*. s.l.:s.n.

Azuma, K. et al., 2014. Association of PD-L1 overexpression with activating EGFR mutations in surgically resected nonsmall-cell lung cancer.. *Annals of oncology : official journal of the European Society for Medical Oncology*, 10, 25(10), pp. 1935-40.

Bader, E. et al., 2016. Identification of proliferative and mature β -cells in the islets of langerhans. *Nature*, 535(7612), pp. 430-434.

Baetens, D., Malaisse-Lagae, F., Perrelet, A. & Orci, L., 1979. Endocrine pancreas: Three-dimensional reconstruction shows two types of islets of Langerhans. *Science*, 14 12, 206(4424), pp. 1323-1325.

Ballian, N. & Brunnicardi, F. C., 2007. *Islet vasculature as a regulator of endocrine pancreas function*. s.l., Springer, pp. 705-714.

Bamgbade, O. A., Rutter, T. W., Nafiu, O. O. & Dorje, P., 2007. Postoperative complications in obese and nonobese patients. *World Journal of Surgery*, 29 3, 31(3), pp. 556-560.

Barak, Y. et al., 1999. PPAR γ is required for placental, cardiac, and adipose tissue development. *Molecular Cell*, 4(4), pp. 585-595.

Barg, S. et al., 2001. Fast exocytosis with few Ca²⁺ channels in insulin-secreting mouse pancreatic B cells. *Biophysical Journal*, 81(6), pp. 3308-3323.

Baron, A. D., Schaeffer, L., Shragg, P. & Kolterman, O. G., 1987. Role of hyperglucagonemia in maintenance of increased rates of hepatic glucose output in type II diabetics. *Diabetes*, 36(3), pp. 274-283.

Bartholomeus, K. et al., 2013. Omentum is better site than kidney capsule for growth, differentiation, and vascularization of immature porcine β -cell implants in immunodeficient rats. *Transplantation*, 27 12, 96(12), pp. 1026-1033.

Basco, D. et al., 2018. α -cell glucokinase suppresses glucose-regulated glucagon secretion. *Nature Communications*, 1 12.9(1).

Batterham, R. L. et al., 2002. Gut hormone PYY₃₋₃₆ physiologically inhibits food intake. *Nature*, 8 8, 418(6898), pp. 650-654.

Beck, J. et al., n.d. Islet Encapsulation: Strategies to Enhance Islet Cell Functions.

Bélanger, P., Couturier, K., Latour, M. G. & Lavoie, J. M., 2000. Effects of supranormal liver glycogen content on hyperglucagonemia-induced liver glycogen breakdown. *European Journal of Applied Physiology*, 83(4-5), pp. 328-335.

Bennett, B. C. et al., 2016. An electrostatic mechanism for Ca²⁺-mediated regulation of gap junction channels. *Nature Communications*, 12 1. Volume 7.

- Benninger, R. K. et al., 2011. Gap junctions and other mechanisms of cell-cell communication regulate basal insulin secretion in the pancreatic islet. *Journal of Physiology*, 15 11, 589(22), pp. 5453-5466.
- Benninger, R. K. & Hodson, D. J., 2018. New understanding of β -cell heterogeneity and in situ islet function. *Diabetes*, 1 4, 67(4), pp. 537-547.
- Benninger, R. K. & Piston, D. W., 2014. *Cellular communication and heterogeneity in pancreatic islet insulin secretion dynamics*. s.l.:Elsevier Inc..
- Benninger, R. K. et al., 2008. Gap junction coupling and calcium waves in the pancreatic islet. *Biophysical Journal*, 1 12, 95(11), pp. 5048-5061.
- Bensellam, M., Jonas, J. C. & Laybutt, D. R., 2018. *Mechanisms of β -cell dedifferentiation in diabetes: Recent findings and future research directions*. s.l.:BioScientifica Ltd..
- Berglund, E. D. et al., 2008. Glucose metabolism in vivo in four commonly used inbred mouse strains. *Diabetes*, 7, 57(7), pp. 1790-1799.
- Bergsten, P., 1995. Slow and fast oscillations of cytoplasmic Ca^{2+} in pancreatic islets correspond to pulsatile insulin release.. *The American journal of physiology*, 2, 268(2 Pt 1), pp. E282-7.
- Bergsten, P. et al., 1994. Synchronous oscillations of cytoplasmic Ca^{2+} and insulin release in glucose-stimulated pancreatic islets. *Journal of Biological Chemistry*, 25 3, 269(12), pp. 8749-8753.
- Bertelli, E. & Bendayan, M., 2005. Association between endocrine pancreas and ductal system. More than an epiphenomenon of endocrine differentiation and development?. *The journal of histochemistry and cytochemistry : official journal of the Histochemistry Society*, 27 9, 53(9), pp. 1071-86.
- Berthoud, H. R. & Powley, T. L., 1990. Identification of vagal preganglionics that mediate cephalic phase insulin response. *American Journal of Physiology - Regulatory Integrative and Comparative Physiology*, 258(2 27-2).
- Bertram, R. et al., 2000. The phantom burster model for pancreatic β -cells. *Biophysical Journal*, 79(6), pp. 2880-2892.
- Bertram, R., Satin, L. S. & Sherman, A. S., 2018. Closing in on the mechanisms of pulsatile insulin secretion. *Diabetes*, 1 3, 67(3), pp. 351-359.
- Bertram, R., Sherman, A. & Satin, L. S., 2007. *Metabolic and electrical oscillations: Partners in controlling pulsatile insulin secretion*. s.l.:American Physiological Society.
- Betz, C., Lenard, A., Belting, H. G. & Affolter, M., 2016. *Cell behaviors and dynamics during angiogenesis*. s.l.:Company of Biologists Ltd.
- Bishop, A. E. et al., 1980. The location of VIP in the pancreas of man and rat. *Diabetologia*, 1, 18(1), pp. 73-78.

Blackman, B., 1961. The use of glucagon in insulin coma therapy. *The Psychiatric Quarterly*, 9, 35(3), pp. 482-487.

Boden, G., 2003. *Effects of free fatty acids (FFA) on glucose metabolism: Significance for insulin resistance and type 2 diabetes*. s.l.:s.n.

Boden, G., Chen, X. & Polansky, M., 1999. Disruption of circadian insulin secretion is associated with reduced glucose uptake in first-degree relatives of patients with type 2 diabetes. *Diabetes*, 1 11, 48(11), pp. 2182-2188.

Bogorad, M. I. et al., 2015. *Review: In vitro microvessel models*. s.l.:Royal Society of Chemistry.

Bonner-Weir, S., 1988. Morphological Evidence for Pancreatic Polarity of β -Cell Within Islets of Langerhans. *Diabetes*, 1 5, 37(5), pp. 616-621.

Bosco, D. et al., 2010. Unique arrangement of α - and β -cells in human islets of Langerhans. *Diabetes*, 5, 59(5), pp. 1202-1210.

Bowe, J. E. et al., 2014. Assessing glucose homeostasis in rodent models. *Journal of Endocrinology*, 9, 222(3), pp. 13-25.

Bratusch-Marrain, P. R., Komjati, M. & Waldhausl, W. K., 1986. Efficacy of pulsatile versus continuous insulin administration on hepatic glucose production and glucose utilization in type I diabetic humans. *Diabetes*, 8, 35(8), pp. 922-926.

Braun, M., Ramracheya, R. & Rorsman, P., 2012. Autocrine regulation of insulin secretion. *Diabetes, Obesity and Metabolism*, 10, 14(SUPPL.3), pp. 143-151.

Briant, L. R. T. S. I. M. C. R. B. a. R. P., 2017. δ -cells and β -cells are electrically coupled and regulate α -cell activity via somatostatin. *The Journal of Physiology*, 596((2)), pp. pp.197-215.

Brissova, M. et al., 2005. Assessment of human pancreatic islet architecture and composition by laser scanning confocal microscopy. *The journal of histochemistry and cytochemistry : official journal of the Histochemistry Society*, 27 9, 53(9), pp. 1087-97.

Brissova, M. et al., 2004. Intra-islet Endothelial Cells Contribute to Revascularization of Transplanted Pancreatic Islets. *Diabetes*, 5, 53(5), pp. 1318-1325.

Brissova, M. et al., 2015. Human Islets Have Fewer Blood Vessels than Mouse Islets and the Density of Islet Vascular Structures Is Increased in Type 2 Diabetes. *Journal of Histochemistry and Cytochemistry*, 29 8, 63(8), pp. 637-645.

Brom, M. et al., 2014. Non-invasive quantification of the beta cell mass by SPECT with ¹¹¹In-labelled exendin. *Diabetologia*, 1 2, 57(5), pp. 950-959.

Brunnicardi, F. C. et al., n.d. *Perspectives in Diabetes Microcirculation of the Islets of Langerhans Long Beach Veterans Administration Regional Medical Education Center Symposium*, s.l.: s.n.

Burant, C. F. et al., 1997. Troglitazone action is independent of adipose tissue. *Journal of Clinical Investigation*, 1 12, 100(11), pp. 2900-2908.

- Butler, A. E. et al., 2003. β -cell deficit and increased β -cell apoptosis in humans with type 2 diabetes. *Diabetes*, 1 1, 52(1), pp. 102-110.
- Canzano, J. S. et al., 2019. Islet Microvasculature Alterations With Loss of Beta-cells in Patients With Type 1 Diabetes. *Journal of Histochemistry & Cytochemistry*, 17 1, 67(1), pp. 41-52.
- Cao, L., Kobayakawa, S., Yoshiki, A. & Abe, K., 2012. High resolution intravital imaging of subcellular structures of mouse abdominal organs using a microstage device. *PLoS ONE*, 27 3.7(3).
- Capey, S., 2007. Isoflurane. In: *xPharm: The Comprehensive Pharmacology Reference*. s.l.:Elsevier Inc., pp. 1-4.
- Capozzi, M. E. et al., 2019. β Cell tone is defined by proglucagon peptides through cAMP signaling. *JCI insight*, 7 3.4(5).
- Capozzi, M. E. et al., 2019. Glucagon lowers glycemia when β cells are active. *JCI Insight*, 22 8.4(16).
- Carlsson, P. O., Jansson, L., Östenson, C. G. & Källskog, Ö., 1997. Islet capillary blood pressure increase mediated by hyperglycemia in NIDDM GK rats. *Diabetes*, 6, 46(6), pp. 947-952.
- Carlsson, P. O., Palm, F., Andersson, A. & Liss, P., 2001. Markedly decreased oxygen tension in transplanted rat pancreatic islets irrespective of the implantation site. *Diabetes*, 1 3, 50(3), pp. 489-495.
- Case, R. M., 2006. Is the rat pancreas an appropriate model of the human pancreas?. *Pancreatology*, 1 7, 6(3), pp. 180-190.
- Cernea, S. & Dobreanu, M., 2013. *Diabetes and beta cell function: From mechanisms to evaluation and clinical implications*. s.l.:Croatian Society for Medical Biochemistry and Laboratory Medicine.
- Chen, C. et al., 2016. Alterations in β -cell calcium dynamics and efficacy outweigh islet mass adaptation in compensation of insulin resistance and prediabetes onset. *Diabetes*, 1 9, 65(9), pp. 2676-2685.
- Cherrington, A. D., 2010. Glucagon Physiology. *Canadian Journal of Diabetes*, 24 1, 34(3), pp. 187-188.
- Chiu, Y. C. et al., 2012. 3-D imaging and illustration of the perfusive mouse islet sympathetic innervation and its remodelling in injury. *Diabetologia*, 30 12, 55(12), pp. 3252-3261.
- Chow, C. C., Tsang, L. W., Sorensen, J. P. & Cockram, C. S., 1995. Comparison of insulin with or without continuation of oral hypoglycemic agents in the treatment of secondary failure in NIDDM patients. *Diabetes Care*, 1 3, 18(3), pp. 307-314.
- Christoffersson, G. et al., 2010. Clinical and experimental pancreatic islet transplantation to striated muscle: Establishment of a vascular system similar to that in native islets. *Diabetes*, 10, 59(10), pp. 2569-2578.
- Civelek, V. N. et al., 1996. Temporal sequence of metabolic and ionic events in glucose-stimulated clonal pancreatic β -cells (HIT). *Biochemical Journal*, 1 5, 315(3), pp. 1015-1019.

- Cnop, M. et al., 2002. The concurrent accumulation of intra-abdominal and subcutaneous fat explains the association between insulin resistance and plasma leptin concentrations: Distinct metabolic effects of two fat compartments. *Diabetes*, 51(4), pp. 1005-1015.
- Coca-Prados, M., 2014. The blood-aqueous barrier in health and disease. *Journal of Glaucoma*, 10 12, 23(8), pp. S36-S38.
- Cohrs, C. M. et al., 2017. Vessel network architecture of adult human islets promotes distinct cell-cell interactions in situ and is altered after transplantation. *Endocrinology*, 15, 158(5), pp. 1373-1385.
- Colberg, S. R. et al., 2016. *Physical activity/exercise and diabetes: A position statement of the American Diabetes Association*. s.l.:American Diabetes Association Inc..
- Collins, S. C. et al., 2010. Progression of Diet-Induced Diabetes in C57BL6J Mice Involves Functional Dissociation of Ca²⁺ Channels From Secretory Vesicles.
- Craig, L. E., Spelman, J. P., Strandberg, J. D. & Zink, M. C., 1998. Endothelial cells from diverse tissues exhibit differences in growth and morphology. *Microvascular Research*, 1 1, 55(1), pp. 65-76.
- Crofford, O. B., Genuth, S. & Baker, L., 1987. Diabetes Control and Complications Trial (DCCT): Results of feasibility study. *Diabetes Care*, 1 1, 10(1), pp. 1-19.
- Cryer, P. E., 2012. *Minireview: Glucagon in the pathogenesis of hypoglycemia and hyperglycemia in diabetes*. s.l.:s.n.
- Cypess, A. M., Unson, C. G., Wu, C. R. & Sakmar, T. P., 1999. Two cytoplasmic loops of the glucagon receptor are required to elevate cAMP or intracellular calcium. *Journal of Biological Chemistry*, 2 7, 274(27), pp. 19455-19464.
- Dai, C. et al., 2013. Pancreatic islet vasculature adapts to insulin resistance through dilation and not angiogenesis. *Diabetes*, 12, 62(12), pp. 4144-4153.
- Dakin, C. L. et al., 2001. Oxyntomodulin inhibits food intake in the rat. *Endocrinology*, 10, 142(10), pp. 4244-4250.
- D'Alessio, D., 2011. The role of dysregulated glucagon secretion in type 2 diabetes. *Diabetes, Obesity and Metabolism*, 10, 13(SUPPL. 1), pp. 126-132.
- Day, J. W. et al., 2009. A new glucagon and GLP-1 co-agonist eliminates obesity in rodents. *Nature Chemical Biology*, 10, 5(10), pp. 749-757.
- De Vos, A. et al., n.d. *Rapid Publication Human and Rat Beta Cells Differ in Glucose Transporter but Not in Glucokinase Gene Expression*, s.l.: s.n.
- DeFronzo, R. A., 2010. *Insulin resistance, lipotoxicity, type 2 diabetes and atherosclerosis: The missing links. The Claude Bernard Lecture 2009*. s.l.:Springer Verlag.
- DeFronzo, R. A., Tobin, J. D. & Andres, R., 1979. Glucose clamp technique: A method for quantifying insulin secretion and resistance. *American Journal of Physiology Endocrinology Metabolism and Gastrointestinal Physiology*, 6(3).

- Deng, S. et al., 2004. Structural and Functional Abnormalities in the Islets Isolated from Type 2 Diabetic Subjects. *Diabetes*, 13, 53(3), pp. 624-632.
- Deng, W. et al., 2003. Adenoviral gene transfer of eNOS: High-level expression in ex vivo expanded marrow stromal cells. *American Journal of Physiology - Cell Physiology*, 11, 285(5 54-5), pp. C1322-9.
- Desborough, J. P. et al., 1993. Isoflurane inhibits insulin secretion from isolated rat pancreatic islets of Langerhans. *British journal of anaesthesia*, 12, 71(6), pp. 873-6.
- Diez, J. A. et al., 2017. Pancreatic Islet Blood Flow Dynamics in Primates. *Cell Reports*, 8 8, 20(6), pp. 1490-1501.
- DiMeglio, L. A., Evans-Molina, C. & Oram, R. A., 2018. *Type 1 diabetes*. s.l.:Lancet Publishing Group.
- DM, N. et al., 1993. The Effect of Intensive Treatment of Diabetes on the Development and Progression of Long-Term Complications in Insulin-Dependent Diabetes Mellitus. *New England Journal of Medicine*, 30 9, 329(14), pp. 977-986.
- Dobbins, R. L. et al., 1998. A fatty acid-dependent step is critically important for both glucose- and non-glucose-stimulated insulin secretion. *Journal of Clinical Investigation*, 1 6, 101(11), pp. 2370-2376.
- Dolenšek, J., Slak Rupnik, M. & Stožer, A., 2015. Structural similarities and differences between the human and the mouse pancreas.
- Dolenšek, J., Rupnik, M. S. & Stožer, A., 2015. *Structural similarities and differences between the human and the mouse pancreas*. s.l.:Taylor and Francis Inc..
- Dolenšek, J. et al., 2013. The Relationship between Membrane Potential and Calcium Dynamics in Glucose-Stimulated Beta Cell Syncytium in Acute Mouse Pancreas Tissue Slices. *PLoS ONE*, 6 12, 8(12), p. e82374.
- Dominguez-Gutierrez, G., Xin, Y. & Gromada, J., 2019. *Heterogeneity of human pancreatic β -cells*. s.l.:Elsevier GmbH.
- Donath, M. Y. et al., 2005. Mechanisms of beta-cell death in type 2 diabetes. *Diabetes*, 12, Volume 54 Suppl 2, pp. S108-13.
- Dorrell, C. et al., 2016. Human islets contain four distinct subtypes of β cells. *Nature Communications*, 11 7, Volume 7, p. 11756.
- Drucker, D. J., Habener, J. F. & Holst, J. J., 2017. *Discovery, characterization, and clinical development of the glucagon-like peptides*. s.l.:American Society for Clinical Investigation.
- Duca, F. A. et al., 2015. Metformin activates a duodenal Ampk-dependent pathway to lower hepatic glucose production in rats. *Nature Medicine*, 1 5, 21(5), pp. 506-511.
- Dutchak, P. A. et al., 2012. Fibroblast growth factor-21 regulates PPAR γ activity and the antidiabetic actions of thiazolidinediones. *Cell*, 3 2, 148(3), pp. 556-567.

- Dwulet, J. et al., 2019. How heterogeneity in glucokinase and gap junction coupling determines the islet electrical response. *Biophysical Journal*, 8 7.p. 696096.
- Eich, T., Eriksson, O. & Lundgren, T., 2007. Visualization of Early Engraftment in Clinical Islet Transplantation by Positron-Emission Tomography. *New England Journal of Medicine*, 28 6, 356(26), pp. 2754-2755.
- Elizondo, D. M. et al., 2020. Pancreatic islets seeded in a novel bioscaffold forms an organoid to rescue insulin production and reverse hyperglycemia in models of type 1 diabetes. *Scientific Reports*, 1 12, 10(1), pp. 1-11.
- El, K. & Campbell, J. E., 2019. *The role of GIP in α -cells and glucagon secretion*. s.l.:Elsevier Inc..
- Ellenbroek, J. H. et al., 2013. Topologically Heterogeneous Beta Cell Adaptation in Response to High-Fat Diet in Mice.
- Eriksson, J. et al., 1989. Early Metabolic Defects in Persons at Increased Risk for Non-Insulin-Dependent Diabetes Mellitus. *New England Journal of Medicine*, 10 8, 321(6), pp. 337-343.
- Eriksson, J. W. et al., 2016. Sulphonylurea compared to DPP-4 inhibitors in combination with metformin carries increased risk of severe hypoglycemia, cardiovascular events, and all-cause mortality. *Diabetes Research and Clinical Practice*, 1 7, Volume 117, pp. 39-47.
- Eriksson, O. et al., 2014. On the use of [18F]DOPA as an imaging biomarker for transplanted islet mass. *Annals of Nuclear Medicine*, 29 1, 28(1), pp. 47-52.
- Ernst, S. et al., 2011. Mechanisms in the adaptation of maternal β -cells during pregnancy. *Diabetes Management*, 3, 1(2), pp. 239-248.
- Evron, Y. et al., 2018. Long-term viability and function of transplanted islets macroencapsulated at high density are achieved by enhanced oxygen supply. *Scientific Reports*, 1 12, 8(1), pp. 1-13.
- F Carvalho, C. P. et al., 2012. Impaired-cell-cell coupling mediated by Cx36 gap junctions in prediabetic mice. *Am J Physiol Endocrinol Metab*, Volume 303, pp. 144-151.
- Fagerholm, V. et al., 2010. Assessment of islet specificity of dihydrotetrabenazine radiotracer binding in rat pancreas and human pancreas. *Journal of Nuclear Medicine*, 9, 51(9), pp. 1439-1446.
- Fang, L., Karakiulakis, G. & Roth, M., 2020. Are patients with hypertension and diabetes mellitus at increased risk for COVID-19 infection?.
- Farnsworth, N. L., Hemmati, A., Pozzoli, M. & Benninger, R. K., 2014. Fluorescence recovery after photobleaching reveals regulation and distribution of connexin36 gap junction coupling within mouse islets of Langerhans. *Journal of Physiology*, 15 10, 592(20), pp. 4431-4446.
- Fendler, B., Zhang, M., Satin, L. & Bertram, R., 2009. Synchronization of pancreatic islet oscillations by intrapancreatic ganglia: A modeling study. *Biophysical Journal*, 97(3), pp. 722-729.

- Fernandez-Alvarez, J. et al., 1994. Enzymatic, metabolic and secretory patterns in human islets of Type 2 (non-insulin-dependent) diabetic patients. *Diabetologia: Clinical and Experimental Diabetes and Metabolism*, 37(2), pp. 177-181.
- Ferrannini, E. & Solini, A., 2012. SGLT2 inhibition in diabetes mellitus: rationale and clinical prospects. *Nature Reviews Endocrinology*, Volume 8, pp. 495-502.
- Ferrannini, E., Veltkamp, S. A. & Smulders, R. A., 2013. Renal Glucose Handling Impact of chronic kidney disease and sodium-glucose cotransporter 2 inhibition in patients with type 2 diabetes.
- Fiaschi-Taesch, N. M. et al., 2008. Hepatocyte growth factor enhances engraftment and function of nonhuman primate islets. *Diabetes*, 1 10, 57(10), pp. 2745-2754.
- Filippatos, T. D., Panagiotopoulou, T. V. & Elisaf, M. S., 2014. *Adverse Effects of GLP-1 Receptor Agonists*. s.l.:Society for Biomedical Diabetes Research.
- Finan, B., Capozzi, M. E. & Campbell, J. E., 2020. Repositioning glucagon action in the physiology and pharmacology of diabetes. *Diabetes*, 1 4, 69(4), pp. 532-541.
- Fong, D. S. et al., 2003. *Diabetic retinopathy*. s.l.:American Diabetes Association Inc..
- Freedman, R. et al., 1992. Initial studies of embryonic transplants of human hippocampus and cerebral cortex derived from schizophrenic women. *Biological Psychiatry*, 15 12, 32(12), pp. 1148-1163.
- Frisk, G. & Diderholm, H., 2000. *Tissue Culture of Isolated Human Pancreatic Islets Infected with Different Strains of Coxsackievirus B4: Assessment of Virus Replication and Effects on Islet Morphology and Insulin Release*, s.l.: s.n.
- Fu, Z., R. Gilbert, E. & Liu, D., 2012. Regulation of Insulin Synthesis and Secretion and Pancreatic Beta-Cell Dysfunction in Diabetes. *Current Diabetes Reviews*, 19 12, 9(1), pp. 25-53.
- Gale, E. A., 2002. *The rise of childhood type 1 diabetes in the 20th century*. s.l.:American Diabetes Association Inc..
- Gallichan, W. S. et al., 1998. Lentivirus-mediated transduction of islet grafts with interleukin 4 results in sustained gene expression and protection from insulinitis. *Human Gene Therapy*, 10 12, 9(18), pp. 2717-2726.
- Galsgaard, K. D. et al., 2019. *Glucagon receptor signaling and lipid metabolism*. s.l.:Frontiers Media S.A..
- Gan, M. J., Albanese-O'Neill, A. & Haller, M. J., 2012. Type 1 diabetes: Current concepts in epidemiology, pathophysiology, clinical care, and research. *Current Problems in Pediatric and Adolescent Health Care*, 1 11, 42(10), pp. 269-291.
- Gao, T. et al., 2014. Pdx1 maintains β cell identity and function by repressing an α cell program. *Cell Metabolism*, 4 2, 19(2), pp. 259-271.

- Gelling, R. W. et al., 2003. Lower blood glucose, hyperglucagonemia, and pancreatic α cell hyperplasia in glucagon receptor knockout mice. *Proceedings of the National Academy of Sciences of the United States of America*, 4 2, 100(3), pp. 1438-1443.
- Gerich, J. E., 2010. Role of the kidney in normal glucose homeostasis and in the hyperglycaemia of diabetes mellitus: therapeutic implications. *Diabet. Med*, Volume 27, pp. 136-142.
- Gill, G. V., Lucas, S. & Kent, L. A., 1996. Prevalence and characteristics of brittle diabetes in Britain.. *QJM : monthly journal of the Association of Physicians*, 11, 89(11), pp. 839-43.
- Gilon, P., Chae, H. Y., Rutter, G. A. & Ravier, M. A., 2014. *Calcium signaling in pancreatic β -cells in health and in Type 2 diabetes*. s.l.:Churchill Livingstone.
- Gilon, P., Shepherd, R. M. & Henquin, J. C., 1993. Oscillations of secretion driven by oscillations of cytoplasmic Ca^{2+} as evidenced in single pancreatic islets. *Journal of Biological Chemistry*, 268(30), pp. 22265-22268.
- Giordano, E., Bosco, D., Cirulli, V. & Meda, P., 1991. Repeated glucose stimulation reveals distinct and lasting secretion patterns of individual rat pancreatic B cells. *Journal of Clinical Investigation*, 87(6), pp. 2178-2185.
- Girard, J., 2017. *Glucagon, a key factor in the pathophysiology of type 2 diabetes*. s.l.:Elsevier B.V..
- Giuliani, M. et al., 2005. *Central Necrosis in Isolated Hypoxic Human Pancreatic Islets: Evidence for Postisolation Ischemia*, s.l.: s.n.
- Góes, R. M., Barbosa, F. L., De Faria-e-sousa, S. J. & Haddad, A., 2008. Morphological and Autoradiographic Studies on the Corneal and Limbal Epithelium of Rabbits. *The Anatomical Record: Advances in Integrative Anatomy and Evolutionary Biology*, 1 2, 291(2), pp. 191-203.
- Goldman, C. K. et al., 1993. Epidermal growth factor stimulates vascular endothelial growth factor production by human malignant glioma cells: A model of glioblastoma multiforme pathophysiology. *Molecular Biology of the Cell*, 4(1), pp. 121-133.
- Goldstein, D. E. et al., 2004. *Tests of Glycemia in Diabetes*, s.l.: s.n.
- Golocheikine, A. et al., 2010. Cooperative signaling for angiogenesis and neovascularization by VEGF and HGF following islet transplantation. *Transplantation*, 15 10, 90(7), pp. 725-731.
- Goodner, C. J., Sweet, I. R. & Courtenay Harrison, H., 1988. Rapid reduction and return of surface insulin receptors after exposure to brief pulses of insulin in perfused rat hepatocytes. *Diabetes*, 1 10, 37(10), pp. 1316-1323.
- Goodwin, A. M., 2007. *In vitro assays of angiogenesis for assessment of angiogenic and anti-angiogenic agents*. s.l.:NIH Public Access.
- Gosak, M. et al., 2017. Critical and supercritical spatiotemporal calcium dynamics in beta cells. *Frontiers in Physiology*, 22 12.8(DEC).

- Gosmain, Y. et al., 2012. Pax6 is crucial for β -cell function, insulin biosynthesis, and glucose-induced insulin secretion. *Molecular Endocrinology*, 14, 26(4), pp. 696-709.
- Graham, T., 2005. Serum retinol binding protein 4 contributes to insulin resistance in obesity and type 2 diabetes CHIP-seq motif analysis View project Retinol Binding Protein 4 Biology View project.
- Graham, T., Mody, N. & Preitner, F., 2005. Serum retinol binding protein 4 contributes to insulin resistance in obesity and type 2 diabetes CHIP-seq motif analysis View project Retinol Binding Protein 4 Biology View project.
- Gram, D. X. et al., 2007. Capsaicin-sensitive sensory fibers in the islets of Langerhans contribute to defective insulin secretion in Zucker diabetic rat, an animal model for some aspects of human type 2 diabetes. *European Journal of Neuroscience*, 19, 25(1), pp. 213-223.
- Granger, C. W. J., 1969. *Investigating Causal Relations by Econometric Models and Cross-spectral Methods*, s.l.: s.n.
- Grodsky, G. M. & Bennett, L. L., 1966. Cation requirements for insulin secretion in the isolated perfused pancreas. *Diabetes*, 15, 15(12), pp. 910-913.
- Gross, J. L. et al., 2005. *Diabetic nephropathy: Diagnosis, prevention, and treatment*. s.l.:American Diabetes Association.
- Gutierrez, G. D., Gromada, J. & Sussel, L., 2017. Heterogeneity of the Pancreatic Beta Cell. *Frontiers in Genetics*, 8, 8(MAR), p. 22.
- Gylfe, E., 2016. *Glucose control of glucagon secretion—‘There’s a brand-new gimmick every year’*. s.l.:Taylor and Francis Ltd.
- Habener, J. F. & Stanojevic, V., 2013. *Alpha cells come of age*. s.l.:s.n.
- Halban, P. A. et al., 2014. β -Cell failure in type 2 diabetes: Postulated mechanisms and prospects for prevention and treatment. *Journal of Clinical Endocrinology and Metabolism*, 94(6), pp. 1983-1992.
- Hancock, A. S. et al., 2010. Glucagon deficiency reduces hepatic glucose production and improves glucose tolerance in adult mice. *Molecular Endocrinology*, 24, 24(8), pp. 1605-1614.
- Hart, N. J. & Powers, A. C., 2019. *Use of human islets to understand islet biology and diabetes: progress, challenges and suggestions*. s.l.:Springer Verlag.
- Hathout, E. et al., 2009. In vivo imaging demonstrates a time-line for new vessel formation in islet transplantation. *Pediatric Transplantation*, 11, 13(7), pp. 892-897.
- Hauge-Evans, A. C. et al., 2009. Somatostatin secreted by islet δ -cells fulfills multiple roles as a paracrine regulator of islet function. *Diabetes*, 58, 58(2), pp. 403-411.
- Hauner, H., 2002. The mode of action of thiazolidinediones. *Diabetes/Metabolism Research and Reviews*, 18(SUPPL. 2).

- Hayden, M. R. et al., 2008. *Attenuation of endocrine-exocrine pancreatic communication in type 2 diabetes: pancreatic extracellular matrix ultrastructural abnormalities*. s.l.:NIH Public Access.
- Hayreh, S. S., 2006. *Orbital vascular anatomy*. s.l., Nature Publishing Group, pp. 1130-1144.
- Hayreh, S. S. & Edwards, J., 1971. Ophthalmic arterial and venous pressures effects of acute intracranial hypertension. *British Journal of Ophthalmology*, 55(10), pp. 649-663.
- Haythorne, E. et al., 2019. Diabetes causes marked inhibition of mitochondrial metabolism in pancreatic β -cells. *Nature Communications*, 10(1), pp. 1-17.
- Head, W. S. et al., 2012. Connexin-36 Gap Junctions Regulate In Vivo First-and Second-Phase Insulin Secretion Dynamics and Glucose Tolerance in the Conscious Mouse. *Diabetes*, Volume 61, pp. 1700-1707.
- Hellman, B., Dansk, H. & Grapengiesser, E., 2004. Pancreatic β -cells communicate via intermittent release of ATP. *American Journal of Physiology-Endocrinology and Metabolism*, 5, 286(5), pp. E759-E765.
- Henderson, S. J. et al., 2016. Robust anti-obesity and metabolic effects of a dual GLP-1/glucagon receptor peptide agonist in rodents and non-human primates. *Diabetes, Obesity and Metabolism*, 18(12), pp. 1176-1190.
- Henquin, J.-C., 2000. *Perspectives in Diabetes Triggering and Amplifying Pathways of Regulation of Insulin Secretion by Glucose*, s.l.: s.n.
- Henquin, J. C., 1992. *The fiftieth anniversary of hypoglycaemic sulphonamides. How did the mother compound work?*. s.l.:Springer-Verlag.
- Henquin, J. C., 2012. *Do pancreatic β cells "taste" nutrients to secrete insulin?*. s.l.:s.n.
- Hevener, A. L. et al., 2007. Macrophage PPAR γ is required for normal skeletal muscle and hepatic insulin sensitivity and full antidiabetic effects of thiazolidinediones. *Journal of Clinical Investigation*, 117(6), pp. 1658-1669.
- Hex, N. et al., 2012. Estimating the current and future costs of Type1 and Type2 diabetes in the UK, including direct health costs and indirect societal and productivity costs. *Diabetic Medicine*, 7, 29(7), pp. 855-862.
- Hodson, D. J. et al., 2013. Lipotoxicity disrupts incretin-regulated human β cell connectivity. *Journal of Clinical Investigation*, 123(10), pp. 4182-4194.
- Hodson, D. J. et al., 2010. *Investigating and Modelling Pituitary Endocrine Network Function*. s.l.:s.n.
- Hodson, D. J. et al., 2012. Existence of long-lasting experience-dependent plasticity in endocrine cell networks. *Nature Communications*, 3(1), pp. 1-10.
- Holst, J. J., 2007. *The physiology of glucagon-like peptide 1*. s.l.:American Physiological Society.

- Holz, G. G., 2004. *Epac: A New cAMP-Binding Protein in Support of Glucagon-like Peptide-1 Receptor-Mediated Signal Transduction in the Pancreatic β -Cell*. s.l.:s.n.
- Hoppa, M. B. et al., 2009. Chronic Palmitate Exposure Inhibits Insulin Secretion by Dissociation of Ca^{2+} Channels from Secretory Granules. *Cell Metabolism*, 12, 10(6), pp. 455-465.
- Hovorka, R. et al., 2014. Overnight closed-loop insulin delivery in young people with type 1 diabetes: A free-living, randomized clinical trial. *Diabetes Care*, 37(5), pp. 1204-1211.
- Huypens, P., Ling, Z., Pipeleers, D. & Schuit, F., 2000. Glucagon receptors on human islet cells contribute to glucose competence of insulin release. *Diabetologia*, 43(8), pp. 1012-1019.
- Idevall-Hagren, O. & Tengholm, A., 2020. *Metabolic regulation of calcium signaling in beta cells*. s.l.:Elsevier Ltd.
- Ilegems, E. et al., 2013. Reporter islets in the eye reveal the plasticity of the endocrine pancreas. *Proceedings of the National Academy of Sciences of the United States of America*, 110(51), pp. 20581-20586.
- Isaji, M., 2007. *Sodium-glucose cotransporter inhibitors for diabetes*. s.l.:s.n.
- Isomaa, B. O. et al., n.d. *Cardiovascular Morbidity and Mortality Associated With the Metabolic Syndrome*, s.l.: s.n.
- Itoh, T. et al., 2017. The spleen is an ideal site for inducing transplanted islet graft expansion in mice. *PLoS ONE*, 12(1), pp. 1-12.
- Itoh, Y. et al., 2003. Free fatty acids regulate insulin secretion from pancreatic β cells through GPR40. *Nature*, 422(6928), pp. 173-176.
- Jackson, C. J. & Nguyen, M., 1997. Human microvascular endothelial cells differ from macrovascular endothelial cells in their expression of matrix metalloproteinases. *International Journal of Biochemistry and Cell Biology*, 10(10), pp. 1167-1177.
- Jacobowitz, D. & Laties, A. M., 1970. Adrenergic reinnervation of the cat ovary transplanted to the anterior chamber of the eye. *Endocrinology*, 86(4), pp. 921-924.
- James Shapiro, A. M., 2012. *Islet transplantation in type 1 diabetes: Ongoing challenges, refined procedures, and long-term outcome*. s.l.:s.n.
- Jampol, L. M. et al., 1988. Hyperbaric and transcorneal delivery of oxygen to the rabbit and monkey anterior segment. *Archives of Ophthalmology*, 106(6), pp. 825-829.
- Janah, L. et al., 2019. *Molecular Sciences Glucagon Receptor Signaling and Glucagon Resistance*.
- Janssen, M. M., Snoek, F. J. & Heine, R. J., 2000. Assessing impaired hypoglycemia awareness in type 1 diabetes: Agreement of self-report but not of field study data with the autonomic symptom threshold during experimental hypoglycemia. *Diabetes Care*, 23(4), pp. 529-532.
- Jansson, L. et al., 2016. *Pancreatic islet blood flow and its measurement*. s.l.:Taylor and Francis Ltd.

- Jansson, L. & Hellerström, C., 1983. Stimulation by glucose of the blood flow to the pancreatic islets of the rat. *Diabetologia*, 7, 25(1), pp. 45-50.
- Jaworski, J. et al., 2003. Inducible cAMP early repressor, an endogenous antagonist of cAMP responsive element-binding protein, evokes neuronal apoptosis in vitro. *Journal of Neuroscience*, 16, 23(11), pp. 4519-4526.
- Johansson, H. et al., 2005. Tissue factor produced by the endocrine cells of the islets of langerhans is associated with a negative outcome of clinical islet transplantation. *Diabetes*, 16, 54(6), pp. 1755-1762.
- Johnston, N. R. et al., 2016. Beta Cell Hubs Dictate Pancreatic Islet Responses to Glucose. *Cell Metabolism*, 13, 24(3), pp. 389-401.
- Jonas, J.-C., n.d. Signals and Pools Underlying Biphasic Insulin Secretion.
- Jones, B. J., Tan, T. & Bloom, S., 2012. *Minireview: Glucagon in stress and energy homeostasis*. s.l.:s.n.
- Jørgensen, M. S., Tornqvist, K. S. & Hvid, H., 2017. Calculation of glucose dose for intraperitoneal glucose tolerance tests in lean and obese mice. *Journal of the American Association for Laboratory Animal Science*, 11, 56(1), pp. 95-97.
- Jurczak, M. J. et al., 2011. SGLT2 deletion improves glucose homeostasis and preserves pancreatic β -cell function. *Diabetes*, 3, 60(3), pp. 890-898.
- Juster-Switlyk, K. & Smith, A. G., 2016. *Updates in diabetic peripheral neuropathy*. s.l.:Faculty of 1000 Ltd.
- Kabadi, U. M., 1993. *Hepatic regulation of pancreatic α -cell function*. s.l.:s.n.
- Kahn, S. E., Hull, R. L. & Utzschneider, K. M., 2006. *Mechanisms linking obesity to insulin resistance and type 2 diabetes*. s.l.:Nature Publishing Group.
- Karg, M. V. et al., 2018. SGLT-2-inhibition with dapagliflozin reduces tissue sodium content: A randomised controlled trial. *Cardiovascular Diabetology*, 17(1).
- Kawamori, D. et al., 2009. Insulin Signaling in α Cells Modulates Glucagon Secretion In Vivo. *Cell Metabolism*, 8, 9(4), pp. 350-361.
- Kennedy, R. T., Kauri, L. M., Dahlgren, G. M. & Jung, S. K., 2002. *Metabolic oscillations in β -cells*. s.l., American Diabetes Association, pp. S152-S161.
- Kiekens, R. et al., 1992. Differences in glucose recognition by individual rat pancreatic B cells are associated with intercellular differences in glucose-induced biosynthetic activity. *Journal of Clinical Investigation*, 89(1), pp. 117-125.
- Kilkenny, D. M. & Rocheleau, J. V., 2008. Fibroblast growth factor receptor-1 signaling in pancreatic islet β -cells is modulated by the extracellular matrix. *Molecular Endocrinology*, 1, 22(1), pp. 196-205.

- Kim, A. et al., 2009. Islet architecture: A comparative study.. *Islets*, 1(2), pp. 129-136.
- Kim, C. Y., Kuehn, M. H., Anderson, M. G. & Kwon, Y. H., 2007. Intraocular pressure measurement in mice: a comparison between Goldmann and rebound tonometry. *Eye*, Volume 21, pp. 1202-1209.
- Kim, J. et al., 2019. Intraocular Pressure Monitoring Following Islet Transplantation to the Anterior Chamber of the Eye.
- Kim, J. et al., 2020. Intraocular Pressure Monitoring following Islet Transplantation to the Anterior Chamber of the Eye. *Nano Letters*, 11 3, 20(3), pp. 1517-1525.
- Kim, J. M. & Kim, D. J., 2015. *The optimal cutoff value of glycated hemoglobin for detection of diabetic retinopathy*. s.l.:Korean Diabetes Association.
- Kim, T. et al., 2018. Hepatic glucagon receptor signaling enhances insulin-stimulated glucose disposal in rodents. *Diabetes*, 1 11, 67(11), pp. 2157-2166.
- Kimura, H. et al., 1994. Vasoactive intestinal peptide released by acetylcholine in the dog ileum. *Journal of the Autonomic Nervous System*, 1 7, 48(2), pp. 167-174.
- King, P., Peacock, I. & Donnelly, R., 1999. *The UK Prospective Diabetes Study (UKPDS): Clinical and therapeutic implications for type 2 diabetes*. s.l.:Wiley-Blackwell.
- Knowles, M. R. et al., 1995. A controlled study of adenoviral-vector-mediated gene transfer in the nasal epithelium of patients with cystic fibrosis. *New England Journal of Medicine*, 28 9, 333(13), pp. 823-831.
- Koffert, J. P. et al., 2017. Metformin treatment significantly enhances intestinal glucose uptake in patients with type 2 diabetes: Results from a randomized clinical trial. *Diabetes Research and Clinical Practice*, 1 9, Volume 131, pp. 208-216.
- Kreymann, B. et al., 1989. Characterization of glucagon-like peptide-1-(7-36)amide in the hypothalamus. *Brain Research*, 20 11, 502(2), pp. 325-331.
- Kumagai-Braesch, M. et al., 2013. The theracyte™ device protects against islet allograft rejection in immunized hosts. *Cell Transplantation*, 22(7), pp. 1137-1146.
- Kumar, M. et al., 2007. Gene therapy of diabetes using a novel GLP-1/IgG1-Fc fusion construct normalizes glucose levels in db/db mice. *Gene Therapy*, 31 1, 14(2), pp. 162-172.
- Lammert, E., Cleaver, O. & Melton, D., 2001. Induction of pancreatic differentiation by signals from blood vessels. *Science*, 19 10, 294(5542), pp. 564-567.
- Larraufie, P. et al., 2019. Important Role of the GLP-1 Axis for Glucose Homeostasis after Bariatric Surgery. *Cell Reports*, 5 2, 26(6), pp. 1399-1408.e6.
- Le Gurun, S. et al., 2003. Connexin-36 contributes to control function of insulin-producing cells. *Journal of Biological Chemistry*, 26 9, 278(39), pp. 37690-37697.

- Le Lay, J. et al., 2009. CRTC2 (TORC2) Contributes to the Transcriptional Response to Fasting in the Liver but Is Not Required for the Maintenance of Glucose Homeostasis. *Cell Metabolism*, 8 7, 10(1), pp. 55-62.
- Lean, M. E. et al., 2018. Primary care-led weight management for remission of type 2 diabetes (DiRECT): an open-label, cluster-randomised trial. *The Lancet*, 10 2, 391(10120), pp. 541-551.
- Lei, C. L. et al., 2018. Beta-cell hubs maintain Ca²⁺ oscillations in human and mouse islet simulations. *Islets*, 4 7, 10(4), pp. 151-167.
- Leon, B. M., 2015. Diabetes and cardiovascular disease: Epidemiology, biological mechanisms, treatment recommendations and future research. *World Journal of Diabetes*, 6(13), p. 1246.
- Leung, P. S. & Ip, S. P., 2006. *Pancreatic acinar cell: Its role in acute pancreatitis*. s.l.:Int J Biochem Cell Biol.
- Li, D. S. et al., 2009. A protocol for islet isolation from mouse pancreas. *Nature Protocols*, 22 10, 4(11), pp. 1649-1652.
- Li, L., Seno, M., Yamada, H. & Kojima, I., 2001. Promotion of β -Cell Regeneration by Betacellulin in Ninety Percent-Pancreatectomized Rats. *Endocrinology*, 1 12, 142(12), pp. 5379-5385.
- Lindsay, R. S. & Loeken, M. R., 2017. Metformin use in pregnancy: promises and uncertainties. *Diabetologia*, 2 9, 60(9), pp. 1612-1619.
- Liu, J. et al., 2017. Effects of SGLT2 inhibitors on UTIs and genital infections in type 2 diabetes mellitus: A systematic review and meta-analysis. *Scientific Reports*, 1 12, 7(1), pp. 1-11.
- Liu, Y. J. et al., 1998. Origin of slow and fast oscillations of Ca²⁺ in mouse pancreatic islets. *Journal of Physiology*, 15 4, 508(2), pp. 471-481.
- Liu, Y. M. et al., 1993. Dynamic in vivo observation of rat islet microcirculation. *Pancreas*, 8(1), pp. 15-21.
- Li, X. C., Liao, T. D. & Zhuo, J. L., 2008. Long-term hyperglucagonaemia induces early metabolic and renal phenotypes of Type 2 diabetes in mice. *Clinical Science*, 5, 114(9-10), pp. 591-601.
- Ludwig, B. et al., 2010. *Islet versus pancreas transplantation in type 1 diabetes: Competitive or complementary?*. s.l.:s.n.
- Lundquist, I. et al., 2003. Carbon monoxide stimulates insulin release and propagates Ca²⁺ signals between pancreatic β -cells. *American Journal of Physiology-Endocrinology and Metabolism*, 11, 285(5), pp. E1055-E1063.
- Luo, J. et al., 2007. A protocol for rapid generation of recombinant adenoviruses using the AdEasy system. *Nature Protocols*, 17 5, 2(5), pp. 1236-1247.
- Maahs, D. M., West, N. A., Lawrence, J. M. & Mayer-Davis, E. J., 2010. *Epidemiology of type 1 diabetes*. s.l.:NIH Public Access.

- Mahadevan, V., 2019. *Anatomy of the pancreas and spleen*. s.l.:Elsevier Ltd.
- Maida, A., Lamont, B. J., Cao, X. & Drucker, D. J., 2011. Metformin regulates the incretin receptor axis via a pathway dependent on peroxisome proliferator-activated receptor- α in mice. *Diabetologia*, 2, 54(2), pp. 339-349.
- Makhmutova, M. et al., 2019. Pancreatic Islets Communicate With the Brain via Vagal Sensory Neurons. *bioRxiv*, 24 9.p. 780395.
- Malaisse, W. J. et al., 1979. The stimulus secretion coupling of glucose-induced insulin release. Effect of lactate upon islet function. *Archives of Biochemistry and Biophysics*, 15 4, 194(1), pp. 49-62.
- Malecki, M. T. et al., 1999. Mutations in NEUROD1 are associated with the development of type 2 diabetes mellitus. *Nature Genetics*, 11, 23(3), pp. 323-328.
- Marchetti, P. et al., 2017. Pancreatic Beta Cell Identity in Humans and the Role of Type 2 Diabetes. *Frontiers in Cell and Developmental Biology*, 23 5, 5(MAY), p. 55.
- Marchetti, P. et al., 2007. The endoplasmic reticulum in pancreatic beta cells of type 2 diabetes patients. *Diabetologia*, 30 12, 50(12), pp. 2486-2494.
- Marchetti, P. et al., 2004. Pancreatic islets from type 2 diabetic patients have functional defects and increased apoptosis that are ameliorated by metformin. *Journal of Clinical Endocrinology and Metabolism*, 11, 89(11), pp. 5535-5541.
- Marcu, R. et al., 2018. Human Organ-Specific Endothelial Cell Heterogeneity. *iScience*, 29 6, Volume 4, pp. 20-35.
- Mårin, P. et al., 1996. Assimilation of triglycerides in subcutaneous and intraabdominal adipose tissues in vivo in men: effects of testosterone.. *The Journal of Clinical Endocrinology & Metabolism*, 3, 81(3), pp. 1018-1022.
- Markee, J. E., 1978. Menstruation in intraocular endometrial transplants in the Rhesus monkey. *American Journal of Obstetrics and Gynecology*, 1 7, 131(5), pp. 558-559.
- Markovič, R. et al., 2015. Progressive glucose stimulation of islet beta cells reveals a transition from segregated to integrated modular functional connectivity patterns. *Scientific Reports*, 19 1, 5(1), pp. 1-10.
- Marso, S. P. et al., 2016. Semaglutide and Cardiovascular Outcomes in Patients with Type 2 Diabetes. *New England Journal of Medicine*, 10 11, 375(19), pp. 1834-1844.
- Masson, V. et al., 2002. Mouse aortic ring assay: A new approach of the molecular genetics of angiogenesis. *Biological Procedures Online*, 4(1), pp. 24-31.
- Mather, A. & Pollock, C., 2011. *Glucose handling by the kidney*.. s.l.:s.n.
- Mattsson, G., Jansson, L. & Carlsson, P. O., 2002. Decreased vascular density in mouse pancreatic islets after transplantation. *Diabetes*, 51(5), pp. 1362-1366.

- Mazzone, S. B. & Canning, B. J., 2002. *Central nervous system control of the airways: Pharmacological implications*. s.l.:Elsevier BV.
- McCulloch, L. J. et al., 2011. GLUT2 (SLC2A2) is not the principal glucose transporter in human pancreatic beta cells: Implications for understanding genetic association signals at this locus. *Molecular Genetics and Metabolism*, 12, 104(4), pp. 648-653.
- Mcdougal, D. H. & Gamlin, P. D., n.d. Autonomic control of the eye.
- Meda, P. et al., 1984. THE TOPOGRAPHY OF ELECTRICAL SYNCHRONY AMONG β -CELLS IN THE MOUSE ISLET OF LANGERHANS. *Quarterly Journal of Experimental Physiology*, 10 10, 69(4), pp. 716-735.
- MEDAWAR, P. B., 1948. Immunity to homologous grafted skin; the fate of skin homografts transplanted to the brain, to subcutaneous tissue, and to the anterior chamber of the eye.. *British journal of experimental pathology*, 2, 29(1), pp. 58-69.
- Mehta, A., Marso, S. P. & Neeland, I. J., 2017. Liraglutide for weight management: a critical review of the evidence. *Obesity Science & Practice*, 19 3, 3(1), pp. 3-14.
- Meier, J. J., Veldhuis, J. D. & Butler, P. C., 2005. *Pulsatile Insulin Secretion Dictates Systemic Insulin Delivery by Regulating Hepatic Insulin Extraction In Humans*, s.l.: s.n.
- Menegaz, D. H. D. A. J. C. C. R.-D. R. M. J. D. R. B. M. S. P. N. R. L. F. K. C. S. R. G. H. B. P. B. S. C. A. a. P. E., 2019. Menegaz, D., Hagan, D., Almaça, J., Cianciaruso, C., Rodriguez-Diaz, R., Molina, J., Dolan, R., Becker, M., Schwalie, P., Nano, R., Lebreton, Mechanism and effects of pulsatile GABA secretion from cytosolic pools in the human beta cell. *Nature Metabolism*, 1((11)), pp. pp.1110-1126.
- Merani, S., Toso, C., Emamaullee, J. & Shapiro, A. M. J., 2008. Optimal implantation site for pancreatic islet transplantation. *British Journal of Surgery*, 1 12, 95(12), pp. 1449-1461.
- Mestrinerr, A. C. D. & Haddad, A., 1994. Serum albumin enters the posterior chamber of the eye permeating the blood-aqueous barrier. *Graefe's Archive for Clinical and Experimental Ophthalmology*, 4, 232(4), pp. 242-251.
- Moberg, L. et al., 2002. Production of tissue factor by pancreatic islet cells as a trigger of detrimental thrombotic reactions in clinical islet transplantation. *Lancet*, 21 12, 360(9350), pp. 2039-2045.
- Moens, K. et al., 1998. Dual Glucagon Recognition by Pancreatic β -Cells via Glucagon and Glucagon-Like Peptide 1 Receptors. *Diabetes*, 1 1, 47(1), pp. 66-72.
- Moens, K. et al., 1996. Expression and functional activity of glucagon, glucagon-like peptide I, and glucose-dependent insulinotropic peptide receptors in rat pancreatic islet cells. *Diabetes*, 45(2), pp. 257-261.
- Molina, J. et al., 2014. Control of insulin secretion by cholinergic signaling in the human pancreatic islet. *Diabetes*, 8, 63(8), pp. 2714-2726.

- Moore, R. A., Rosenblum, H. B., Tolins, S. H. & Melchionna, R. H., 1937. The physiological response of prostatic and vesicular transplants in the anterior chamber of the eye. *Journal of Experimental Medicine*, 19, 66(3), pp. 281-289.
- Mori, Y. et al., 1999. Effect of troglitazone on body fat distribution in type 2 diabetic patients. *Diabetes Care*, 22(6), pp. 908-912.
- Mukai, E. et al., 2007. Efficient gene transfer into murine pancreatic islets using adenovirus vectors. *Journal of Controlled Release*, 125(1), pp. 136-141.
- Müller, T. D. et al., 2019. *Glucagon-like peptide 1 (GLP-1)*. s.l.:Elsevier GmbH.
- Muniappan, L. & Ozcan, S., 2009. Adenoviral gene transfer into isolated pancreatic islets. *Methods in molecular biology (Clifton, N.J.)*, Volume 590, pp. 131-142.
- Murakami, T. et al., 1993. The Insulo-Acinar Portal and Insulo-Venous Drainage Systems in the Pancreas of the Mouse, Dog, Monkey and Certain Other Animals: A Scanning Electron Microscopic Study of Corrosion Casts. *archives of histology and cytology*, 6, 56(2), pp. 127-147.
- Murakami, T. et al., n.d. Pancreatic insulo-acinar portal systems in humans, rats, and some other mammals: scanning electron microscopy of vascular casts. *Microscopy research and technique*, 37(5-6), pp. 478-88.
- Nair, G. et al., 2011. Effects of common anesthetics on eye movement and electroretinogram. *Documenta Ophthalmologica*, 6, 122(3), pp. 163-176.
- Nano, R. et al., 2019. *Islets for research: Nothing is perfect, but we can do better*. s.l.:American Diabetes Association Inc..
- Nathan, D. M. et al., 2013. *Diabetes control and complications trial/epidemiology of diabetes interventions and complications study at 30 years: Advances and contributions*. s.l.:American Diabetes Association.
- Nattrass, M., 2010. *Diabetic ketoacidosis*. s.l.:Elsevier Ltd.
- Naziruddin, B. et al., 2014. Evidence for instant blood-mediated inflammatory reaction in clinical autologous islet transplantation. *American Journal of Transplantation*, 14(2), pp. 428-437.
- Nesto, R. W. et al., 2004. *Thiazolidinedione Use, Fluid Retention, and Congestive Heart Failure: A consensus statement from the American Heart Association and American Diabetes Association*. s.l., American Diabetes Association, pp. 256-263.
- Nguyen, L. M., Pozzoli, M., Hraha, T. H. & Benninger, R. K., 2014. Decreasing Cx36 gap junction coupling compensates for overactive K ATP channels to restore insulin secretion and prevent hyperglycemia in a mouse model of neonatal diabetes. *Diabetes*, 63(5), pp. 1685-1697.
- Nicol, L. E. et al., 2013. Pancreatic inflammation and increased islet macrophages in insulin-resistant juvenile primates. *Journal of Endocrinology*, 177(2), pp. 207-213.
- Niederhorn, J. Y., 2006. *See no evil, hear no evil, do no evil: The lessons of immune privilege*. s.l.:s.n.

- Nikolova, G. et al., 2006. The vascular basement membrane: A niche for insulin gene expression and β cell proliferation. *Developmental Cell*, 3, 10(3), pp. 397-405.
- Nilsson, J. et al., 2020. Recruited fibroblasts reconstitute the peri-islet membrane: a longitudinal imaging study of human islet grafting and revascularisation. *Diabetologia*, 1 1, 63(1), pp. 137-148.
- Nimmerjahn, A., Kirchhoff, F. & Helmchen, F., 2005. Neuroscience: Resting microglial cells are highly dynamic surveillants of brain parenchyma in vivo. *Science*, 27 5, 308(5726), pp. 1314-1318.
- Nolan, C. J. et al., 2006. *Fatty acid signaling in the β -cell and insulin secretion*. s.l.:s.n.
- Nunemaker, C. S. et al., 2005. Individual mice can be distinguished by the period of their islet calcium oscillations: Is there an intrinsic islet period that is imprinted in vivo?. *Diabetes*, 1 12, 54(12), pp. 3517-3522.
- Nyman, L. R., Ford, E., Powers, A. C. & Piston, D. W., 2010. Glucose-dependent blood flow dynamics in murine pancreatic islets in vivo. *American Journal of Physiology - Endocrinology and Metabolism*, 4, 298(4), pp. E807-E814.
- Nyman, L. R. et al., 2008. Real-time, multidimensional in vivo imaging used to investigate blood flow in mouse pancreatic islets. *Journal of Clinical Investigation*, 3 11, 118(11), pp. 3790-3797.
- Nyqvist, D., Köhler, M., Wahlstedt, H. & Berggren, P. O., 2005. Donor islet endothelial cells participate in formation of functional vessels within pancreatic islet grafts. *Diabetes*, 1 8, 54(8), pp. 2287-2293.
- Nyqvist, D. et al., 2011. Donor islet endothelial cells in pancreatic islet revascularization. *Diabetes*, 10, 60(10), pp. 2571-2577.
- Okamoto, H. et al., 2017. Glucagon receptor inhibition normalizes blood glucose in severe insulin-resistant mice. *Proceedings of the National Academy of Sciences of the United States of America*, 7 3, 114(10), pp. 2753-2758.
- Olofsson, C. S. et al., 2007. Long-term exposure to glucose and lipids inhibits glucose-induced insulin secretion downstream of granule fusion with plasma membrane. *Diabetes*, 7, 56(7), pp. 1888-1897.
- Olsson, R., Maxhuni, A. & Carlsson, P. O., 2006. Revascularization of transplanted pancreatic islets following culture with stimulators of angiogenesis. *Transplantation*, 82(3), pp. 340-347.
- Olsson, R., Olerud, J., Pettersson, U. & Carlsson, P. O., 2011. Increased numbers of low-oxygenated pancreatic islets after intraportal islet transplantation. *Diabetes*, 9, 60(9), pp. 2350-2353.
- Omar, B. A. et al., 2014. Fibroblast growth factor 21 (FGF21) and glucagon-like peptide 1 contribute to diabetes resistance in glucagon receptor-deficient mice. *Diabetes*, 1, 63(1), pp. 101-110.
- Omar-Hmeadi, M. et al., 2020. Paracrine control of α -cell glucagon exocytosis is compromised in human type-2 diabetes. *Nature Communications*, 20 12, 11(1), p. 1896.

- Ota, K. et al., 2015. Induction of PD-L1 expression by the EML4-ALK oncoprotein and down stream signaling pathways in non-small cell lung cancer. *Clinical Cancer Research*, 19, 21(17), pp. 4014-4021.
- Otonkoski, T. et al., 2007. Physical exercise-induced hypoglycemia caused by failed silencing of monocarboxylate transporter 1 in pancreatic β cells. *American Journal of Human Genetics*, 81(3), pp. 467-474.
- Otonkoski, T. et al., 2006. Noninvasive diagnosis of focal hyperinsulinism of infancy with [^{18}F]-DOPA positron emission tomography. *Diabetes*, 55(1), pp. 13-18.
- Owen, M. R., Doran, E. & Halestrap, A. P., 2000. Evidence that metformin exerts its anti-diabetic effects through inhibition of complex 1 of the mitochondrial respiratory chain. *Biochemical Journal*, 348(3), pp. 607-614.
- Orskov, N. K. et al., 1996. *Mechanisms of Sulfonylurea's Stimulation of Insulin Secretion In Vivo Selective Amplification of Insulin Secretory Burst Mass*, s.l.: s.n.
- Palti, Y. et al., 1996. Islets of Langerhans generate wavelike electric activity modulated by glucose concentration. *Diabetes*, 45(5), pp. 595-601.
- Pancholi, J. et al., 2014. Biologically targeted probes for Zn^{2+} : A diversity oriented modular "click-SNAr-click" approach. *Chemical Science*, 5(9), pp. 3528-3535.
- Paolisso, G. et al., 1988. Pulsatile insulin delivery is more efficient than continuous infusion in modulating islet cell function in normal subjects and patients with type 1 diabetes. *Journal of Clinical Endocrinology and Metabolism*, 66(6), pp. 1220-1226.
- Parikh, A. A. et al., 2003. Expression and regulation of the novel vascular endothelial growth factor receptor neuropilin-1 by epidermal growth factor in human pancreatic carcinoma. *Cancer*, 98(4), pp. 720-729.
- Parish, R. & Petersen, K. F., 2005. *Mitochondrial dysfunction and type 2 diabetes*. s.l.:Current Science Ltd.
- Parker, J. C. et al., 2002. Glycemic control in mice with targeted disruption of the glucagon receptor gene. *Biochemical and Biophysical Research Communications*, 290(2), pp. 839-843.
- Parnaud, G. et al., 2009. Signaling pathways implicated in the stimulation of β -cell proliferation by extracellular matrix. *Molecular Endocrinology*, 23(8), pp. 1264-1271.
- Parnaud, G. et al., 2006. Blockade of β 1 integrin-laminin-5 interaction affects spreading and insulin secretion of rat β -cells attached on extracellular matrix. *Diabetes*, 55(5), pp. 1413-1420.
- Paschen, M. et al., 2016. Non-invasive cell type selective in vivo monitoring of insulin resistance dynamics. *Scientific Reports*, 6. Volume 6.
- Paschen, M. et al., 2019. Diet-induced β -cell insulin resistance results in reversible loss of functional β -cell mass. *FASEB Journal*, 33(1), pp. 204-218.

- Peiris, H. et al., 2014. *The β -cell/EC axis: How do islet cells talk to each other?*. s.l.:American Diabetes Association.
- Pénicaud, L., 2017. *Autonomic nervous system and pancreatic islet blood flow*. s.l.:Elsevier B.V..
- Pepper, A. R., Gala-Lopez, B., Ziff, O. & Shapiro, A. M. J., 2013. Revascularization of Transplanted Pancreatic Islets and Role of the Transplantation Site. *Clinical and Developmental Immunology*, Volume 2013, p. 13.
- Perkovic, V. et al., 2019. Canagliflozin and Renal Outcomes in Type 2 Diabetes and Nephropathy. *New England Journal of Medicine*, 13 6, 380(24), pp. 2295-2306.
- Petersen, M. C., Vatner, D. F. & Shulman, G. I., 2017. *Regulation of hepatic glucose metabolism in health and disease*. s.l.:Nature Publishing Group.
- Petruzzo, P. et al., 2006. Metabolic consequences of pancreatic systemic or portal venous drainage in simultaneous pancreas-kidney transplant recipients. *Diabetic Medicine*, 1 6, 23(6), pp. 654-659.
- Picard, F. & Auwerx, J., 2002. PPAR γ AND GLUCOSE HOMEOSTASIS. *Annual Review of Nutrition*, 7, 22(1), pp. 167-197.
- Pipeleers, D., 1987. *The biosociology of pancreatic B cells**, s.l.: s.n.
- Pipeleers, D., De Mesmaeker, I., Robert, T. & Van Hulle, F., 2017. *Heterogeneity in the Beta-Cell Population: a Guided Search Into Its Significance in Pancreas and in Implants*. s.l.:Current Medicine Group LLC 1.
- Pipeleers, D. G., 1992. Heterogeneity in Pancreatic β -cell Population. *Diabetes*, 1 7, 41(7), pp. 777-781.
- Pipeleers, D. G., 1992. *Heterogeneity in pancreatic β -cell population*. s.l.:s.n.
- PIPELEERS, D. G. et al., 1985. Interplay of Nutrients and Hormones in the Regulation of Insulin Release*. *Endocrinology*, 9, 117(3), pp. 824-833.
- PIPELEERS, D. G., SCHUIT, F. C., SCHRAVENDIJK, C. F. H. V. & WINKEL, M. V. D., 1985. Interplay of Nutrients and Hormones in the Regulation of Glucagon Release*. *Endocrinology*, 9, 117(3), pp. 817-823.
- Plotnick, L. P., Clark, L. M., Brancati, F. L. & Erlinger, T., 2003. Safety and effectiveness of insulin pump therapy in children and adolescents with type 1 diabetes. *Diabetes Care*, 1 4, 26(4), pp. 1142-1146.
- Pocai, A. et al., 2009. Glucagon-like peptide 1/glucagon receptor dual agonism reverses obesity in mice. *Diabetes*, 10, 58(10), pp. 2258-2266.
- Pories, W. J. et al., 1995. *Who Would Have Thought It? An Operation Proves to Be the Most Effective Therapy for Adult-Onset Diabetes Mellitus*, s.l.: Lippincott-Raven Publishers.

- Pralong, W. F., Bartley, C. & Wollheim, C. B., 1990. Single islet beta-cell stimulation by nutrients: relationship between pyridine nucleotides, cytosolic Ca²⁺ and secretion.. *The EMBO journal*, 1, 9(1), pp. 53-60.
- Pratley, R. E. et al., 2010. *Liraglutide versus sitagliptin for patients with type 2 diabetes who did not have adequate glycaemic control with metformin: a 26-week, randomised, parallel-group, open-label trial*, s.l.: s.n.
- Proks, P. et al., 2002. *Sulfonylurea stimulation of insulin secretion*. s.l., American Diabetes Association, pp. S368-S376.
- Purnell, J. Q., 2000. *Definitions, Classification, and Epidemiology of Obesity*. s.l.:MDText.com, Inc..
- Purnell, J. Q. et al., 2003. Relationship of family history of type 2 diabetes, hypoglycemia, and autoantibodies to weight gain and lipids with intensive and conventional therapy in the diabetes control and complications trial. *Diabetes*, 1 10, 52(10), pp. 2623-2629.
- Quiñones, M. et al., 2015. Hypothalamic CaMKK β mediates glucagon anorectic effect and its diet-induced resistance. *Molecular Metabolism*, 12, 4(12), pp. 961-970.
- Raskin, P. & Mora, P. F., 2010. Glycaemic control with liraglutide: the phase 3 trial programme. *International Journal of Clinical Practice*, 23 9, 64(SUPPL. 167), pp. 21-27.
- Ravier, M. A. et al., 2005. Loss of connexin36 channels alters β -cell coupling, islet synchronization of glucose-induced Ca²⁺ and insulin oscillations, and basal insulin release. *Diabetes*, 6, 54(6), pp. 1798-1807.
- Ravier, M. A. & Rutter, G. A., 2010. Isolation and culture of mouse pancreatic islets for ex vivo imaging studies with trappable or recombinant fluorescent probes.. *Methods in molecular biology (Clifton, N.J.)*, Volume 633, pp. 171-184.
- Ravier, M., Sehlin, J. & Henquin, J., 2002. Disorganization of cytoplasmic Ca²⁺ oscillations and pulsatile insulin secretion in islets from ob/ob mice. *Diabetologia*, 8, 45(8), pp. 1154-1163.
- Razavi, R. et al., 2006. TRPV1+ Sensory Neurons Control β Cell Stress and Islet Inflammation in Autoimmune Diabetes. *Cell*, 15 12, 127(6), pp. 1123-1135.
- Reaven, G. M. et al., 1987. Documentation of hyperglucagonemia throughout the day in nonobese and obese patients with noninsulin-dependent diabetes mellitus. *Journal of Clinical Endocrinology and Metabolism*, 1, 64(1), pp. 106-110.
- Redfield, R. R., Rickels, M. R., Naji, A. & Odorico, J. S., 2016. *Pancreas Transplantation in the Modern Era*. s.l.:W.B. Saunders.
- Reinert, R. B. et al., 2013. Vascular endothelial growth factor-a and islet vascularization are necessary in developing, but not adult, pancreatic islets. *Diabetes*, 1 12, 62(12), pp. 4154-4164.
- Rena, G., Hardie, D. G. & Pearson, E. R., 2017. *The mechanisms of action of metformin*. s.l.:Springer Verlag.

- Rendell, M., 2004. *The Role of Sulphonylureas in the Management of Type 2 Diabetes Mellitus*, s.l.: s.n.
- Rines, A. K., Sharabi, K., Tavares, C. D. & Puigserver, P., 2016. *Targeting hepatic glucose metabolism in the treatment of type 2 diabetes*. s.l.:Nature Publishing Group.
- Rizza, R. A., 2010. Pathogenesis of Fasting and Postprandial Hyperglycemia in Type 2 Diabetes: Implications for Therapy.
- Rocheleau, J. V. et al., 2006. Critical role of gap junction coupled KATP channel activity for regulated insulin secretion. *PLoS Biology*, 2, 4(2), pp. 221-227.
- Roden, M. & Bernroider, E., 2003. *Hepatic glucose metabolism in humans - Its role in health and disease*. s.l.:Bailliere Tindall Ltd.
- Rodriguez-Diaz, R. et al., 2011. Innervation patterns of autonomic axons in the human endocrine pancreas. *Cell Metabolism*, 6 7, 14(1), pp. 45-54.
- Rodriguez-Diaz, R. & Caicedo, A., 2013. *Novel Approaches to Studying the Role of Innervation in the Biology of Pancreatic Islets*. s.l.:NIH Public Access.
- Rodriguez-Diaz, R. et al., 2018. Paracrine Interactions within the Pancreatic Islet Determine the Glycemic Set Point. *Cell Metabolism*, 6 3, 27(3), pp. 549-558.e4.
- Rodriguez-Diaz, R. et al., n.d. Noninvasive in vivo model demonstrating the effects of autonomic innervation on pancreatic islet function.
- Rodriguez-Diaz, R. et al., 2012. Noninvasive in vivo model demonstrating the effects of autonomic innervation on pancreatic islet function. *Proceedings of the National Academy of Sciences of the United States of America*, 26 12, 109(52), pp. 21456-21461.
- Rodriguez-Diaz, R., Tamayo, A., Hara, M. & Caicedo, A., 2019. The Local Paracrine Actions of the Pancreatic Alpha Cell. *Diabetes*, 27 12.p. dbi190002.
- Rorsman, P. & Braun, M., 2013. Regulation of Insulin Secretion in Human Pancreatic Islets. *Annual Review of Physiology*, 10 2, 75(1), pp. 155-179.
- Rorsman, P., Braun, M. & Zhang, Q., 2012. Regulation of calcium in pancreatic α - and β -cells in health and disease. *Cell Calcium*.
- Rorsman, P. & Renström, E., 2003. *Insulin granule dynamics in pancreatic beta cells*. s.l.:Springer.
- Rosenstock, J. & Ferrannini, E., 2015. *Euglycemic diabetic ketoacidosis: A predictable, detectable, and preventable safety concern with sglt2 inhibitors*. s.l.:American Diabetes Association Inc..
- Rosenstock, J. et al., 2019. Effect of Linagliptin vs Glimepiride on Major Adverse Cardiovascular Outcomes in Patients with Type 2 Diabetes: The CAROLINA Randomized Clinical Trial. *JAMA - Journal of the American Medical Association*, 24 9, 322(12), pp. 1155-1166.

- Rossi, D. L. et al., 2015. State of the art paper Sulfonylureas and their use in clinical practice. *Arch Med Sci*, Volume 11, pp. 840-848.
- Rother, K. I. & Harlan, D. M., 2004. Challenges facing islet transplantation for the treatment of type 1 diabetes mellitus.. *The Journal of clinical investigation*, 10, 114(7), pp. 877-83.
- Roumie, C. L. et al., 2012. Comparative effectiveness of sulfonylurea and metformin monotherapy on cardiovascular events in type 2 diabetes mellitus: A cohort study. *Annals of Internal Medicine*, 6 11, 157(9), pp. 601-610.
- Rubino, F., Schauer, P. R., Kaplan, L. M. & Cummings, D. E., 2010. Puget Sound Health Care System. *Annu. Rev. Med*, Volume 61, pp. 393-411.
- Rutter, G., 2019. Pancreatic islet secretion: gabbling via GABA. *Nature Metabolism*, 1((11)), pp. pp. 1032-1033.
- Rutter, G. A., Pullen, T. J., Hodson, D. J. & Martinez-Sanchez, A., 2015. *Pancreatic β -cell identity, glucose sensing and the control of insulin secretion*. s.l.:Portland Press Ltd.
- Ryan, E. A. et al., 2001. Clinical outcomes and insulin secretion after islet transplantation with the edmonton protocol. *Diabetes*, 50(4), pp. 710-719.
- Sabatini, P. V., Speckmann, T. & Lynn, F. C., 2019. *Friend and foe: β -cell Ca^{2+} signaling and the development of diabetes*. s.l.:Elsevier GmbH.
- Salem, V. & Delgadillo Silva, L., n.d. Leader β -cells coordinate Ca^{2+} dynamics across pancreatic islets in vivo.
- Salem, V. et al., 2016. Glucagon increases energy expenditure independently of brown adipose tissue activation in humans. *Diabetes, Obesity and Metabolism*, 1 1, 18(1), pp. 72-81.
- Salem, V. et al., 2019. Leader β -cells coordinate Ca^{2+} dynamics across pancreatic islets in vivo. *Nature Metabolism*, 1 6, 1(6), pp. 615-629.
- Salem, V. et al., 2019. Leader β -cells coordinate Ca^{2+} dynamics across pancreatic islets in vivo. *Nature Metabolism*, 1(6).
- Saltiel, A. R. & Olefsky, J. M., 1996. *Perspectives in Diabetes Thiazolidinediones in the Treatment of Insulin Resistance and T²e II Diabetes*, s.l.: s.n.
- Samols, E., Marri, G. & Marks, V., 1966. Interrelationship of glucagon, insulin and glucose. The insulinogenic effect of glucagon.. *Diabetes*, 1 12, 15(12), pp. 855-866.
- Samols, E., Stagner, J. I., Ewart, R. B. & Marks, V., 1988. The order of islet microvascular cellular perfusion is B \rightarrow A \rightarrow D in the perfused rat pancreas. *Journal of Clinical Investigation*, 82(1), pp. 350-353.
- Samulski, R. J. & Muzyczka, N., 2014. Downloaded from www.annualreviews.org Access provided by 185. *Annu. Rev. Virol*, Volume 1, p. 250.

- Sansbury, F. H. et al., 2012. SLC2A2 mutations can cause neonatal diabetes, suggesting GLUT2 may have a role in human insulin secretion. Volume 55, pp. 2381-2385.
- Santos, A. & Blazquez, E., 1982. Regulatory effect of glucagon on its own receptor concentrations and target-cell sensitivity in the rat.. *Diabetologia*, 5, 22(5), pp. 362-71.
- Sasada, T., Azuma, K., Ohtake, J. & Fujimoto, Y., 2016. Immune Responses to Epidermal Growth Factor Receptor (EGFR) and Their Application for Cancer Treatment. *Frontiers in Pharmacology*, 26 10, 7(OCT), p. 405.
- Satin, L. Z. Q. a. R. P., 2020. "Take Me To Your Leader": An Electrophysiological Appraisal of the Role of Hub Cells in Pancreatic Islets.. *Diabetes*, 69((5)), pp. pp.830-836.
- Schäfer, M. K. et al., 2013. Species-specific vesicular monoamine transporter 2 (VMAT2) expression in mammalian pancreatic beta cells: Implications for optimising radioligand-based human beta cell mass (BCM) imaging in animal models. *Diabetologia*, 5, 56(5), pp. 1047-1056.
- Scheen, A. J., 2003. *PATHOPHYSIOLOGY OF TYPE 2 DIABETES Continuing Medical Education*, s.l.: s.n.
- Schreier, B., Gekle, M. & Grossmann, C., 2014. Role of epidermal growth factor receptor in vascular structure and function. *Current Opinion in Nephrology and Hypertension*, 3, 23(2), pp. 113-121.
- Schuit, F., Moens, K., Heimberg, H. & Pipeleers, D., 1999. Cellular origin of hexokinase in pancreatic islets. *Journal of Biological Chemistry*, 12 11, 274(46), pp. 32803-32809.
- Schuit, F. et al., 2012. *β -cell-specific gene repression: A mechanism to protect against inappropriate or maladjusted insulin secretion?*. s.l.:American Diabetes Association.
- Schulla, V. et al., 2003. Impaired insulin secretion and glucose tolerance in β cell-selective Cav1.2 Ca²⁺ channel null mice. *EMBO Journal*, 1 8, 22(15), pp. 3844-3854.
- Seino, S., 2012. *Cell signalling in insulin secretion: The molecular targets of ATP, cAMP and sulfonylurea*. s.l.:Springer.
- Shapiro, A. J. et al., 2000. Islet Transplantation in Seven Patients with Type 1 Diabetes Mellitus Using a Glucocorticoid-Free Immunosuppressive Regimen. *New England Journal of Medicine*, 27 7, 343(4), pp. 230-238.
- Sharabi, K., Tavares, C. D., Rines, A. K. & Puigserver, P., 2015. *Molecular pathophysiology of hepatic glucose production*. s.l.:Elsevier Ltd.
- Sharifipour, F. et al., 2013. Oxygen Tension in the Aqueous Humor of Human Eyes under Different Oxygenation Conditions. *Journal of Ophthalmic & Vision Research*, 8(2), p. 119.
- Shaw, J. E., Sicree, R. A. & Zimmet, P. Z., 2010. *Global estimates of the prevalence of diabetes for 2010 and 2030*. s.l.:Elsevier.
- Shaw, R. J. et al., 2005. Medicine: The kinase LKB1 mediates glucose homeostasis in liver and therapeutic effects of metformin. *Science*, 9 12, 310(5754), pp. 1642-1646.

- Sherwood, L. M., Parris, E. E. & Unger, R. H., 1971. *Glucagon Physiology and Pathophysiology*. s.l.:s.n.
- Shishido, A. et al., 2016. Clinical intraocular islet transplantation is not a number issue.. *CellIR4--repair, replacement, regeneration, & reprogramming*, 4(4).
- Short, K. W., Steve Head, W. & Piston, D. W., 2014. Connexin 36 mediates blood cell flow in mouse pancreatic islets. *American Journal of Physiology - Endocrinology and Metabolism*, 1 2, 306(3), pp. E324-31.
- Shulman, G. I., 2000. *Cellular mechanisms of insulin resistance*. s.l.:The American Society for Clinical Investigation.
- Sigismund, S., Avanzato, D. & Lanzetti, L., 2018. *Emerging functions of the EGFR in cancer*. s.l.:John Wiley and Sons Ltd..
- Simpson, R. G. et al., 1968. Early phase of insulin release.. *Diabetes*, 1 11, 17(11), pp. 684-692.
- Situ, I. et al., 1995. *Magnitude and Modulation of Pancreatic 13-Cell Gap Junction Electrical Conductance*, s.l.: s.n.
- Sloop, K. W. et al., 2004. Hepatic and glucagon-like peptide-1-mediated reversal of diabetes by glucagon receptor antisense oligonucleotide inhibitors. *The Journal of Clinical Investigation*, 113(11).
- Smith, P., Millard, P. J., Fewtrell, C. M. & Ashcroft, F. M., 1997. Heterogeneity of β -cell Ca^{2+} responses to glucose. *Advances in Experimental Medicine and Biology*, Volume 426, pp. 253-257.
- Snowling, N. J. & Hopkins, W. G., 2006. Effects of different modes of exercise training on glucose control and risk factors for complications in type 2 diabetic patients: A meta-analysis. *Diabetes Care*, 11, 29(11), pp. 2518-2527.
- Sola, D. et al., 2015. *Sulfonylureas and their use in clinical practice*. s.l.:Termedia Publishing House Ltd..
- Soltani, N. Q. H. A. M. G. Y. Z. F. L. R. L. Y. Z. N. C. R. N. T. J. T. Z. H. L. W. F. Z. P. G. a. W. Q., 2011. GABA exerts protective and regenerative effects on beta-cells and reverses diabetes. *Proceedings of the National Academy of Sciences*, 108((28)), pp. pp. 11692-11697.
- Song, M. Y., Bae, U. J., Jang, K. Y. & Park, B. H., 2014. Transplantation of betacellulin-transduced islets improves glucose intolerance in diabetic mice. *Experimental and Molecular Medicine*, 46(5), p. e98.
- Song, W. J. et al., 2013. Pancreatic b-cell response to increased metabolic demand and to pharmacologic secretagogues requires epac2a. *Diabetes*, 8, 62(8), pp. 2796-2807.
- Souza, F. et al., 2006. Longitudinal noninvasive PET-based β cell mass estimates in a spontaneous diabetes rat model. *Journal of Clinical Investigation*, 1 6, 116(6), pp. 1506-1513.
- Speier, S. et al., 2007. Cx36-mediated coupling reduces β -cell heterogeneity, confines the stimulating glucose concentration range, and affects insulin release kinetics. *Diabetes*, 1 4, 56(4), pp. 1078-1086.

- Speier, S. et al., 2008. Noninvasive in vivo imaging of pancreatic islet cell biology. *Nature Medicine*, 5, 14(5), pp. 574-578.
- Staton, C. A., Reed, M. W. & Brown, N. J., 2009. *A critical analysis of current in vitro and in vivo angiogenesis assays*. s.l.:Wiley-Blackwell.
- Steiner, D. J., Kim, A., Miller, K. & Hara, M., 2010. *Pancreatic islet plasticity: Interspecies comparison of islet architecture and composition*. s.l.:Landes Bioscience.
- Stendahl, J. C., Kaufman, D. B. & Stupp, S. I., 2009. *Extracellular matrix in pancreatic islets: Relevance to scaffold design and transplantation*. s.l.:NIH Public Access.
- Stice, M. J. et al., 2018. Omental Pouch Technique for Combined Site Islet Autotransplantation Following Total Pancreatectomy. *Cell Transplantation*, 1 10, 27(10), pp. 1561-1568.
- Stožer, A., Dolencek, J. & Rupnik, M. S., 2013. Glucose-Stimulated Calcium Dynamics in Islets of Langerhans in Acute Mouse Pancreas Tissue Slices. *PLoS ONE*, 24 1, 8(1), p. e54638.
- Stožer, A. et al., 2013. Functional Connectivity in Islets of Langerhans from Mouse Pancreas Tissue Slices. *PLoS Computational Biology*, 28 2, 9(2), p. e1002923.
- Strömberg, I. & Ebendal, T., 1989. Aged adrenal medullary tissue survives intraocular grafting, forms nerve fibers and responds to nerve growth factor. *Journal of Neuroscience Research*, 1 6, 23(2), pp. 162-171.
- Sun, K. & Scherer, P. E., 2012. The PPAR γ -FGF1 axis: An unexpected mediator of adipose tissue homeostasis. *Cell Research*, 10, 22(10), pp. 1416-1418.
- Svensson, J., Lau, J., Sandberg, M. & Carlsson, P.-O., 2011. High vascular density and oxygenation of pancreatic islets transplanted in clusters into striated muscle. *Cell transplantation*, 1 6, 20(5), pp. 783-8.
- Swisa, A. et al., 2017. PAX6 maintains β cell identity by repressing genes of alternative islet cell types. *Journal of Clinical Investigation*, 3 1, 127(1), pp. 230-243.
- Taborsky, G. J., 2011. *Islets have a lot of nerve! or do they?*. s.l.:Cell Press.
- Takahashi, R. et al., 2007. Efficient and controlled gene expression in mouse pancreatic islets by arterial delivery of tetracycline-inducible adenoviral vectors. *Journal of Molecular Endocrinology*, 2, 38(1-2), pp. 127-136.
- Tanabe, K., 2003. *Calcineurin inhibitors in renal transplantation: What is the best option?*. s.l.:s.n.
- Tanaka, K. et al., 2014. In Vivo Characterization of Neutrophil Extracellular Traps in Various Organs of a Murine Sepsis Model. *PLoS ONE*, 5 11, 9(11), p. e111888.
- Taneera, J. J. Z. J. Y. M. S. Z. E. L. S. S. A. K. O. R. E. G. L. a. B. B., 2012. γ -Aminobutyric acid (GABA) signalling in human pancreatic islets is altered in type 2 diabetes. *Diabetologia*, 55((7)), pp. pp. 1985-1994.

- Tan, T. M. et al., 2013. Coadministration of glucagon-like peptide-1 during glucagon infusion in humans results in increased energy expenditure and amelioration of hyperglycemia. *Diabetes*, 4, 62(4), pp. 1131-1138.
- Tarasov, A., Dusonchet, J. & Ashcroft, F., 2004. *Metabolic Regulation of the Pancreatic-Cell ATP-Sensitive K Channel A Pas de Deux*, s.l.: s.n.
- Taylor, B. L., Liu, F. F. & Sander, M., 2013. Nkx6.1 Is Essential for Maintaining the Functional State of Pancreatic Beta Cells. *Cell Reports*, 26 9, 4(6), pp. 1262-1275.
- Teff, K. L., Mattes, R. D. & Engelman, K., 1991. Cephalic phase insulin release in normal weight males: Verification and reliability. *American Journal of Physiology - Endocrinology and Metabolism*, 261(4 24-4).
- Tesfaye, N. & Seaquist, E. R., 2010. Neuroendocrine responses to hypoglycemia. *Annals of the New York Academy of Sciences*, Volume 1212, pp. 12-28.
- Tessonnier, L. et al., 2010. Limited Value of 18F-F-DOPA PET to Localize Pancreatic Insulin-Secreting Tumors in Adults with Hyperinsulinemic Hypoglycemia. *The Journal of Clinical Endocrinology & Metabolism*, 1 1, 95(1), pp. 303-307.
- Thorens, B., 2015. *GLUT2, glucose sensing and glucose homeostasis*. s.l.:Springer Verlag.
- Thorens, B. et al., n.d. Ins1 Cre knock-in mice for beta cell-specific gene recombination.
- Thorens, B. et al., 1990. Reduced expression of the liver/beta-cell glucose transporter isoform in glucose-insensitive pancreatic beta cells of diabetic rats. *Proceedings of the National Academy of Sciences of the United States of America*, 87(17), pp. 6492-6496.
- Tian, J. et al., 2017. *Bile acid signaling and bariatric surgery*. s.l.:KeAi Communications Co..
- Tibaldi, J. M., 2012. *Evolution of insulin development: Focus on key parameters*. s.l.:Springer.
- Tornehave, D. et al., 2008. Expression of the GLP-1 receptor in mouse, rat, and human pancreas. *Journal of Histochemistry and Cytochemistry*, 9, 56(9), pp. 841-851.
- Turner, R. C., 1998. *The U.K. Prospective Diabetes Study: A review*. s.l., American Diabetes Association, pp. C35-C38.
- Turner, R. C., Cull, C. A., Frighi, V. & Holman, R. R., 1999. Glycemic control with diet, sulfonylurea, metformin, or insulin in patients with type 2 diabetes mellitus. Progressive requirement for multiple therapies (UKPDS 49). *Journal of the American Medical Association*, 2 6, 281(21), pp. 2005-2012.
- Turner, R. C. & Holman, R. R., 1995. Lessons from UK prospective diabetes study. *Diabetes Research and Clinical Practice*, 1 1, Volume 28, pp. S151-S157.
- Turton, M. D. et al., 1996. A role for glucagon-like peptide-1 in the central regulation of feeding. *Nature*, 4 1, 379(6560), pp. 69-72.

- Unger, R. H. & Orci, L., 1975. The essential role of glucagon in the pathogenesis of diabetes mellitus.. *Lancet (London, England)*, 4 1, 1(7897), pp. 14-6.
- Unson, C. G., 2002. *Molecular determinants of glucagon receptor signaling*. s.l.:s.n.
- Van De Bunt, M. & Gloyn, A. L., 2012. *A tale of two glucose transporters: How GLUT2 re-emerged as a contender for glucose transport into the human beta cell*. s.l.:Springer.
- van Gurp, L. et al., 2016. Sequential intravital imaging reveals in vivo dynamics of pancreatic tissue transplanted under the kidney capsule in mice. *Diabetologia*, 21 11, 59(11), pp. 2387-2392.
- van Krieken, P. P. et al., 2019. Translational assessment of a genetic engineering methodology to improve islet function for transplantation. *EBioMedicine*, 1 7, Volume 45, pp. 529-541.
- Van Schravendijk, C. F., Kiekens, R. & Pipeleers, D. G., 1992. Pancreatic β cell heterogeneity in glucose-induced insulin secretion. *Journal of Biological Chemistry*, 267(30), pp. 21344-21348.
- Viollet, B. et al., 2012. *Cellular and molecular mechanisms of metformin: An overview*. s.l.:s.n.
- Wang, X. et al., 2013. Regional Differences in Islet Distribution in the Human Pancreas - Preferential Beta-Cell Loss in the Head Region in Patients with Type 2 Diabetes. *PLoS ONE*, 24 6.8(6).
- Wang, Z., Liu, G., Zheng, H. & Chen, X., 2014. Rigid nanoparticle-based delivery of anti-cancer siRNA: Challenges and opportunities. *Biotechnology Advances*, 32(4), pp. 831-843.
- Watada, H. et al., 1996. PDX-1 Induces Insulin and Glucokinase Gene Expressions in TC1 Clone 6 Cells in the Presence of Betacellulin. *Diabetes*, 1 12, 45(12), pp. 1826-1831.
- Weigert, R. et al., 2010. *Intravital microscopy: A novel tool to study cell biology in living animals*. s.l.:NIH Public Access.
- Weihe, E., Schäfer, M. K., Erickson, J. D. & Eiden, L. E., 1994. Localization of vesicular monoamine transporter isoforms (VMAT1 and VMAT2) to endocrine cells and neurons in rat. *Journal of Molecular Neuroscience*, 9, 5(3), pp. 149-164.
- Weinberg, N. et al., 2007. Lineage tracing evidence for in vitro dedifferentiation but rare proliferation of mouse pancreatic β -cells. *Diabetes*, 5, 56(5), pp. 1299-1304.
- Weinstock, R. S. et al., 2013. Severe hypoglycemia and diabetic ketoacidosis in adults with type 1 diabetes: Results from the T1D exchange clinic registry. *Journal of Clinical Endocrinology and Metabolism*, 8, 98(8), pp. 3411-3419.
- Welsh, M., Nielsen, D. A., MacKrell, A. J. & Steiner, D. F., 1985. Control of insulin gene expression in pancreatic β -cells and in an insulin-producing cell line, RIN-5F cells. II. Regulation of insulin mRNA stability. *Journal of Biological Chemistry*, 260(25), pp. 13590-13594.
- Wendt, A. & Eliasson, L., 2020. Pancreatic α -cells – The unsung heroes in islet function. *Seminars in Cell & Developmental Biology*, 1.

- Westacott, M. J., Ludin, N. W. & Benninger, R. K., 2017. Spatially Organized β -Cell Subpopulations Control Electrical Dynamics across Islets of Langerhans. *Biophysical Journal*, 5 9, 113(5), pp. 1093-1108.
- White, S. A., Shaw, J. A. & Sutherland, D. E., 2009. *Pancreas transplantation*. s.l.:s.n.
- Wiederkehr, A. & Wollheim, C. B., 2008. *Impact of mitochondrial calcium on the coupling of metabolism to insulin secretion in the pancreatic β -cell*. s.l.:Elsevier Ltd.
- Wieduwilt, M. J. & Moasser, M. M., 2008. *The epidermal growth factor receptor family: Biology driving targeted therapeutics*. s.l.:NIH Public Access.
- Windeløv, J. A., Pedersen, J. & Holst, J. J., 2016. Use of anesthesia dramatically alters the oral glucose tolerance and insulin secretion in C57Bl/6 mice. *Physiological Reports*, 1 6.4(11).
- Winer, S. et al., 2003. Autoimmune islet destruction in spontaneous type 1 diabetes is not β -cell exclusive. *Nature Medicine*, 1 2, 9(2), pp. 198-205.
- Winzell, M. S. et al., 2007. Glucagon receptor antagonism improves islet function in mice with insulin resistance induced by a high-fat diet. *Diabetologia*, 7, 50(7), pp. 1453-1462.
- Witkowski, M., Landmesser, U. & Rauch, U., 2016. *Tissue factor as a link between inflammation and coagulation*. s.l.:Elsevier Inc..
- Wojtuszczyński, A. et al., 2008. Insulin secretion from human beta cells is heterogeneous and dependent on cell-to-cell contacts. *Diabetologia*, 30 10, 51(10), pp. 1843-1852.
- Wollheim, C. B. & Sharp, G. W., 1981. *Regulation of insulin release by calcium*. s.l.:s.n.
- Wragg, L. E., Machado, C. R., Snyder, S. H. & Axelrod, J., 1967. Anterior chamber pineal transplants: Their metabolic activity and independence of environmental lighting. *Life Sciences*, 1 1, 6(1), pp. 31-38.
- Wynne, K. et al., 2006. Oxyntomodulin increases energy expenditure in addition to decreasing energy intake in overweight and obese humans: A randomised controlled trial. *International Journal of Obesity*, 21 12, 30(12), pp. 1729-1736.
- Wynne, K. et al., 2005. Subcutaneous oxyntomodulin reduces body weight in overweight and obese subjects: A double-blind, randomized, controlled trial. *Diabetes*, 1 8, 54(8), pp. 2390-2395.
- Xiong, Q.-Y. et al., 2017. Key proteins involved in insulin vesicle exocytosis and secretion. *Biomedical Reports*, 2, 6(2), pp. 134-139.
- Yap, W. T. et al., 2013. *Collagen IV-modified scaffolds improve islet survival and function and reduce time to euglycemia*. s.l., Mary Ann Liebert Inc., pp. 2361-2372.
- Yeung, J. C. et al., 2012. Ex vivo adenoviral vector gene delivery results in decreased vector-associated inflammation pre- and post-lung transplantation in the pig. *Molecular Therapy*, 20(6), pp. 1204-1211.

- Yokota, Y. et al., 2015. Endothelial Ca²⁺ oscillations reflect VEGFR signaling-regulated angiogenic capacity in vivo. *eLife*, 20 11.4(NOVEMBER2015).
- Yoshitomi, H. & Zaret, K. S., 2004. Endothelial cell interactions initiate dorsal pancreas development by selectively inducing the transcription factor Ptf1a. *Development*, 15 2, 131(4), pp. 807-817.
- You, W. P. & Henneberg, M., 2016. Type 1 diabetes prevalence increasing globally and regionally: The role of natural selection and life expectancy at birth. *BMJ Open Diabetes Research and Care*, 1 3, 4(1), p. e000161.
- Yukawa, M., Takeuchi, T., Watanabe, T. & KITAMURA, S., 1999. Proportions of Various Endocrine Cells in the Pancreatic Islets of Wood Mice (*Apodemus speciosus*). *Anatomia, Histologia, Embryologia: Journal of Veterinary Medicine Series C*, 1 3, 28(1), pp. 13-16.
- Zaccardi, F., Webb, D. R., Yates, T. & Davies, M. J., 2016. *Pathophysiology of type 1 and type 2 diabetes mellitus: A 90-year perspective*. s.l.:BMJ Publishing Group.
- Zarrouki, B. et al., 2014. Epidermal growth factor receptor signaling promotes pancreatic β -cell proliferation in response to nutrient excess in rats through mTOR and FOXM1. *Diabetes*, 3, 63(3), pp. 982-993.
- Zhang, C. et al., 2006. siRNA-containing liposomes modified with polyarginine effectively silence the targeted gene. *Journal of Controlled Release*, 15 5, 112(2), pp. 229-239.
- Zhang, M. et al., 2008. Long lasting synchronization of calcium oscillations by cholinergic stimulation in isolated pancreatic islets. *Biophysical Journal*, 15 11, 95(10), pp. 4676-4688.
- Zhang, W. W. et al., 2018. The First Approved Gene Therapy Product for Cancer Ad-p53 (Gendicine): 12 Years in the Clinic. *Human Gene Therapy*, 1 2, 29(2), pp. 160-179.
- Zhu, L. et al., 2020. Association of Blood Glucose Control and Outcomes in Patients with COVID-19 and Pre-existing Type 2 Diabetes. *Cell Metabolism*, 1 5.